Universitat d'Alacant
Universidad de Alicante

Electrocatalytic studies of formic acid oxidation on Pt model surfaces

Juan Víctor Perales Rondón

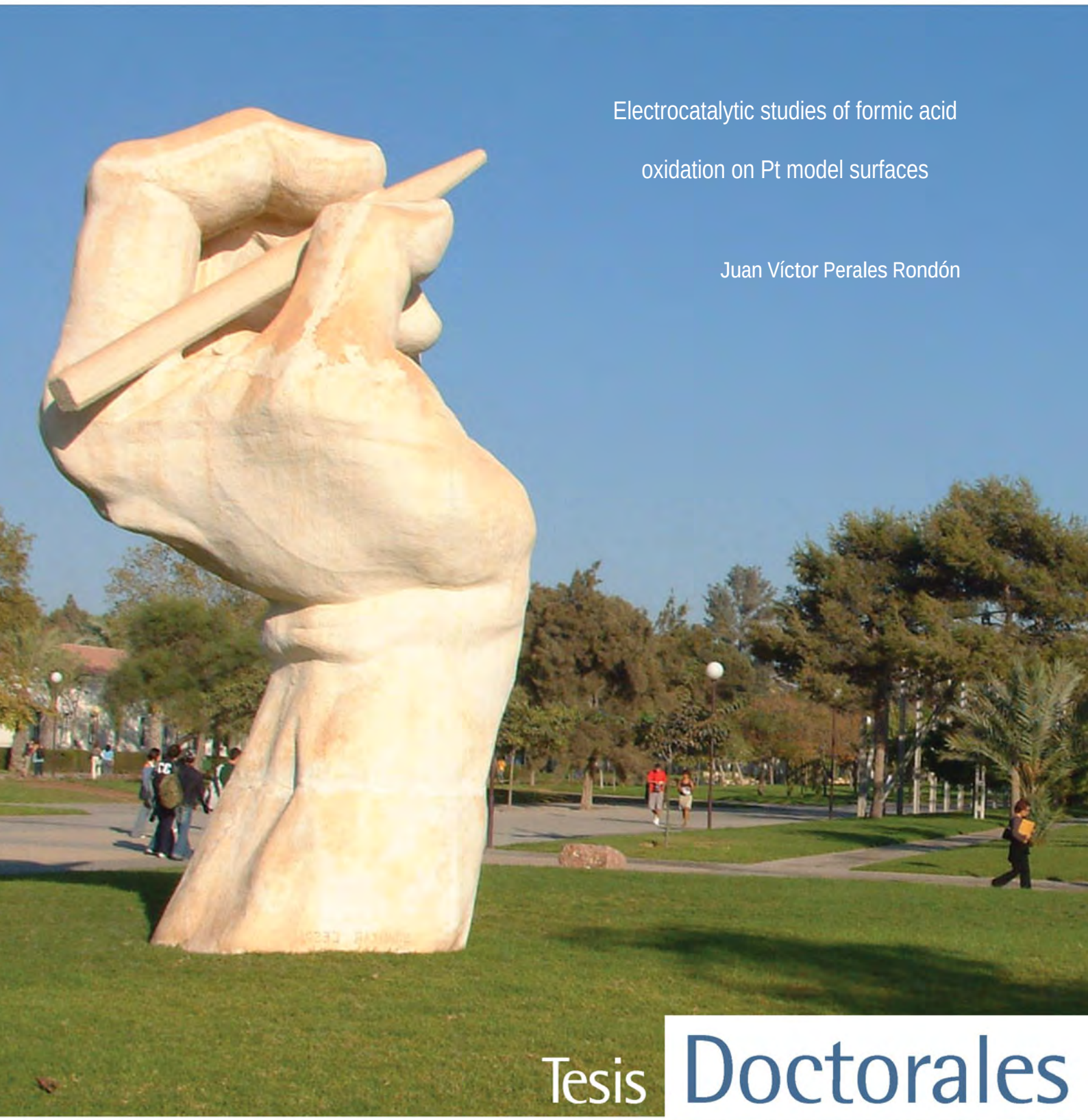

Tesis Doctorales

www.eltallerdigital.com

UNIVERSIDAD de ALICANTE

Universitat d'Alacant
Universidad de Alicante

Instituto Universitario de Electroquímica

Facultad de Ciencias

Electrocatalytic studies of formic acid oxidation on Pt model surfaces

Juan Víctor Perales Rondón

Tesis presentada para aspirar al grado de

DOCTOR POR LA UNIVERSIDAD DE ALICANTE

MENCIÓN DE DOCTOR INTERNACIONAL

Programa de Doctorado Electroquímica. Ciencia y Tecnología RD 99/2011

Dirigida por:

Enrique Herrero Rodríguez
Catedrático de Universidad en el
Dpto. de Química Física de la
Universidad de Alicante

Carlos M. Sánchez-Sánchez
Chargé de Recherche CNRS (HDR)
Laboratoire Interfaces et Systèmes
Electrochimiques
Sorbonne Universités, UPMC Univ Paris 06

Alicante, Julio 2016

Este trabajo ha sido financiado por la Generalitat Valenciana a través de la Beca para la formación de personal investigador, en centros de investigación de la Comunitat Valenciana GRISOLIA/2011/029.

Agradecimientos / Acknowledgements

"Sólo un exceso es recomendable en
el mundo: el exceso de gratitud"
Jean de la Bruyère

El camino de realizar una tesis doctoral es, como la mayoría saben, un sendero largo y que implica mucho esfuerzo. Las experiencias que adquieres durante ese tiempo no sólo aportan para tu formación profesional, sino que además son clave para un crecimiento personal integral. Después de todo, no dejan de ser cuatro años de tu vida en la que aprendes a saborear victorias y desaciertos, buenos momentos y no tan buenos. En fin, el tránsito por este camino no habría sido posible si no hubiese tenido a mi lado un ingente número de personas que de forma directa o indirecta han aportado su grano (o en algunos casos puños llenos) de arena al desarrollo exitoso de este trabajo de tesis.

Quiero empezar agradeciendo a **Dios**, por quien soy y tengo todo, a quien debo mis alcances, mis victorias y aun mis derrotas. Sé que gracias a Él he culminado con éxito la realización de esta tesis. Gracias.

Al Prof. **Enrique Herrero**, por tener paciencia conmigo durante todo este tiempo, y por estar dispuesto a ayudarme y a responder mis dudas cuando las he tenido. Gracias por guiarme en la realización del trabajo, y por recomendarme experimentos que han terminado siendo exitosos con resultados publicables.

Al Dr. **Carlos Sánchez** quien me ha ayudado con mucha paciencia y entrega en las diversas fases de este trabajo de tesis. Gracias por aportar un valor de excelencia a mis escritos y a mis presentaciones. Por enseñarme que con esfuerzo y trabajo se pueden lograr

las cosas que se proponen. Gracias también por las palabras de aliento y reconocimiento que, sin tu saberlo, me han levantado en momentos de decaída.

Al Prof. **Juan Feliu**, quien siempre demuestra mucha pasión por lo que hace y quien solía plantearme dudas que me aportaban ideas para hacer nuevos experimentos. Gracias por aportarme, no sólo a mí sino a todos los demás alumnos, los electrodos que necesitamos para trabajar, y gracias también por los consejos, tanto académicos como personales, consejos estos que detrás de las risas esconden una gran verdad.

Al Dr. **Jose Solla**, por formar parte directa de muchos de los trabajos que he publicado durante el desarrollo de la tesis. Jose es el tipo de personas que te enseña mucho esas cosas prácticas que sólo te puede aportar gente de experiencia en laboratorio como él. Gracias también por tener paciencia y atenderme cuando lo he necesitado, así como por aportar las nanopartículas que usé en varios trabajos de la tesis.

Al Prof. **Víctor Climent**, quien ha aportado algunos consejos y respuestas a mis dudas con mucho criterio.

A los compañeros del laboratorio de Electroquímica de Superficies de la Universidad de Alicante, quienes con su ayuda y compañerismo han creado un clima agradable que ha facilitado el trabajo del día a día. Entre ellos quiero mencionar a **Ana B, Calos B, Rosa A, Betzhy C, Valentín B, Ricardo M, Fran, Paula S, Sara C, Rubén R, Rubén G, Jonnathan H, Miguel A, Naiara, Leticia, Ariadna B, Ana C, Nacho, Dr. David V, Dr. Fran Vidal y Alicia**. No quiero olvidar por supuesto aquellos que han pasado de estancia por nuestro laboratorio y han dejado una impronta en mí, entre ellos: **Sara T, Manuel, Ottavio L, Juliane, Elton S, Natalia A, Natalia, Andrea y Gisele.**

A los profesores que me recibieron en sus laboratorios para hacer estancias en mi etapa doctoral (Prof. **Bing-Wei Mao** y Prof. **Vincent Vivier**). ¡Cuántos conocimientos aprendí durante esas estancias!. Son etapas invaluables. También aprovecho a agradecer a

mis compañeros de laboratorio en esas estancias, en especial: **Dingwen, Tang, Meng, Zong, Xie, Larbi, Caio, Stephane, Malika y Alessandro.** Gracias por hacer mucho más fácil mi integración en los distintos lugares donde tuve la dicha de trabajar.

Muy especialmente quiero agradecer a **Maribel Viedma**, ya que su ayuda con los documentos concernientes a mi estadía en España ha sido clave para continuar sin ningún contratiempo.

Quiero agradecer también a la gente de la Iglesia Cristo Vive "San Vicente". En este tiempo del desarrollo de mi tesis no sólo han sido amigos, han sido una gran familia para mí. Especialmente quiero agradecer a personas como: **Carlos J, Ana O y familia; Marcos C; Dolores A y familia, Jose A y Loida; Anita, Arturo, Nice y Sofia.** Gracias por haber sido un gran apoyo durante todo este tiempo, no sólo personal sino también principalmente espiritual.

Finalmente, quiero agradecer a mis Padres **Isoris Rondón y Felix Perales** y mis hermanos **Carlos Perales y David Perales**, quienes siempre me han apoyado en mis decisiones y han creído en mí y en que puedo alcanzar las metas que me he trazado. Siempre me han apoyado desde que empecé este camino y sin ustedes nada de esto hubiese sido posible. Gracias a mis tíos maternos, en especial **Gladys R** quien ha formado parte de la aventura de venir aquí. Gracias a mi abuela **Ester de R**, que con sus buenos deseos y sus oraciones ha formado parte de este éxito. No quiero dejar de nombrar también a **Maria E**, quien de forma silenciosa pero efectiva ha estado allí para animarme a seguir y dar lo mejor de mí. Ella es la muestra de lo bien que te puede hacer una persona cuando cree en ti. Gracias por creer en mí.

En definitiva, a todas aquellas personas que no alcancé a mencionar en este escrito pero que, no por eso, no dejo de estar agradecido también con ellos.

“La perfección no existe, pero si la buscamos

alcanzaremos la excelencia”

Anónimo

A mis padres, mis hermanos y mis sobrinos

Contents

Resumen

Abstract

Resumen

El aumento de los problemas ocasionados por el cambio climático ha llevado al planteamiento de nuevas tecnologías que puedan minimizar la emisión de gases de efecto invernadero a la atmósfera [1, 2], tales como CO_2 o CH_4. Entre ellas cabe destacar el papel relevante de las células de combustible [3, 4]. Estas son dispositivos capaces de generar electricidad directamente a partir de la reacción electroquímica de un combustible, convirtiendo la energía química almacenada en los enlaces, en energía eléctrica. Esta conversión directa implica que el rendimiento máximo teórico no se ve limitado por el ciclo de Carnot, pudiendo ser mayor comparado con los procesos de combustión convencionales. Sin embargo, el rendimiento energético de las pilas de combustible está aún lejos de alcanzar los valores máximos teóricos. Por tanto, es imperativo conseguir la mejora de su eficiencia, lo que conllevaría una disminución sustancial en las emisiones de gases de efecto invernadero (GHG) a la atmósfera.

Entre las células de combustible más destacadas se encuentran las de membrana polimérica (PEMFC). Estas funcionan a bajas temperaturas ($T < 100ºC$), y permiten operar con combustibles líquidos como metanol, etanol o ácido fórmico, que presentan la ventaja de un fácil manejo, una elevada densidad energética por molécula, así como un elevado potencial de célula teórico [5, 6].

Uno de los combustibles más estudiados en este sentido ha sido el ácido fórmico, especialmente para aplicaciones portátiles y de pequeña potencia [7, 8]. Adicionalmente, la

reacción de ácido fórmico presenta un gran interés en electrocatálisis, debido a que su oxidación involucra sólo dos electrones, no necesita oxígeno adicional para generar CO_2 como producto y, por último, es una reacción claramente sensible a la estructura superficial del electrodo [9]. Por estos motivos puede considerarse una reacción modelo en electrocatálisis, cuyo mecanismo puede servir para comprender reacciones de oxidación más complejas.

Debido a que uno de los metales más usados en electrocatálisis es el Pt, en la bibliografía se pueden encontrar numerosos estudios sobre la oxidación de ácido fórmico en este metal, tanto a nivel fundamental como en un ámbito más aplicado. A nivel fundamental se ha estudiado la electrocatálisis en electrodos de Pt con superficies bien definidas [10, 11], aportando datos que puedan elucidar el mecanismo a través del cual ocurre la reacción, mientras que en un ámbito más aplicado, usando nanopartículas metálicas (Pt y Pt modificadas con adatomos) con tamaños y formas definidas, a fin de aportar datos catalíticos sobre materiales aplicables en células de combustible [12, 13].

A pesar de que la investigación de la oxidación de ácido fórmico en electrodos de Pt está en una fase avanzada, su mecanismo de reacción dista mucho de ser ampliamente comprendido; de hecho, existe aún disputa respecto de la naturaleza y configuración de las especies que participan como intermedios en las diferentes vías de reacción. Hasta ahora se sabía que la reacción de oxidación de ácido fórmico seguía un mecanismo dual, con dos claras vías de reacción diferentes [14-16]: la llamada vía directa, que implica la formación de un intermedio activo que luego es oxidado a CO_2 a valores de potenciales menos positivos; y la vía indirecta, que conlleva la formación de un intermedio venenoso, identificado como CO [17], cuya oxidación a CO_2 requiere de potenciales elevados. A pesar de que este mecanismo está ampliamente extendido y aceptado entre la comunidad

científica, recientemente se ha planteado un nuevo mecanismo de tres vías [18], sustentado por datos teóricos y experimentales [19-21], que viene a ampliar la propuesta hecha inicialmente por Capon y Parsons [14]. El mecanismo de tres vías plantea la existencia de una vía indirecta, que al igual que en el caso anterior, implica la formación de CO en la superficie electródica, el cual participa como intermedio venenoso; una vía directa, que pasa por la formación de un intermedio activo, cuya naturaleza y configuración aún está bajo fuerte discusión, y finalmente una tercera vía conocida como la vía del formiato, que como su nombre indica, conlleva la formación de formiato adsorbido en configuración "bidentada" o "puente" en la superficie electródica, el cual participa como una especie espectadora y/o facilitadora, debido a su dificultad para ser oxidado a CO_2. Esto ha sido ampliamente demostrado en numerosos estudios teóricos donde se ha puesto de manifiesto la alta barrera energética asociada al paso del formiato adsorbido en configuración "puente" a CO_2.

Estudios hechos con electrodos de Pt con superficies bien definidas [Pt(*hkl*)] (o electrodos monocristalinos) muestran la dependencia de cada una de estas vías de reacción con la estructura superficial del electrodo [22, 23]. La diferencia de actividad entre los distintos planos de base (Pt(111), Pt(100) y Pt(110)) es bastante notoria. Un ejemplo claro se encuentra en la voltametría cíclica para la oxidación del ácido fórmico en medio ácido. Así, la histéresis entre los barridos positivo y negativo para el Pt(111) es muy pequeña, lo cual implica que este electrodo se ve muy poco afectado por la vía del intermedio venenoso, mientras que un comportamiento contrario se observa para el caso del Pt(100), donde la marcada histéresis muestra su mayor sensibilidad hacia el envenenamiento con CO. Las diferencias en las reactividades de estos dos planos bases señala uno de los

problemas claves para catalizar esta reacción: la selectividad hacia cada una de las vías antes mencionadas.

Lo expuesto anteriormente muestra uno de los grandes retos que hay que enfrentar en la investigación de la electroxidación de ácido fórmico en superficies de Pt: suprimir la formación de veneno o intermedios espectadores, favoreciendo de este modo la oxidación a través del intermedio activo. Para ello es necesario tener un amplio conocimiento acerca de su mecanismo, y de la dependencia de este con la estructura y composición superficial de los electrodos de Pt, parámetros estos que modulan la cinética y el rendimiento de la reacción.

Una vez ha quedado demostrada la importancia de la reacción de oxidación de ácido fórmico, debido a su uso como reacción modelo en electrocatálisis, y su posible aplicación en células de combustible, es fácil entender por qué se ha planteado la realización de este trabajo de tesis doctoral, cuyo objetivo principal es el estudio de la electrooxidación de ácido fórmico en electrodos de Pt, en dos niveles: El primero comprende un enfoque fundamental, mediante la determinación de parámetros cinéticos y termodinámicos usando electrodos monocristalinos para, partiendo de estos datos, plantear un modelo de reacción satisfactorio. Un segundo nivel de estudio que comprende la modificación superficial de electrodos monocristalinos o nanopartículas de Pt, a fin de mejorar su actividad electrocatalítica para la oxidación de ácido fórmico. Se hará especial énfasis en la disminución en el sobrepotencial aplicado, así como el aumento de la densidad de corriente para un valor de potencial dado; empleando para todo ello técnicas electroquímicas convencionales (voltametría cíclica, voltametría de pulso, cronoamperometría), así como técnicas más vanguardistas, como la microscopía electroquímica de barrido (SECM) [24].

Consecuente con el cumplimiento de este objetivo general, el contenido de la tesis se ha dividido en 8 capítulos, atendiendo a los dos enfoques presentados anteriormente. La presentación del trabajo de tesis se hará por compendio de las publicaciones en revistas indexadas logradas en el desarrollo de la misma, lo que se ajusta al reglamento de la Universidad de Alicante. Adicionalmente, la memoria de la tesis será escrita parcialmente en inglés, con el fin de cumplir los requisitos necesarios para obtener el título de Doctor con mención internacional. Los mencionados capítulos se describen brevemente a continuación:

En el capítulo 1 se muestra una introducción que pretende aportar las bases teóricas imprescindibles para entender los aspectos mecanísticos y aplicados de la reacción de oxidación de ácido fórmico en electrodos de Pt. Se presentará por tanto una revisión bibliográfica mostrando el estado del arte acerca del mecanismo de reacción, así como de los sistemas M-Pt (Pt modificado por otro metal (M)), haciendo énfasis en aquellos que han presentado una mayor actividad catalítica hasta ahora, y finalizando con la descripción de las nanopartículas de Pt con forma preferencial y su aplicación en la oxidación del ácido fórmico.

En el capítulo 2 se aborda la descripción de los protocolos experimentales generales utilizados a lo largo de esta tesis doctoral, comenzando con algunas nociones sobre cristalografía de superficies, y con especial énfasis en la notación típica de las superficies monocristalinas (índices de Miller). En los capítulos subsiguientes se mantendrá la nomenclatura introducida en esta sección. La segunda parte del capítulo está dedicada a la descripción de las técnicas experimentales empleadas, así como las configuraciones experimentales utilizadas para el desarrollo de este trabajo. Finalmente, se hace también

una descripción de la célula electroquímica, así como de los reactivos que fueron usados a lo largo del desarrollo de este trabajo de tesis.

El capítulo 3 se dedica a la presentación de los resultados derivados del estudio de la electrooxidación de ácido fórmico en un electrodo de Pt(111) bajo diferentes condiciones de pH y usando diferentes electrolitos [25]. Para este estudio se utilizó como herramienta fundamental la determinación de la energía de activación aparente ($E_a{}^{app}$) de la reacción en todo el rango de potenciales donde el Pt(111) presenta actividad, lo que permitió establecer comparaciones entre diferentes pHs y medios electrolíticos estudiados.

El comportamiento de la $E_a{}^{app}$ en función del pH mostró que la reacción de oxidación del ácido fórmico se ve favorecida con el aumento de pH. Relacionando este hecho con los resultados voltamétricos, en los que se aprecia un aumento claro de la densidad de corriente máxima de oxidación con el pH, fue posible concluir que el formiato en disolución tiene una participación activa en el mecanismo de la reacción, lo cual concuerda con los resultados obtenidos y publicados recientemente por Joo *et al*. [26].

Al estudiar el efecto de la presencia de distintos aniones sobre las energías de activación, se pudo observar que el anión sulfato provoca una disminución de la $E_a{}^{app}$ en Pt(111), lo que implica que la adsorción del sulfato tiene un inesperado efecto positivo en la oxidación de ácido fórmico sobre Pt(111), sugiriendo que los aniones adsorbidos (espectadores) también pueden estar implicados en el mecanismo de reacción. Usando estos datos experimentales y relacionándolos con trabajos teóricos llevados a cabo en colaboración con otros grupos donde se hacen cálculos de DFT, se propone la participación del anión sulfato como un agente promotor de la adsorción del formiato en una configuración adecuada que da lugar a su oxidación total a CO_2 con una menor E_a, lo que permite explicar satisfactoriamente los resultados experimentales obtenidos.

En el capítulo 4 se presenta un estudio comparado de la E_a^{app} de la electroxidación de ácido fórmico sobre los planos bases Pt(111) y Pt(100), así como sobre dos superficies escalonadas, a saber, Pt(544) y Pt(554), que son escalonadas del tipo Pt*(s)*[*n(111)x(100)*] y Pt*(s)*[*(n-1)(111)x(110)*] respectivamente [27]. Para ello se hicieron experimentos de voltametría de pulso a diferentes temperaturas. Obtenidas las curvas cronoamperométricas, estas se ajustaron a un modelo cinético planteado con anterioridad en la bibliografía [28, 29] y se obtuvieron de este modo los valores de energía de E_a^{app} en todo el rango de potenciales para cada uno de los 4 electrodos estudiados, tal y como ya se hizo en el capítulo anterior para el Pt(111).

Las diferencias encontradas en la E_a^{app} para los planos bases, muestra la sensibilidad a la estructura de la reacción de electrooxidación de ácido fórmico, encontrándose valores de E_a^{app} más bajos, a menores sobrepotenciales para el Pt(100) frente a los obtenidos para el Pt(111). Sin embargo, a sobrepotenciales elevados se observa el comportamiento contrario. Por otro lado, la energía de activación aparente en las superficies de Pt escalonadas muestra un comportamiento similar al del Pt(111), presentando valores mayores de E_a^{app} en casi todo el rango de potencial, lo que explica la influencia que tiene la densidad de escalones en la reactividad de la superficie y en la modulación del mecanismo de reacción, tal y como ya lo describió Grozovski *et al*. [28, 29] en otra tesis doctoral del mismo grupo de investigación (Electroquímica de Superficies de la Universidad de Alicante). Además, se pone de manifiesto, una vez más, la participación del anión sulfato en el mecanismo de reacción, por cuanto la incorporación de estos aniones que presentan adsorción específica, provoca una disminución de la energía de activación en la mayoría de los casos. Por tanto, estos datos apuntan hacia un

efecto positivo por parte del sulfato en el mecanismo de reacción para el electrodo Pt(100), tal y como se describió en el capítulo 3 para el Pt(111).

En vista de que el pH de la disolución y la adsorción específica de los aniones presentes en la misma, constituyen parámetros fundamentales que pueden gobernar en gran medida el mecanismo de reacción, parece razonable la realización de un estudio donde se amplíe el rango de pH a estudiar, sin que esto suponga la adición de aniones que puedan tener adsorción específica. Con este fin se realizó el trabajo que se presenta en el capítulo 5, donde se estudia la cinética de la oxidación de ácido fórmico en un electrodo de Pt poliorientado en un rango amplio de pHs (1-14) y con aniones con diferente capacidad de adsorción como ClO_4^-, SO_4^{2-}, PO_4^{3-} y Cl^- [30].

En esta parte de la tesis doctoral se pone de manifiesto como a medida que se aumenta el pH en un rango comprendido entre 0 y 5, las densidades de corriente de oxidación máximas van aumentando, con lo que una vez más se muestra con claridad la participación del formiato en disolución en el mecanismo de la reacción de oxidación del ácido fórmico. De hecho, de los resultados se desprende que esta última especie en disolución es la precursora del intermedio activo, tal como se ha sugerido con anterioridad [26, 31, 32]. Por otro lado, el estudio de la influencia del anión presente en el electrolito y su capacidad de adsorción sobre el Pt muestra que en medio PO_4^{3-}, anión con adsorción específica sobre Pt, la relación densidad de corriente máxima vs pH presenta una forma gausiana, teniendo un máximo a un valor de pH igual a 3.7 que coincide con el p*Ka* del ácido fórmico; al contrario de lo que ocurre en el caso del ClO_4^- o SO_4^{2-}, donde la curva presenta un plató y alcanza la densidad de corriente máxima de oxidación de ácido fórmico alrededor de pH 5. Gracias a todos estos datos experimentales fue posible plantear un mecanismo de reacción que puede explicar satisfactoriamente el comportamiento de la

densidad de corriente máxima para la oxidación de ácido fórmico a diferentes valores de pH, en los diferentes medios electrolíticos estudiados.

Hasta este momento de la tesis, sólo se ha estudiado el mecanismo de reacción de la oxidación de ácido fórmico en electrodos de Pt sin ningún tipo de modificación superficial, con el objetivo de conseguir una visión amplia de la reacción, e intentar modelizar los comportamientos voltamétricos descritos, tal como se ha hecho en los capítulos 3, 4 y 5. No obstante, en el capítulo 6 se introduce una nueva variable, que es la modificación superficial de los electrodos monocristalinos de Pt. Concretamente, se estudia el electrodo de Pt(111) modificado con Bi, que es uno de los sistemas que presenta un mayor incremento de su actividad catalítica para la oxidación de ácido fórmico [33].

En este caso, el electrodo de Pt(111) fue modificado con varios recubrimientos de Bi (θ_{Bi}) y se trabajó a distintas temperaturas con el fin de determinar la energía de activación de la reacción de oxidación de ácido fórmico en todo el rango de potenciales, usando para ello el barrido de potencial en sentido positivo de la curva voltamétrica. Los resultados obtenidos muestran como a medida que se aumenta el recubrimiento, la energía de activación presenta una disminución respecto a la del electrodo de Pt sin modificar, especialmente a potenciales inferiores a 0.6 V vs. *RHE*, lo que demuestra el importante efecto electrocatalítico del Bi como modificador superficial [34]. Por otro lado, al contrastar los valores de las energías de activación obtenidos experimentalmente con aquellos obtenidos por cálculos de DFT, fue posible concluir que la energía de activación para la ruptura del enlace C-H en el formiato es realmente baja en estas condiciones. Así pues, los cálculos y observaciones anteriores permitieron proponer un mecanismo en el que se plantea como etapa inicial la adsorción de una molécula de formiato sobre el átomo de bismuto. Dada la baja electronegatividad de este, el formiato se adsorbe a través de uno de

sus átomos de oxígeno, lo que permite una rotación libre de la molécula en el eje que forma el enlace C-O. En estas condiciones, la molécula se orienta con el enlace C-H hacia la superficie electródica, favoreciendo la adsorción del hidrógeno sobre un átomo de Pt adyacente, lo que facilita la formación y posterior liberación de CO_2 como producto de oxidación. Así, la energía de activación de la ruptura de este último enlace (C-H) es, como se mencionó anteriormente, realmente baja y casi despreciable [33, 35].

En los cuatro capítulos de resultados detallados hasta ahora, se ha tratado de dar explicación a todos los datos experimentales obtenidos y se ha desarrollado para ello un mecanismo de reacción plausible para la oxidación de ácido fórmico, sin hacer especial énfasis en cómo mejorar la electrocatálisis del electrodo de Pt. Uno de los métodos que se puede usar para lograr este último fin es la modificación superficial del electrodo de Pt, ya sea por adsorción irreversible o por electrodeposición a bajo potencial (UPD por su acrónimo en inglés) de un adátomo, o también por formación de una aleación superficial. Así pues, en el capítulo 7 de esta tesis doctoral se detalla la modificación superficial de electrodos de Pt(111), Pt(100) y superficies vecinales, con Tl como adátomo, y su efecto en la actividad catalítica para la reacción de oxidación de ácido fórmico. En concreto, se intenta aportar un conocimiento fundamental que permita explicar el importante aumento de actividad para la oxidación de ácido fórmico, ya demostrado en nanopartículas de Pt modificadas con Tl [36]. Gracias a estos nuevos datos se demostró que la reacción presenta sensibilidad a la superficie de los electrodos modificados, siendo uno de los más activos el sistema Tl-Pt(100), el cual presenta una densidad de corriente normalizada máxima a 0.42 V vs. *RHE*. Así mismo, la presencia de Tl provoca una disminución importante del potencial de inicio de la oxidación, mostrado aumentos de actividad en los barridos positivos de la voltametría cíclica correspondiente. Los electrodos de la serie

Pt*(s)*[*n(100)x(111)*] modificados con Tl presentan un comportamiento similar al del Pt(100). Por otro lado, para el sistema Tl-Pt(111) el cambio más significativo corresponde a la disminución del potencial de inicio de la oxidación, siendo su mejora en actividad destacable, especialmente a bajos potenciales (< 0.40 V vs. *RHE*). Las observaciones anteriores, unidas a datos obtenidos por espectroscopia infrarroja FT-IR apuntan a que el Tl presenta tanto un efecto de tercer cuerpo (por cuanto suprime el envenenamiento del electrodo por CO) como un efecto bifuncional, evidenciado en el marcado aumento de la actividad para el caso del electrodo Pt(100).

Por último, el trabajo detallado en el capítulo 8 tiene un corte más aplicado. En él se presenta la actividad catalítica de nanopartículas de Pt con formas preferenciales, modificadas superficialmente con Pb. Las nanopartículas estudiadas fueron las 111-Pt (octaédricas), las 100-Pt (cúbicas) y las Pt poly (esféricas). Al modificar cada uno de los electrodos anteriores con Pb, se observó como a medida que se aumenta el recubrimiento de Pb hay un incremento notable en su actividad para la oxidación de ácido fórmico. Esto se demostró tanto por datos voltamétricos como usando microscopía electroquímica de barrido (SECM) [24], mediante la cual se pudo obtener el mapa de actividades de un ultramicroelectrodo de Pt (diámetro = 100 μm) antes y después de ser modificado con Pb, observándose corrientes entre 4 y 7 veces mayores a las correspondientes al electrodo de Pt sin modificar. Para este experimento se usó un protocolo de trabajo introducido por Rodríguez-López *et al*. [37], y basado en la liberación de una cantidad controlada de ácido fórmico desde una micropipeta y su posterior colección-reacción en el electrodo que actúa de sustrato, en este caso Pt y Pt-Pb. En concreto, este experimento consiste en llenar una micropipeta (diámetro apertura ~ 15 μm) con una disolución de ácido fórmico en un disolvente orgánico (dicloroetano, DCE), con la que se barre la cercanía de la superficie

del electrodo que actúa de sustrato. Todo ello en presencia de la disolución acuosa de interés para la reacción de oxidación. Así pues, cuando la micropipeta se pone en contacto con el medio acuoso, se establece un gradiente de concentración entre el ácido fórmico del interior de la micropipeta y la disolución acuosa en el exterior, el cual está regido por la constante de reparto del ácido fórmico entre las dos fases líquidas (orgánica y acuosa). Esto permite la liberación de forma controlada del ácido fórmico desde el interior de la micropipeta hacia la disolución acuosa del exterior. De este modo, el ácido fórmico liberado será oxidado al encontrarse con una superficie electroactiva. Finalmente, la representación de la corriente del sustrato en función de la posición de la micropipeta sobre el plano XY permite obtener un mapa de la actividad catalítica del mismo e identificar sus zonas más y/o menos activas. Para el estudio de la oxidación de ácido fórmico, el experimento de SECM se utilizó únicamente como test preliminar para hacer una evaluación rápida de la modificación superficial de electrodos de Pt con Pb. Sin embargo, esta misma técnica se ha utilizado también como método para discernir la actividad entre distintos electrocatalizadores para otras reacciones, como por ejemplo la reducción de cloroformo sobre nanopartículas de Ag [38].

Por otro lado, los test de actividad catalítica convencionales llevados a cabo por cronoamperometría para las nanopartículas de Pt con forma superficial controlada y modificadas con Pb, mostraron que las nanopartículas más activas son las octaédricas (Pb_θ/111-Pt NPs), mostrando densidades de corriente máximas de alrededor de 7 $mA.cm^{-2}$, comparado con los 4 $mA.cm^{-2}$ de las nanopartículas cúbicas (Pb_θ/100-Pt NPs), ambas a un potencial de 0.5 V vs. *RHE* en una disolución de ácido fórmico 0.1 M. Las curvas cronoamperométricas a 0.3 V y 0.5 V vs. *RHE* muestran como las nanopartículas de Pt con forma superficial controlada y modificadas con Pb presentan una estabilidad aceptable y

superior a la de otros adátomos, tales como Sb o Tl, siendo su disminución de actividad con el tiempo entre el 10-20% para la mayoría de los casos.

El capítulo final presenta las principales conclusiones del trabajo de tesis, haciendo énfasis en aquellas que se refieren a los modelos mecanísticos propuestos tanto para Pt como para Pt modificado por adatomos. En el caso del Pt, resaltando el efecto del anión del electrolito (o del mismo reactivo), ya que este participa en el mecanismo de la oxidación de ácido fórmico, presentando un posible efecto promotor de la adsorción del intermedio activo en una configuración adecuada. Por otro lado, demostrando también que el formiato es el precursor del intermedio activo, el cual se propone como el formiato adsorbido en una configuración con el enlace C-H orientado hacia la superficie electródica, esto último apoyado por cálculos DFT. En el caso de los electrodos de Pt modificados por adátomos, se describe un mecanismo similar para el sistema Bi-Pt(111), donde el formiato se adsorbe por uno de los átomos de oxígeno sobre el átomo de Bi. En estas condiciones, el enlace C-O es libre en su rotación y se orienta con el enlace C-H hacia la superficie electródica, favoreciendo la formación de CO_2 con una energía de activación despreciable. Por otro lado, cuando electrodos monocristalinos de Pt son modificados con Tl, este tiene un efecto positivo en la mejora de la actividad catalítica, disminuyendo el potencial de inicio de la oxidación de ácido fórmico y siendo más notorio el efecto en el Tl-Pt(100) que en Tl-Pt(111). Estas mejoras pueden asociarse con un efecto de tercer cuerpo, que evita la formación de CO, así como un efecto bifuncional, que disminuye la energía de activación de la vía de reacción directa. Finalmente, cuando se modifican nanopartículas de Pt con forma controlada usando Pb como adátomo, es clara la mejora en la actividad y la estabilidad de los catalizadores. De hecho, la mejora absoluta en la densidad de corriente mostrada por Pb_{θ}/111-Pt NPs es 2.7 y 2.3 veces aquella encontrada para otros sistemas

similares como el Tl_θ/100-Pt NPs y Sb_θ/111-Pt NPs, respectivamente. Tal aumento de actividad podría ser explicado por una sinergia entre un efecto de tercer cuerpo (supresión de la formación de CO) y un efecto bifuncional, donde el formiato es adsorbido inicialmente sobre el Pb, lo cual facilita su posterior oxidación sobre el Pt, pero con una menor barrera energética, asumiendo un mecanismo análogo al descrito en el caso del Bi-Pt(111) [25, 35].

Referencias

[1] M. I. Hoffert, K. Caldeira, G. Benford, D. R. Criswell, C. Green, H. Herzog, A. K. Jain, H. S. Kheshgi, K. S. Lackner, J. S. Lewis, H. D. Lightfoot, W. Manheimer, J. C. Mankins, M. E. Mauel, L. J. Perkins, M. E. Schlesinger, T. Volk and T. M. L. Wigley, "Advanced Technology Paths to Global Climate Stability: Energy for a Greenhouse Planet" *Science* **2002**, 298, 981-987.

[2] D. A. King, "Climate Change Science: Adapt, Mitigate, or Ignore?" *Science* **2004**, 303, 176-177.

[3] L. Carrette, K. A. Friedrich and U. Stimming, "Fuel Cells: Principles, Types, Fuels, and Applications" *ChemPhysChem* **2000**, 1, 162-193.

[4] S. Srinivasan, "Fuel Cells: From fundamental to Applications", Springer, **2006**.

[5] Y. Wang, K. S. Chen, J. Mishler, S. C. Cho and X. C. Adroher, "A review of polymer electrolyte membrane fuel cells: Technology, applications, and needs on fundamental research" *Applied Energy* **2011**, 88, 981-1007.

[6] J. Garche and L. Jörissen, "PEMFC fuel cell systems", in *Handbook of Fuel Cells*, John Wiley & Sons, Ltd, **2010**.

[7] S. Uhm, H. J. Lee and J. Lee, "Understanding underlying processes in formic acid fuel cells" *Physical Chemistry Chemical Physics* **2009**, 11, 9326-9336.

[8] C. Rice, R. I. Ha, R. I. Masel, P. Waszczuk, A. Wieckowski and T. Barnard, "Direct formic acid fuel cells" *Journal of Power Sources* **2002**, 111, 83-89.

[9] C. Rice, S. Ha, R. I. Masel and A. Wieckowski, "Catalysts for direct formic acid fuel cells" *Journal of Power Sources* **2003**, 115, 229-235.

[10] J. M. Feliu and E. Herrero, "Formic acid oxidation", in *Handbook of Fuel Cells - Fundamentals, Technology and Applications, vol. 2*, W. Vielstich, H. Gasteiger and A. Lamm (Eds.) John Wiley & Sons, Ltd., Chichester, **2003**, pp. 625-634.

[11] M. T. M. Koper, "Fuel Cell Catalysis: A Surface Science Approach", *Electrocatalysis and Electrochemistry* A. Wieckowski (Ed.), John Wiley & Sons, Hoboken, New Jersey, **2009**.

[12] J. Solla-Gullón, P. Rodríguez, E. Herrero, A. Aldaz and J. M. Feliu, "Surface characterization of platinum electrodes" *Physical Chemistry Chemical Physics* **2008**, 10, 1359-1373.

[13] J. Solla-Gullón, F. J. Vidal-Iglesias, A. López-Cudero, E. Garnier, J. M. Feliu and A. Aldaz, "Shape-dependent electrocatalysis: methanol and formic acid electrooxidation on preferentially oriented Pt nanoparticles" *Physical Chemistry Chemical Physics* **2008**, 10, 3689-3698.

[14] A. Capon and R. Parsons, "The oxidation of formic acid at noble metal electrodes Part III. Intermediates and mechanism on platinum electrodes " *Journal of Electroanalytical Chemistry* **1973**, 45, 205-231.

[15] A. Capon and R. Parsons, "The oxidation of formic acid on noble metal electrodes: II. A comparison of the behaviour of pure electrodes " *Journal of Electroanalytical Chemistry* **1973**, 44, 239-254.

[16] A. Capon and R. Parsons, "The oxidation of formic acid at noble metal electrodes: I. Review of previous work " *Journal of Electroanalytical Chemistry* **1973**, 44, 1-7.

[17] K. Kunimatsu, "Infrared spectroscopic study of methanol and formic acid adsorbates on a platinum electrode: Part I. Comparison of the infrared absorption intensities of linear CO(a) derived from CO, CH_3OH and HCOOH " *Journal of Electroanalytical Chemistry* **1986**, 213, 149-157.

[18] Y. X. Chen, M. Heinen, Z. Jusys and R. B. Behm, "Kinetics and mechanism of the electrooxidation of formic acid - Spectroelectrochemical studies in a flow cell" *Angewandte Chemie, International Edition in English* **2006**, 45, 981-985.

[19] Y. X. Chen, M. Heinen, Z. Jusys and R. J. Behm, "Bridge-bonded formate: Active intermediate or spectator species in formic acid oxidation on a Pt film electrode?" *Langmuir* **2006**, 22, 10399-10408.

[20] Y. X. Chen, M. Heinen, Z. Jusys and R. J. Behm, "Kinetic isotope effects in complex reaction networks: Formic acid electro-oxidation" *ChemPhysChem* **2007**, 8, 380-385.

[21] J. Xu, D. F. Yuan, F. Yang, D. Mei, Z. B. Zhang and Y. X. Chen, "On the mechanism of the direct pathway for formic acid oxidation at a Pt(111) electrode" *Physical Chemistry Chemical Physics* **2013**, 15, 4367-4376.

[22] J. Clavilier, R. Parsons, R. Durand, C. Lamy and J. M. Leger, "Formic acid oxidation on single crystal platinum electrodes. Comparison with polycrystalline platinum" *Journal of Electroanalytical Chemistry* **1981**, 124, 321-326.

[23] C. Lamy, J. M. Leger, J. Clavilier and R. Parsons, "Structural effects in electrocatalysis: A comparative study of the oxidation of CO, HCOOH and CH_3OH on single crystal Pt electrodes" *Journal of Electroanalytical Chemistry* **1983**, 150, 71-77.

[24] A. J. Bard and M. V. Mirkin, "Scanning Electrochemical Microscopy, Second Edition", CRC Press, **2012**.

[25] J. V. Perales-Rondon, E. Herrero and J. M. Feliu, "Effects of the anion adsorption and pH on the formic acid oxidation reaction on Pt(111) electrodes" *Electrochimica Acta* **2014**, 140, 511-517.

[26] J. Joo, T. Uchida, A. Cuesta, M. T. M. Koper and M. Osawa, "Importance of Acid-Base Equilibrium in Electrocatalytic Oxidation of Formic Acid on Platinum" *Journal of the American Chemical Society* **2013**, 135, 9991-9994.

[27] J. V. Perales-Rondón, E. Herrero and J. M. Feliu, "On the activation energy of the formic acid oxidation reaction on platinum electrodes" *Journal of Electroanalytical Chemistry* **2015**, 742, 90-96.

[28] V. Grozovski, V. Climent, H. Herrero and J. M. Feliu, "INtrinsic Activity and Poison Rate for HCOOH Oxidation at Pt(100) and Vicinal Surfaces Containing Monoatomic (111) Steps " *ChemPhysChem* **2009**, 10, 1922-1926.

[29] V. Grozovski, V. Climent, E. Herrero and J. M. Feliu, "Intrinsic activity and poisoning rate for HCOOH oxidation on platinum stepped surfaces" *Physical Chemistry Chemical Physics* **2010**, 12, 8822-8831.

[30] J. V. Perales-Rondón, S. Brimaud, J. Solla-Gullón, E. Herrero, R. Jürgen Behm and J. M. Feliu, "Further Insights into the Formic Acid Oxidation Mechanism on Platinum: pH and Anion Adsorption Effects" *Electrochimica Acta* **2015**, 180, 479-485.

[31] J. Joo, T. Uchida, A. Cuesta, M. T. M. Koper and M. Osawa, "The effect of pH on the electrocatalytic oxidation of formic acid/formate on platinum: A mechanistic study by surface-enhanced infrared spectroscopy coupled with cyclic voltammetry" *Electrochimica Acta* **2014**, 129, 127-136.

[32] S. Brimaud, J. Solla-Gullon, I. Weber, J. M. Feliu and R. J. Behm, "Formic Acid Electrooxidation on Noble-Metal Electrodes: Role and Mechanistic Implications of pH, Surface Structure, and Anion Adsorption" *ChemElectroChem* **2014**, 1, 1075-1083.

[33] J. V. Perales-Rondon, A. Ferre-Vilaplana, J. M. Feliu and E. Herrero, "Oxidation Mechanism of Formic Acid on the Bismuth Adatom-Modified Pt(111) Surface" *Journal of the American Chemical Society* **2014**, 136, 13110-13113.

[34] E. Leiva, T. Iwasita, E. Herrero and J. M. Feliu, "Effect of adatoms in the electrocatalysis of HCOOH oxidation. A theoretical model" *Langmuir* **1997**, 13, 6287-6293.

[35] A. Ferre-Vilaplana, J. V. Perales-Rondon, J. M. Feliu and E. Herrero, "Understanding the Effect of the Adatoms in the Formic Acid Oxidation Mechanism on Pt(111) Electrodes" *ACS Catalysis* **2015**, 5, 645-654.

[36] C. Buso-Rogero, J. V. Perales-Rondon, M. J. S. Farias, F. J. Vidal-Iglesias, J. Solla-Gullon, E. Herrero and J. M. Feliu, "Formic acid electrooxidation on thallium-decorated shape-controlled platinum nanoparticles: an improvement in electrocatalytic activity" *Physical Chemistry Chemical Physics* **2014**, 16, 13616-13624.

[37] C.-L. Lin, J. Rodríguez-López and A. J. Bard, "Micropipet Delivery−Substrate Collection Mode of Scanning Electrochemical Microscopy for the Imaging of Electrochemical Reactions and the Screening of Methanol Oxidation Electrocatalysts" *Analytical Chemistry* **2009**, 81, 8868-8877.

[38] O. Lugaresi, J. V. Perales-Rondon, A. Minguzzi, J. Solla-Gullon, S. Rondinini, J. M. Feliu and C. M. Sanchez-Sanchez, "Rapid screening of silver nanoparticles for the catalytic degradation of chlorinated pollutants in water" *Applied Catalysis B* **2015**, 163, 554-563.

Abstract

The increasing problem of global warming provokes the appearance of new technologies for minimizing the emission of greenhouse gases (GHG) to the atmosphere, such as CO_2 and CH_4 [1, 2]. Among these technologies, fuel cells devices emerge as one of the possible solutions to mitigate this problem [3, 4]. Fuel cells are devices that can produce electrical energy through the electrochemical combustion of a fuel, which involves the direct conversion of the energy contained within chemical bonds into electrical energy. The maximum energetic efficiency using that direct conversion system is not limited by the Carnot cycle and this may exhibit a better performance than the one achieved by classical electrical generators. However, its energetic efficiency at present is still far from achieving maximum practical energetic efficiencies.

Among all fuel cell types, one of the most developed is the proton exchange membrane fuel cell (PEMFC). Those cells work at low temperature ($T<100^{o}C$), and may use liquid fuels such as methanol, ethanol or formic acid, which present several advantages, such as, easy handled, high energy density per molecule and high theoretical output cell potential [5, 6].

One of the fuels more widely studied in the last years is formic acid, especially for portable and small power devices [7, 8]. In addition, formic acid presents particular interest in electrocatalysis because its oxidation reaction only involves two electrons, no additional oxygen is needed to generate CO_2 as a final product, and finally, it is clearly a surface

sensitive reaction (a very important parameter in electrocatalysis) [9]. For that reason, it is considered as a model oxidation reaction in electrocatalysis, providing valuable data to understand more complex oxidation reactions of other fuels, such as methanol or ethanol.

One of the most used metals in electrocatalysis is Pt, because of that, numerous studies can be found in the literature regarding formic acid oxidation on this metal, both at a fundamental and an applied level. Firstly, this doctoral thesis addresses the study of electrocatalysis using Pt electrodes with a specific surface structure (known as Pt single crystal electrodes in the literature)[10, 11], in order to elucidate the mechanism of the formic acid oxidation reaction. Secondly, this doctoral thesis is focussed on applications using shape controlled Pt and Pt modified nanoparticles, which can be used as a real catalysts in fuel cells [12, 13].

Despite the formic acid electrooxidation reaction on Pt electrodes is in a mature stage, so far the reaction mechanism is not completely understood: In fact, there is currently a strong controversy regarding the nature and configuration of the intermediate species participating in the different reaction pathways. So far, it was only well established in the literature that formic acid oxidation reaction follows a dual path mechanism, with two different reaction pathways [14-16], the so called direct pathway, which involves the formation of an active intermediate, whose nature is under strong debate, which is oxidized into CO_2 at low overpotentials; and the indirect pathway, which leads to the formation of a poisoning intermediate, identified as CO [17], which is only converted into CO_2 at high overpotentials. In spite of the acceptance of this mechanism, recently a new three path mechanism comprising three possible reaction via has been set out [18]. This is supported by both theoretical and experimental data [19-21], and come out to extend the proposal initially introduced by Capon and Parsons [14]. The three path mechanism establishes the

existence of an indirect via, similar to the previous mechanism, implying the formation of CO on the electrode surface, acting as poisoning intermediate; a direct via, which goes through the formation of an active intermediate, whose nature and configuration is still under discussion; and finally, a third path known as the formate via, which assumes the adsorption of formate ion in a bridge bonded configuration on the electrode surface. This adsorbed formate acts as spectator species, because of its difficulty to be oxidized into CO_2. The later reaction has been widely demonstrated in numerous theoretical studies where it was revealed the high energetic barrier associated to the conversion of bridge bonded formate adsorbed into CO_2.

Some studies using Pt single crystal electrodes [Pt(*hkl*)] show the dependency of each reaction pathway with the electrode surface structure [22, 23]. A remarkable difference in activity is found for every basal plane, as it is evident from their corresponding cyclic voltammetry in acid solution. For Pt(111), the hysteresis between the positive and negative sweep is very low, which implies that this electrode is barely affected by the poisoning via. On the contrary, Pt(100) exhibits a remarkable hysteresis that confirms its high sensitivity towards the poisoning by CO. The large activity difference between this two Pt basal planes drive one of the key problems to be solved to catalyse this reaction: the surface selectivity towards each particular reaction pathway and, consequently, a specific reaction product, which would be controlled by the type of sites at the Pt electrode.

All that explained above shows one of the largest challenge regarding the research of formic acid electrooxidation on Pt electrodes: the decreasing or totally suppression of the poison (or spectator intermediate) formation, favouring the oxidation through the active intermediate. To achieve this goal, it is necessary to have a wide knowledge about its

reaction mechanism, and its dependency with the surface structure and composition of the Pt electrodes, which modulates the reaction kinetics.

Once the importance of the formic acid oxidation reaction as a model reaction in electrocatalysis (specially using Pt electrodes), as well as its possible application in fuel cells, has been demonstrated, it is easy to understand why this doctoral thesis has been carried out, since its main goal is study formic acid oxidation reaction on Pt electrodes from two different approaches. The first one involves a fundamental point of view, through the determination of kinetic and thermodynamic parameters, using Pt single crystal electrodes, whose surface structure is well defined. In this way, using the data collected, it is possible to propose a plausible mechanistic model. The second approach comprises the surface adatom modification of both Pt single crystal and Pt nanoparticles electrodes, in order to improve their catalytic activity towards formic acid oxidation. Special emphasis is put on the diminution of the overpotential applied, as well as the increasing in the current density. In order to evaluate those parameters, classical electrochemical experiments (cyclic voltammetry, chronoamperometry, etc.) are used, as well as advanced screening techniques, such as scanning electrochemical microscopy (SECM) [24].

Consequently, for achieving the main goal proposed on this doctoral thesis, the overall work has been divided in eight chapters according to the two main approaches mentioned before. This doctoral thesis will be presented by a compendium of publications in peer reviewed scientific journals, achieved in the development of this doctoral thesis, which complies with the regulations of the University of Alicante. The thesis document will be written partially in English, in order to fulfil all the needed requirements to obtain the title "International PhD" mention. The mentioned chapters are briefly described as follows:

In chapter 1, a general introduction is shown to provide the theoretical background needed to understand the mechanistic aspects and some applications of the formic acid oxidation on Pt electrodes. It presents a literature review to show the state of the art about the reaction mechanism at present, as well as the M-Pt catalysts (Pt electrodes modified by another metal or semi-metal (M)), highlighting the most active M-Pt catalysts, to end up with a detailed description of shaped controlled Pt nanoparticles and its applications in a reaction of interest in fuel cells, such as formic acid oxidation.

In chapter 2, a detailed description of all experimental protocols, methodologies and techniques used along this thesis is presented. First of all, some basic notions of crystallography of surfaces are given, emphasising the nomenclature system (Miller Index). In subsequent chapters, this nomenclature introduced here remains unchanged. The second part of this chapter is focused on describing all experimental techniques and configurations used along this thesis work. Finally, a proper and detailed description of the electrochemical cells is also included, as well as a table with all the reagents formula, purity and supplier used in this doctoral thesis.

Chapter 3 describes the results obtained studying the electrooxidation of formic acid on Pt(111) electrode, under different pH and electrolytic conditions in solution [25]. In order to carry out that study, the apparent activation energy ($E_a{}^{app}$) of the reaction over all the potential range where Pt(111) presents activity is quantified, which allows to set a faire comparison between different pHs and electrolytic solutions.

The behaviour of the $E_a{}^{app}$ as a function of pH, shows that formic acid oxidation reaction is favoured when the solution pH increases. Relating this fact with voltammetric results, in which a clear increase of the maximum current density with increasing pH

values is exhibited, it is concluded that formate anion in solution plays an active role in the reaction mechanism, which agrees with those results recently reported by Joo *et al*. [26].

The effect of different anions in solution on the activation energy of the reaction shows that the presence of sulphate causes a diminution of the E_a^{app}, which implies that sulphate adsorption presents a positive effect on the formic acid oxidation on Pt(111), which suggests that some adsorbed anions (spectators) could play a relevant role in the oxidation mechanism through the active intermediate. These experimental data, in combination with some DFT calculations performed in collaboration with other group of research, allow proposing the active participation of sulphate anion as a promotor of the adsorption of formate in a proper configuration, leading to its complete oxidation to CO_2 and implying lower activation energy.

In chapter 4 is presented a comparison of the E_a^{app} of the formic acid oxidation on basal planes Pt(111) and Pt(100), as well as Pt(544) and Pt(554), which are stepped surfaces type Pt*(s)*[*n(111)x(100)*] and Pt*(s)*[*(n-1)(111)x(110)*], respectively [27]. Pulsed voltammetry experiments at different temperature values are done in order to calculate their corresponding activation energy. For doing that the cronoamperometric curves obtained are adjusted to a proper kinetic model previously described in the literature [28, 29] in order to get the intrinsic activity ($j_{\theta=0}$). Then a plot of intrinsic activity at different temperatures allows getting the activation energy at each potential value. This is done for all 4 electrodes studied, as is described in the previous chapter for Pt(111) as a function of the solution composition.

The differences obtained on the E_a^{app} values for the basal planes, show the relevant surface sensitivity of formic acid oxidation reaction, evidenced in lower activation energy values for Pt(100), compared with those obtained for Pt(111) at low overpotentials.

Nevertheless, at high overpotentials, the inverse behaviour is observed. On the other hand, the E_a^{app} on the studied stepped surfaces shows a similar behaviour to Pt(111), but exhibiting higher energy values almost over the whole potential range, which explains the influence of steps density in the electrode surface reactivity, and hence in the modulation of the reaction mechanism, as was previously described by Grozovski *et al*. [28, 29] in another doctoral thesis from the same group of research (Surface Electrochemistry at the University of Alicante). Moreover, the role of the sulphate anion on the oxidation mechanism is revealed, since its promoting effect on the reaction is shown by a diminution on the E_a^{app}, which is especially relevant in large terraces domains. Those data point out a positive effect of sulphate adsorption on the oxidation reaction over Pt(100), as was already demonstrated in chapter 3 for Pt(111).

Once it has been proved that solution pH and specific anion adsorption comprise fundamental parameters that could strongly modulate the reaction mechanism, it seems reasonable to study the reaction within a broad pH range in the presence of different anions with specific adsorption in solution. Thus, chapter 5 presents results with this aim, where formic acid oxidation kinetics are studied in a polycrystalline Pt electrode over a wide pH range (1-14), using electrolytes with different adsorption strength (ClO_4^-, SO_4^{2-}, PO_4^{3-} and Cl^-) [30].

The results in this chapter show the continue increasing of the maximum oxidation current density as the pH move from 0 to 5, which clearly shows the participation of formate in solution within the oxidation mechanism of formic acid. In fact, from those results is demonstrated that this species in solution is precursor of the active intermediate, as has been previously stated by different researchers [26, 31, 32]. On the other hand, the effect of the electrolyte anion adsorbed on the electrode surface for the case of PO_4^{3-},

which is an anion with specific adsorption, shows that the maximum current density plotted as a function of solution pH presents a Gaussian shape, displaying a maximum at a pH value of 3.7, which matches the pK_a value of formic acid. On the contrary, for the cases of ClO_4^- o SO_4^{2-}, that curve presents a plateau, reaching a maximum current density at pH 5. Then, a new reaction mechanism that could satisfactorily explain the behaviour of the maximum current density over the whole pH range and all different electrolytic solutions studied is proposed in this doctoral thesis by combining all experimental data obtained.

So far in this thesis, the mechanism of the formic acid oxidation reaction has been only studied on Pt electrodes (single crystal and polycrystalline) without changing its surface composition. This provides a global overview and makes easier to model the voltammetric behaviour observed, as it has been done in chapters 3, 4 and 5. However, in chapter 6, a new variable is introduced, which is the surface modification of Pt single crystal electrodes. In particular, Pt(111) modified by Bi adatoms is studied in detail, since represents one of the most active catalysts for formic acid oxidation [33].

In that case, Pt(111) electrode is modified varying the Bi coverage value (θ_{Bi}) and the E_a^{app} of the formic acid oxidation at different temperatures is determined over the whole potential range, using only the positive sweep of the corresponding cyclic voltammogram. The results obtained show a diminution of the E_a^{app} compared with the unmodified Pt electrode, as the Bi coverage increases, especially at potentials below 0.6 V vs. RHE, which points out the relevant catalytic effect due to the Bi presence as surface modifier on Pt electrodes [34]. On the other hand, when comparing the experimental values of E_a^{app} with those obtained by DFT calculations was possible to conclude that the activation energy for the C-H bond cleavage in formate is negligible in those conditions. Then, those previous calculations and observations allow proposing a reaction mechanism

in which the initial reaction step corresponds to the formate molecule adsorption on the Bi atom. Thanks to the low electronegativity of Bi, the formate is adsorbed on it through one of the oxygen atoms, which allows free rotation of the molecule along the C-O bond. In such conditions, the molecule is oriented with the C-H bond towards the surface of the electrode, which favours the hydrogen adsorption over an adjacent free Pt atom and facilitates the formation and subsequent release of CO_2 as a final oxidation product. Thus, the activation energy for the C-H bond cleavage is, as mentioned previously, really low and almost negligible [33, 35].

So far, all four previous chapters about results try to give some mechanistic explanation to the results obtained, developing a plausible reaction mechanism for formic acid oxidation on model surfaces, without searching to improve the activity (electrocatalysis) of Pt electrodes. However, this is also a relevant goal in this doctoral thesis. Thus, one of the methods used to achieve the latter is the surface modification of Pt electrodes, either by irreversible adsorption or under potential deposition (UPD) of an adatom as well as by the formation of a surface alloy. For this reason, in chapter 7, the surface modification of Pt(111), Pt(100) and vicinal surfaces with Tl is performed in order to study its electrocatalytic effect over the formic acid oxidation reaction. In particular, this study on model Pt surfaces tries to provide fundamental knowledge to understand the recently reported enhancement on formic acid oxidation activity exhibited by thallium (Tl) modified Pt nanoparticles (NPs) [36]. Thanks to this new fundamental data, it is demonstrated in this doctoral thesis that the reaction presents surface sensitivity to the modified electrodes, being Tl-Pt(100), the most active catalyst , whose maximum normalized current is achieved at 0.42 V. Likewise, the presence of Tl provokes an important diminution of the oxidation onset potential, enhancing the catalytic activity in

the positive sweep of the corresponding cyclic voltammogram. Furthermore, the electrodes belonging to the series Pt*(s)*[*n(100)x(111)*] modified by Tl, present a similar behaviour to the one displayed by the basal plane Pt(100). On the other hand, for the catalyst Tl-Pt(111), the most significant change in comparison with non-modified Pt is the diminution on the onset potential of the oxidation, being its activity enhancement especially remarkable, at low overpotentials (<0.40 V vs RHE). Some Fourier transformed infrared radiation experiments (FT-IR), joined to the previous observations, support the idea that Tl role is based on both effects, a third body effect (by supressing the poisoning of the electrode by CO) and an bifunctional effect, evidenced in a remarkable enhancement of the activity on Pt(100).

Finally, chapter 8 presents a more applied work, since it is devoted to study the catalytic activity of shape controlled Pt nanoparticles, modified by lead (Pb). In particular, 111-Pt NPs (octahedral), 100-Pt NPs (cubic) and Pt polycrystalline NPs (spherical) are studied. When modifying all 3 types of Pt NPs with Pb is observed an important enhancement on the activity of formic acid oxidation as the Pb coverage increases. This is demonstrated by cyclic voltammetry as well as scanning electrochemical microscopy (SECM) [24]. This local technique provides a map of catalytic activity for a Pt ultramicroelectrode (100 μm of diameter) before and after being modified by Pb, which provides currents between 4 and 7 times larger than the one exhibited by the unmodified Pt electrode. To perform this SECM experiment, an experimental protocol introduced by Rodríguez-López *et al.* [37] is used. This is based in the controlled release of formic acid from a micropipette to the substrate, and its subsequent reaction-collection on the substrate electrode (in this case Pt and Pt-Pb electrodes). In particular, this experiment consists in filling a micropipette (open diameter ~ 15 μm) with a solution of formic acid in an organic

solvent (dichloroethane, DCE), in which formic acid is partially soluble, and uses this micropipette to release a controlled amount of formic acid meanwhile scans the surface of the electrode acting as a substrate. Moreover, the substrate is immersed in an aqueous solution of interest for the formic acid oxidation reaction. Thus, when the micropipette is in contact with the aqueous solution of interest, a concentration gradient of formic acid is stablished between the inner and the outer solutions. Such a gradient is governed by the partition coefficient of the formic acid in both media (aqueous and organic), and allows the controlled release of formic acid from the micropipette to the outside solution, which is initially free of formic acid. Once formic acid is delivered in the aqueous solution, it is only oxidized when reaches an electroactive surface (active spot). Finally, the representation of the substrate current as a function of the micropipette position in the XY plane allows getting a map of the substrate catalytic activity and identifying its active and inactive zones. In the case of formic acid oxidation, the SECM experiment is only used as a prelaminary test to evaluate, in a fast way, the effect of the surface modification on Pt electrodes by Pb adatoms. However, SECM has been also used as a screening technique for an array of several nanoparticles catalysts. For instance, the chloroform reduction on different types of Ag nanoparticles has been already studied using SECM [38].

On the other hand, the catalytic activity evaluation of shape controlled Pt NPs modified by Pb is performed by chronoamperometry, which points out that the most active nanoparticles are the octahedral ones (Pb_θ/111-Pt NPs), achieving a maximum current density of 7 $mA.cm^{-2}$, compared with 4 $mA.cm^{-2}$ for the Pb_θ/100-Pt NPs, in both cases at 0.5 V vs RHE in a 0.1 M formic acid solution. Chronoamperometric curves at 0.3 and 0.5 V show high stability for the Pb-Pt NPs catalyst, particularly at maximum Pb coverage,

where the diminution in activity after 600 s remains low (10-20 %). This stability is superior than that reported in the literature for Sb or Tl modified shape controlled Pt NPs.

The final chapter of this doctoral thesis presents the most remarkable conclusions achieved, emphasizing those referred to the mechanistic models proposed for both, Pt and Pt modified by adatoms electrodes. In the case of Pt electrodes, highlighting the effect of the electrolytic solution anion (or formate), since that spectator adsorption displays an active role in the oxidation mechanism by promoting the adsorption of the active intermediate in a proper configuration, which facilitates the complete oxidation of formic acid into CO_2. On the other hand, it is also demonstrated that formate in solution is the precursor of the active intermediate species, which is proposed as formate adsorbed in a configuration with its C-H bond towards the electrode surface. This is also supported by DFT calculations. In the case of Pt electrodes modified by adatoms, it is described a similar mechanism for the catalyst Bi-Pt(111), where formate is adsorbed on the Bi atom by one of its oxygen atoms. In such conditions, the C-O bond is free to rotate along its axis, allowing the C-H bond to be pointed towards the electrode surface, favouring the CO_2 formation with negligible activation energy. On the other hand, when Pt single crystal electrodes are modified by Tl, this adatom presents a positive effect by enhancing the catalytic activity and decreasing the formic acid oxidation onset potential. This effect is more evident in Tl-Pt(100) than on Tl-Pt(111) electrodes. Such behaviour is due to a third body effect, which avoids the formation of CO, preventing the electrode blockage and a simultaneous bifunctional effect, which decreases the activation energy of the direct reaction pathway. Finally, it is demonstrated a clear improvement in the catalytic activity and stability of shape controlled Pt NPs, when they are modified by Pb adatoms. In fact, the absolute enhancement in the current density exhibited by Pb_θ/111-Pt NPs is 2.7 and 2.3

times larger than that found in the literature for similar catalysts as Tl_{θ}/100-Pt NPs y Sb_{θ}/111-Pt NPs, respectively. Such an improvement may be explained by a synergy of the third body effect (suppression of CO formation), and the bifunctional effect, where the formate is adsorbed initially on the Pb adatom, which favours the subsequent oxidation of formate with a lower activation energy, showing a similar mechanism than the one described for Bi-Pt(111) [25, 35].

References

[1] M. I. Hoffert, K. Caldeira, G. Benford, D. R. Criswell, C. Green, H. Herzog, A. K. Jain, H. S. Kheshgi, K. S. Lackner, J. S. Lewis, H. D. Lightfoot, W. Manheimer, J. C. Mankins, M. E. Mauel, L. J. Perkins, M. E. Schlesinger, T. Volk and T. M. L. Wigley, "Advanced Technology Paths to Global Climate Stability: Energy for a Greenhouse Planet" *Science* **2002**, 298, 981-987.

[2] D. A. King, "Climate Change Science: Adapt, Mitigate, or Ignore?" *Science* **2004**, 303, 176-177.

[3] L. Carrette, K. A. Friedrich and U. Stimming, "Fuel Cells: Principles, Types, Fuels, and Applications" *ChemPhysChem* **2000**, 1, 162-193.

[4] S. Srinivasan, "Fuel Cells: From fundamental to Applications", Springer, **2006**.

[5] Y. Wang, K. S. Chen, J. Mishler, S. C. Cho and X. C. Adroher, "A review of polymer electrolyte membrane fuel cells: Technology, applications, and needs on fundamental research" *Applied Energy* **2011**, 88, 981-1007.

[6] J. Garche and L. Jörissen, "PEMFC fuel cell systems", in *Handbook of Fuel Cells*, John Wiley & Sons, Ltd, **2010**.

[7] S. Uhm, H. J. Lee and J. Lee, "Understanding underlying processes in formic acid fuel cells" *Physical Chemistry Chemical Physics* **2009**, 11, 9326-9336.

[8] C. Rice, R. I. Ha, R. I. Masel, P. Waszczuk, A. Wieckowski and T. Barnard, "Direct formic acid fuel cells" *Journal of Power Sources* **2002**, 111, 83-89.

[9] C. Rice, S. Ha, R. I. Masel and A. Wieckowski, "Catalysts for direct formic acid fuel cells" *Journal of Power Sources* **2003**, 115, 229-235.

[10] J. M. Feliu and E. Herrero, "Formic acid oxidation", in *Handbook of Fuel Cells - Fundamentals, Technology and Applications, vol. 2*, W. Vielstich, H. Gasteiger and A. Lamm (Eds.) John Wiley & Sons, Ltd., Chichester, **2003**, pp. 625-634.

[11] M. T. M. Koper, "Fuel Cell Catalysis: A Surface Science Approach", *Electrocatalysis and Electrochemistry* A. Wieckowski (Ed.), John Wiley & Sons, Hoboken, New Jersey, **2009**.

[12] J. Solla-Gullón, P. Rodríguez, E. Herrero, A. Aldaz and J. M. Feliu, "Surface characterization of platinum electrodes" *Physical Chemistry Chemical Physics* **2008**, 10, 1359-1373.

[13] J. Solla-Gullón, F. J. Vidal-Iglesias, A. López-Cudero, E. Garnier, J. M. Feliu and A. Aldaz, "Shape-dependent electrocatalysis: methanol and formic acid electrooxidation on preferentially oriented Pt nanoparticles" *Physical Chemistry Chemical Physics* **2008**, 10, 3689-3698.

[14] A. Capon and R. Parsons, "The oxidation of formic acid at noble metal electrodes Part III. Intermediates and mechanism on platinum electrodes " *Journal of Electroanalytical Chemistry* **1973**, 45, 205-231.

[15] A. Capon and R. Parsons, "The oxidation of formic acid on noble metal electrodes: II. A comparison of the behaviour of pure electrodes " *Journal of Electroanalytical Chemistry* **1973**, 44, 239-254.

[16] A. Capon and R. Parsons, "The oxidation of formic acid at noble metal electrodes: I. Review of previous work " *Journal of Electroanalytical Chemistry* **1973**, 44, 1-7.

[17] K. Kunimatsu, "Infrared spectroscopic study of methanol and formic acid adsorbates on a platinum electrode: Part I. Comparison of the infrared absorption intensities of linear CO(a) derived from CO, CH_3OH and HCOOH " *Journal of Electroanalytical Chemistry* **1986**, 213, 149-157.

[18] Y. X. Chen, M. Heinen, Z. Jusys and R. B. Behm, "Kinetics and mechanism of the electrooxidation of formic acid - Spectroelectrochemical studies in a flow cell" *Angewandte Chemie, International Edition in English* **2006**, 45, 981-985.

[19] Y. X. Chen, M. Heinen, Z. Jusys and R. J. Behm, "Bridge-bonded formate: Active intermediate or spectator species in formic acid oxidation on a Pt film electrode?" *Langmuir* **2006**, 22, 10399-10408.

[20] Y. X. Chen, M. Heinen, Z. Jusys and R. J. Behm, "Kinetic isotope effects in complex reaction networks: Formic acid electro-oxidation" *ChemPhysChem* **2007**, 8, 380-385.

[21] J. Xu, D. F. Yuan, F. Yang, D. Mei, Z. B. Zhang and Y. X. Chen, "On the mechanism of the direct pathway for formic acid oxidation at a Pt(111) electrode" *Physical Chemistry Chemical Physics* **2013**, 15, 4367-4376.

[22] J. Clavilier, R. Parsons, R. Durand, C. Lamy and J. M. Leger, "Formic acid oxidation on single crystal platinum electrodes. Comparison with polycrystalline platinum" *Journal of Electroanalytical Chemistry* **1981**, 124, 321-326.

[23] C. Lamy, J. M. Leger, J. Clavilier and R. Parsons, "Structural effects in electrocatalysis: A comparative study of the oxidation of CO, HCOOH and CH_3OH on single crystal Pt electrodes" *Journal of Electroanalytical Chemistry* **1983**, 150, 71-77.

[24] A. J. Bard and M. V. Mirkin, "Scanning Electrochemical Microscopy, Second Edition", CRC Press, **2012**.

[25] J. V. Perales-Rondon, E. Herrero and J. M. Feliu, "Effects of the anion adsorption and pH on the formic acid oxidation reaction on Pt(111) electrodes" *Electrochimica Acta* **2014**, 140, 511-517.

[26] J. Joo, T. Uchida, A. Cuesta, M. T. M. Koper and M. Osawa, "Importance of Acid-Base Equilibrium in Electrocatalytic Oxidation of Formic Acid on Platinum" *Journal of the American Chemical Society* **2013**, 135, 9991-9994.

[27] J. V. Perales-Rondón, E. Herrero and J. M. Feliu, "On the activation energy of the formic acid oxidation reaction on platinum electrodes" *Journal of Electroanalytical Chemistry* **2015**, 742, 90-96.

[28] V. Grozovski, V. Climent, E. Herrero and J. M. Feliu, "Intrinsic Activity and Poisoning Rate for HCOOH Oxidation at Pt(100) and Vicinal Surfaces Containing Monoatomic (111) Steps" *ChemPhysChem* **2009**, 10, 1922-1926.

[29] V. Grozovski, V. Climent, E. Herrero and J. M. Feliu, "Intrinsic activity and poisoning rate for HCOOH oxidation on platinum stepped surfaces" *Physical Chemistry Chemical Physics* **2010**, 12, 8822-8831.

[30] J. V. Perales-Rondón, S. Brimaud, J. Solla-Gullón, E. Herrero, R. Jürgen Behm and J. M. Feliu, "Further Insights into the Formic Acid Oxidation Mechanism on Platinum: pH and Anion Adsorption Effects" *Electrochimica Acta* **2015**, 180, 479-485.

[31] J. Joo, T. Uchida, A. Cuesta, M. T. M. Koper and M. Osawa, "The effect of pH on the electrocatalytic oxidation of formic acid/formate on platinum: A mechanistic study by surface-enhanced infrared spectroscopy coupled with cyclic voltammetry" *Electrochimica Acta* **2014**, 129, 127-136.

[32] S. Brimaud, J. Solla-Gullon, I. Weber, J. M. Feliu and R. J. Behm, "Formic Acid Electrooxidation on Noble-Metal Electrodes: Role and Mechanistic Implications of pH, Surface Structure, and Anion Adsorption" *ChemElectroChem* **2014**, 1, 1075-1083.

[33] J. V. Perales-Rondon, A. Ferre-Vilaplana, J. M. Feliu and E. Herrero, "Oxidation Mechanism of Formic Acid on the Bismuth Adatom-Modified Pt(111) Surface" *Journal of the American Chemical Society* **2014**, 136, 13110-13113.

[34] E. Leiva, T. Iwasita, E. Herrero and J. M. Feliu, "Effect of adatoms in the electrocatalysis of HCOOH oxidation. A theoretical model" *Langmuir* **1997**, 13, 6287-6293.

[35] A. Ferre-Vilaplana, J. V. Perales-Rondon, J. M. Feliu and E. Herrero, "Understanding the Effect of the Adatoms in the Formic Acid Oxidation Mechanism on Pt(111) Electrodes" *ACS Catalysis* **2015**, 5, 645-654.

[36] C. Buso-Rogero, J. V. Perales-Rondon, M. J. S. Farias, F. J. Vidal-Iglesias, J. Solla-Gullon, E. Herrero and J. M. Feliu, "Formic acid electrooxidation on thallium-decorated shape-controlled platinum nanoparticles: an improvement in electrocatalytic activity" *Physical Chemistry Chemical Physics* **2014**, 16, 13616-13624.

[37] C.-L. Lin, J. Rodríguez-López and A. J. Bard, "Micropipet Delivery−Substrate Collection Mode of Scanning Electrochemical Microscopy for the Imaging of Electrochemical Reactions and the Screening of Methanol Oxidation Electrocatalysts" *Analytical Chemistry* **2009**, 81, 8868-8877.

[38] O. Lugaresi, J. V. Perales-Rondon, A. Minguzzi, J. Solla-Gullon, S. Rondinini, J. M. Feliu and C. M. Sanchez-Sanchez, "Rapid screening of silver nanoparticles for the catalytic degradation of chlorinated pollutants in water" *Applied Catalysis B* **2015**, 163, 554-563.

Chapter I

Introduction

English acronyms used in this thesis

Acronyms	Meaning
AES	Auger Electron Spectroscopy
ATR-SEIRAS	Surface Enhanced Infrared Reflectance Absorption Spectroscopy in an Attenuated Total Reflection
CV	Cyclic Voltammetry
DEMS	Differential Electrochemical Mass Spectrometry
DFAFC	Direct Formic Acid Fuel Cell
DLFC	Direct Liquid Fuel Cell
EMIRS	Electrochemically Modulated Infrared Reflectance Spectroscopy
EOR	Ethanol Oxidation Reaction
FAOR	Formic Acid Oxidation Reaction
FTIR	Fourier Transformed Infrared
HER	Hydrogen Evolution Reaction
HOR	Hydrogen Oxidation Reaction
ICE	Internal Combustion Engine
L-H	Langmuir-Hinshelwood Mechanism
LEED	Low Energy Electron Diffraction
MCFC	Molten Carbonate Fuel Cell
MD-SC	Micropipette Delivery Substrate Collection
MOR	Methanol Oxidation Reaction
NPs	Nanoparticles
OCP	Open Circuit Potential
ORR	Oxygen Reduction Reaction
PAFC	Phosphoric Acid Fuel Cell
PEMFC	Polymer Electrolyte Membrane Fuel Cell
PMG	Precious Metal Group

PZTC	Potential of Zero Total Charge
RDE	Rotating Disk Electrode
RDS	Rate Determining Step
RHE	Reversible Hydrogen Electrode
SECM	Scanning Electrochemical Microscopy
SG-TC	Substrate Generation Tip Collection
SOFC	Solid Oxide Fuel Cell
SOMs	Small Organic Molecules
TG-SC	Tip Generation Substrate Collection
UHV	Ultra-High Vacuum
UME	UltraMicroelectrode
UPD	Under Potential Deposition

1. Introduction

1.1. Development of surface electrochemistry

Electrochemistry is the part of chemistry concerned with the interrelations of electrical and chemical effects [1]. A large part of this field deals with the study of chemical changes driven by an electrical current, and the production of electrical energy from chemical reactions [1, 2]. In most cases, electrochemical processes involve the study of charge transfer (electrons or ions) reactions, taking place through an interphase. For that reason, it is highly important to know the relevant processes at the interphase, and how they are affected by an electrical driving force (potential). Thus, the study of the interphases represents a fundamental research area of this science.

The most common interphase in Electrochemistry, for its numerous applications at an industrial level, is the solid-liquid interphase. One of the phases is usually a metal conductor known as electrode (electronic conductor), while the other phase contains an electrolytic solution (ionic conductor). Thus, most electrochemical processes are heterogeneous in nature, and the interphase is the place where the most relevant events occur. Figure 1.1 represents a typical electrochemical system.

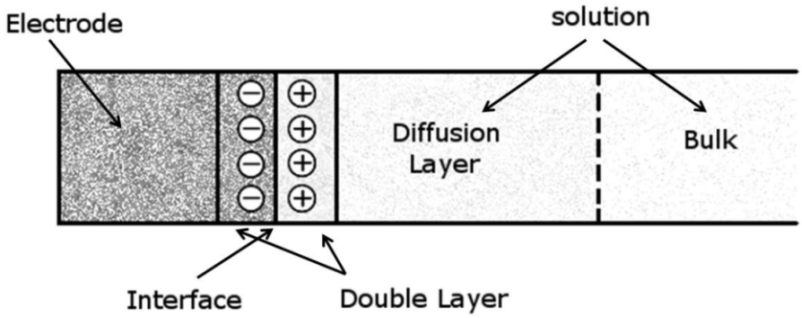

Figure 1.1. Spatial structure of an electrochemical system adapted from [3].

Electrode reactions such as de hydrogen evolution reaction (HER),

$$2H^+ + 2e^- \longrightarrow H_{2(g)} \qquad \textit{Eq. 1.1}$$

or the plating of copper,

$$Cu^{2+} + 2e^- \longrightarrow Cu \qquad \textit{Eq. 1.2}$$

or the formic acid oxidation reaction (FAOR),

$$HCOOH \longrightarrow CO_2 + H_2O + 2e^- \qquad \textit{Eq. 1.3}$$

can only take place at the interphase between the electrode and the electrolytic solution. The important point is that the electrode can only affect or sense the part of the solution in immediate contact with itself. For instance, no formic acid molecules can be oxidized if they are not located at the interphase. In fact, electrode reactions tend to change the composition in the nearby solution (diffusion layer), which will be different from that located further away (bulk). The latter statement is true because, in order to produce the electrochemical reaction, an electron transfer is required, and this process can only take place through the interphase.

According to the nature of the changes produced in the species upon the electron transfer, the electrochemical reactions, which belong to the heterogeneous chemical reactions, can be classified in two main types: outer-sphere and inner-sphere electrochemical reactions (Figure 1.2). The outer-sphere electrochemical reactions are those where the reactants, products, and/or intermediates do not interact strongly with the electrode material and the electron transfer occurs by tunneling across at least a monolayer of solvent. On the other hand, in the inner-sphere electrochemical reaction, there is a strong interaction of reactants, products and/or intermediates with the electrode surface [4]. Thus,

in an electrochemical inner-sphere reaction (electrocatalytic reaction), the reactants, intermediates, or products are often specifically adsorbed on the electrode surface in at least one of the reaction steps. This necessarily means that the reaction path and thus, the product selectivity would depend on the composition and the surface structure of the electrode.

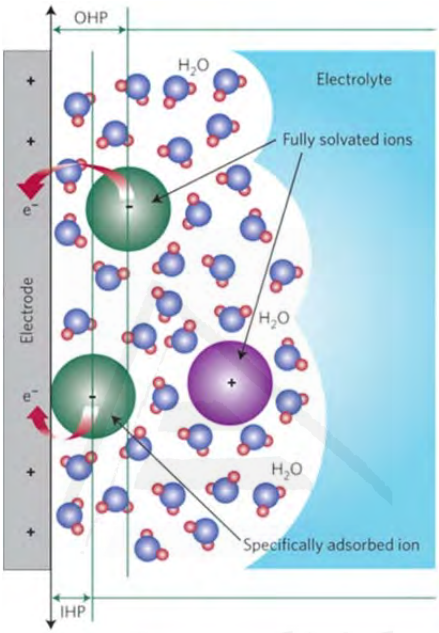

Figure 1.2. Schematic illustration of inner-sphere (IHP region) and outer-sphere (OHP region) electron transfer reaction mechanisms. Taken from [5].

Almost all the interesting reactions from an applied point of view are inner-sphere reactions, and as aforementioned, all these reactions are, necessarily, surface sensitive, since at some point in their reaction pathway appears the adsorption-desorption of species on the electrode surface. If the adsorption process leads to a diminution of the activation energy (see Figure 1.3) the electrode will have an electrocatalytic effect on the reaction. Further electrocatalysis can be achieved by modifying the electrode surface either in composition, or in structure, since those two parameters control the strength of the interaction between the adsorbed molecule and the electrode surface. Additionally, reaction

paths that are energetically inaccessible in homogeneous catalysis become accessible at the metal-solution interface [4] thanks to the electrocatalytic effect, bringing some valuable information that can be eventually used for the development of better catalytic materials for industrial applications.

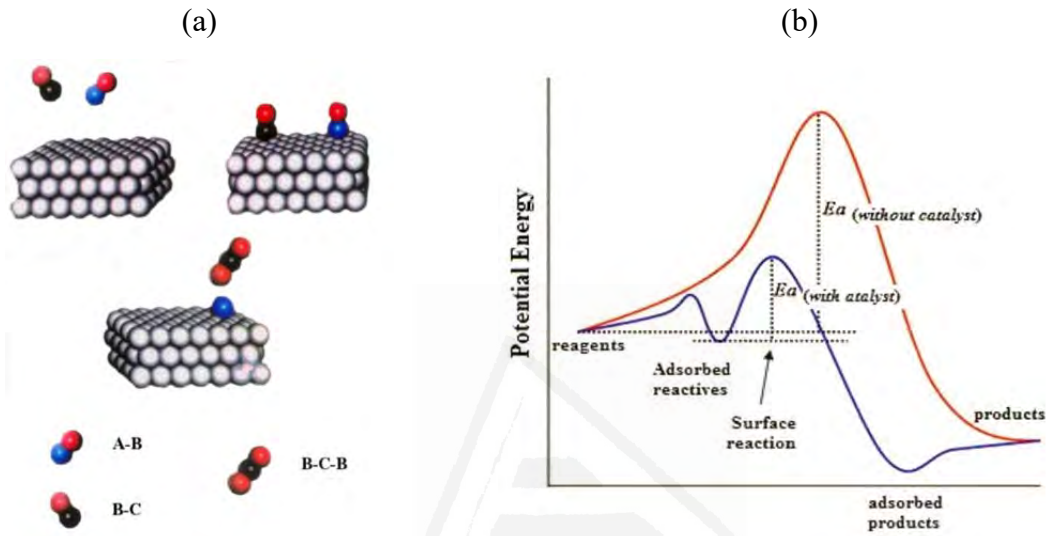

Figure 1.3. (a) Scheme representative of a surface reaction with some adsorption steps. (b) Energetic profile of an outer-sphere reaction (red line) and inner sphere reaction (blue line) [6].

Due to the relevance of heterogeneous gas-phase chemical reactions at industrial level, a large number of techniques that allow the study of the solid-gas interphase at a high precision level were developed starting in the 50s [7-9]. They are known as ultra-high vacuum (UHV) techniques, due to the requirements of UHV conditions for these studies. Some examples could be using low energy electron diffraction (LEED) to assess the surface order or Auger electron spectroscopy (AES) to check surface cleanliness. Despite being a good approach for characterization of reactions in the solid-gas interphase, its application to study electrochemical processes seems to be limited to those not being affected by the emersion of the electrode from the solution to the UHV environment. Thus, some years later, a series of novel techniques that allow the study of reactions at the solid-

liquid interphase appeared, enabling the use of electrochemical conditions, making possible to study the surface electron transfer processes. This approach must include not only the interactions between the electrode and the reactant, intermediate and product species, but also the interactions of water and ions from the supporting electrolyte with the electrode and the adsorbed species. Moreover, the complex dependence of all these interactions with the applied potential should be established. Thus, in order to get a specific characterization of those systems, a perfect characterization of the surface structure of the electrode is required as an initial condition. The use of surfaces with defined crystallographic structures, as was done previously in UHV studies [8-10], appears as a suitable way to control the electrode surface structure. In this respect, experiments with single-crystal electrodes have the advantage of a defined nominal atomic density and thanks to this fact, a relationship between the charge density transferred in a given process and the atomic density at the electrode can be perfectly established. Additionally, because of the very strict control of surface properties, the results of experiments (such as those related to reactivity) are valid, not only with respect to reaction kinetics but also regarding fundamental double-layer thermodynamic parameters. Nevertheless, it was not until 1981, when J. Clavilier *et al.* published their work about preparation and cleaning of platinum single crystals, Pt(*hkl*) [11-14], when the studies of surface electrochemistry using model single crystal electrodes became possible. In these works, it was demonstrated that in order to make reproducible studies, it is not only important to have electrodes whose surface structure is well-characterized and well-defined from a crystallographic point of view, but also cleaned by the flame annealing method [12]. Thus, controlling the preparation and cleaning conditions of the single crystal electrodes with high precision became, then, in key steps for the future development of surface electrochemistry. Thanks to the understanding of model systems, like Pt(*hkl*) at a fundamental level, new information about

key kinetic parameters of important electrocatalytic reactions, such as, formic acid (FAOR) [15, 16] and ethanol oxidations (EOR) [17, 18], or oxygen reduction reactions (ORR) [19-21], have been reported and some relevant improvements in activity and durability for those electrocatalytic reactions have been already achieved.

The great advance reached in the 80s, opened new and exciting opportunities to develop, in a rational way, the electrocatalysis research, which involves the catalysis of a specific reaction taking place in a metallic-solution interphase, subjected to an electrical potential. With this picture in mind, is reasonable to expect that very important areas like fuel cell or batteries research have taken advantage of this new knowledge spectrum, achieving some spectacular advances in the last 30 years. In fact, nowadays some fuel cells prototypes are being commercialized, especially for the transportation field. For instance, in 2015 two fuel cell vehicles have been introduced for commercial lease and sale in limited quantities: the *Toyota Mirai* and the *Hyundai ix35 FCEV*. Additional demonstration models include the *Honda FCX Clarity*, and *Mercedes-Benz F-Cell* [22].

1.2. Background in fuel cells

A fuel cell is an electrochemical device, which can continuously and directly convert the chemical energy of a fuel and an oxidant into electrical energy, by a process involving essentially, electrode-electrolyte systems [23, 24] based on electrocatalytic reactions. The great advantage of fuel cells in transportation systems compared with conventional internal combustion engine (ICE) generators lies in the theoretical efficiency in the energy conversion, which is not limited by the Carnot cycle. For instance, current phosphoric acid fuel cells (PAFC) offer 42% conversion efficiency, whereas, it is predicted that molten

carbonate fuel cells (MCFC) may achieve electrical efficiencies as high as 60%. In contrast, only about 14% - 30% of the energy from the fuel is effectively used in ICE [25]. Additionally, since fuel cells contain fewer moving parts, they have higher reliability than ICE generators.

Fuel cells are different from batteries. In fact, fuel cells require a continuous source of fuel to sustain the chemical reaction, whereas in a battery the chemical species react with each other within the electrode-electrolyte interphase to generate energy in a closed system, until all the reactants are consumed. For the rechargeable batteries, the reactants can be regenerated when electrical energy is supplied to the device so that the opposite reaction occurs, which is not the case in fuel cells. In contrast, fuel cells can produce electricity continuously as long as these inputs are supplied; moreover, fuel cells are generally considered as viable candidates to replace batteries in portable power devices, due to the fast capability of refueling, allowing 24/7 operation.

A typical fuel cell (see Figure 1.4a) consists of an anode compartment, where the oxidation of the fuel takes place, a cathode side, for the reduction of the oxidant (typically oxygen), and a separator (often a membrane), which separates the two compartment avoiding the direct combination of reactants or products.

There are several types of fuel cells that can be classified depending on the working temperature as follow:

- **Proton exchange membrane fuel cells (PEMFCs) and alkaline fuel cells (AFCs):** They are low temperature fuel cells (T < 100 ºC) whose main feature

is the separation of the anode and cathode compartments by a proton exchange membrane (typically Nafion® membranes), which act as electrolyte and allows proton transport. PEMFCs represent one of the most developed and investigated types of fuel cells for applications in transportation and small power supply. Hydrogen-oxygen and hydrogen-air fuel cells or direct liquid fuel cells (DLFCs) represent typical examples under development at this moment (Figure 1.4b) [26].

- **Phosphoric acid fuel cells (PAFCs):** They are intermediate temperature fuel cells, since they commonly work in temperatures ranging from 150 to 200 ºC. This temperature will cause energy loss if the heat is not removed and used properly. In these cells phosphoric acid is used as electrolyte, in which protons are charge carriers in the electrolyte. PAFCs are mainly used for stationary energy production [27].

- **Solid oxide fuel cells (SOFCs) and molten carbonate fuel cells (MCFCs):** They are cells that are able to work at high temperatures. SOFCs working at temperatures about 1000 ºC, and the MCFCs using carbonate salts as electrolyte, and operating at about 650 ºC [28].

In spite of the promising solution that represents fuel cells to produce electrical energy, its application at the moment is still overshadowed by a low efficiency and high cost. Among others, anode fuel type and electrocatalyst selection are key factors for getting high overall efficiencies and power densities. For instance, hydrogen fuel is capable to

produce high energy efficiencies, but presents as a drawback the absence of natural sources of hydrogen, and its subsequent storage. For this reason, new alternative liquid fuels such as, formic acid, methanol, ethanol or formaldehyde have emerged. In particular, DLFCs have the advantage of easy transport and handling of the fuel, but typically suffer from lower energy efficiencies compared with the hydrogen one and high fuel crossover by the membrane, which results in a loss of efficiency at the fuel cell.

Among the different types of DLFC, direct formic acid fuel cells (DFAFC) overcomes most of the issues of DLFCs, having low fuel crossover, low toxicity and a reasonable power density at low temperature [29-31]. Table 1.1 compares the main thermodynamic values of some DLFCs and the H_2/O_2 fuel cell. For instance, the volumetric energy density for formic acid (2104 Wh L^{-1}) is low as compared to methanol (4900 Wh L^{-1}). However, this deficiency in DFAFCs is compensated by a minimum crossover of formic acid through the Nafion® membrane, allowing high fuel concentrations in solution, between 5 and 12 M of formic acid [32, 33]. Additionally, the theoretical open circuit potential (OCP) is 1.48 V, compared to 1.23 V for hydrogen or 1.21 V for methanol fuel cells. All these characteristics make DFAFC a valuable candidate for energy supply in portable devices [30, 31].

(a)

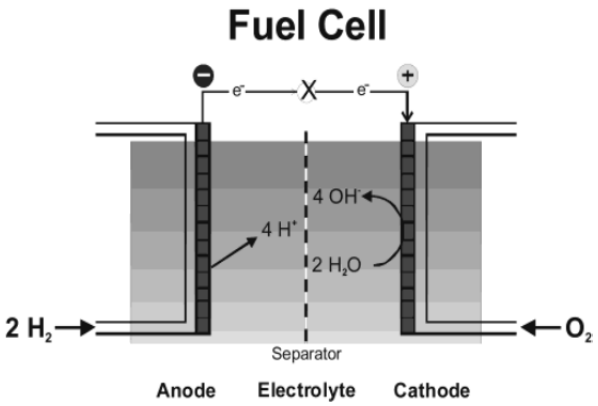

(b)

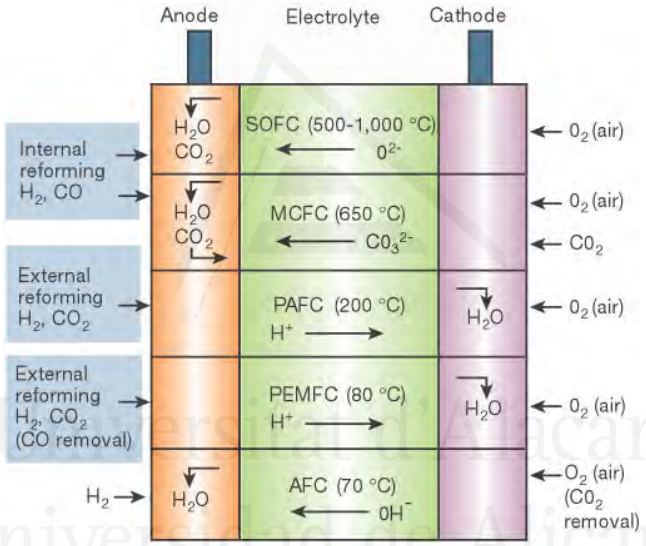

Figure 1.4. (a) A fuel cell showing the continuous supply of reactants (hydrogen at the anode and oxygen at the cathode) and redox reactions in the cell. Taken from [34]. The oxidation reaction takes place at the anode (+) and involves the liberation of electrons ($H_2 = 2H^+ + 2e^-$). These electrons travel round the external circuit producing electrical energy by means of the external load, and arrive at the cathode (-) to participate in the reduction reaction ($1/2\ O_2 + 2H^+ + 2e^- = H_2O$). (b) Different types of fuel cells. The reaction products are formed at the anode for SOFC, MCFC and AFC types, and at the cathode for PAFC and PEMFC types. This difference has implications for the design of the entire fuel-cell system, including pumps and heat exchangers. For instance, to maintain the composition of the electrolyte component in the MCFC system, CO_2 has to be recirculated from the anode exhaust to the cathode input. Taken from [35].

Other important aspect concerning the fuel cell efficiency is the nature of the electrode (electrocatalyst). Platinum (Pt) (and its alloys) has been extensively used in PEMFC, since it is one of the most active pure metal not just for hydrogen oxidation reaction (HOR), but also for the oxidation of small organic molecules (SOMs) with one or two carbon atoms(C1 or C2). For this reason, platinum is one of the most studied precious metals in electrocatalysis. The main target for the electrocatalyst in the anode is to produce the most oxidised species (CO_2 or H^+ depending on the fuel), with the highest current density and at the lowest overpotential. Thus, such a process involves the break and formation of different carbon bonds when SOMs are used as a fuel, and this would be preceded by adsorption/desorption processes, as was aforementioned when electrocatalysis was defined. The strength and extension of those adsorption/desorption reaction steps would be directly related with the surface structure and composition of the electrode. A general mechanism for the SOMs oxidation (having a single carbon atom) on Pt, have been proposed earlier (Scheme 1.1) [36-40].

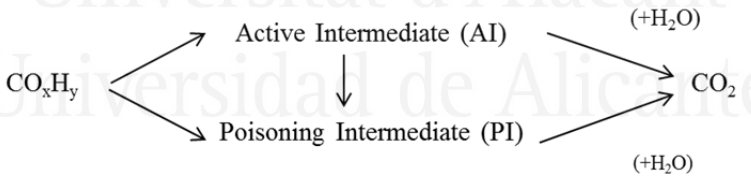

Scheme 1.1. General mechanism for small organic molecules oxidation C1 type[41].

According to this, the reactant initially gets adsorbed on the electrode surface by the carbon atom, losing a hydrogen atom in the process, to form an intermediate which evolves to yield the active intermediate (AI). At this point, the intermediate can be oxidize directly into CO_2, involving water adsorbed molecules, or eventually can be decomposed to produce a poisoning intermediate (PI), generally CO, which is a low reactivity compound

strongly adsorbed on the Pt surface. Moreover, the PI can be formed directly from the initial adsorbed molecule depending on the interaction between the electrode surface and the reactant. A general scheme of the process is represented in Scheme 1.1.

Table 1.1. Theoretical thermodynamics values at 25ºC for different fuel cells.

Fuel	***Reaction***	$\frac{\Delta G^0}{Kcal.mol^{-1}}$	$\frac{E^0}{V}$	***Fuel Cell***
Formic acid	$HCOOH + {}^1/_2\, O_2 \longrightarrow CO_2 + H_2O$	-68.2	1.48	DFAFCs
Methanol	$CH_3OH + {}^3/_2\, O_2 \longrightarrow CO_2 + 2H_2O$	-166.77	1.21	DMFCs
Formaldehyde	$CH_2O + O_2 \longrightarrow CO_2 + H_2O$	-124.7	1.35	
Hydrogen	$H_2 + {}^1/_2\, O_2 \longrightarrow H_2O$	-56.69	1.23	PEMFCs

Formic acid represents one of the most promising fuels in DLFCs, and also platinum is the anodic electrocatalyst conventionally used in this kind of devices. For this reason, the study of FAOR on platinum electrodes is the main goal of this thesis being one of the main targets to make some insight into the reaction mechanism, in order to use this knowledge to design and produce better and more efficient electrocatalysts.

1.3. Formic acid electrooxidation reaction

FAOR is one of the most studied reactions in electrocatalysis, given that its oxidation process only involves two electrons, it is not needed additional oxygen to produce CO_2, and finally, it is a reaction clearly sensitive to the surface structure of the electrocatalyst. For this reason, it is usually considered as a suitable model reaction for the oxidation of

SOMs. On the other hand, formic acid has been proposed as a possible fuel for fuel cells in portables and small power devices, another reason to stimulate its study [30, 31, 42].

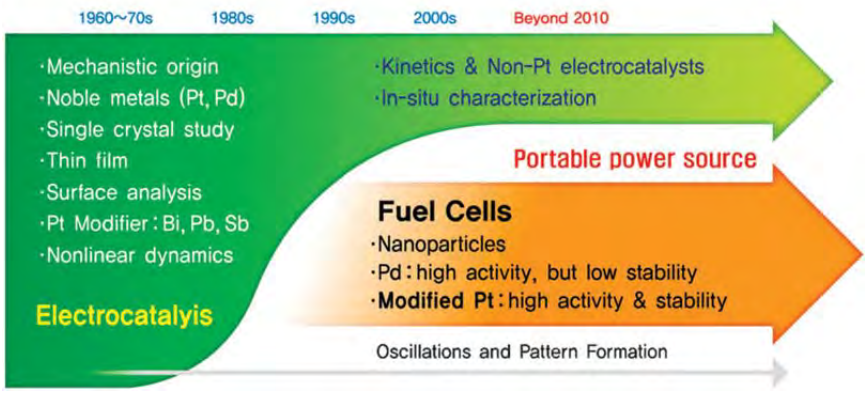

Figure 1.5. An overview of formic acid research in electrochemistry, from understanding the mechanistic origin of electro-oxidation to applications in fuel cells. Taken from [29].

The interest in formic acid research is shown in Figure 1.5, emphasizing that since 2000´s have had a strong attempt to develop DFAFCs as a portable power source, taking advantage of the activity and stability presented by the modified Pt anodes [29]. Formic acid has the same oxidation valency as CO; both require two electrons for complete oxidation to CO_2 [43], however, when comparing with CO, the reaction mechanism of FAOR is more complex although its elecrocatalysis is simpler. Actually, FAOR onset potential is as low as 0.2 V *vs. RHE* in Pt electrodes. For this reason, FAOR has been already widely studied using different types of Pt electrodes from single crystal to nanoparticles electrodes [44].

1.3.1. General mechanism for the formic acid oxidation reaction. CO as poisoning intermediate

To try to enhance the activity of any catalyst for a specific reaction is very important to understand in a deep way such a reaction mechanism. Since most of the electrochemical reactions imply some adsorption steps, is reasonable to think about different possible reaction pathways to justify the whole FAOR. In this sense, the first step towards unravelling its mechanism is the identification of the PI (Scheme 1.1). Initially, several candidates were proposed, namely CO, COH and CHO, but the only one identified by electrochemical and spectroscopic techniques was CO. In fact, using techniques as electrochemically modulated infrared reflectance spectroscopy (EMIRS) and fourier transformed infrared (FTIR) spectroscopy, Kunimatsu *et al*. [45] identified CO as PI and demonstrated that the linear CO is the predominant intermediate species detected in the FAOR on Pt. Since CO oxidation to CO_2 on Pt takes place at significant rates only above 0.6 V *vs. RHE*, CO could be detected by IR spectroscopy at potentials as low as 0.2 V *vs. RHE*. Later, using differential electrochemical mass spectrometry (DEMS) was possible to unequivocally identify CO as the PI, and not acting as an active intermediate.

In that experiment (Figure 1.6), the Pt electrode was immersed into a $H^{13}COOH$ solution. After the ^{13}CO is spontaneously formed at the Pt surface, the electrode was taken into a new solution containing $H^{12}COOH$. While running a CV, the formation of CO_2 was followed using DEMS (see Figure 1.6). In this case, it was possible to detect that the $^{12}CO_2$ formation preceded the $^{13}CO_2$, which indicated the presence of an AI, different from the CO [46, 47]. Those experiments not only demonstrated that CO is the PI, but also confirmed the existence of a parallel reaction pathway yielding CO_2 as a common product in the whole mechanism.

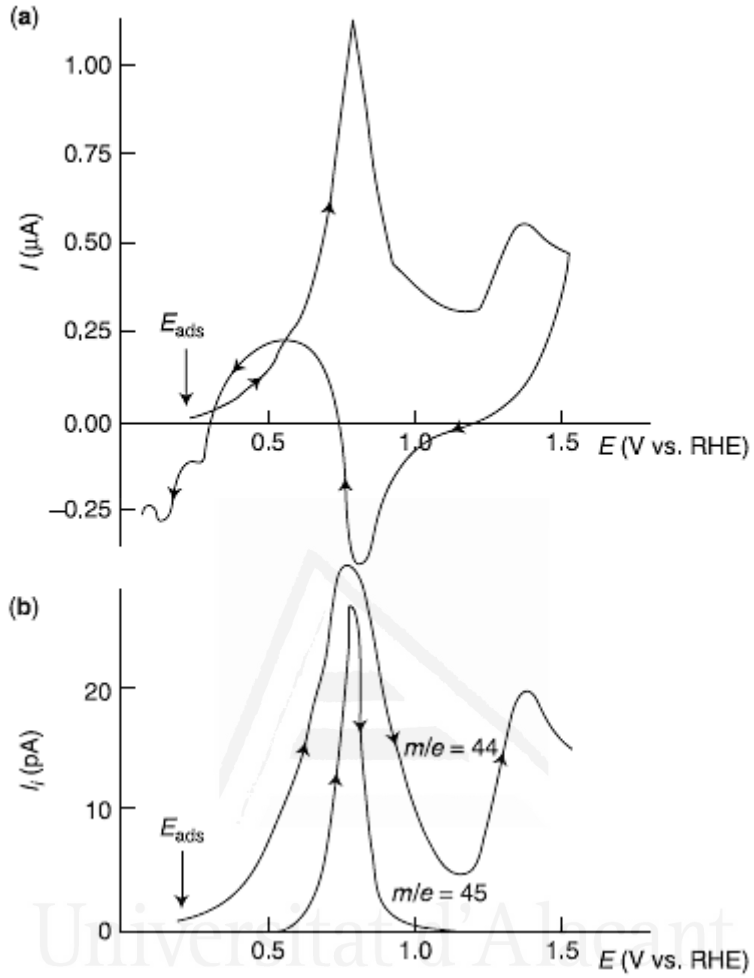

Figure 1.6. Oxidation of 0.01 M $H^{12}COOH$ in 0.5 M H_2SO_4 on a polycrystalline electrode pre-covered with ^{13}CO. (a) Voltammetric currents. (b) Mass signals for $^{12}CO_2$ (m/e = 44) and $^{13}CO_2$ (m/e = 45). (Reproduced from[46]).

Later, Clavilier *et al*. [48] showed that the quantity and fraction of Pt blocked surface by CO, depends on the surface structure of the electrode, and some ensemble effects prevent the formation of CO layer that blocks completely the surface. This was confirmed later by Llorca *et al*. [49] who demonstrated the requirement of a minimum amount of free

and contiguous Pt sites to allow the CO formation from spontaneous formic acid dehydratation.

Summarizing, the formation and reaction of the PI can be written in two steps as follow:

$$HCOOH + Pt^* \longrightarrow CO_{ads} + H_2O_{ads} \longrightarrow CO_2 + 2H^+ + 2e^- + Pt^* \quad Eq.\ 1.4$$

The first part of the reaction described in equation 4 is the decomposition of the formic acid, yielding CO and water (dehydratation reaction). This step is a chemical reaction, and no electrons are involved in this process; also the reaction takes place at open circuit potential. The second part involves the CO oxidation by the Langmuir-Hinshelwood (*L-H*) mechanism [50], which has been extensively studied [51-56].

Finally, the above pathway shows one of the main persisting problems for using formic acid in fuel cells: the poisoning of the electrode, which has as a consequence the deactivation of the electrocatalyst. This problem needs to be overcome to successfully improve the efficiency in DFAFC.

1.3.2. The active intermediate dilemma

Initially, adsorbed species such as –COH or CHO [57], -COOH [17, 58] and formate ($HCOO_{ads}$) [59, 60] were suggested as AI (see figure 1.8), mainly based on electrochemical and in situ FTIR experiments. Nevertheless, most of these studies had the problem of using external reflection configuration, making difficult to eliminate some by-product interferences. It was not until Osawa *et al*. successfully performed some ATR-SEIRAS [59, 60] experiments where the presence of formate in a bridge bonded configuration (*b*-

$HCOO_{ads}$) species was clearly observed and it was proposed as the AI (initially identified by Miki *et al*. [61]). They also found a qualitative correlation between the observed reactivity for FAOR and the amount of *b*-$HCOO_{ads}$ obtained from the spectroscopic data [60].

By the previous experimental facts, it can be demonstrated that FAOR has two different reaction pathways: one of them (direct pathway) implies the adsorption of an AI, presumably *b*-$HCOO_{ads}$. Then, this is oxidized into CO_2. The other reaction pathway involves the CO formation (indirect pathway) on the electrode surface through irreversible dissociation of formic acid, and its subsequent oxidation into CO_2 at higher potentials (aforementioned). A representation of the process is shown in Scheme 1.2.

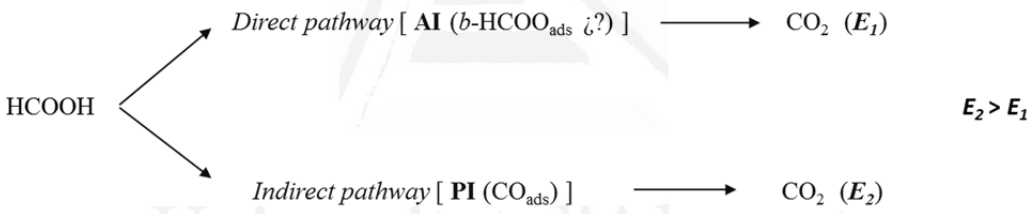

Scheme 1.2. Dual path mechanism for formic acid oxidation on Pt electrodes.

The previous dual path mechanism agrees with the earlier observations made by Capon and Parsons [36-39], who were the first one to propose this kind of mechanism in FAOR on Pt electrodes.

Despite *b*-$HCOO_{ads}$ was considered to be the AI species in subsequent contributions [62-65], in other reports this species was considered, conversely, as a site-blocking spectator reactive, and the oxidation was proposed to proceed via a weakly adsorbed formic acid molecule (*w*-$HCOOH_{ads}$) [66-70]. Although these authors also identified

adsorbed formate, they argued that the calculated amount of CO_2 coming from the oxidation of *b*-$HCOO_{ads}$ would not be able to justify the total amount of CO_2 produced during FAOR. For this reason, they proposed a third pathway, called the formate pathway. Scheme 1.3 illustrates the triple pathway for formic acid oxidation, proposed by Chen *et al*. [66].

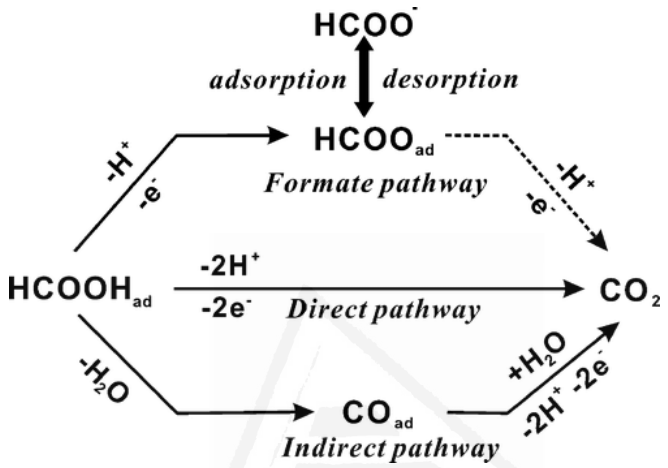

Scheme 1.3. Schematic description of the "triple pathway" reaction mechanism for formic acid oxidation as proposed in reference [66].

In this new scheme, the direct pathway implies the dehydrogenation of *w*-$HCOOH_{ads}$, whereas *b*-$HCOO_{ads}$ belong to the third pathway (formate pathway) and acts as a spectator species.

Nowadays, the nature and role of the AI are still under debate [69, 71] and more insights are required to clarify these mechanistic considerations. In this sense, some theoretical studies have been devoted to understand the system in an extensible way. For instance, Neurock *et al*. [72] showed that the C-H breaking might lead the formation of the AI through the direct pathway, while *b*-$HCOO_{ads}$ is just a spectator, supporting experiments by Chen *et al*. These authors also found that applied potential has little effect on the barriers of *b*-$HCOO_{ads}$ oxidation, but significantly influence on CO oxidation. Those

theoretical calculations demonstrated that once *b*-$HCOO_{ads}$ is formed, its oxidation is energetically not favoured. Later, Wang and Liu [73] used continuum solvation approaches to model the Pt/H_2O interface, and proposed that a weakly adsorbed HCOOH with its C-H bond in a "down" configuration (*w*-$HCOOH_{C\text{-}H\ down}$) is the AI. Their results also suggested that applied potentials have minor effects on *w*-$HCOOH_{ads}$ oxidation barriers. In contrast, Gao *et al*. [74] concluded that FAOR on platinum proceeds via a formate pathway having *b*-$HCOO_{ads}$ as intermediate and a direct pathway from $HCOOH_{ads}$ via a highly transient CO_2 intermediate, in agreement with the mechanism proposed by Chen *et al*. (see Scheme 1.3). In addition, they proposed that the presence of other adsorbed species (CO_{ad}, OH_{ad} or anions) may be also important, since such co-adsorbates might additionally influence the reaction mechanism.

More recently, some new FAOR experiments using polycrystalline platinum have shown that weakly adsorbed formate (*w*-$HCOO_{ads}$) and not *w*-$HCOOH_{ads}$ may be the AI. In those experiments, the pH effect has been evaluated, showing that the current is proportional with the pH increasing (formate concentration increasing) [75, 76]. Those results are also supported by a similar conclusion achieved by Brimaud *et al*. [77].

Until now there are two main proposals regarding the AI dilemma. One of them claims the existence of a direct pathway involving *b*-$HCOO_{ads}$, supported by ATR-SEIRAS experimental data under the dual pathway mechanism. The other proposal argues that *w*-$HCOOH_{ads}$ or *w*-$HCOO_{ads}$ is the main AI, under the triple pathway mechanism framework, where *b*-$HCOO_{ads}$ could act as a spectator. In this second proposal, both the *w*-$HCOOH_{ads}$ and *w*-$HCOO_{ads}$ are presented as weakly adsorbed intermediates, suggesting the most possible adsorption structure as the C-H "down" configuration (see Figure 1.7).

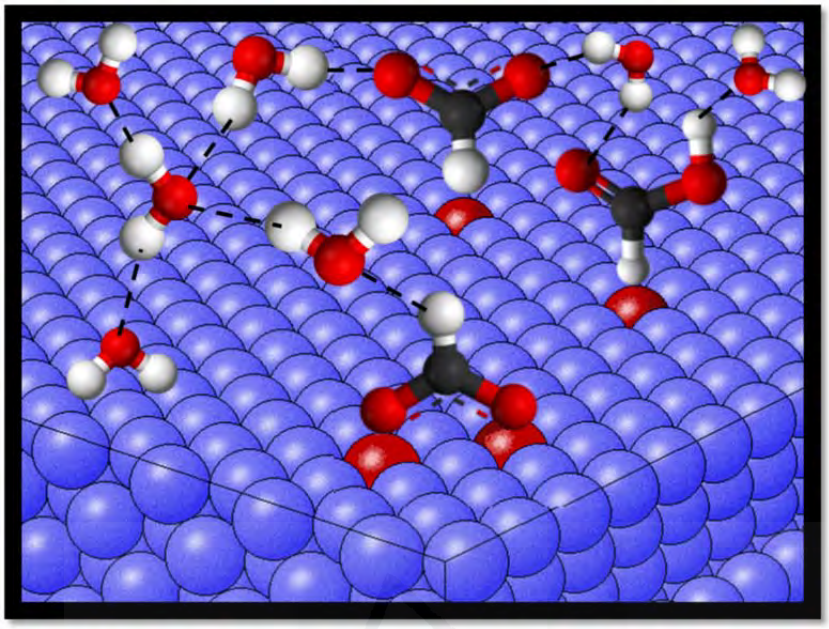

Figure 1.7. Different formate/formic acid configuration adsorbed species proposed so far. From up to down w-$HCOO_{ads}$, w-$HCOOH_{ads}$ and b-$HCOO_{ads}$.

1.3.3. Formic acid oxidation reaction in Pt single crystal electrodes Pt(*hkl*)

The surface sensitivity of the FAOR on Pt was put in evidence firstly by Clavilier *et al*. [78] who observed that the corresponding voltammetric profile for the three basal planes (Pt(111), Pt(100) and Pt(110)) were completely different. This was also observed by Lamy *et al*. [79] and Adzic *et al*. [80]. Taking two representative cases, Pt(111) and Pt(100), Figure 1.10 shows substantial differences in the activity for FAOR displayed on both electrodes (Figure 1.8). The Pt(100) electrode (see Figure 1.8 b) presents a higher activity compared with Pt(111), however, this is only in the backward cycle, given that, in the forward direction, the surface is almost completely blocked by CO. The remarkable hysteresis observed in this electrode put in evidence the high reactivity of this surface for both reaction pathways, AI and PI. In contrast, the behaviour of Pt(111) (see Figure 1.8 a)

electrode is completely different. It presents a very small hysteresis when comparing backward and forward scans, which is in agreement with its remarkable resistance to the catalytic poisoning [81]; however, it yields a much less overall activity (current density) when comparing with Pt(100) electrode. It is also worth noting that, as formic acid oxidation comprises surface adsorption steps, the involved species must compete for reaching Pt free sites in the electrode surface; sites that are eventually occupied by water, protons or anions, all of them potential-dependant adsorbates. This fact, is responsible for the typical bell shaped cyclic voltammetry curve obtained for FAOR on the Pt(111) electrode [82].

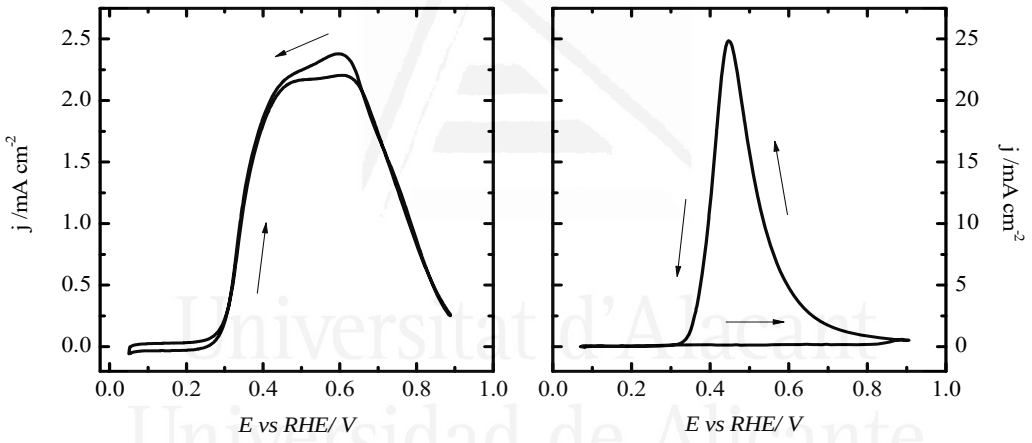

Figure 1.8. Voltammetric profile for HCOOH 0.1 M + H_2SO_4 0.5 M deaerated solution. (a) Pt(111) and (b) Pt(100). Scan rate 50 $mV.s^{-1}$.

Numerous studies to understand FAOR in stepped Pt surfaces have been also done. One of the first studies in this sense was conducted by Motoo *et al*. [83], who confirmed that both reaction pathways (AI and PI) present a structure sensitive mechanism. Thus, when the density of (100) steps sites in an Pt(111) electrode is increased [Pt(111)x(100)], the activity for FAOR also increases. After different experiments modullating the defects density on the electrode surface they concluded that a minimum number of 5 or 6 terrace

atoms with (111) symmetry is needed to get the maximum activity, with the minimum poisoning effect [84].

1.4. How to study the mechanism of formic acid oxidation on Pt(*hkl*) electrodes

1.4.1. Active intermediate

In order to study and characterize the overall FAOR mechanism using voltammetric techniques, each pathway should be studied separately. In this sense, to investigate the AI kinetics, the experiments should be conducted in the absence of adsorbed CO. One way to achieve this is using the pulse voltammetry. In this case, a potential positive enough to remove CO from the surface is chosen as initial potential, after that the current due to the FAOR by the AI is measured by stepping at any potential within the specific potential window under study for a short time (Figure 1.9). This procedure allows measuring the current transients in the surface free of CO. With the use of this technique, intrinsic activities (which is the current at no poisoning interference) for Pt(100) electrode of ca. 30 $mA \cdot cm^{-2}$ were measured. This value implies a conversion index of 70 molecules per Pt site and per second [85].

In contrast, for Pt(111) electrode, the intrinsic activity is low compared with Pt(100) electrode, being its conversion rate around 6 molecules per Pt site and per second. These differences in activity between Pt(100) and Pt(111) evidence one of the key problems regarding their use in fuel cells applications, which is controlling the product selectivity coming from each reaction pathway through the electrode surface control. Thus, the ideal

electrocatalysts should have high rate of direct oxidation pathway, suppressing, as much as possible the poisoning pathway.

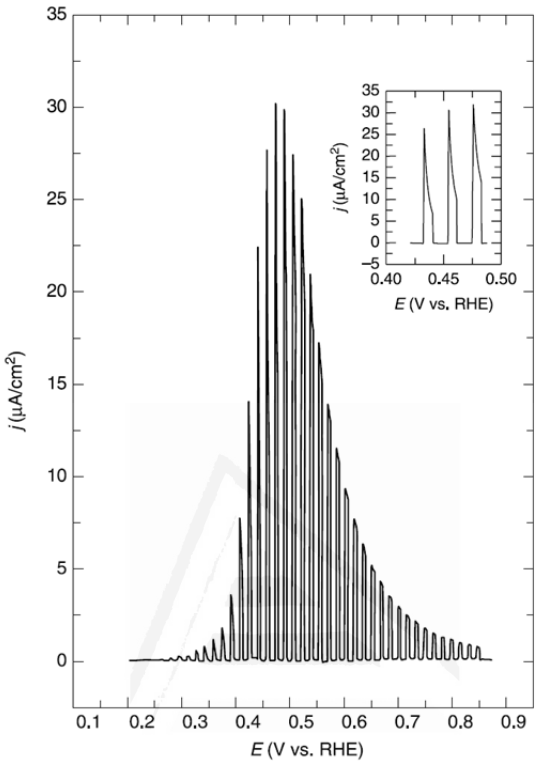

Figure 1.9. Pulse voltammetry of a Pt(100) electrode in 0.5 M H_2SO_4 0.25 M HCOOH. The inset is an expansion of the region between 0.4 and 0.5 V *vs. RHE* to show the decay in the current due to the poisoning of the surface. During the pulse at high potentials (0.9 V *vs. RHE*) to remove the poison, the current was not recorded (baseline between pulses). Adapted from [85] .

Sun *et al*. [86] performed quantitative determinations in this respect, obtaining activation energies and Tafel slopes for the FAOR in Pt single crystal electrodes. Thus, for Pt(100) electrode, a Tafel slope of about 120 mV was obtained. Using a different strategy, namely, preventing CO formation by blocking all the defect sites in Pt(111) electrodes, the same Tafel slope was measured [87]. The classical interpretation of such a Tafel slope would suggest that the rate determining step (rds) for the FAOR through the AI is the first

electron transfer. Since two electrons are exchanged in the reaction, the step that leads to the formation of the AI is the slowest step. Once this is formed, the following reaction will proceed much more rapidly.

1.4.2. Poisoning intermediate

The poisoning intermediate is easier to study, given that this is formed even at OCP in the electrode surface [48]. In addition, when CO is adsorbed, remains stable on the surface in the low potential range. Earlier studies using Pt single crystal electrodes have shown that the formic acid dissociates irreversibly and spontaneously on the Pt electrode surface [48]. This process is known as dissociative adsorption. Despite this phenomenon, it is important to point out that the CO does not completely cover the Pt surface, but the coverage always takes a maximum value of 70% of that required to block completely the surface. This observation shows that the specific surface requirements of the dissociative adsorption open a new via to improve the electrocatalysis of the whole reaction.

The kinetics of this reaction also have been studied by Sun *et al*. [86], in formic acid diluted solutions ($<10^{-3}$ M), to promote the reaction occurring mainly by the PI pathway. Using these low concentrations, it was determined that the maximum CO coverage in Pt(100) is formed before 100 sec, which explains how fast the poisoning process happens in this surface even in diluted solutions. This result compared with the one obtained for Pt(111) electrode, whose blocking time is larger than 500 sec in solutions 10^{-2} M [88], shows one more time the poisoning resistance of the later surface electrode.

It is also important to highlight that CO kinetics can be also studied using data coming from pulse voltammetry experiments such as those already described for studying the AI (Figure 1.9). In fact, some of these studies have found the potential range in which CO formation is favoured near by the potential of zero total charge (PZTC). Actually, the poison formation on Pt(111) electrodes has been associated with the presence of defective sites with other crystallography on their surface. This was demonstrated by, selectively covering the defects on such electrodes by adatoms, which prevented the formation of CO on the electrode surface [87, 89-91].

1.5. Improvement of the Pt electrocatalytic activity. Alloys and bimetallic surfaces

A way to enhance the activity of Pt for FAOR consists in modifying its chemical nature by combining this with other elements (metallic or non-metallic) looking for a synergetic effect. This can be achieved in two different ways; *i*) only modifying the chemical nature of the electrode surface creating bi or trimetallic surfaces, by the modification of the atomic surface composition of the Pt electrode, or *ii*) synthesizing Pt alloys, which have a homogeneous composition in the bulk and in the surface of all metals forming part of the alloy (Figure 1.10).

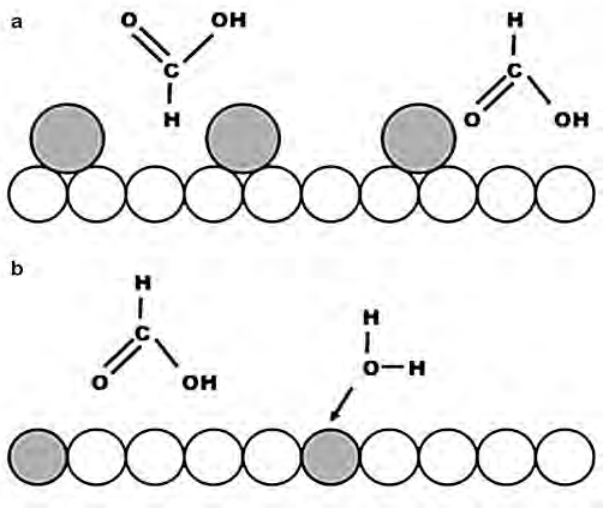

Figure 1.10. FAOR mediated by adatoms modified or bimetallic Pt surfaces. (a) Bimetalic surface. (b) Alloy [92].

All these combined new Pt-based electrode materials have unique electrocatalytic properties, which are different from the participating metals separately [93]. The electrocatalytic performance enhancement achieved by this modified electrodes is attributed to three main effects. *i*) the so-called bifunctional effect [94], the presence of foreign adatoms on the Pt surface can reduce the overpotential for CO_{ads} oxidation easily providing activated oxygen-species at lower potentials to produce its oxidation to CO_2, *ii*) the so-called electronic effect [81, 84, 95], in which one of the metals modifies the electronic properties of the other to enhance the global catalytic activity, and finally, *iii*) the so-called third body effect [95], in which one of the metals acts partially blocking the surface by a steric effect to suppress one of the reaction pathways (the PI pathway, in this case), enhancing the activity in the other route. All these three effects can appear combined in the different Pt alloys or bimetallic surfaces studied here [96].

Taking into account the combination of these effects mentioned above, one of the main requirements for the second participant metal would be the capability of suppressing the poison formation on the Pt-modified surface. Most of the metals present in Table 1.2

have been recently studied for enhancing the catalytic activity of Pt in FAOR by modifying either the Pt surface or bulk chemical composition. Pt alloys with metals from the precious metal group (PMG) are expected to have a better activity and stability for FAOR in comparison with alloys using other transition metals, due to the similarity in the physical features. In particular, Pt-Pd and Pt-Ru alloys have been widely studied.

Table 1.2. Metals used in Pt-modified electrodes to enhance the activity for FAOR [29].

Group	Metals
Group I (Precious Metals, PGM)	**Pt, Pd, Ru, Au, Ir**
Group II (Transition Metals, except PGM)	**Cr, Cu, Fe, Mo, Nb, V**
Group III (Post Transition Metals)	**Bi, Pb, Sb, Sn**

In contrast, other metals tested belonging to the group II in Table 1.2 have exhibited stability issues in the long term (problems due to their selective dissolution), which makes really difficult its application in fuel cells. The third group of metals in Table 1.2, so-called post-transition metal group (group III), have been widely tested towards FAOR in combination with Pt exhibiting promising activity results. These metals or semi-metals present a unique feature which is the ability to be adsorbed and electrodeposited at potentials below its massive deposition, also known as under potential deposition (UPD), thus Pt-UPD electrodes show a reasonable stability. Among these metals in group III, Bi emerges as a promising adatom to modified the Pt surface, not just for its high resistance to the PI adsorption, due to a third body effect [95], but also due to the moderate stability of the Bi-Pt system in a wide potential range.

1.5.1. Pt bulk alloys and screening techniques

An important number of studies have been done trying to find the most active combination of Pt with some other PGM. In particular, the combination of Pt and Pd provides a synergistic effect in Pt and enhances its activity as both metals possess similar properties such as the electronegativity [97-99]. However, the performance obtained from the Pt-Pd alloy is much lower than that on pure Pd, although the high degradation rate observed in Pd electrodes is somewhat alleviated in the Pt-Pd alloy.

Pt-Ru alloys have been reported as one of the best electrocatalysts for SOMs oxidation due to their high activity following the bifunctional mechanism, which involves the adsorption of OH species on Ru and then, the complete oxidation of CO to CO_2 [30, 100]. However, FAOR proceeds via a combination of different reaction mechanisms, and for this reason, Ru- (Pt or Pd) alloys are not as effective as pure Pd catalyst. Alternatively, Pt-Au [98, 100-102] or Pt-Ir [103] have been suggested as promising PMG alloys for enhancing FAOR by reducing poison formation due to the third body effect. However, FAOR investigations on such type of alloys are very limited, probably because PGM alloys have no clear inherent advantage for lowering the catalyst cost, although they may provide interesting information from a mechanistic point of view.

Voltammetric techniques have been widely used for the characterization and study of binary and ternary alloys. However, the screening of different alloys using a combinatorial approach varying the combination of metals and the ratio of each metal within the alloy represents a time consuming task, which is out of the scope of one single thesis. Nevertheless, recently new rapid high-throughput screening techniques have been introduced as an extremely versatile tool to evaluate the activity of a set of different

catalysts in one single experiment [104-108]. One of those promising screening techniques is the scanning electrochemical microscopy (SECM) [109], an useful new electroanalytical tool, which improves the output speed in the electrocatalyst screening step and allows to study a wide number of electrochemical processes with high temporal and spatial resolution. SECM applications in electrocatalysis are still under development and for this reason novel modes of use for the SECM are developed here to study FAOR in Pt modified electrodes.

1.5.2. Bimetallic Pt-modified surfaces

Some systematic studies of the effect of different adatoms on the poison formation on well-defined surfaces were first carried out on Pt(100) and Pt(111) surfaces [110, 111], and later, they were extended to Pt(110) and stepped surfaces [112, 113]. A key issue modifying Pt(*hkl*) electrodes is controlling the amount of surface modified by the foreign adatom in order to know the final coverage achieved. In some cases, adatoms suffer surface processes to form an oxygenated surface compound (i.e. oxide formation), in a potential range in which the platinum substrate is stable. Thus, the adatom coverage may be estimated electrochemically from the charge involved in these processes and compared to the charge displayed by the bare platinum electrode or from the charge diminution observed in the hydrogen UPD signals due to the blocking effect of the adatoms incorporated at the Pt surface. In this way, it is possible to quantify and modulate the amount of adatom, in order to produce the desired activity improvement. A deep knowledge about the coverage stoichiometry and the location of the adatoms on the Pt surface is of main interest, given that it can give an idea of the domain in which the

reaction is taking place, and how the reactive species interact with the Pt sites neighbouring the adatom. It could also be of interest knowing the reactive sites for oxygen adsorption, so it would help understand the enhancement of the CO oxidation rate in the presence of those adatoms.

Similar to the bare platinum electrode, for adatom modified Pt surfaces, both the poison formation and the direct pathway for the FAOR have been studied. For instance, in the case of the adatom modified-Pt(100), the third body effect seems to explain reasonably the improvement exhibited in the catalytic activity. Sb, Bi and Te [114, 115] adatoms irreversibly adsorbed on well-defined Pt(100) electrodes exhibit long term poisoning resistance. Herrero *et al.* concluded that the amount of poison that can be accumulated on those Pt-modified electrodes decreases linearly with the adatom coverage. At relatively high adatom coverages, where the free platinum sites are probably isolated, the poison formation is completely inhibited. Under these circumstances, the direct oxidation of formic acid may take place and the surface has become selective for the reaction by the direct pathway, yielding the highest currents in the positive-going scan [42].

In the case of adatom modified-Pt(111) electrodes two different types of behaviour have been found for the poison formation reaction. In the first one, the amount of the poison decreases linearly with the adatom coverage and becomes zero at relatively high adatom coverage. This is the case of S or Se adatoms [49]. In the second case, however, very small amounts of the adatom on the Pt surface cause a deep decrease in the poison accumulation. This is the case of irreversibly adsorbed Bi [81]. In fact, CO is not present on the surface at Bi coverage as low as 0.04, i.e., when about 90% of the platinum sites remain free. This behaviour is related to the blocking of the reactive sites for the PI pathway. As aforementioned, defects are responsible for the formation of the PI on the

Pt(111) electrode [81] and the adsorption and deposition of Bi occurs preferentially on those sites. A similar PI inhibition behaviour has been observed with Sb [116] , Te [117], as well as with As [81], Sn [118] and Pb [119] adatoms on Pt. In relation to the FAOR by the direct pathway, for Bi on Pt(111) electrodes, the oxidation rate becomes more than ten times higher than that corresponding to the intrinsic activity of Pt(111), resulting in turnover rates as high as 250 molecules per Pt(111) site and per second. However, if the electrode is fully blocked with Bi becomes inactive. Sb [116] and Te [117] on Pt(111) electrodes also catalyse strongly the FAOR by the direct pathway. Finally, it can be highlighted that the bimetallic Pt-modified surfaces that exhibit an enhancement in the FAOR are those formed by adatoms, which are electropositive with respect to platinum, i.e., the adatoms that modify the electronic properties of platinum donating electrons to its *d* orbitals [42].

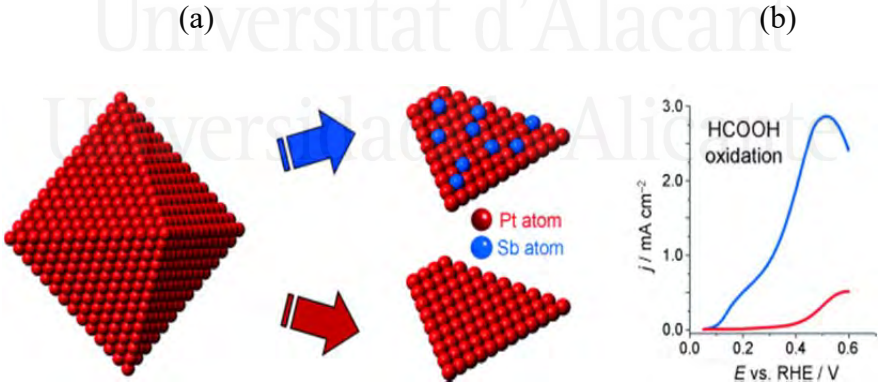

Figure 1.11. (a) Representation of the surface modification of octahedral Pt NPs by antimony adatom. (b) Activity of the Sb modified octahedral Pt NPs (blue line) compared with bare octahedral Pt NPs (red line) in the forward cycle [120].

Pt nanoparticles (Pt NPs) have been also decorated with adatoms such as Pd [121, 122], Bi [123, 124] or Sb [125]. The case of Sb modified octahedral Pt NPs electrodes is presented in Figure 1.11 as a clear example of a successful system based on bimetallic surface modified Pt NPs, which improves catalyst activity towards FAOR.

1.6. Platinum nanoparticles as electrocatalyst

The studies in the electrocatalysis of SOMs conducted with Pt single crystal electrodes presents the advantage of obtaining information about the reaction mechanism, providing some experimental valuable results really useful for further verification of theoretical modelling [42, 44, 121]. However, for real applications in fuel cells it is necessary to jump into some kind of electrocatalyst that can be spread in cathodes or anodes contained in the device set up. Faced to this challenge, the development of different Pt NPs syntheses represents a rational approach to prepare real catalysts for fuel cells. Nanomaterials have the advantage of minimizing the amount of platinum used in the preparation of the electrodes, due to their high fraction of available surface atoms as compared to conventional bulk materials. Metal NPs usually present different characteristics from their corresponding bulk phase metals because of their finite size or equivalently the large fraction of atoms located near or at the particle surface, which can lead to significant changes in the structural and chemical properties of the metal. Additionally, catalyst activities depend critically on their size-dependent properties [122].

In recent years, the synthesis of shape-controlled Pt NPs using capping agents has been widely explored, with the main target of obtaining more efficient catalysts by controlling their surface structure [106, 122-124]. Thus, it has been clearly shown that the

reactivity and selectivity of the Pt NPs can be modulated by controlling their morphology because, depending on their shape, the surface of the NPs may contain very different reactive surface sites [123, 125]. Figure 1.12 shows an example of a growing process for a (100) preferential oriented Pt NPs In addition, hape-controlled Pt NPs are ideal to understand the reactivity on practical electrodes, since they provide the missing link with the model surfaces, that is, the single-crystal electrodes.

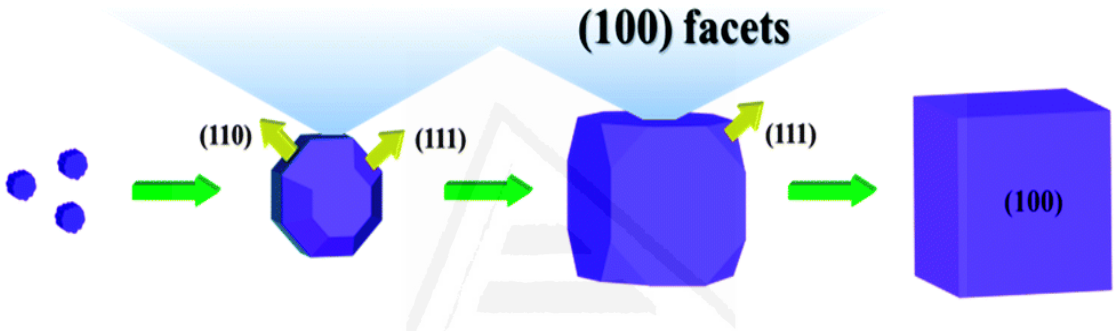

Figure 1.12. Schematic illustration of the formation mechanism of the cubic Pt NPs. Taken from [126].

Since the advent of shape-controlled NPs, similar electrocatalytic studies to those reported on single crystal electrodes have become possible at nanometric scale. Solla-Gullón *et al*. [127] studied the FAOR on (111), (100) and (100)-(111) Pt NPs. In Figure 1.13 are shown the reaction mechanism models predominant on octahedral (111) and cubic (100) NPs, as well as its model nanocatalyst structure. They argued that the surface structure of the NPs plays an important role on the reactivity of both oxidation pathways, and thus the electrocatalytic properties strongly depend on the surface structure/shape of the NPs. Among the Pt NPs studied so far, those containing a preferential (111) orientation are clearly the most active (in the long-term) towards FAOR, because of their low poisoning rate, the same feature exhibited by the Pt(111) electrode.

Although the Pt NPs catalytic activity is improved by the shape modification, it is important to point out that the stability of such NPs is not too high. Thus, the oxygen adsorption promotes the surface oxidation and this may damage the shape of the NPs which, eventually, could transform them into polyoriented Pt NPs. For this reason, a more restrictive potential window must be used in order to prevent the surface structure modification on shape-controlled Pt NPs.

(a) (b)

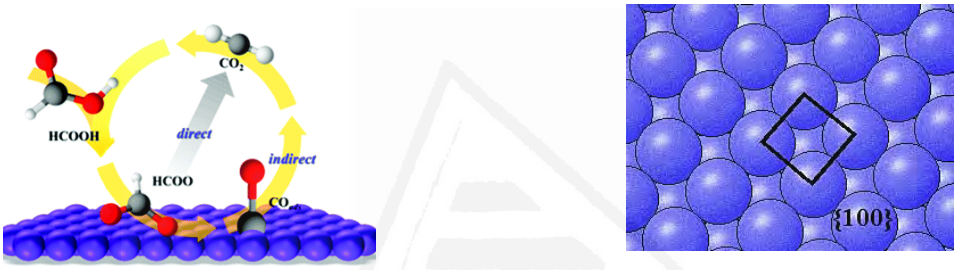

Figure 1.13. (a) Mechanism of FAOR on the catalyst Cubic Pt-based nanostructure catalysts with dominant (100) facets [126]. (b) Surface structure of the {111} and {100} domains.

1.7. References

[1] A. J. Bard and L. R. Faulkner, "Electrochemical Methods. Fundamental and Applications", John Wiley & Sons, Inc., New York, **2001**.

[2] J. O. M. Bockris and A. K. N. Reddy, "Modern Electrochemistry", Plenum, New York, **1970**.

[3] L. R. Faulkner, "Understanding electrochemistry: Some distinctive concepts" *Journal of Chemical Education* **1983**, 60, 262.

[4] A. J. Bard, "Inner-Sphere Heterogeneous Electrode Reactions. Electrocatalysis and Photocatalysis: The Challenge" *Journal of the American Chemical Society* **2010**, 132, 7559-7567.

[5] N. M. Markovic, "Electrocatalysis: Interfacing electrochemistry" *Nature Materials* **2013**, 12, 101-102.

[6] C. Apuntes, "Catalisis - http://apuntescientificos.org/catalisis-ibq2.html", in, Apuntes Científicos, **2012**.

[7] G. Somorjai and Y. Li, "Introduction to Surface Chemistry and Catalysis", Willey, **2010**.

[8] B. Lang, R. W. Joyner and G. A. Somorjai, "Low energy electron diffraction studies of chemisorbed gases on stepped surfaces of platinum" *Surface Science* **1972**, 30, 454-474.

[9] B. Lang, R. W. Joyner and G. A. Somorjai, "Low energy electron diffraction studies of high index crystal surfaces of platinum" *Surface Science* **1972**, 30, 440-453.

[10] K. Christmann and G. Ertl, "Interaction of Hydrogen with platinum(111): the role of atomic steps" *Surface Science* **1976**, 60, 365-384.

[11] J. Clavilier, R. Durand, G. Guinet and R. Faure, "Electrochemical adsorption behaviour of Pt(100) in sulphuric acid solution " *Journal of Electroanalytical Chemistry* **1981**, 127, 281-287.

[12] J. Clavilier, R. Faure, G. Guinet and R. Durand, "Preparation of monocrystalline Pt microelectrodes and electrochemical study of the plane surfaces cut in the direction of the {111} and {110} planes " *Journal of Electroanalytical Chemistry* **1980**, 107, 205-209.

[13] J. Clavilier, D. Armand, S. G. Sun and M. Petit, "Electrochemical adsorption behaviour of platinum stepped surfaces in sulphuric acid solutions " *Journal of Electroanalytical Chemistry* **1986**, 205, 267-277.

[14] J. Clavilier, "The role of anion on the electrochemical behaviour of a {111} platinum surface; an unusual splitting of the voltammogram in the hydrogen region " *Journal of Electroanalytical Chemistry* **1980**, 107, 211-216.

[15] M. D. Maciá, E. Herrero and J. M. Feliu, "Formic acid oxidation on Bi-Pt(111) electrode in perchloric acid media. A kinetic study" *Journal of Electroanalytical Chemistry* **2003**, 554, 25-34.

[16] J. V. Perales-Rondon, A. Ferre-Vilaplana, J. M. Feliu and E. Herrero, "Oxidation Mechanism of Formic Acid on the Bismuth Adatom-Modified Pt(111) Surface" *Journal of the American Chemical Society* **2014**, 136, 13110-13113.

[17] C. Lamy and J. M. Leger, "Electrocatalytic oxidation of small organic molecules at platinum single crystals" *Journal de Chimie Physique et de Physico-Chimie Biologique* **1991**, 88, 1649-1671.

[18] S. C. S. Lai and M. T. M. Koper, "Ethanol electro-oxidation on platinum in alkaline media" *Physical Chemistry Chemical Physics* **2009**, 11, 10446-10456.

[19] T. P. Johansson, E. T. Ulrikkeholm, P. Hernandez-Fernandez, M. Escudero-Escribano, P. Malacrida, I. E. L. Stephens and I. Chorkendorff, "Towards the elucidation of the high oxygen electroreduction activity of PtxY: Surface science and electrochemical studies of Y/Pt(111)" *Physical Chemistry Chemical Physics* **2014**, 16, 13718-13725.

[20] E. T. Ulrikkeholm, A. F. Pedersen, T. P. Johansson, P. Malacrida, M. E. Escribano, P. Hernandez-Fernandez, U. G. Vej-Hansen, C. M. Pedersen, D. Friebel, J. Rossmeisl, I. Stephens, A. Nilsson and I. Chorkendorff, "Correlating Structure and Oxygen Reduction Activity on Y/Pt(111) and Gd/Pt(111) Single Crystals" *Electrochemical Society. Meeting Abstracts (Online)* **2015**, MA2015-03.

[21] D. Strmcnik, M. Escudero-Escribano, K. Kodama, R. StamenkovicVojislav, A. Cuesta and N. M. Marković, "Enhanced electrocatalysis of the oxygen reduction reaction based on patterning of platinum surfaces with cyanide" *Nature Chemistry* **2010**, 2, 880-885.

[22] v. Hydrogen, "Hydrogen vehicle - https://en.wikipedia.org/wiki/Hydrogen_vehicle", in, Wikipedia, the free encyclopedia, **2016**.

[23] G. Sandstede, E. J. Cairns, V. S. Bagotsky and K. Wiesener, "History of low temperature fuel cells", in *Handbook of Fuel Cells*, John Wiley & Sons, Ltd, **2010**.

[24] M. T. M. Koper, "Fuel Cell Catalysis: A Surface Science Approach", *Electrocatalysis and Electrochemistry* A. Wieckowski (Ed.), John Wiley & Sons, Hoboken, New Jersey, **2009**.

[25] Y. Demirel, "Energy and Energy Types", in *Energy: Production, Conversion, Storage, Conservation, and Coupling*, Springer London, London, **2012**, pp. 27-70.

[26] V. M. Vishnyakov, "Proton exchange membrane fuel cells" *Vacuum* **2006**, 80, 1053-1065.

[27] V. S. Bagotsky, "Phosphoric Acid Fuel Cells", in *Fuel Cells*, John Wiley & Sons, Inc., **2012**, pp. 99-106.

[28] R. M. Ormerod, "Solid oxide fuel cells" *Chemical Society Reviews* **2003**, 32, 17-28.

[29] S. Uhm, H. J. Lee and J. Lee, "Understanding underlying processes in formic acid fuel cells" *Physical Chemistry Chemical Physics* **2009**, 11, 9326-9336.

[30] C. Rice, S. Ha, R. I. Masel and A. Wieckowski, "Catalysts for direct formic acid fuel cells" *Journal of Power Sources* **2003**, 115, 229-235.

[31] C. Rice, R. I. Ha, R. I. Masel, P. Waszczuk, A. Wieckowski and T. Barnard, "Direct formic acid fuel cells" *Journal of Power Sources* **2002**, 111, 83-89.

[32] Y.-W. Rhee, S. Y. Ha and R. I. Masel, "Crossover of formic acid through Nafion® membranes" *Journal of Power Sources* **2003**, 117, 35-38.

[33] X. Wang, J.-M. Hu and I. M. Hsing, "Electrochemical investigation of formic acid electro-oxidation and its crossover through a Nafion® membrane" *Journal of Electroanalytical Chemistry* **2004**, 562, 73-80.

[34] M. Winter and R. J. Brodd, "What Are Batteries, Fuel Cells, and Supercapacitors?" *Chemical Reviews (Washington, DC, United States)* **2004**, 104, 4245-4270.

[35] B. C. H. Steele and A. Heinzel, "Materials for fuel-cell technologies" *Nature* **2001**, 414, 345-352.

[36] A. Capon and R. Parsons, "The oxidation of formic acid at noble metal electrodes: I. Review of previous work " *Journal of Electroanalytical Chemistry* **1973**, 44, 1-7.

[37] A. Capon and R. Parsons, "The oxidation of formic acid on noble metal electrodes: II. A comparison of the behaviour of pure electrodes " *Journal of Electroanalytical Chemistry* **1973**, 44, 239-254.

[38] A. Capon and R. Parsons, "The oxidation of formic acid at noble metal electrodes Part III. Intermediates and mechanism on platinum electrodes " *Journal of Electroanalytical Chemistry* **1973**, 45, 205-231.

[39] R. Parsons and T. Vandernoot, "The oxidation of small organic molecules: A survey of recent fuel cell related research" *Journal of Electroanalytical Chemistry* **1988**, 257, 9-45.

[40] A. Nilsson, L. G. M. Pettersson and J. Norskov, "Chemical Bonding at Surfaces and Interfaces", Elsevier Science, **2011**.

[41] P. Strasser and H. Ogasawara, "Chemical Bonding at Surfaces and Interfaces. Chapter 6, Surface Electrochemistry", Elsevier, Ansterdam, The Netherlands **2008**.

[42] J. M. Feliu and E. Herrero, "Formic acid oxidation", in *Handbook of Fuel Cells - Fundamentals, Technology and Applications, vol. 2*, W. Vielstich, H. Gasteiger and A. Lamm (Eds.) John Wiley & Sons, Ltd., Chichester, **2003**, pp. 625-634.

[43] V. S. Bagotzky, Y. B. Vassiliev and O. A. Khazova, "Generalized scheme of chemisorption, electrooxidation and electroreduction of simple organic compounds on platinum group metals" *Journal of Electroanalytical Chemistry and Interfacial Electrochemistry* **1977**, 81, 229-238.

[44] M. T. M. Koper, S. C. S. Lai and E. Herrero, "Mechanisms of the Oxidation of Carbon Monoxide and Small Organic Molecules at Metal Electrodes", in *Fuel Cell Catalysis, A Surface Science Approach*, M. T. M. Koper (Ed.) John Wiley & Sons, Inc, Hoboken, NJ, **2009**, pp. 159-208.

[45] K. Kunimatsu, "Infrared spectroscopic study of methanol and formic acid adsorbates on a platinum electrode: Part I. Comparison of the infrared absorption

intensities of linear CO(a) derived from CO, CH_3OH and HCOOH " *Journal of Electroanalytical Chemistry* **1986**, 213, 149-157.

[46] J. Willsau and J. Heitbaum, "Analysis of adsorbed intermediates and determination of surface potential shifts by DEMS" *Electrochimica Acta* **1986**, 31, 943-948.

[47] O. Wolter, J. Willsau and J. Heitbaum, "Reaction Pathways of the Anodic Oxidation of Formic Acid on Pt Evidenced by 18O Labeling—A DEMS Study" *Journal of The Electrochemical Society* **1985**, 132, 1635-1638.

[48] J. Clavilier and S. G. Sun, "Electrochemical Study of the Chemisorbed Species Formed from Formic-Acid Dissociation at Platinum Single-Crystal Electrodes" *Journal of Electroanalytical Chemistry* **1986**, 199, 471-480.

[49] M. J. Llorca, E. Herrero, J. M. Feliu and A. Aldaz, "Formic acid oxidation on Pt(111) electrodes modified by irreversibly adsorbed selenium" *Journal of Electroanalytical Chemistry* **1994**, 373, 217-225.

[50] S. Gilman, "The Mechanism of Electrochemical Oxidation of Carbon Monoxide and Methanol on Platinum. II. The "Reactant-Pair" Mechanism for Electrochemical Oxidation of Carbon Monoxide and Methanol" *Journal of Physical Chemistry B* **1964**, 68, 70.

[51] B. Love and J. Lipkowski, "Effect of surface crystallography on electrocatalytic oxidation of carbon-monoxide on platinum-electrodes." *Acs Symposium Series* **1988**, 378, 484-496.

[52] M. T. M. Koper, A. P. J. Jansen, R. A. van Santen, J. J. Lukkien and P. A. J. Hilbers, "Monte Carlo simulations of a simple model for the electrocatalytic CO oxidation on platinum" *Journal of Chemical Physics* **1998**, 109, 6051-6062.

[53] N. P. Lebedeva, M. T. M. Koper, J. M. Feliu and R. A. van Santen, "Role of crystalline defects in electrocatalysis: Mechanism and kinetics of CO adlayer oxidation on stepped platinum electrodes" *Journal of Physical Chemistry B* **2002**, 106, 12938-12947.

[54] C. A. Angelucci, E. Herrero and J. M. Feliu, "Modeling CO Oxidation on Pt(111) Electrodes" *Journal of Physical Chemistry C* **2010**, 114, 14154-14163.

[55] E. Herrero, J. M. Feliu, S. Blais, Z. Radovic-Hrapovic and G. Jerkiewicz, "Temperature dependence of CO chemisorption and its oxidative desorption on the Pt(111) electrode" *Langmuir* **2000**, 16, 4779-4783.

[56] F. A. Hanc-Scherer, C. M. Sánchez-Sánchez, P. Ilea and E. Herrero, "Surface-Sensitive Electrooxidation of Carbon Monoxide in Room Temperature Ionic Liquids" *ACS Catalysis* **2013**, 3, 2935-2938.

[57] S. Wilhelm, W. Vielstich, H. W. Buschmann and T. Iwasita, "Direct proof of the hydrogen in the methanol adsorbate at platinum — an ECTDMS study" *Journal of Electroanalytical Chemistry and Interfacial Electrochemistry* **1987**, 229, 377-384.

[58] S. G. Sun, J. Clavilier and A. Bewick, "The mechanism of electrocatalytic oxidation of formic acid on Pt (100) and Pt (111) in sulphuric acid solution: an emirs study" *Journal of Electroanalytical Chemistry* **1988**, 240, 147-159.

[59] G. Samjeské, A. Miki, S. Ye, A. Yamakata, Y. Mukouyama, H. Okamoto and M. Osawa, "Potential Oscillations in Galvanostatic Electrooxidation of Formic Acid on Platinum: A Time-Resolved Surface-Enhanced Infrared Study" *The Journal of Physical Chemistry B* **2005**, 109, 23509-23516.

[60] G. Samjeské and M. Osawa, "Current Oscillations during Formic Acid Oxidation on a Pt Electrode: Insight into the Mechanism by Time-Resolved IR Spectroscopy" *Angewandte Chemie International Edition* **2005**, 44, 5694-5698.

[61] A. Miki, S. Ye and M. Osawa, "Surface-enhanced IR absorption on platinum nanoparticles: an application to real-time monitoring of electrocatalytic reactions" *Chemical Communications* **2002**, 1500-1501.

[62] G. Samjeské, A. Miki, S. Ye and M. Osawa, "Mechanistic Study of Electrocatalytic Oxidation of Formic Acid at Platinum in Acidic Solution by Time-Resolved Surface-Enhanced Infrared Absorption Spectroscopy" *The Journal of Physical Chemistry B* **2006**, 110, 16559-16566.

[63] A. Cuesta, G. Cabello, C. Gutierrez and M. Osawa, "Adsorbed formate: the key intermediate in the oxidation of formic acid on platinum electrodes" *Physical Chemistry Chemical Physics* **2011**, 13, 20091-20095.

[64] M. Osawa, K. Komatsu, G. Samjeske, T. Uchida, T. Ikeshoji, A. Cuesta and C. Gutierrez, "The Role of Bridge-Bonded Adsorbed Formate in the Electrocatalytic Oxidation of Formic Acid on Platinum" *Angewandte Chemie-International Edition* **2011**, 50, 1159-1163.

[65] A. Cuesta, G. Cabello, M. Osawa and C. Gutiérrez, "Mechanism of the Electrocatalytic Oxidation of Formic Acid on Metals" *ACS Catalysis* **2012**, 2, 728-738.

[66] Y. X. Chen, M. Heinen, Z. Jusys and R. B. Behm, "Kinetics and mechanism of the electrooxidation of formic acid - Spectroelectrochemical studies in a flow cell" *Angewandte Chemie, International Edition in English* **2006**, 45, 981-985.

[67] Y. X. Chen, M. Heinen, Z. Jusys and R. J. Behm, "Bridge-bonded formate: Active intermediate or spectator species in formic acid oxidation on a Pt film electrode?" *Langmuir* **2006**, 22, 10399-10408.

[68] Y. X. Chen, M. Heinen, Z. Jusys and R. J. Behm, "Kinetic isotope effects in complex reaction networks: Formic acid electro-oxidation" *ChemPhysChem* **2007**, 8, 380-385.

[69] J. Xu, D. Yuan, F. Yang, D. Mei, Z. Zhang and Y.-X. Chen, "On the mechanism of the direct pathway for formic acid oxidation at a Pt(111) electrode" *Physical Chemistry Chemical Physics* **2013**, 15, 4367-4376.

[70] Y. X. Chen, S. Ye, M. Heinen, Z. Jusys, M. Osawa and R. J. Behm, "Application of in-situ attenuated total reflection-Fourier transform infrared spectroscopy for the understanding of complex reaction mechanism and kinetics: Formic acid oxidation on a Pt film electrode at elevated temperatures" *Journal of Physical Chemistry B* **2006**, 110, 9534-9544.

[71] H. Okamoto, Y. Numata, T. Gojuki and Y. Mukouyama, "Different behavior of adsorbed bridge-bonded formate from that of current in the oxidation of formic acid on platinum" *Electrochimica Acta* **2014**, 116, 263-270.

[72] M. Neurock, M. Janik and A. Wieckowski, "A first principles comparison of the mechanism and site requirements for the electrocatalytic oxidation of methanol and formic acid over Pt" *Faraday Discussions* **2009**, 140, 363-378.

[73] H.-F. Wang and Z.-P. Liu, "Formic Acid Oxidation at Pt/H2O Interface from Periodic DFT Calculations Integrated with a Continuum Solvation Model" *Journal of Physical Chemistry C* **2009**, 113, 17502-17508.

[74] W. Gao, J. A. Keith, J. Anton and T. Jacob, "Theoretical Elucidation of the Competitive Electro-oxidation Mechanisms of Formic Acid on Pt(111)" *Journal of the American Chemical Society* **2010**, 132, 18377-18385.

[75] J. Joo, T. Uchida, A. Cuesta, M. T. M. Koper and M. Osawa, "Importance of Acid-Base Equilibrium in Electrocatalytic Oxidation of Formic Acid on Platinum" *Journal of the American Chemical Society* **2013**, 135, 9991-9994.

[76] J. Joo, T. Uchida, A. Cuesta, M. T. M. Koper and M. Osawa, "The effect of pH on the electrocatalytic oxidation of formic acid/formate on platinum: A mechanistic study by surface-enhanced infrared spectroscopy coupled with cyclic voltammetry" *Electrochimica Acta* **2014**, 129, 127-136.

[77] S. Brimaud, J. Solla-Gullón, I. Weber, J. M. Feliu and R. J. Behm, "Formic Acid Electrooxidation on Noble-Metal Electrodes: Role and Mechanistic Implications of pH, Surface Structure, and Anion Adsorption" *ChemElectroChem* **2014**, 1, 1075-1083.

[78] J. Clavilier, R. Parsons, R. Durand, C. Lamy and J. M. Leger, "Formic acid oxidation on single crystal platinum electrodes. Comparison with polycrystalline platinum" *Journal of Electroanalytical Chemistry* **1981**, 124, 321-326.

[79] C. Lamy, J. M. Leger, J. Clavilier and R. Parsons, "Structural effects in electrocatalysis: A comparative study of the oxidation of CO, HCOOH and CH_3OH on single crystal Pt electrodes" *Journal of Electroanalytical Chemistry* **1983**, 150, 71-77.

[80] R. R. Adzic, A. V. Tripkovic and W. E. O'Grady, "Structural effects in electrocatalysis" *Nature* **1982**, 296, 137-138.

[81] E. Herrero, A. Fernández-Vega, J. M. Feliu and A. Aldaz, "Poison formation reaction from formic acid and methanol on Pt(111) electrodes modified by irreversibly adsorbed Bi and As " *Journal of Electroanalytical Chemistry* **1993**, 350, 73-88.

[82] T. Iwasita, X. H. Xia, H. D. Liess and W. Vielstich, "Electrocatalysis of Organic Oxidations - Influence of Water- Adsorption on the Rate of Reaction" *Journal of Physical Chemistry B* **1997**, 101, 7542-7547.

[83] S. Motoo and N. Furuya, "Effect of terraces and steps in the electrocatalysis for formic acid oxidation on platinum" *Berichte Der Bunsen-Gesellschaft-Physical Chemistry Chemical Physics* **1987**, 91, 457-461.

[84] M. Shibata, N. Furuya, M. Watanabe and S. Motoo, "Electrocatalysis by ad-atoms. Part XXIV. Effect of arrangement of Bi ad-atoms on formic acid oxidation" *Journal of Electroanalytical Chemistry* **1989**, 263, 97-108.

[85] J. Clavilier, "Pulsed linear sweep voltammetry with pulses of constant level in a potential scale, a polarization demanding condition in the study of platinum single-crystal electrodes" *Journal of Electroanalytical Chemistry* **1987**, 236, 87-94.

[86] S. G. Sun, Y. Lin, N. H. Li and J. Q. Mu, "Kinetics of Dissociative Adsorption of Formic-Acid on Pt(100), Pt(610), Pt(210) and Pt(110) Single-Crystal Electrodes in Perchloric-Acid Solutions" *Journal of Electroanalytical Chemistry* **1994**, 370, 273-280.

[87] M. D. Maciá, E. Herrero, J. M. Feliu and A. Aldaz, "Formic acid self-poisoning on bismuth-modified stepped electrodes" *Journal of Electroanalytical Chemistry* **2001**, 500, 498-509.

[88] T. Iwasita, X. H. Xia, E. Herrero and H. D. Liess, "Early stages during the oxidation of HCOOH on single-crystal Pt electrodes as characterized by infrared spectroscopy" *Langmuir* **1996**, 12, 4260-4265.

[89] M. D. Maciá, E. Herrero, J. M. Feliu and A. Aldaz, "Formic acid self-poisoning on bismuth-modified Pt(755) and Pt(775) electrodes" *Electrochemistry Communications* **1999**, 1, 87-89.

[90] M. D. Maciá, E. Herrero and J. M. Feliu, "Formic acid self-poisoning on adatom-modified stepped electrodes" *Electrochimica Acta* **2002**, 47, 3653-3661.

[91] S. P. E. Smith, K. F. Ben-Dor and H. D. Abruna, "Poison formation upon the dissociative adsorption of formic acid on bismuth-modified stepped platinum electrodes" *Langmuir* **2000**, 16, 787-794.

[92] C. A. Rice and A. Wieckowski, "Electrocatalysis of Formic Acid Oxidation", in *Electrocatalysis in Fuel Cells: A Non- and Low- Platinum Approach*, M. Shao (Ed.) Springer London, London, **2013**, pp. 43-67.

[93] J. Schwank, "Bimetallic catalysts: Discoveries, concepts, and applications. By John H. Sinfelt, John Wiley & Sons, 1983. XI + 164 pp" *AIChE Journal* **1985**, 31, 1405-1405.

[94] M. Watanabe and S. Motoo, "Electrocatalysis by ad-atoms: Part III. Enhancement of the oxidation of carbon monoxide on platinum by ruthenium ad-atoms" *Journal of Electroanalytical Chemistry* **1975**, 60, 275-283.

[95] E. Leiva, T. Iwasita, E. Herrero and J. M. Feliu, "Effect of adatoms in the electrocatalysis of HCOOH oxidation. A theoretical model" *Langmuir* **1997**, 13, 6287-6293.

[96] M. T. M. Koper, "Electrocatalysis on bimetallic and alloy surfaces" *Surface Science* **2004**, 548, 1-3.

[97] M. Baldauf and D. M. Kolb, "Formic acid oxidation on ultrathin Pd films on Au(hkl) and Pt(hkl) electrodes" *Journal of Physical Chemistry* **1996**, 100, 11375-11381.

[98] N. Kristian, Y. Yan and X. Wang, "Highly efficient submonolayer Pt-decorated Au nano-catalysts for formic acid oxidation" *Chemical Communications* **2008**, 353-355.

[99] S. E. Habas, H. Lee, V. Radmilovic, G. A. Somorjai and P. Yang, "Shaping binary metal nanocrystals through epitaxial seeded growth" *Nature Materials* **2007**, 6, 692-697.

[100] J.-H. Choi, K.-J. Jeong, Y. Dong, J. Han, T.-H. Lim, J.-S. Lee and Y.-E. Sung, "Electro-oxidation of methanol and formic acid on PtRu and PtAu for direct liquid fuel cells" *Journal of Power Sources* **2006**, 163, 71-75.

[101] R. Larsen, S. Ha, J. Zakzeski and R. I. Masel, "Unusually active palladium-based catalysts for the electrooxidation of formic acid" *Journal of Power Sources* **2006**, 157, 78-84.

[102] S. Ha, R. Larsen, Y. Zhu and R. I. Masel, "Direct Formic Acid Fuel Cells with 600 mA cm–2 at 0.4 V and 22 °C" *Fuel Cells* **2004**, 4, 337-343.

[103] X. Wang, Y. Tang, Y. Gao and T. Lu, "Carbon-supported Pd–Ir catalyst as anodic catalyst in direct formic acid fuel cell" *Journal of Power Sources* **2008**, 175, 784-788.

[104] C. Jung, C. M. Sánchez-Sánchez, C.-L. Lin, J. Rodríguez-López and A. J. Bard, "Electrocatalytic Activity of Pd−Co Bimetallic Mixtures for Formic Acid Oxidation Studied by Scanning Electrochemical Microscopy" *Analytical Chemistry* **2009**, 81, 7003-7008.

[105] C.-L. Lin, J. Rodríguez-López and A. J. Bard, "Micropipet Delivery−Substrate Collection Mode of Scanning Electrochemical Microscopy for the Imaging of Electrochemical Reactions and the Screening of Methanol Oxidation Electrocatalysts" *Analytical Chemistry* **2009**, 81, 8868-8877.

[106] C. M. Sanchez-Sanchez, J. Solla-Gullon, F. J. Vidal-Iglesias, A. Aldaz, V. Montiel and E. Herrero, "Imaging Structure Sensitive Catalysis on Different Shape-Controlled Platinum Nanoparticles" *Journal of the American Chemical Society* **2010**, 132, 5622-5624.

[107] O. Lugaresi, J. V. Perales-Rondon, A. Minguzzi, J. Solla-Gullon, S. Rondinini, J. M. Feliu and C. M. Sanchez-Sanchez, "Rapid screening of silver nanoparticles for the catalytic degradation of chlorinated pollutants in water" *Applied Catalysis B* **2015**, 163, 554-563.

[108] J. L. Fernández, D. A. Walsh and A. J. Bard, "Thermodynamic Guidelines for the Design of Bimetallic Catalysts for Oxygen Electroreduction and Rapid Screening by Scanning Electrochemical Microscopy. M−Co (M: Pd, Ag, Au)" *Journal of the American Chemical Society* **2005**, 127, 357-365.

[109] A. J. Bard and M. V. Mirkin, "Scanning Electrochemical Microscopy, Second Edition", CRC Press, **2012**.

[110] A. Fernández-Vega, J. M. Feliu, A. Aldaz and J. Clavilier, "Heterogeneous electrocatalysis on well defined platinum surfaces modified by controlled amounts of irreversible adsorbed adatoms. 2. Formic acid oxidation on the Pt(100)-Sb system" *Journal of Electroanalytical Chemistry* **1989**, 258, 101-113.

[111] J. Clavilier, A. Fernández-Vega, J. M. Feliu and A. Aldaz, "Heterogeneous electrocatalysis on well defined platinum surfaces modified by controlled amounts of irreversibly adsorbed adatoms. 1. Formic-acid oxidation on the Pt (111) - Bi system" *Journal of Electroanalytical Chemistry* **1989**, 258, 89-100.

[112] A. Boronat-Gonzalez, E. Herrero and J. M. Feliu, "Fundamental aspects of HCOOH oxidation at platinum single crystal surfaces with basal orientations and modified by irreversibly adsorbed adatoms" *Journal of Solid State Electrochemistry* **2014**, 18, 1181-1193.

[113] A. Lopez-Cudero, F. J. Vidal-Iglesias, J. Solla-Gullon, E. Herrero, A. Aldaz and J. M. Feliu, "Formic acid electrooxidation on Bi-modified Pt(110) single crystal electrodes" *Journal of Electroanalytical Chemistry* **2009**, 637, 63-71.

[114] E. Herrero, J. M. Feliu and A. Aldaz, "Poison formation reaction from formic acid on Pt(100) electrodes modified by irreversibly adsorbed bismuth and antimony " *Journal of Electroanalytical Chemistry* **1994**, 368, 101-108.

[115] E. Herrero, M. J. Llorca, J. M. Feliu and A. Aldaz, "Oxidation of formic acid on Pt(100) electrodes modified by irreversibly adsorbed tellurium" *Journal of Electroanalytical Chemistry* **1995**, 383, 145-154.

[116] V. Climent, E. Herrero and J. M. Feliu, "Electrocatalysis of formic acid and CO oxidation on antimony-modified Pt(111) electrodes" *Electrochimica Acta* **1998**, 44, 1403-1414.

[117] E. Herrero, M. J. Llorca, J. M. Feliu and A. Aldaz, "Oxidation of formic acid on Pt(111) electrodes modified by irreversibly adsorbed tellurium" *Journal of Electroanalytical Chemistry* **1995**, 394, 161-167.

[118] S. A. Campbell and R. Parsons, "Effect of Bi and Sn adatoms on formic acid and methanol oxidation at well defined platinum surfaces" *Journal of the Chemical Society, Faraday Transactions* **1992**, 88, 833-841.

[119] H.-W. Lei, H. Hattori and H. Kita, "Electrocatalysis by Pb adatoms of HCOOH oxidation at Pt(111) in acidic solution" *Electrochimica Acta* **1996**, 41, 1619-1628.

[120] F. J. Vidal-Iglesias, A. López-Cudero, J. Solla-Gullón and J. M. Feliu, "Towards More Active and Stable Electrocatalysts for Formic Acid Electrooxidation: Antimony-Decorated Octahedral Platinum Nanoparticles" *Angewandte Chemie International Edition* **2013**, 52, 964-967.

[121] E. Herrero, J. M. Feliu and A. Aldaz, "Electrocatalysis", in *Encyclopedia of Electrochemistry - Interfacial Kinetics and Mass Transport, vol. 2*, A. J. Bard and M. Stratmann (Eds.) Wiley-VCH Verlag, Weinheim, Germany, **2003**, pp. 443-465.

[122] J. Solla-Gullon, F. J. Vidal-Iglesias and J. M. Feliu, "Shape dependent electrocatalysis" *Annual Reports on the Progress of Chemistry, Section C: Physical Chemistry* **2011**, 107, 263-297.

[123] M. T. M. Koper, "Structure sensitivity and nanoscale effects in electrocatalysis" *Nanoscale* **2011**, 3, 2054-2073.

[124] I. Lee, F. Delbecq, R. Morales, M. A. Albiter and F. Zaera, "Tuning selectivity in catalysis by controlling particle shape" *Nature Materials* **2009**, 8, 132-138.

[125] Q. S. Chen, J. Solla-Gullon, S. G. Sun and J. M. Feliu, "The potential of zero total charge of Pt nanoparticles and polycrystalline electrodes with different surface structure The role of anion adsorption in fundamental electrocatalysis" *Electrochimica Acta* **2010**, 55, 7982-7994.

[126] J.-Y. Lee, D.-H. Kwak, Y.-W. Lee, S. Lee and K.-W. Park, "Synthesis of cubic PtPd alloy nanoparticles as anode electrocatalysts for methanol and formic acid oxidation reactions" *Physical Chemistry Chemical Physics* **2015**, 17, 8642-8648.

[127] J. Solla-Gullón, F. J. Vidal-Iglesias, A. López-Cudero, E. Garnier, J. M. Feliu and A. Aldaz, "Shape-dependent electrocatalysis: methanol and formic acid electrooxidation on preferentially oriented Pt nanoparticles" *Physical Chemistry Chemical Physics* **2008**, 10, 3689-3698.

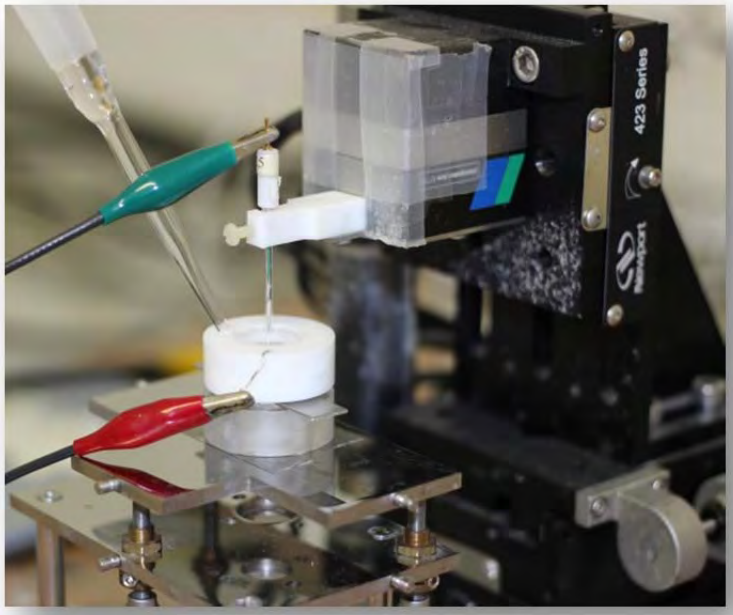

Chapter II

Experimental and Techniques

2. Methods and Experimental Techniques

2.1. Pt single crystal electrode surfaces [1-6]

A single crystal surface is obtained when cutting a Pt crystalized bead in a specific orientation. If we accept that the Pt atoms remain at the same position after the cutting process, then it is possible to obtain an *ideal surface*. If the cutting and polishing process is fine enough it is possible to get single crystal surfaces, which are very similar to the ideal ones and are known as *single crystal surfaces atomically well defined.* These have been traditionally used as a model surfaces in heterogeneous catalysis and electrocatalysis. Metals such as Pt, Au, Pd, Ru or Rh are the most studied in this field; furthermore, extensive characterization of this metals has been done using different electrochemical and spectroscopic techniques.

It is possible to get a geometrical description of the single crystal surface, taking into account the crystallographic axes and planes present within the crystal. Miller indexes are used to define the type of surface from a crystallographic point of view. In particular, platinum presents a face-centered cubic (fcc) crystal structure that only uses three digits enclosed in parentheses (h k l). These correspond to the minimum integers proportional to the inverse value of the intersession between the crystallographic axes and the crystal plane. For instance, assuming that "a, b, c" are the intersession with the crystallographic axes "x, y, z" respectively, then the Miller index of such crystalline surface is given by h, k, l as follows:

$$(h\ k\ l) = \left(\frac{1}{a}\ \frac{1}{b}\ \frac{1}{c}\right) \qquad \textit{Eq. 2.1}$$

In order to simplify the values obtained, it is required to multiply each fraction by the minimum common multiple, so that the final values will be the minimum ratio in an integer value. If the plane does not intercept any of the crystallographic axes, then the corresponding Miller index is cero (0). In contrast, if the interception is negative, a slash is placed above the corresponding digit of the Miller index.

For all materials displaying a fcc structure, for instance Pt and Au, the Miller index determine a vector whose orientation is normal to the plane of the surface. This fact makes easier the calculation of the geometric parameters, for instance, angles between two different surfaces. Figure 2.1 shows the surfaces with low Miller indexes, which correspond to the basal planes for a fcc structure. As can be seen, both the surface structure and atomic density will depend on the crystal organization and the cutting angle. Thus, (111) facet is the most compact surface and shows a hexagonal symmetry. The (100) facet shows a cubic arrangement, while a rectangular structure is characteristic of (110) facets. Hence, the coordination number of the atoms in the surface is clearly different in all three cases, being 9 for the (111) facet, 8 for the (100) and finally 6 for (110) facet, in comparison with a coordination number of 12 in the bulk Pt structure.

The surfaces with low Miller indexes represent the simplest single crystals surfaces and are placed in the stereographic triangle vertex (see figure 2.2). Those are known as the *basal planes*, a only display a single symmetry site. However, it is also possible to get intermediate surfaces between different basal planes, which simultaneously present two kinds of surface symmetry sites, when moving in a specific edge of the stereographic triangle. These surfaces are known as *stepped surfaces*, due to the presence of terraces with the same surface symmetry of the closest basal plane, and monoatomic steps with the same symmetry of the farthest basal plane.

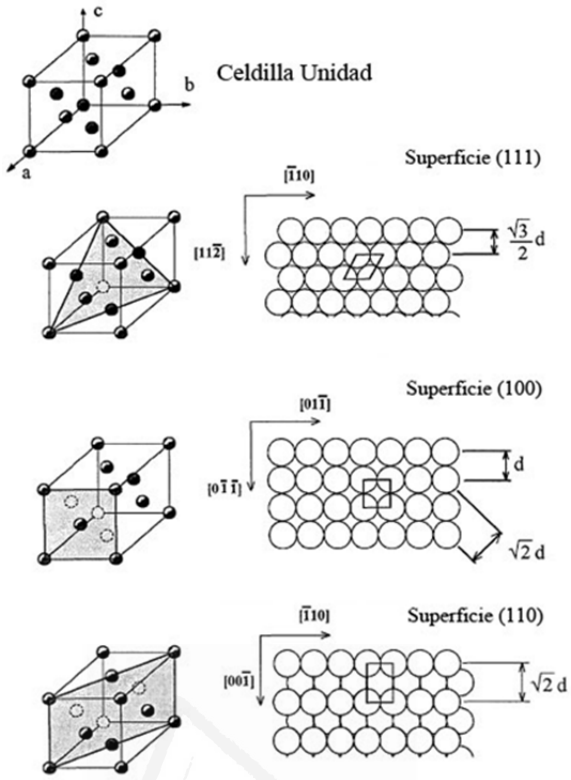

Figure 2.1. Hard spheres model for the basal planes in an fcc crystal. The unit cell and the different lattice parameters, which are related with the Miller index values [1].

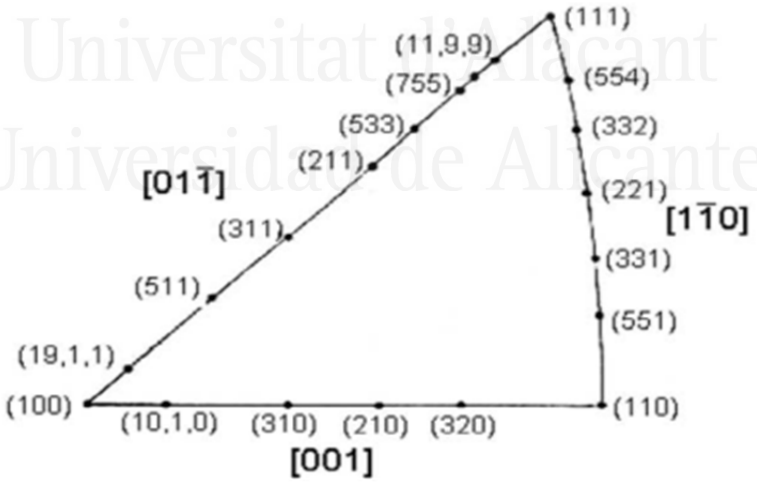

Figure 2.2. Stereographic triangle. The basal planes are in the vertex of the triangle and the stepped surfaces are located in the edges.

From an electrochemical point of view, the electrode surface reactivity depends on the surface structure given that both, the geometry and the electronic surrounding in each one of the surfaces are different. This has been widely demonstrated in a large number of processes. In particular, one of the most studied is the hydrogen under potential deposition (UPD), which is shown as example in figure 2.3.

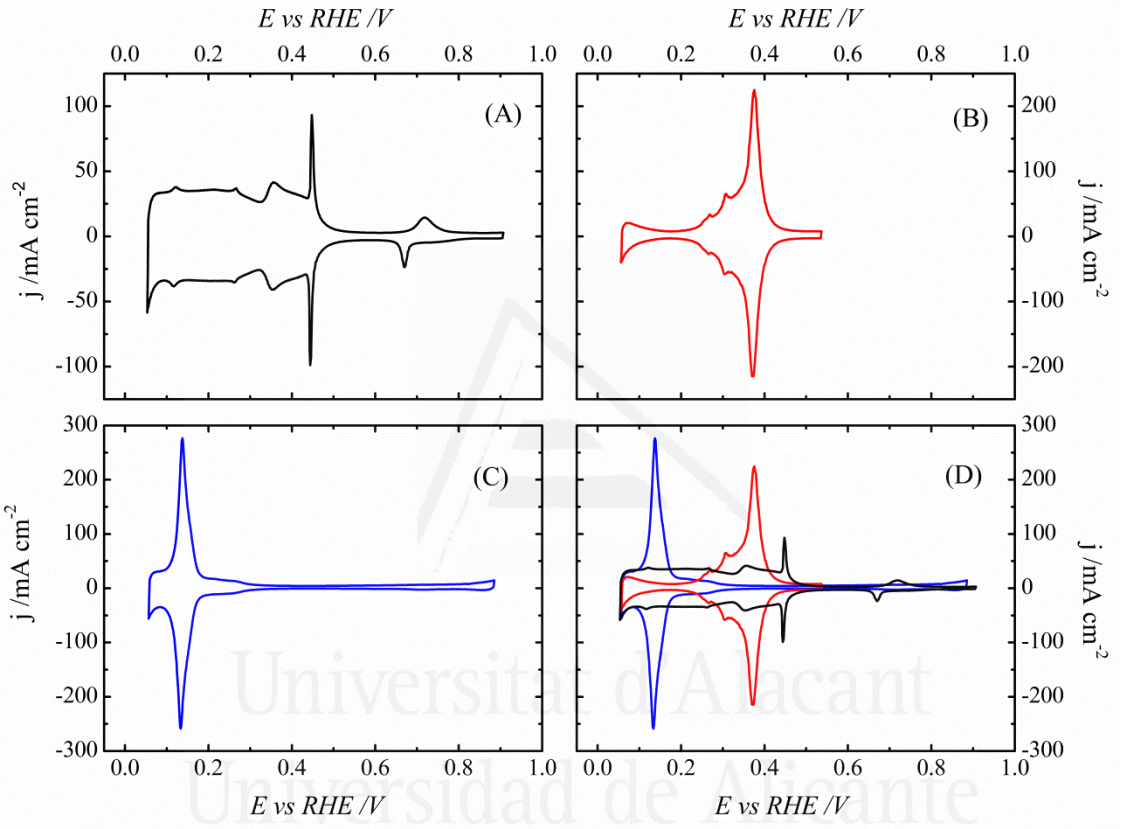

Figure 2.3. Voltammograms of platinum single crystal electrodes in 0.5 M H_2SO_4 solution A) Pt(111), B) Pt(110), C) Pt(100), D) comparison of all three Pt basal planes. Scan rate: 50 mV/s.

Furthermore, those voltammetric profiles in sulfuric solution (figure 2.3) are considered as the fingerprint for each Pt single crystal electrode. On the other hand, it is important to point out that the single crystal surfaces are highly sensitive to small changes in the crystallographic orientation of the electrode and to the species present in the electrolyte solution, especially when they can be adsorbed on the electrode surface.

2.1.1. Preparation of Pt single crystal electrode surfaces

Single crystal electrode surfaces are obtained by orientation, cutting and polishing of spherical platinum beads (figure 2.4), using the method developed by Clavilier [7]. A platinum wire of ca. 0.5 mm in diameter is used to obtain a ball shaped (aprox. 2 mm) crystal, which is formed by heating a platinum wire in a propane-oxygen flame until a ball shaped drop is formed by the high surface tension of the melted platinum metal. The slow cooling of the drop allows the formation of a spherical and crystalline bead. Subsequently, using a goniometer with four axes of rotation and a laser beam, the single crystal is oriented, cut and polished. The cutting process of the electrode is performed using a polishing device placed perpendicular to the axis on the optical bench. Abrasive material such as silicon carbide disks and single crystal diamond paste are used for that purpose.

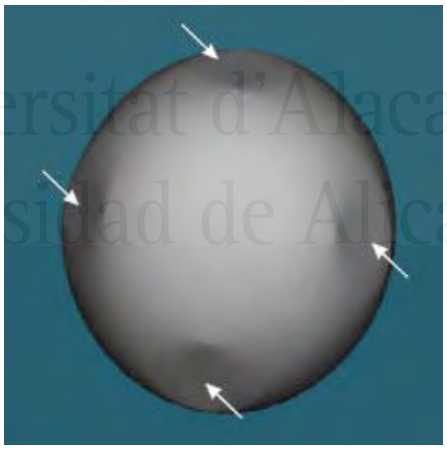

Figure 2.4. Image of a polyoriented Pt bead. The arrows point out the different facets.

Most experiments reported in this doctoral thesis were carried out using single crystal platinum electrodes with low Miller indexes (basal planes), but also some stepped surfaces. In particular, *Pt(111)*, *Pt(100)*, and stepped surface electrodes corresponding to the series

Pt(s)[(n-1)(111)x(110)] and *Pt(s)[n(111)x(100)]*, which are represented in figure 2.5, were used as a model surfaces for studying formic acid oxidation reaction.

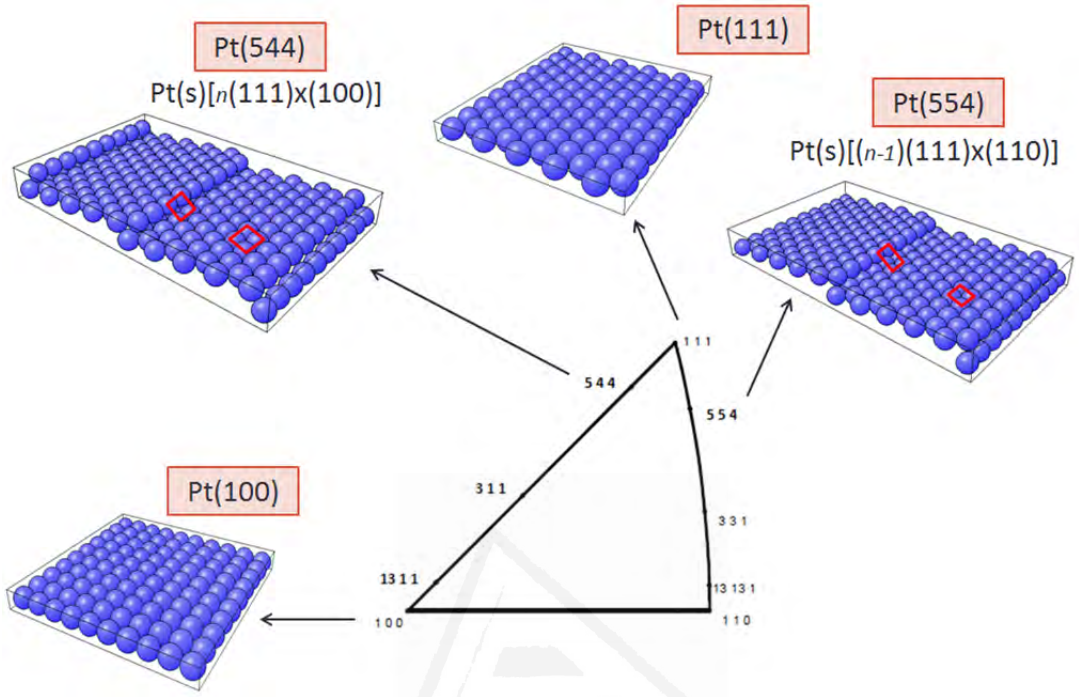

Figure 2.5. Pt single crystal electrodes employed in this thesis.

2.1.2. Surface treatment on Pt single crystal electrodes

One of the most popular methods to clean electrode surfaces involves the implementation of numerous consecutive cycles of oxidation-reduction [8, 9]. However, this kind of cleaning treatment presents some important drawbacks, since it modifies the surface of the single crystal electrode because of the adsorption of oxygen at potentials above 1.0 V [10-12]. Thus, it is only after Clavilier *et al*. [13] presented a new method to clean the Pt electrode surface that Pt single crystal electrodes were reproducible studied. The proposed solution involves the heating treatment of the electrode after polishing, which is capable of oxidizing all species adsorbed on the Pt electrode surface. Additionally, the reached temperature is high enough to reorganize the damaged surface obtained after the polishing process. After the thermal treatment, the surface is protected

with a drop of ultrapure water to avoid the adsorption of any environmental impurity. LEED (low energy electron diffraction) experiments with Pt electrodes treated in this way proved the high quality samples prepared with this procedure [13, 14]. Due to the influence of the adsorption of oxygen at the electrode surface, the use of a reducing atmosphere composed by hydrogen and argon gas is required to prevent oxygen adsorption and to preserve the order in the surface structure. Figure 2.6 shows the scheme of the surface treatment of Pt single crystal electrodes as well as the glassware cleaning procedure.

2.2. Glass material cleaning protocol

An exhaustive cleaning procedure was applied to all glass material used in this work (see figure 2.6):

- Initially, all glass material is immersed in a potassium permanganate solution overnight, or at least during 12 hours. In this way, all organic compounds are oxidized and eliminated in a subsequent treatment.
- The glass material is then taken out from the oxidant solution, and is rinsed thoroughly with water and a hydrogen peroxide solution, which is used to reduce manganese species coming from the precedent process. After that, the material is washed with ultra-pure water.
- Once the material is washed, this is placed into a hot plate to boil ultra-pure water several times, in order to eliminate completely any impurity coming from the walls of the glassware. Between each boiling cycle, a rinsed process using ultra-pure water is applied. This boiling process is repeated three times at least.

- After this cleaning procedure, the material is ready to be used in voltammetric experiments. It is important to point out that, at any moment the glassware must be filled with ultrapure water to avoid further contamination.

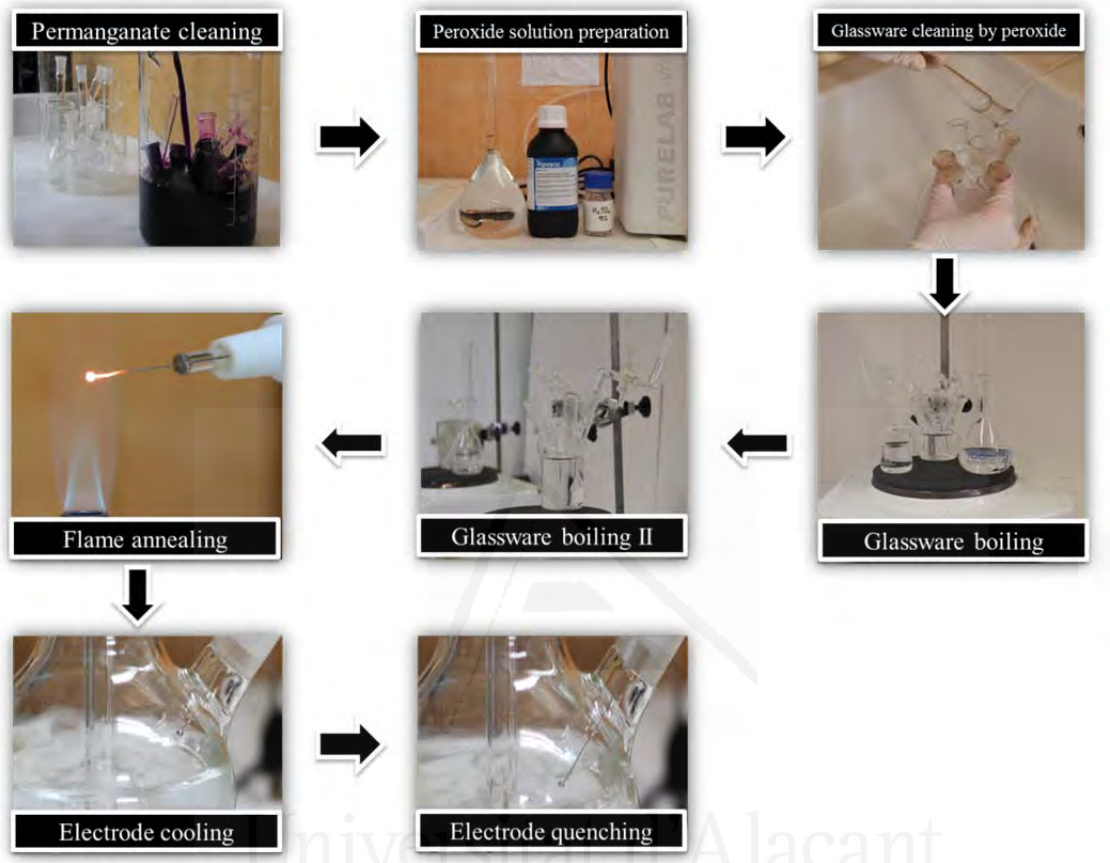

Figure 2.6. Scheme of the glassware and Pt single crystal electrode cleaning protocol before any electrochemistry experiment.

2.3. Shape controlled Pt nanoparticles

For practical applications of platinum electrodes in fuel cells, it is necessary to disperse platinum on a support, generally carbon, in order to increase the exposed area/mass ratio on the platinum catalyst. In this sense, nanoparticles are the most promising materials for real applications in electrocatalysis. The use of nanomaterials in electrocatalysis has had a great importance, mainly in the development of fuel cells. Since the early 70´s, it can be found patents describing platinum nanoparticles used in the developments of fuel cells [15-

18]. Nevertheless, there are still many aspects not optimized yet. The size and surface structure are probably the most important among of them, and for this reason they are extensively and widely studied nowadays.

In the field of nanoparticles is important to control the size of the particle to increase the area/mass ratio, but also to tune the electronic properties of nanoparticles, since they depend on their size. However, it is also relevant to control the nanoparticles surface structure, since adsorption phenomena and electron transfer also depend on the surface structure and orientation of the nanoparticles [15, 19]. Similarly to what is done with single crystal surfaces, there is an intrinsic triangle that connects the symmetry of the facets on nanoparticles and its shape [20], as is shown in figure 2.7. Here, the three vertices represent the coordinates of polyhedral nanocrystals bounded by low index plane facets. Thus, cube, an octahedron and rhombic dodecahedron present mainly (100), (111) and (110) symmetry facets, respectively [20, 21].

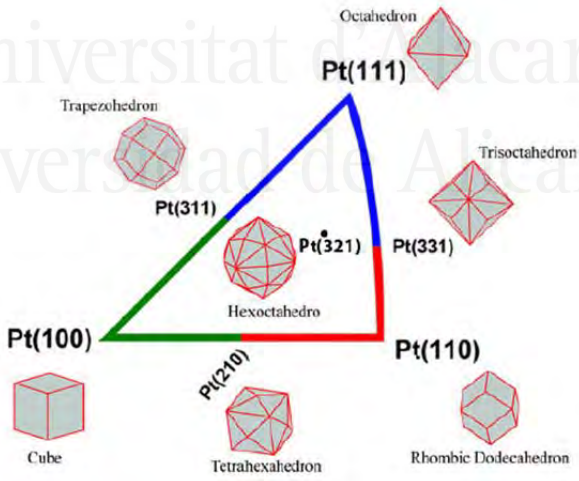

Figure 2.7. The stereographic triangle of polyhedral nanocrystals bounded by different crystal planes taken from [20].

A few years ago, several methods for nanoparticles synthesis controlling their size, shape and surface orientation were developed [22, 23]. These consisted in using some organic compounds, which act as a surfactant, added to a platinum precursor like K_2PtCl_4 to produce a Pt colloidal suspension [24-26]. Then, the platinum precursor is reduced using a reducing agent like hydrogen gas. The nanoparticles prepared in this way are then cleaned using different solutions, and finally washed with enough pure water. Depending on the orientation expected on the nanoparticle, the precursor employed may be different, and also other additional reagents to control the nucleation and growth of the nanoparticle with a specific shape could be added together with the metallic precursor. Despite of the success using this synthesis method, many of these procedures implies adding organic compounds in solution, which are difficult to remove form the Pt nanoparticles surface [15, 27] afterwards. Thus, the presence of those organic compounds adsorbed on the Pt nanoparticles surface limits the use of nanoparticles as electrochemical catalysts. Fortunately, Solla-Gullón et al. [28-30] have recently developed chemical methods of cleaning, which does not affect the surface structure of Pt nanoparticles. These methods are important in obtaining cleaning nanostructured catalysts surfaces without changing the shaped-controlled surface structure.

2.3.1. Synthesis of Pt nanoparticles (NPs)

The spherical polyoriented platinum nanoparticles were synthesized by reduction of H_2PtCl_6 with borohydride using a water in oil (w/o) microemulsion of water/polyethylene glycol-dodecylether (BRIJ® 30)/n-heptane. They were cleaned with acetone and ultrapure water.

For the shape controlled Pt nanoparticles, tree different methods of synthesis were used:

- Pt nanoparticles with preferential cubic shape were synthesized with a colloidal method using sodium polyacrylate (PA, Mw = 2100) as a capping agent and K_2PtCl_4 as a metallic precursor (10^{-4} M aqueous aged solution) [24-26]. This colloidal suspension was bubbled with H_2 gas for 5 min to reduce the Pt precursor. After complete reduction (12-14 hours) these Pt NPs were cleaned with strong alkaline aqueous solution followed by several water washes.
- Pt nanoparticles with preferential octahedral and tetrahedral shape were synthesized by a colloidal method using PA as a capping agent and H_2PtCl_6 as a metallic precursor (10^{-4} M aqueous aged solution) [24-26]. The suspension initial pH (around 8) was adjusted to 7 with 0.1 M HCl solution. This colloidal suspension obtained was bubbled with H_2 gas for 1 min to reduce the Pt precursor. After complete reduction (12-14 hours) these Pt NPs were cleaned with strong alkaline aqueous solution followed by several water washes.

2.4. Cyclic voltammetry

Cyclic voltammetry is a powerful electrochemical technique used to study an electroactive substance in solution or adsorbed on the electrode surface. Using a voltammogram it is possible to get valuable information about the electrochemical behavior of the system. Moreover, it is possible to characterize the reaction and determine whether it is controlled by diffusion, kinetics or surface adsorption. This technique consists of recording the current that flows through the working electrode when a potential sweep is applied. The potential sweep is linear in the time scale, which is achieved by introducing a

triangle signal, whose slope (in absolute value) represents the scan rate, *v*, i.e., the excitation signal change linearly from an initial potential (E_i) to a final one (E_λ), called inversion potential, where the scan direction is reversed until the initial potential is reached again (see figure 2.8) [31, 32]. The scan could be initiated in any direction (positive or negative), and the cycle can be repeated as much as needed.

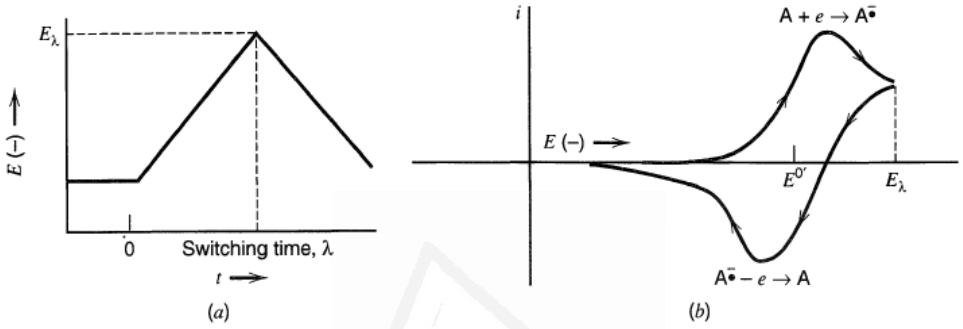

Figure 2.8. (a) Exciting signal from an initial potential to a final on, passing for E_λ. (b) Response to the perturbation in current vs. potential [33].

From now on in this thesis, the general electrochemical reaction used is:

$$A_{sol}^{-} \leftrightarrow A_{sol} + e^{-} \qquad \textit{Eq. 2.2}$$

When a potentiodinamic perturbation is applied to this system, so that the scan is initiated in the positive direction, a potential will be reached where the oxidation reaction will begin. Then, the recorded current will start increasing with a cuasiexponencial shape (see figure 2.9). In the initial part of the curve, the current is controlled by the electron transfer kinetics. Then, when some of the reactant species close to the electrode surface are consumed by the process, the current will depend on the electron transfer kinetics and the diffusion of the electroactive species from the bulk solution to the electrode surface. This region is known as mixed control zone. Finally, the current reach a maximum and start

decreasing due to the depletion of the species in the interfacial region. In this point, the current depends only on the diffusion of the electroactive species to the electrode surface.

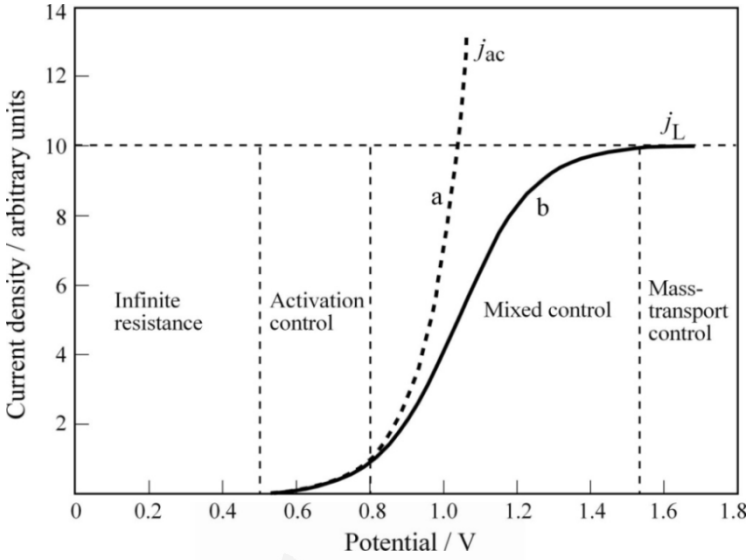

Figure 2.9. Schematic j/E plot for a model for an oxidation reaction. The minimum potential for dc current flow is 0.56 V (onset of oxidation). There are three main specific areas: Activation control (*electron transfer control*); *mixed control* (a mixture between electron transfer and mass control) and *mass transport control*. Adapted from [34].

Once reached the upper potential value, the scan direction is inverted and cathodic current profile due to the reduction of the A species formed is obtained (see figure 2.8). The maximum current in both sweeps are known as peak current (I_{pa} and I_{pc})

When the species involved in the electrochemical process are adsorbed on the electrode surface, as shown in the following reaction,:

$$A_{ads} + e^{-} \leftrightarrow A_{ads}^{-} \qquad \textit{Eq. 2.3}$$

the shape of the voltammogram changes. The following equation describes the electron transfer process on the electrode surface under those conditions [33]:

$$j = nF\frac{d\Gamma_R}{dt} = nF\frac{d\Gamma_O}{dE}v \qquad \textit{Eq. 2.4}$$

where j is the current density, Γ_R and Γ_O are the coverage of the species A_{ads} and A^-_{ads} respectively, in mol cm^{-2}, and v is the scan rate. It is important to notice that the current density is directly proportional to the scan rate, which is a diagnosis method to determine whether the reaction is being controlled by surface adsorption or a diffusion process. In this latter case, the current is proportional to the root square of the scan rate. Thus, if the process is completely reversible and controlled by surface adsorption, the current is given by:

$$j = \left[\frac{\exp\left\{ \frac{nF}{RT}\left(E - E^0\right)\right\}}{\left(1+\exp\left\{ \frac{nF}{RT}\left(E - E^0\right)\right\}\right)^2} \right]\left(\frac{nF}{RT}\right)v \qquad \textit{Eq. 2.5}$$

Figure 2.10 shows the simulation of the voltammetric response using the equation 2.5. Assuming n=1 and lack of lateral interactions (Langmuir isotherm), the peak potentials in both scan directions are the same, due to the lack of diffusive limitations and the high rate of the electron transfer.

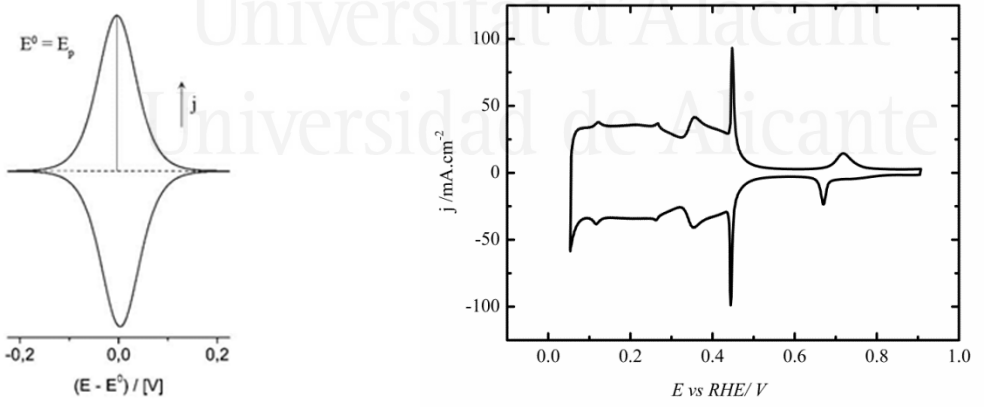

(a) (b)

Figure 2.10. (a) Current vs. Potential response for the oxidation and reduction of an adsorbed species on the electrode surface. The adsorption phenomenon follows a Langmuir isotherm. (b) Voltammetric profile for a Pt(111) electrode in sulphuric acid solution, showing the different hydrogen and anion adsorption-desorption regions.

2.4.1. Electrochemical cell

Most of the experiments were carried out using three electrodes, and a two-compartment electrochemical cell. In the main compartment, which contains the working solution, the counter and working electrodes are placed. The last one is a Pt single crystal electrode or Pt NPs deposited in a proper support. In the second compartment, separated from the first one by a Luggin capillary, a reversible hydrogen electrode (RHE), used as a reference, is placed. Thus all electrode potentials shown in this thesis are quoted vs. the RHE (see figure 2.11)

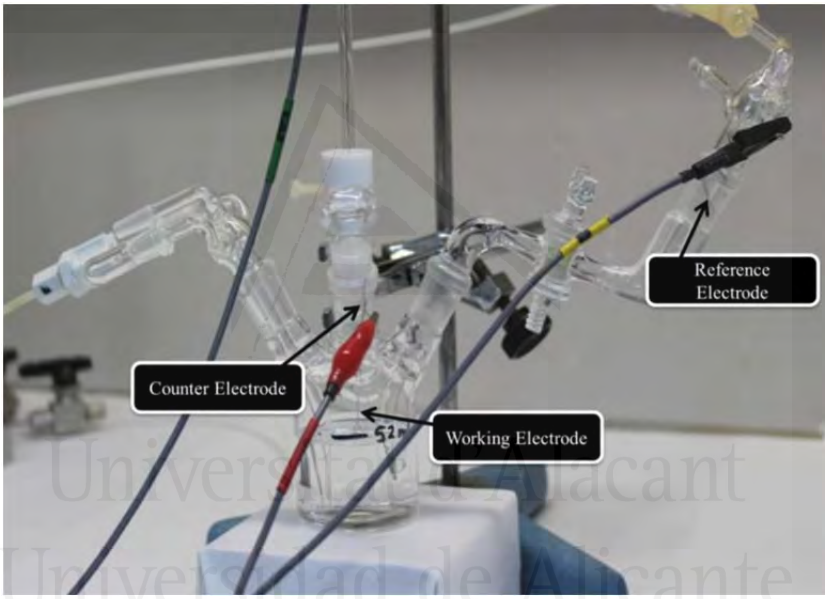

Figure 2.11. Image of the experimental set up for voltammetry.

The working solution is deoxygenated bubbling with $Ar_{(g)}$ by a period of 10 minutes before starting. During the experiment, an argon atmosphere is kept into the cell, in order to minimize the oxygen dissolution.

Before each experiment, all Pt electrodes are heat around 15 seconds in a propane-air flame to reorder the surface atoms and to eliminate any impurity adsorbed on their surface.

After this, the electrode is immediately transferred to a balloon filled with ultrapure water in equilibrium with an atmosphere composed by a mixture of argon and hydrogen gas. The electrode is cooled in this controlled atmosphere to ensure a surface order as high as possible. Once the electrode is cooled, is immersed in the ultrapure water in order to protect the electrode surface while is being transferred to the electrochemical cell. The electrode is immersed in the solution at controlled potential, in a meniscus configuration, so that, the only part of the electrode in contact with the solution is the face of interest. Once this procedure is completed, the electrochemical experiment is run.

2.5. Pulsed voltammetry

This voltammetric technique was firstly used to study electrocatalytic reactions on Pt single crystal electrodes by Clavilier [35]. This involves a pulsed potential program applied over a potential slope, keeping constant the applied upper potential limit, which should be high enough to produce total oxidation of the poison intermediate adsorbed on the Pt electrode surface, but preventing its surface oxidation.

Figure 2.12 presents the pulse programs used in this work. The (a) section is a typical pulsed program, which consists of a pulsed potential scan acquired by repetition of the following sequence: 0.85 V pulse kept for 1 s in order to clean by oxidation the electrode surface from any poison intermediate. Then, the electrode potential is pulsed to the potential value where the kinetics of the reaction is going to be measured for 1 s. After that, the electrode potential is set back to 0.85 V again, and the cycle is repeated, but changing the potential value (20 mV increase) for the measurements in each new cycle. The transient current measured at the sampling potential is used to obtain kinetic parameters, after fitting by the proper kinetic model. In the case of the FAOR, the intrinsic

current through the active reaction intermediate and the poisoning rate of the Pt electrode are obtained from those pulsed voltammetry experiments.

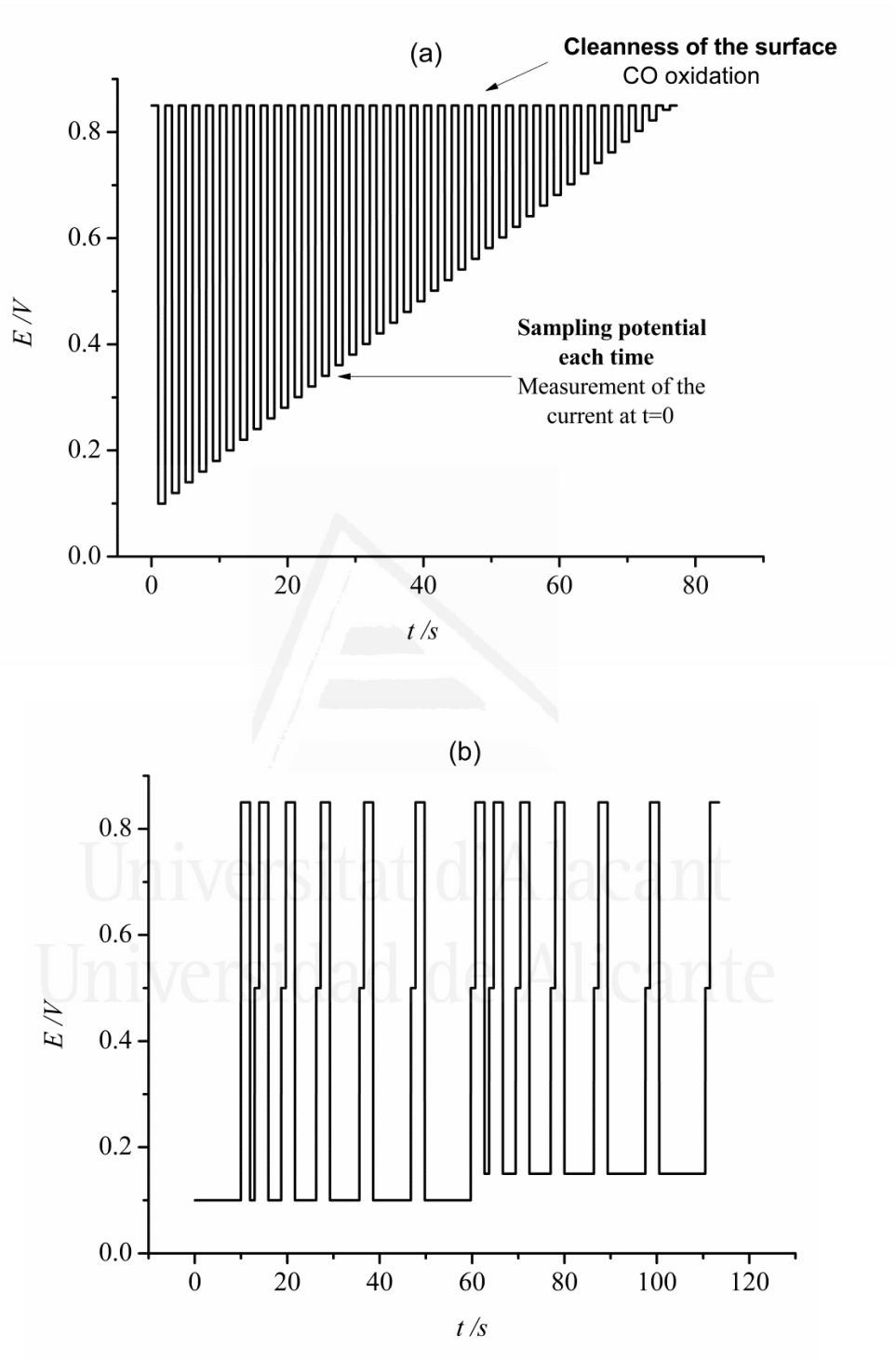

Figure 2.12. Potential program used in the pulsed voltammetry experiments. (a) Potential program used to measure transients at E>0.3 V (b) Potential program used to determine the poison reaction kinetics in stepped surfaces at potentials between 0.1 V and 0.35 V.

However, when the oxidation currents for FAOR are negligible, it is not possible to obtain poisoning rates at those potentials. In this case, a different potential program presented in figure 2.12(b) is applied. The potential program involves one initial pulse for 1 s to 0.85 V to clean the electrode surface. Then, the potential is stepped to the potential value where CO formation is studied for different times and finally the potential is pulsed to 0.5 V where the corresponding transient is recorded during 1 s [36, 37]. The current measured at 0.5 V for different time at the CO formation potentials are used to obtain the poisoning kinetics.

2.6. Rotating disk electrode (RDE) voltammetry [31, 38, 39]

This voltammetric technique is widely used in electrochemistry for measuring electron transfer kinetics for reactions controlled by mass transport. Additionally, it is possible to determine diffusion coefficients for the electroactive species. The equipment used in this case consist in a working electrode, which is a metal disk surrounded by an insulating holder. The disk with its holder is rotated by an electric motor, and rotation is along the vertical axis that passes through the centre of the disk. When the disk rotates, the liquid that is in contact with the surface of the disk electrode is spelled away to its sides, and a new portion of liquid is brought to the centre of the disk from the bulk solution. Figure 2.13 shows the parameter that accounts for the transport regime of the solution in a typical RDE experiment. According to the hydrodynamic theory for laminar flows, near the rotating surface of the disk electrode, a boundary layer with a constant thickness (δ_{bl}) appears. Moreover, a monotone change of the liquid transport speed with respect to the electrode surface is displayed. Then, closer to the electrode surface the role played by diffusion in mass transport is more relevant. So, changes in the concentration of the

reagents near the electrode surface are caused by the diffusion of the electroactive species in the moving liquid. In this sense, the current density (the reaction kinetic) only depends on the diffusion of the electroactive species, making possible to measure limiting currents, due to the accomplishment of stationary conditions.

Thus, in excess of supporting electrolyte, when migration transport is neglected, as usually happens in most electrochemical experiments, Levich equation can be applied to calculate the current (j) measured in RDE experiments:

$$j = \pm 0.62\, nF D_k^{2/3} \omega^{1/2} v^{-1/6} (c_k^0 - c_k^s) \qquad \textit{Eq. 2.6}$$

where F is the Faraday constant; n, the number of electrons exchanged in the electrode process; D_k, the diffusion constant; ω, the radial speed of the rotating electrode; v, kinematic viscosity of the solution; c_k^s, the concentration of the reactant on the surface; c_k^0, the concentration of the reactant in the bulk, and the number 0.62 includes some integration factors.

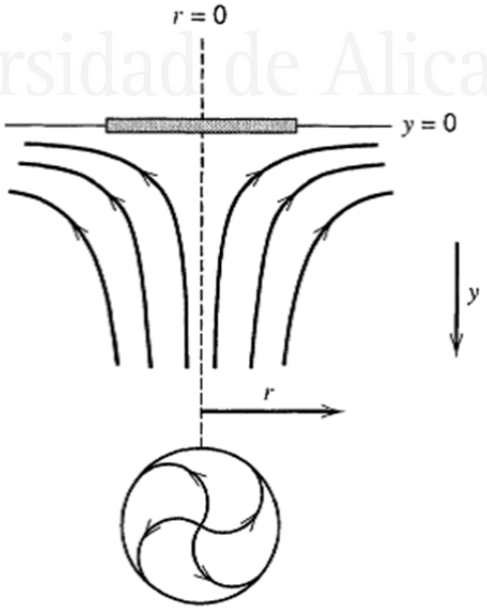

Figure 2.13. Laminar flow regime of the solution through the disk electrode surface [40].

During high polarization, when the current reaches its maximum value, then, the concentration of the reagent close to the surface becomes zero and *Eq. 2.6* transforms into:

$$j_{lim} = \pm 0.62\, nFD_k^{2/3}\omega^{1/2}\nu^{-1/6}\, c_k^0 \qquad \textit{Eq. 2.7}$$

The electrolyte transport regime achieved in RDE experiments does not change the form of the corresponding polarization curve for mass transport controlled process as a function of the electrode rotation speed, but increases the limiting current achieved and decreases the time needed to reach the stationary state (from minutes to less than a second).

RDE experiments are very useful to identify the limiting step in the electrochemical reaction under study, since when the slowest reaction step is the mass-transport process, the current density will be proportional to square root of the rotating speed and on the contrary, if the limiting current does not change with rotation speed, the process does not present diffusion limitations. For the experiments carried out in this doctoral thesis, the RDE voltammetry has been used to ensure a constant flow of electroactive species to the electrode surface, and to corroborate that the current in FAOR does not depend on the mass-transport conditions.

All voltammetric experiments described in sections 2.4, 2.5 and 2.6 were carried out by a potentiostat eDAQ model EA161 attached to an e-Recorder model ED401. In particular, for pulsed voltammetry experiments, a function generator RIGOL DG 3061A was added to the system. Additionally, a PolyScience thermostatic bath was used to control the temperature of the electrochemical cell in the range between 5 and 45ºC. For the RDE experiments, a rotating motor supplied by Radiometer Analytical (Model EDI101) was used. When Pt single crystal electrodes were used as a working electrodes in RDE experiments, those electrodes were attached to the holder, so that the rotation axis

remained normal to the surface and were immersed in the electrolyte solution in a meniscus configuration.

2.7. Fourier Transformed Infrared Reflectance Absorption Spectroscopy (FT-IRRAS)

This spectroscopic technique is based on the analysis of the light (infrared) intensity reflected by a metal surface in contact with a solution, as a function of the wavelength of the incident radiation. The absorption from the molecules on the electrode surface depends on the interaction between the electric field from the beam and the dipolar moment of the molecule.

When a light beam is reflected in a metal surface, the amplitude of the electric field on the surface is the vector sum of the electric field coming from the incident and reflected beams. As shown in figure 2.14(A), the light radiation suffers a phase change of ca. 180º when the polarization plane is perpendicular to the reflection plane (*s* polarization). On the other hand, for a parallel polarization light (*p* polarization) the phase change is almost zero at all incident angles. The consequence of this fact influences the intensity of the normalized electric field on the metal surface, which is maximum at a specific angle (c.a. 80º) for the *p*-polarized incident light (figure 2.14(B)). Furthermore, for the *s*-polarized light, the electric field is almost zero. This is the origin of the surface selection rule, fundamental for this technique: with *p*-polarized light, only the vibrational modes that imply a change in the molecular dipole moment perpendicular to the surface are active in infrared reflection adsorption spectroscopy (IRRAS), meanwhile with *s*-polarized light, only bands resulting from molecular vibrations of species in solution are visible.

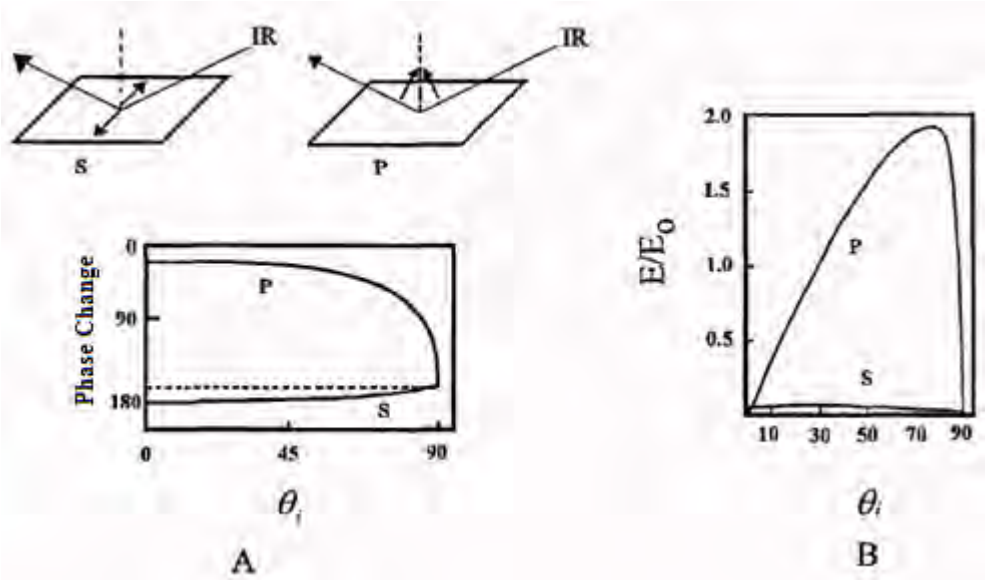

Figure 2.14. (A) Phase change of the electromagnetic radiation with *p* and *s*-polarized light, when is reflected at a metal surface, as function of the incident angle. (B) Electric field normalized on the metal surface, as a function of the incident angle. Figure taken from [41].

The main advantages of using this technique are:

- It allows identifying the chemical nature of the species at the electrode-solution interface, making differences between adsorbed and solution species. In some cases, the band intensity can be used to estimate the surface concentration of the spectroscopically active molecule.
- It can provide information about the adsorption geometry of the molecule on the electrode surface, by taking into account the analysis of the vibrational frequencies and the variation of this parameter as a function of electrode potential.
- It can provide some structural information about the double layer, analysing the shape of the absorption bands.

The detection of the infrared absorbances by submonolayer quantities of species on the electrode surface requires a high level of sensitivity (in most of the cases, transmittance values for the species of interest are in the range of 0.1 to 0.01%). To reach those sensitivity requirements, the adsorption from the solvent should be minimized. One way to achieve it is by decreasing the thickness of the liquid layer, which the light radiation crosses through. For this purpose, the thin solution layer configuration is used. A typical working cell used in IRRAS experiments is presented in figure 2.15. It can be observed that the working electrode (which is often a Pt cut bead) is pressed against a prismatic window, typically CaF_2, so that a 1 to 5 μm liquid thin layer is obtained to perform the spectroelectrochemical measurements (see inset in figure 2.15).

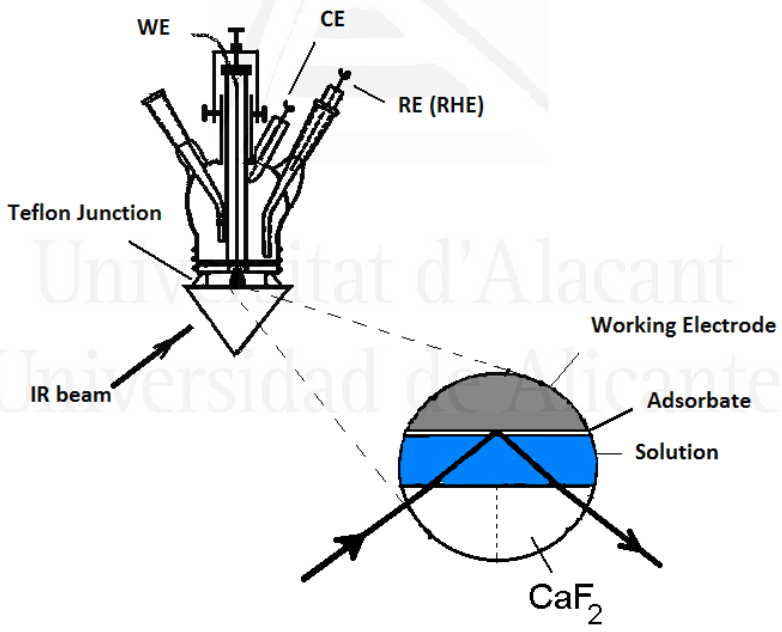

Figure 2.15. Schematic representation of the cell used for the in situ FTIR experiments.

The change of the electrode potential between two values (E_1 and E_2) produces a modulation of the composition in the interfacial electrode-solution region. Figure 2.16 shows the spectrum for a typical FT-IRRAS experiment, where a constant potential (E_{REF})

is selected as reference and the other potential (E_1) varies in the whole range of interest. The infrared signal is measured as a change in reflectivity of the electrode surface by comparing the signals at both potentials (ΔR), and the difference spectrum is obtained by rationing ΔR against the total reflectivity, R. For the small changes that are typically observed in those experiments, $\Delta R/R$ is equivalent to the change in absorbance.

$$A = -\log\left(\frac{R}{R_0}\right) = -\log\left(1 + \frac{R - R_0}{R_0}\right) \cong -\frac{\Delta R}{R_0} \qquad \textit{Eq. 2.8}$$

Figure 2.16 shows schematically the result of subtracting the reflectance at two different potentials.

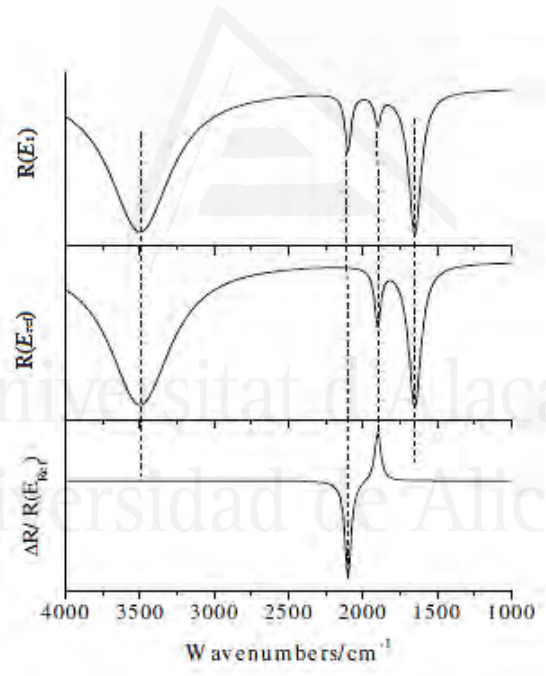

Figure 2.16. Resulting spectrum obtained after subtracting two spectra obtained for different potentials, E_{ref}, reference potential and E_1.

In this doctoral thesis, all the in situ FTIR spectra were acquired using a Nicolet (Model 8700) spectrometer, equipped with an MCT (Mercury - Cadmium–Telluride) detector. The spectroelectrochemical cell is fitted with a prismatic 601 CaF_2 window, as

described previously [42]. The spectra, obtained from the average of 100 interferograms using a resolution of 8 cm^{-1}, were collected at fixed potential intervals. All potentials were measured against RHE. For all FT-IRRAS experiments, *p*-polarized light was employed, since the identification of adsorbed species at the Pt electrode surface during FAO reaction was the main interest of that spectroelectrochemical study.

2.8. Scanning Electrochemical Microscopy (SECM)

This probe technique has emerged as a promising electroanalytical tool to study a wide number of interfacial processes with high temporal and spatial resolution. SECM mainly employs an ultramicroelectrode (UME) or a micropipette probe (tip) to induce chemical changes and collect electrochemical information while approaching or scanning the surface of interest (substrate). This technique provides the great advantage of mapping topography, but also the chemical reactivity of the substrate material, as well as the ability of measuring very rapid heterogeneous electron transfer reaction rates, because of the high rate of mass transfer at the tip and the substrate, and, because it is a steady state measurement with low currents, which are not affected by uncompensated resistance and electrode double layer capacitance.

Initially, SECM applications were mainly based on the feedback current recorded when a redox mediator diffuses in solution within the gap between an UME acting as a tip, and a substrate of interest. However, in the past decades, other modes of actuation in SECM have been developed beyond the initial feedback mode. Thus, in principle, the different modes of SECM can be divided in two main groups: i) Modes based on electrochemically generated reactants, which include tip generation-substrate collection (TG/SC), substrate generation-tip collection (SG/TC), and redox competition (RC) modes,

and ii) Modes based on non-electrochemically generated reactants, namely the micropipette delivery-substrate collection (MD/SC) mode.

As is shown in the figure 2.17, the SECM tip is attached to a 3D motor positioner using stepper or piezo motors depending on the displacement resolution required, which is controlled by a computer. A bipotentiostat controls the potentials of the tip and/or the substrate versus the reference electrode. Most SECM modes of operation can be performed using essentially this experimental setup.

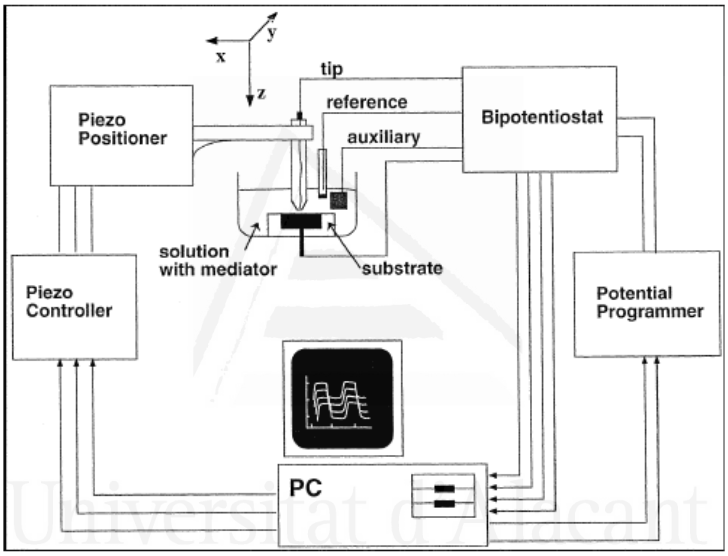

Figure 2.17. Schematic diagram of the SECM setup [43].

2.8.1. SECM working modes

2.8.1.1. Feedback mode

This mode is very useful for controlling the tip-substrate distance. For instance, assuming that a redox-active species, O, is electrogenerated by oxidation from a precursor solution species, R, at the UME tip, which produces a steady-state current at the UME only limited by hemispherical diffusion as is described in figure 2.18.A. Two different behaviours in the tip current could be observed when the tip approaches the substrate

electrode within an electrolytic solution: i) when the tip approaches a conductive substrate, the oxidized species O electrogenerated at the tip may be reduced back to R at the conductive substrate electrode surface depending on the substrate potential, yielding an increase in the tip current and creating a regenerative "positive" feedback loop (figure 2.18.B). The opposite effect is observed when the tip approaches insulating surfaces, as the reduced species R cannot be regenerated and diffusion to the tip UME is inhibited because the close presence of the substrate, which blocks R diffusion. Thus, a "negative" feedback loop is obtained, promoting a decrease in the tip current when approaching an insulator substrate (figure 2.18.C). In addition to the estimation of the tip-substrate distance, the feedback mode results very useful in the elimination of any tilt at the substrate electrode before SECM imaging experiments.

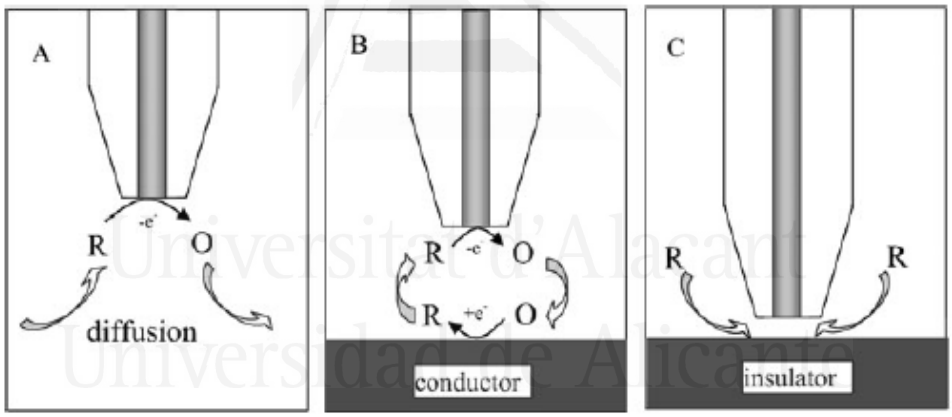

Figure 2.18. Feedback mode of the SECM operation. (A) The UME tip is far from the substrate. (B) Positive feedback: species R is regenerated at the substrate. (C) Negative feedback: diffusion of R to the tip is hindered by the substrate [44].

2.8.1.2. Collection-generation modes

Collection-generation modes are extensively used in electrocatalysis. On the one hand, the TG/SC mode has been successfully used for rapid screening of different micro- and nano-sized bimetallic materials as catalysts for different electrocatalytic reactions,

including the screening of nanoparticles with preferential surface structure [45-47] . In TG/SC mode (figure 2.19.A), the tip is held at a constant potential to electrogenerate under diffusion control conditions the reactant of interest, which is not present in solution initially and is represented as the electroactive species R. After R is generated, the tip is set at a distance where the effective diffusion of R to the substrate is possible and the substrate is held at a proper potential to promote the conversion of R into an oxidized O species. The resulting current at the substrate is "collected" and is directly related with the conversion rate R into O. On the other hand, the reciprocal to this is the SG/TC mode, where the substrate generates a species that is detected at the tip (figure 2.19.B). This mode has been mainly employed for obtaining mechanistic information, such as the number of electrons transferred during the reaction or for detecting short lifetime reaction intermediates. This is because the SG/TC mode does not correspond to a time independent measurement as the TG/SC does.

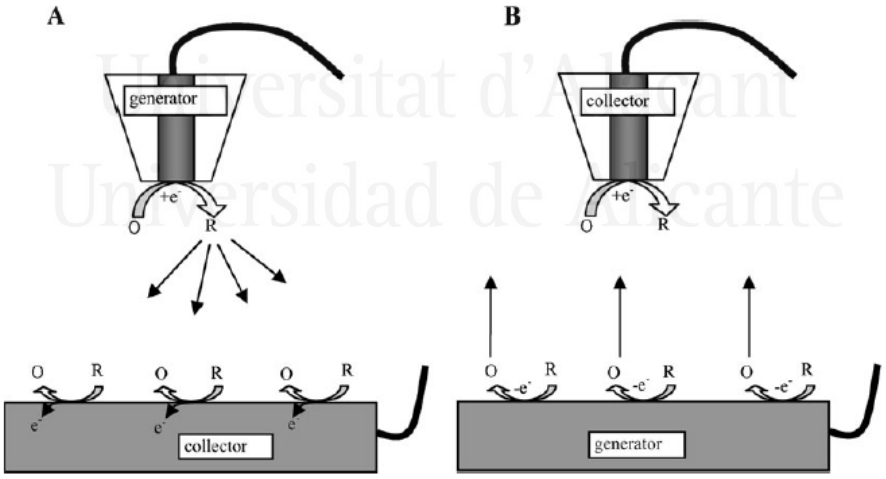

Figure 2.19. Scheme of TG/SC mode (A) and SG/TC mode (B). (A) The tip generates species R by reduction of O in solution; R diffuses toward the substrate and is reoxidized to O. (B) O is electrogenerated at the substrate surface and collected at the tip. The tip and substrate currents are recorded in both cases [44].

2.8.1.3. Micropipette delivered-substrate collection [44, 48, 49]

Despite of the versatility of the working modes revised above, its feasibility seems to be limited by the use of substances that can be electrochemically generated in an UME. For this reason, a new working mode has been proposed, which involves the controlled release of the reactive of interest from a glass micropipette (d < 50 μm). The MD/SC mode was conceived to deliver different neutral species of interest in the vicinity of an electrode, in analogous way to the TG/SC mode, but substituting the UME for a micropipette [50]. The MD/SC mode is based on the exchange of a neutral species of interest (such as HCOOH) across two immiscible solvents (organic and aqueous media) through a liquid-liquid interface. Thus, HCOOH is placed inside the micropipette diluted in an organic solvent (immiscible with water). The transport of HCOOH from the micropipette solution towards the outside solution through the liquid/liquid interphase located at the micropipette apex is perfectly controlled by the partition coefficient of HCOOH between the two immiscible solvents. Once the HCOOH is released, this diffuses near the substrate, where the electrochemical conversion takes place if the substrate is active for FAOR at the applied potential. The amount of electroactive species delivered in solution depends on its specific partition coefficient, and also on the micropipette aperture diameter. The SECM imaging by the MD/SC mode applied to study FAOR used in this doctoral thesis is schematically shown in figure 2.20.

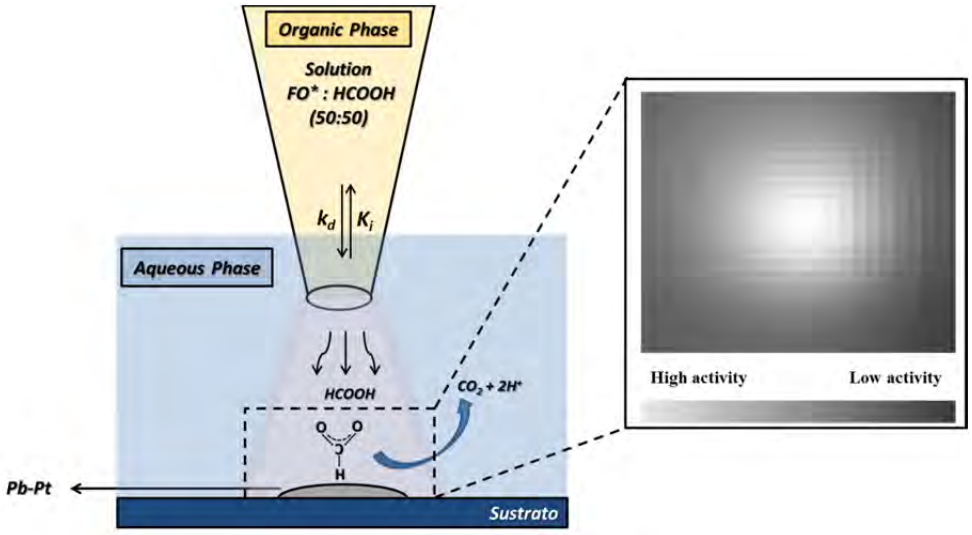

Figure 2.20. Scheme of the imaging process in SECM, using the MD/SC working mode. In the inset is shown the map of activity for an electrocatalyst spot active for formic acid oxidation. k_d y k_i represent the partition rate constants of the HCOOH between two immiscible solventss. [FO* stands for organic phase].

To perform the SECM experiments, a scanning electrochemical microscope CHI 910B from CH Instrument was used. An especial 2 mL Teflon cell with a hole to place the substrate electrode was also used. All approach experiments were performed using an Au UME of 25 µm in diameter provided by CH Instrument. To prepare the micropipettes, borosilicate capillary were pulled using a Puller P-2000 from Sutter Instrument Co, verifying the diameter aperture using an optical microscope BA200 from Motic. Typical micropipette micrographs are shown in figure 2.21, where an empty (a) and filled (b) micropipette are presented.

Figure 2.21. Glass micropipette prepared and silanized before (a) and after (b) filled with FA:DCE (50:50) solution.

2.9. Solutions and reagents

All solutions were prepared using ultrapure water obtained from ELGA PureLab Ultra system (resistivity > 18 MΩ cm at 25 ºC). The reagents and gases used in this thesis are listed in the Table 2.1.

Table 2.1. Reagents used in the thesis work.

Reagent	Formula	Grade	Company
Perchloric acid	$HClO_4$	Suprapur®	Merk
Sulfuric acid	H_2SO_4	Suprapur®	Merk
Sodium perchlorate	$NaClO_4$	Suprapur®	Sigma-Aldrich®
Acetic acid	$C_2H_4O_2$	GR for Analysis 96%	Merk
Phosphoric acid	H_3PO_4	Suprapur®	Merk
Sodium dihydrogen phosphate	NaH_2PO_4	Suprapur®	Merk
Disodium hydrogen phosphate	Na_2HPO_4	Suprapur®	Merk
Thallium(I) sulfate	Tl_2SO_4	99.995 %	Sigma-Aldrich®
Bismuth oxide	Bi_2O_3	Extra pure	Merk
Lead perchlorate hydrated	$Pb(ClO_4)_2 \bullet H_2O$	99.995%	Sigma-Aldrich®
Formic acid	HCOOH	GR for Analysis 98-100%	Merk
Polyethylene glycol dodecyl ether (Brij® 30)	---	---	ACROS Organics
n-heptane	C_7H_{16}	Analysis	ACROS Organics
Sodium borohydride	$NaBH_4$	99.99%	Sigma-Aldrich®
Sodium polyacrylate	$(C_3H_3NaO_2)n$		Sigma-Aldrich®
Potasium tetrachloroplatinate	K_2PtCl_4	99.99%	Sigma-Aldrich®

Hexachloroplatinic acid hexahydrated	$H_2PtCl_6 \cdot 6H_2O$	37.50%	Sigma-Aldrich®
Hydrochloric acid	HCl	37%	Sigma-Aldrich®
Sodium hydroxide	NaOH	Pellets for analysis	Merk
Hydrogen	H_2	N50, 99.999%	Air Liquide
Argon	Ar	N50, 99.999%	Air Liquide

2.10. References

[1] G. A. Somorjai, "Introduction to Surface Chemistry and Catalysis", John Wiley & Sons, Inc., New York, **1994**.

[2] G. Attard and C. Barnes, "Surfaces", **1998**.

[3] R. I. Masel, "Principles of adsorption and reaction on solid surfaces", John Wiley & Sons, Inc., New York, **1996**.

[4] M. A. Van Hove, "Surface Crystallography at the Metal-Gas Interface", *Frontiers of Electrochemistry*, VCH Publishers, Inc., New York, **1993**.

[5] J. F. Nicholas, "An atlas of models of crystal surfaces", Gordon and Breach, Science Publishers, Inc., Londres, **1965**.

[6] D. W. Blakely and G. Somorjai, "The Stability and Structure of High Miller Index Platinum Crystal Surfaces in Vacuum and in the Presence of Adsorbed Carbon and Oxygen" *Surface Science* **1977**, 65, 419.

[7] J. Clavilier, D. Armand, S. G. Sun and M. Petit, "Electrochemical adsorption behaviour of platinum stepped surfaces in sulphuric acid solutions " *Journal of Electroanalytical Chemistry* **1986**, 205, 267-277.

[8] E. Yeager, W. E. Ogrady, M. Y. C. Woo and P. Hagans, "Hydrogen adsorption on single-crystal platinum" *Journal of the Electrochemical Society* **1978**, 125, 348-349.

[9] S. Gilman, "The Mechanism of Electrochemical Oxidation of Carbon Monoxide and Methanol on Platinum. II. The "Reactant-Pair" Mechanism for Electrochemical Oxidation of Carbon Monoxide and Methanol" *Journal of Physical Chemistry B* **1964**, 68, 70.

[10] R. Parsons, "Thermodynamic methods for the study of interfacial regions in electrochemical systems", in, Plenum, New York, **1980**, pp. 1-44.

[11] J. Clavilier, D. Armand and B. L. Wu, "Electrochemical studyof the initial surface condition of platinum surfaces with (100) and (111) orientations" *Journal of Electroanalytical Chemistry* **1982**, 135, 159-166.

[12] N. Furuya and M. Shibata, "Structural changes at various Pt single crystal surfaces with potential cycles in acidic and alkaline solutions" *Journal of Electroanalytical Chemistry* **1999**, 467, 85-91.

[13] J. Clavilier, R. Faure, G. Guinet and R. Durand, "Preparation of monocrystalline Pt microelectrodes and electrochemical study of the plane surfaces cut in the direction of the {111} and {110} planes " *Journal of Electroanalytical Chemistry* **1980**, 107, 205-209.

[14] J. Clavilier, R. Durand, G. Guinet and R. Faure, "Electrochemical adsorption behaviour of Pt(100) in sulphuric acid solution " *Journal of Electroanalytical Chemistry* **1981**, 127, 281-287.

[15] W. Vielstich, H. Gasteiger and A. Lamm, "Electrocatalysis", in, John Wiley & Sons, Ltd Chichester UK, **2003**.

[16] W. H. Lizcano-Valbuena, D. C. de Azevedo and E. R. Gonzalez, "Supported metal nanoparticles as electrocatalysts for low-temperature fuel cells" *Electrochimica Acta* **2004**, 49, 1289-1295.

[17] F. Raimondi, G. G. Scherer, R. tz and A. Wokaun, "Nanoparticles in energy technology: Examples from electrochemistry and catalysis" *Angewandte Chemie - International Edition* **2005**, 44, 2190-2209.

[18] N. Markovic, H. Gasteiger and P. N. Ross, "Kinetics of oxygen reduction on Pt(hkl) electrodes: Implications for the crystallite size effect with supported Pt electrocatalysts" *Journal of the Electrochemical Society* **1997**, 144, 1591-1597.

[19] R. Van Hardeveld and F. Hartog, "Statistics of surface atoms and surface sites on metal crystals" *Surface Science* **1969**, 15, 189-&.

[20] Z.-Y. Zhou, N. Tian, Z.-Z. Huang, D.-J. Chen and S.-G. Sun, "Nanoparticle catalysts with high energy surfaces and enhanced activity synthesized by electrochemical method" *Faraday Discussions* **2009**, 140, 81-92.

[21] N. Tian, Z. Y. Zhou and S. G. Sun, "Platinum Metal Catalysts of High-Index Surfaces: From Single-Crystal Planes to Electrochemically Shape-Controlled Nanoparticles" *Journal of Physical Chemistry C* **2008**, 112, 19801-19817.

[22] T. J. Schmidt, H. A. Gasteiger, G. D. Stab, P. M. Urban, D. M. Kolb and R. J. Behm, "Characterization of High-Surface-Area Electrocatalysts Using a Rotating-Disk Electrode Configuration" *Journal of the Electrochemical Society* **1998**, 145, 2354-2358.

[23] K. A. Friedrich, F. Henglein, U. Stimming and W. Unkauf, "Investigation of Pt particles on gold substrates by IR spectroscopy - Particle structure and catalytic activity" *Colloids and Surfaces A-Physicochemical and Engineering Aspects* **1998**, 134, 193-206.

[24] J. Solla-Gullón, F. J. Vidal-Iglesias, E. Herrero, J. M. Feliu and A. Aldaz, "CO monolayer oxidation on semi-spherical and preferentially oriented (100) and (111) platinum nanoparticles" *Electrochemistry Communications* **2006**, 8, 189-194.

[25] T. S. Ahmadi, Z. L. Wang, T. C. Green, A. Henglein and M. A. El-Sayed, "Shape-controlled synthesis of colloidal platinum nanoparticles" *Science* **1996**, 272, 1924-1926.

[26] J. Solla-Gullón, F. J. Vidal-Iglesias, A. López-Cudero, E. Garnier, J. M. Feliu and A. Aldaz, "Shape-dependent electrocatalysis: methanol and formic acid electrooxidation on preferentially oriented Pt nanoparticles" *Physical Chemistry Chemical Physics* **2008**, 10, 3689-3698.

[27] K. Kinoshita, "Particle Size Effects for Oxygen Reduction on Highly Dispersed Platinum in Acid Electrolytes" *Journal of the Electrochemical Society* **1990**, 137, 845-848.

[28] J. Solla-Gullón, A. Rodes, V. Montiel, A. Aldaz and J. Clavilier, "Electrochemical characterisation of platinum-palladium nanoparticles prepared in a water-in-oil microemulsion" *Journal of Electroanalytical Chemistry* **2003**, 554, 273-284.

[29] J. Solla-Gullón, V. Montiel, A. Aldaz and J. Clavilier, "Synthesis and electrochemical decontamination of platinum-palladium nanoparticles prepared by water-in-oil microemulsion" *Journal of the Electrochemical Society* **2003**, 150, E104-E109.

[30] J. Solla-Gullón, "Caracterización y comportamiento electroquímico de nanopartículas metálicas preparadas en microemulsión", Tesis doctoral, Universitat d'Alacant, **2003**.

[31] D. Pletcher, "A First Course in Electrode Processes", The Electrochemistry Consultancy, Southampton, **1991**.

[32] P. T. K. a. W. R. Heineman, "Cyclic Voltammetry", in: Journal of Chemical Education **1983**.

[33] A. J. Bard and L. R. Faulkner, "Electrochemical Methods. Fundamental and Applications", John Wiley & Sons, Inc., New York, **2001**.

[34] E. Gileadi, "Physical Electrochemistry: Fundamentals, Techniques and Applications", WILEY-VCH Verlag GmbH & Co, **2011**.

[35] J. Clavilier, "Pulsed linear sweep voltammetry with pulses of constant level in a potential scale, a polarization demanding condition in the study of platinum single-crystal electrodes" *Journal of Electroanalytical Chemistry* **1987**, 236, 87-94.

[36] V. Grozovski, V. Climent, E. Herrero and J. M. Feliu, "Intrinsic Activity and Poisoning Rate for HCOOH Oxidation at Pt(100) and Vicinal Surfaces Containing Monoatomic (111) Steps" *ChemPhysChem* **2009**, 10, 1922-1926.

[37] V. Grozovski, V. Climent, E. Herrero and J. M. Feliu, "Intrinsic activity and poisoning rate for HCOOH oxidation on platinum stepped surfaces" *Physical Chemistry Chemical Physics* **2010**, 12, 8822-8831.

[38] A. Bard and L. Faulkner, "Electrochemical Methods: Fundamentals and Applications", John Wiley & Sons, Inc., United States of America, **2001**.

[39] B. B. Damaskin, O. A. Petri and G. A. Tsirilina, "Electrochemistry", 2nd Edition, Moscow, **2006**.

[40] A. B. a. L. Faulkner, "Electrochemical Methods. Fundamentals and Applications", JOHN WILEY & SONS.INC., Texas, United States of America **2001**.

[41] V. Climent, "Nueva aproximación al estudio de los potenciales de carga cero de electrodos monocristalinos del grupo del platino: aplicación al estudio de la adsorción iónica y molecular", Tesis doctoral, Universidad de Alicante, **1999**.

[42] T. Iwasita and F. C. Nart, "In situ infrared spectroscopy at electrochemical interfaces" *Progress in Surface Science* **1997**, 55, 271-340.

[43] A. J. Bard, F.-R. F. Fan, D. T. Pierce, P. R. Unwin, D. O. Wipf and F. Zhou, "Chemical Imaging of Surfaces with the Scanning Electrochemical Microscope" *Science* **1991**, 254, 68-74.

[44] P. Sun, F. O. Laforge and M. V. Mirkin, "Scanning electrochemical microscopy in the 21st century" *Physical Chemistry Chemical Physics* **2007**, 9, 802-823.

[45] C. Jung, C. M. Sánchez-Sánchez, C.-L. Lin, J. Rodríguez-López and A. J. Bard, "Electrocatalytic Activity of Pd−Co Bimetallic Mixtures for Formic Acid Oxidation

Studied by Scanning Electrochemical Microscopy" *Analytical Chemistry* **2009**, 81, 7003-7008.

[46] C. M. Sanchez-Sanchez, J. Solla-Gullon, F. J. Vidal-Iglesias, A. Aldaz, V. Montiel and E. Herrero, "Imaging Structure Sensitive Catalysis on Different Shape-Controlled Platinum Nanoparticles" *Journal of the American Chemical Society* **2010**, 132, 5622-5624.

[47] C. M. Sanchez-Sanchez, F. J. Vidal-Iglesias, J. Solla-Gullon, V. Montiel, A. Aldaz, J. M. Feliu and E. Herrero, "Scanning electrochemical microscopy for studying electrocatalysis on shape-controlled gold nanoparticles and nanorods" *Electrochimica Acta* **2010**, 55, 8252-8257.

[48] A. J. Wain, "Scanning electrochemical microscopy for combinatorial screening applications: A mini-review" *Electrochemistry Communications* **2014**, 46, 9-12.

[49] P. Bertoncello, "Advances on scanning electrochemical microscopy (SECM) for energy" *Energy & Environmental Science* **2010**, 3, 1620-1633.

[50] C.-L. Lin, J. Rodríguez-López and A. J. Bard, "Micropipet Delivery−Substrate Collection Mode of Scanning Electrochemical Microscopy for the Imaging of Electrochemical Reactions and the Screening of Methanol Oxidation Electrocatalysts" *Analytical Chemistry* **2009**, 81, 8868-8877.

Published Articles

Chapter III

Effects of the anion adsorption and pH on the formic acid oxidation reaction on Pt(111) electrodes

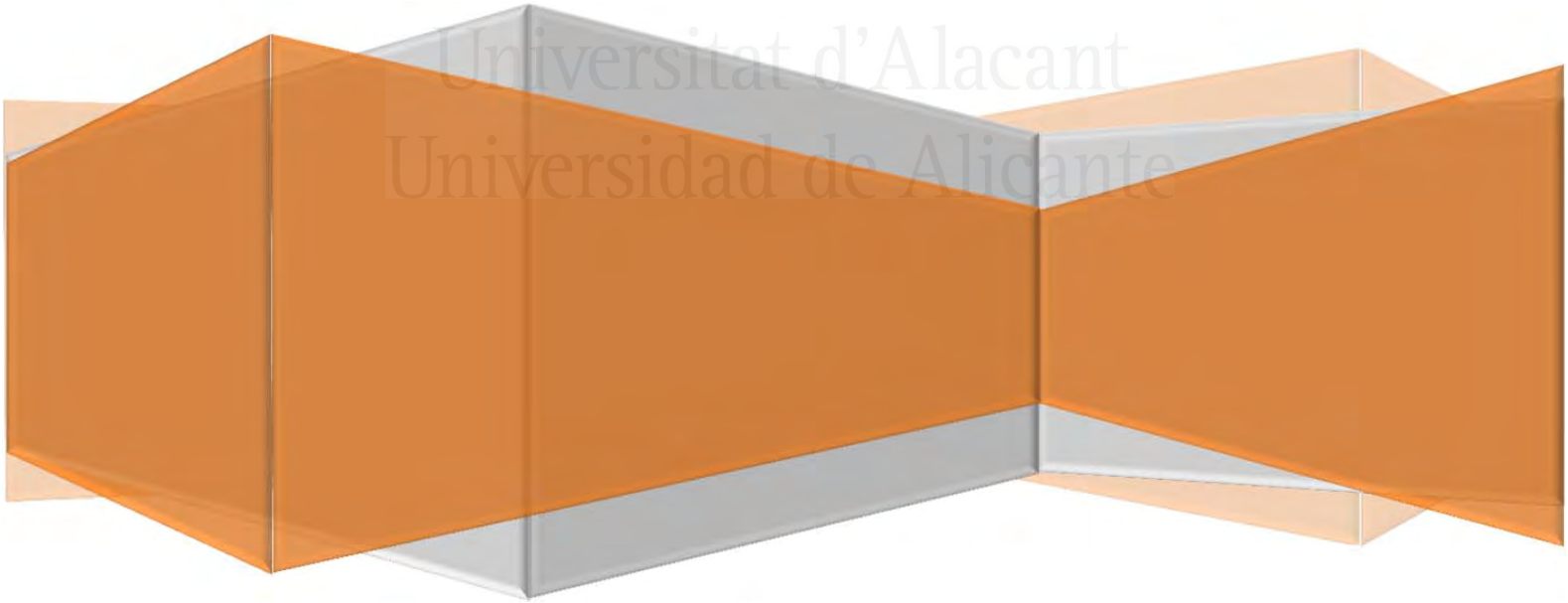

I

Publication I

J. V. Perales-Rondon, E. Herrero and J. M. Feliu, **"Effects of the anion adsorption and pH on the formic acid oxidation reaction on Pt(111) electrodes"** *Electrochimica Acta* **2014**, 140, 511-517. **doi:**10.1016/j.electacta.2014.06.057.

Electrochimica Acta 140 (2014) 511–517

Contents lists available at ScienceDirect

Electrochimica Acta

journal homepage: www.elsevier.com/locate/electacta

Effects of the anion adsorption and pH on the formic acid oxidation reaction on Pt(111) electrodes

Juan V. Perales-Rondón, Enrique Herrero*, Juan M. Feliu

Instituto de Electroquímica, Universidad de Alicante, Apartado 99, E–03080, Alicante, Spain

ARTICLE INFO

Article history:
Received 20 December 2013
Received in revised form 7 June 2014
Accepted 9 June 2014
Available online 14 June 2014

Keywords:
Pt(111) electrode
Formic acid oxidation
Anion adsorption
pH effects

ABSTRACT

The effects of solution pH and anion adsorption for the formic acid oxidation reaction on the Pt(111) electrode have been examined using electrochemical techniques. Regarding the pH effects, it has been found that oxidation currents for this reaction increase with pH, which indicates that solution formate is involved in the reaction mechanism. Unexpectedly, the adsorption of sulfate on the Pt(111) electrode has a positive effect on the oxidation of formic acid, which also suggests that adsorbed anions are also involved in the mechanism. The activation energy calculated from temperature dependent measurements diminishes with the solution pH and also in the presence of adsorbed sulfate. These measurements corroborate the involvement of solution formate and anions in the oxidation mechanism. Using these results, a rate equation for the oxidation of formic acid is proposed. The current values calculated from this equation are in very good agreement with the experimental currents in perchloric acid solutions.

1. Introduction

The formic acid oxidation reaction has been widely studied because its possible use in fuel cell technologies. The reaction involves only two electrons in the oxidation to CO_2, and for that reason, it has a lower energy density (kW/kg) when compared with other organic molecules, such as methanol or ethanol. In spite of that, the practical electrocatalysts (normally composed of platinum or palladium) have higher turnover at comparable potentials. Thus, the cell power per mass of precious metal is higher than that obtained for ethanol or methanol.

The reaction mechanism of the formic acid oxidation reaction has two possible routes, as initially proposed by Capon and Parsons [1–3] and confirmed by DEMS [4]. In one of the routes, the first step is a dehydration step, to yield an adsorbed CO molecule. Adsorbed CO is difficult to oxidize to CO_2 and blocks the surface, hindering the progress of the reaction. The other route goes through the so called active intermediate. In this route, formic acid probably adsorbs on the surface in some form and yields the active intermediate, which is immediately transformed into CO_2. For this reason, this route is more efficient in the oxidation, since the overpotentials are lower, but its performance is hindered by the presence of CO.

Recently, significant efforts have been devoted to determine the nature of the active intermediate [5–7]. The initial works of Osawa and collaborators proposed that adsorbed formate in a bridge-bonded configuration with its two oxygen atoms bound to two surface platinum atoms (bridge bonded bidentate formate geometry) was the active intermediate, since this species was detected in ATR-SEIRAS experiments and a qualitative correlation between the reactivity and the amount of adsorbed formate was found [8–11]. However, other experiments seemed to contradict this initial assignment, proposing other species as the active intermediate [12,13]. All these data resulted in a debate regarding the role of adsorbed bridge bonded bidentate formate in the reaction mechanism, which still is not solved. Recently, a new species has been added to the mechanism, since it has been found that that solution formate plays a very important role in the oxidation mechanism [14].

In all of these manuscripts, polycrystalline electrodes were used. Formic acid oxidation is a reaction very sensitive to the surface structure, as the studies with single crystal electrodes reveal [15]. If a detailed determination of the reaction kinetics is required, the use well-defined surfaces can provide valuable information on the reaction. Very well controlled conditions are normally required in order to untangle the effect of the different parameters and their relationships in the oxidation mechanism. For that reason, the use of low index planes, namely Pt(111), Pt(100) and Pt(110) surfaces, which ideally have only one type of site on the surface, simplifies the problem and allows establishing clear relationships between site and type of reactivity. Among them, the Pt(111) surface is the most stable surface within the potential range of interests [16] and is considered to be the most frequent orientation in practical

* Corresponding author.
E-mail address: herrero@ua.es (E. Herrero).

http://dx.doi.org/10.1016/j.electacta.2014.06.057
0013-4686/

nanoparticles [17]. Under these conditions, it is possible to determine the activity of the electrode for both routes independently [18]. Consequently, absolute reaction rates and potential regions in which each route is active can be determined as a function of the electrode structure [19,20].

In this manuscript, the oxidation of formic acid on Pt(111) electrodes is studied in solutions containing perchloric, sulfuric and acetic acid in the pH range between 0 and 2. From the temperature dependence of the activity through the active intermediate, apparent activation energies are calculated. All these data will be used to determine the role of the adsorbed anion, formic acid and formate concentration in the oxidation mechanism. This will allow establishing an explicit rate equation for the oxidation through the active intermediate route that will be compared to the observed behavior. In this equation, the solution formate concentration, and the coverage of adsorbed formate and that of other adsorbed species will be considered.

2. Experimental

Platinum single crystal electrodes were oriented, cut and polished from small single crystal beads (2.5 mm diameter) following the procedure described by Clavilier and co-workers [21,22]. The electrodes were cleaned by flame annealing, cooled down in H_2/Ar and protected with water in equilibrium with this gas mixture to prevent contamination before immersion in the electrochemical cell, as described in detail elsewhere [22,23]. The voltammetric profiles, and therefore the surface structure of the electrodes, are stable upon cycling provided that oxide formation is avoided. It is known that oxidation/reduction cycles create defects on the electrode surface [16,24]. For that reason, the upper potential limit of the scan is always maintained below 1.1 V for the Pt(111) electrode.

Experiments were carried out in a classical two-compartment electrochemical cell deaerated by using Ar (N50, Air Liquide in all gases used), including a large platinum counter electrode and a reversible hydrogen (N50) electrode (RHE) as reference. For the determination of the activation energy, the electrochemical cell was immersed in a water bath to control the temperature in a range between 278 and 333 K. The reference electrode was kept at room temperature (298 K) and all the measured potentials are referred to a RHE electrode at 298 K. For that reason, the measured potentials were corrected with the thermodiffusion potential using the procedure explained in reference [25]. All the potentials are quoted vs. the RHE at 298 K unless otherwise stated. Solutions were prepared from sulfuric acid, perchloric acid, sodium perchlorate, acetic acid, formic acid (Merck suprapur in all cases) and ultrapure water from Elga. The cleanliness of the solutions was tested by the stability of the characteristic voltammetric features of well-defined single crystal electrodes.

The potential program for the transients was generated with an arbitrary function generator (Rigol, DG3061A) together with a potentiostat (eDAQ EA161) and a digital recorder (eDAQ, ED401). To avoid any interference of the diffusion of formic acid in the reaction rate, stationary conditions were attained by using a hanging meniscus rotating disk configuration at 900 rpm (controlled by a Radiometer CTV 101).

3. Results

3.1. Effect of the solution pH.

It has been recently shown that the pH affects significantly the currents for formic acid oxidation on platinum polycrystalline electrodes [14]. These experiments were carried out in different phosphate buffers. In order to verify the effects of pH in the oxidation

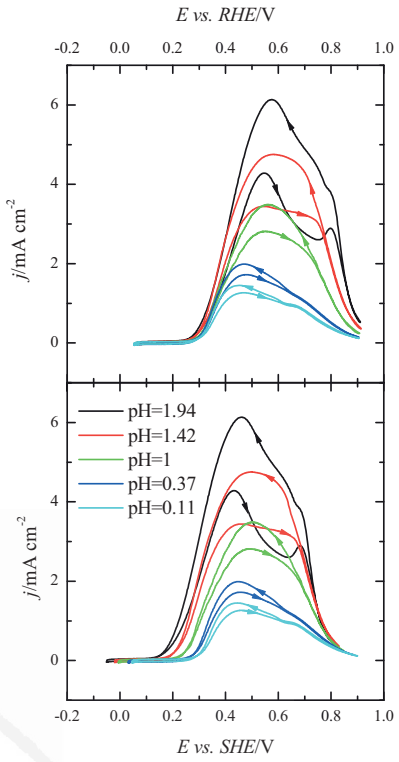

Fig. 1. Voltammetric profiles for the oxidation of 0.1 M formic acid in different solutions on the Pt(111) electrode: 1 M $HClO_4$ (pH = 0.11), 0.5 M $HClO_4$ (pH = 0.37), 0.1 M $HClO_4$ (pH = 1.0), 0.05 M $HClO_4$ + 0.05 $NaClO_4$ (pH = 1.42) and 0.01 M $HClO_4$ + 0.09 $NaClO_4$ (pH = 1.94).

of formic acid on Pt(111) electrodes, the oxidation currents for this electrode at different pHs have been measured. However, to prevent any possible interference in the oxidation currents as the pH changes, solutions have to be chosen carefully. First, specific adsorption of anions should be avoided, since this process can alter the reaction kinetics, as will be shown later. On the other hand, special care should be taken to maintain the interfacial pH constant during the process, since two protons are generated per formic acid molecule. Thus, solutions with a large buffering power should be used. The absence of specific adsorption precludes the use of the typical buffering solutions, such as phosphate buffers, since the different phosphate anions adsorb specifically on the (111) surface [26,27]. For that reason, the solutions were prepared with perchloric acid and sodium perchlorate and the higher studied pH was close to 2.

As can be seen in fig. 1, an increase in the oxidation currents are observed as the pH shifts from ca. 0 to 2. Also, the overall shape of the voltammetric profile in the negative scan remains almost constant. On the other hand, the difference between the currents measured in the positive and negative scan directions also increases with pH. This hysteresis is associated to the formation of CO in the dehydration reaction of formic acid at low potential values [1–4], which blocks the surface and affects the currents measured in the positive scan direction. For the Pt(111) electrode, CO formation is restricted to the defects on the surface and takes place at potentials below 0.3 V [20,28,29]. There is a clear relationship between the hysteresis and the CO formation rate as shown in the studies with stepped surfaces [20], and thus the larger hysteresis as the pH increases has to be associated to an increase in the CO formation

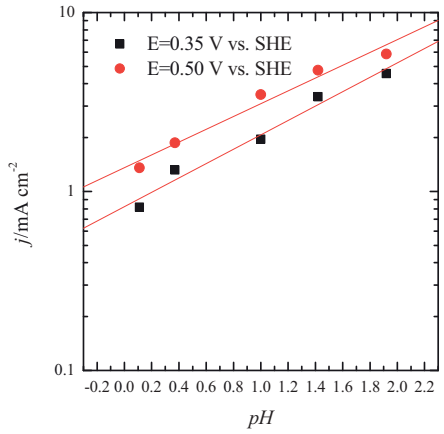

Fig. 2. Currents at constant potential for formic acid oxidation vs. solution pH. Data taken from fig. 1.

rate at defects at low potentials. Since CO is oxidized above 0.75 V [30], the currents measured in the negative scan direction correspond exclusively to the oxidation of formic acid through the active intermediate route [20]. The constancy of the shape in the negative scan direction suggests that the oxidation mechanism is the same, so that the current increase should be related to the increase in concentration of a relevant species in the oxidation mechanism. Being formic acid a weak acid with a $pK_a = 3.75$, the change in pH alters the ratio between formate and formic acid in solution. Thus, the current increase can be related to the increase in the concentration of formate in solution, as has been previously proposed [14]. In the RHE scale (fig. 1, top panel), the onset for formic acid oxidation only moves slightly towards more negative values as the pH increases.

To check the reaction order with respect to the concentration of formate, currents at constant absolute potential (vs. SHE) from fig. 1 lower panel have been plotted vs. pH. Fig. 2 shows the currents measured at 0.35 and 0.50 V vs. SHE in the negative scan direction, which correspond exclusively to the activity of the surface trough the active intermediate route in absence of CO [20]. As can be seen, there is a linear relationship between the pH and the logarithm of the current density, in which the slope is between 0.35 and 0.4. Since in this pH range, solution formate concentration is proportional to the proton concentration, the slope of this plot can also be considered the reaction order for solution formate in the rate equation.

3.2. Effect of the specific adsorption of anions

Adsorbed species on the electrode surface alter the reactivity since they change the interaction between the relevant species in the mechanism and the surface. As solution pH affects the formic acid oxidation currents (and therefore the reaction rate), the study of the effect of the specifically adsorbed anions in the reaction rate should be carried out at constant pH. Fig. 3 show the voltammetric profiles for the clean electrolyte and for formic acid oxidation in 0.5 M $HClO_4$ and 0.5 M H_2SO_4, solutions whose pHs can be considered very similar. As can be seen, maximum currents for both media are almost the same. However, it should be noted that currents for the sulfuric acid solution are slightly higher and the onset is displaced towards more negative potentials. This behavior is rather unexpected. From the pH perspective, solution pH in the sulfuric acid solution can be somehow higher due to the second acid/base equilibrium of the molecule. According to the previous results, the higher pH should correspond to lower currents. Also, the presence

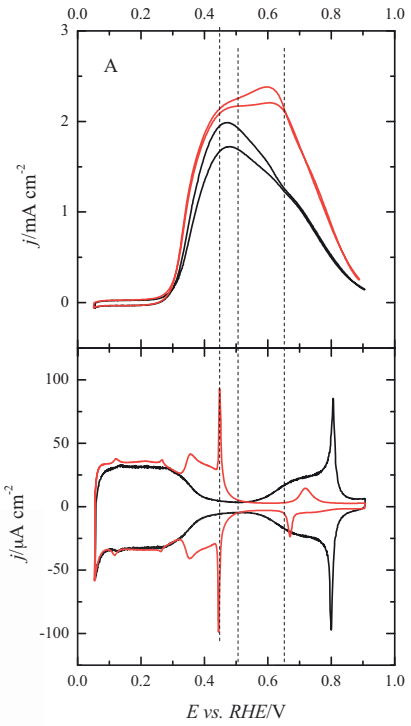

Fig. 3. A) Voltammetric profile for the Pt(111) electrode in 0.5 M $HClO_4$ + 0.1 M HCOOH (black line) and 0.5 M H_2SO_4 + 0.1 M HCOOH (red line) B) Voltammetric profile for the Pt(111) electrode in 0.5 M $HClO_4$ (black line) and 0.5 M H_2SO_4 (red line).

of strongly adsorbed sulfate should lead to a significant diminution in the currents, as happens to other organic molecules such as methanol [31]. On the other hand, significant currents for formic acid oxidation are obtained in the region where sulfate anions are adsorbed [32] and the current decay after the maximum takes place at more positive potential values for the sulfuric acid solution. All these results indicate that the adsorption of sulfate on the electrode surface has an unexpected positive effect for the oxidation of formic acid.

To check whether this enhancement is exclusive of sulfate or can be observed with other anions, the effect of acetic acid was also studied. In order to maintain the solution pH below to 2, 1 mM acetic acid was added to a 0.1 M perchloric acid solution (fig. 4). For comparison, the effect of the addition of 1 mM H_2SO_4 was also studied. It should be borne in mind that the adsorption of acetate is stronger than that of sulfate, as can be observed in the voltammetry of the Pt(111) electrode (see fig. 10). As shown in this figure, the effects of the addition of sulfate and acetate to the 0.1 M perchloric acid solution are similar. In this case, the change in the onset is negligible, due to the lower concentration of the anions. However, in spite of the specific adsorption of anions, currents are maintained when compared to pure perchloric acid solutions.

3.3. Determination of the activation energy for the direct oxidation path

Additional information on the mechanism of formic acid oxidation can be obtained if the activation energy is determined. To ensure that the activation energy corresponds to the direct route,

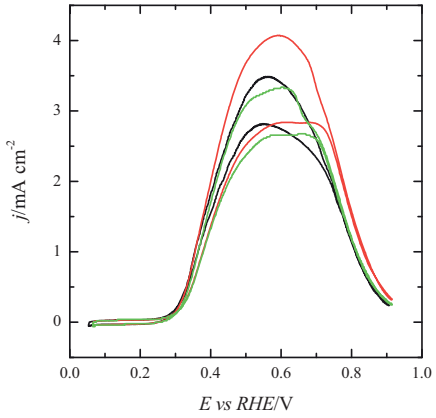

Fig. 4. A) Voltammetric profile for the Pt(111) electrode in 0.1 M $HClO_4$ + 0.1 M HCOOH (black line), 0.1 M $HClO_4$ + 1 mM H_2SO_4 + 0.1 M HCOOH (red line) and 0.1 M $HClO_4$ + 1 mM HAc + 0.1 M HCOOH (green line).

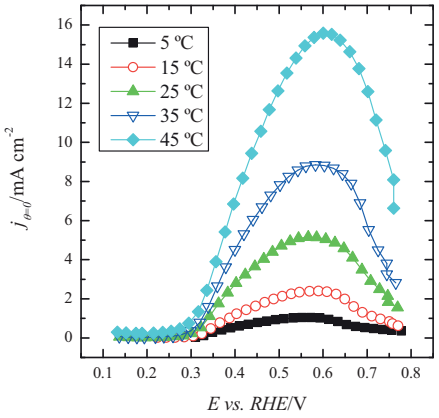

Fig. 5. Values of $j_{\theta=0}$ at different temperatures vs. electrode potential measured in 0.1 M $HClO_4$ + 0.1 M HCOOH solutions for the Pt(111) electrode.

pulsed voltammetry has been used [18,19]. Each transient obtained from the pulsed voltammetry has been fitted to the equation

$$j = j_{\theta=0}\left(\frac{1}{1+k_{ads}t(p-1)}\right)^{\frac{1}{p-1}} \quad (1)$$

where $j_{\theta=0}$ represents the current through the direct route in absence of poison, the so-called intrinsic activity of the electrode [18], k_{ads} is the CO formation rate from formic acid and p is the number of sites required for the adsorption of formic acid to yield CO. According to this model, the transients should have a decay, which depends on the value of k_{ads}, and the extrapolation of the transients to $t = 0$ gives the value of $j_{\theta=0}$. This equation has been proved to fit adequately the observed transients for formic acid oxidation on single crystal electrodes [19,20] and nanoparticle electrodes [33]. For all the observed transients, the decay was very small and therefore no accurate determination of the parameter p could be made. As the usual value is close to 2 [19,20], in all the fittings for this electrode the value of p was set to 2.

Transients for the oxidation of 0.1 M formic acid with the pulsed voltammetry technique were recorded between 5 and 45 °C to determine the change of $j_{\theta=0}$ with potential and temperature for the following supporting solutions: 0.1 M $HClO_4$, 0.5 M H_2SO_4, 0.1 M $HClO_4$ + 10 mM H_2SO_4 and 0.1 M $HClO_4$ + 10 mM CH_3COOH, 0.05 M $HClO_4$ + 0.05 M $KClO_4$ (pH = 1.42) and 0.01 M $HClO_4$ + 0.09 M $KClO_4$ (pH = 1.94). With these solutions, the anion and pH effects in the activation energy can be studied. Fig. 5 shows the results of $j_{\theta=0}$ obtained for the oxidation of 0.1 M HCOOH in 0.1 M $HClO_4$ at selected temperatures. It should be noted that the error in the determination of $j_{\theta=0}$ is well below 1% in all cases, due to almost negligible k_{ads} values obtained from the fittings. As expected, currents increase with temperature and the onset for the oxidation shifts towards more negative values.

The activation energy can be obtained from the Arrhenius plots as shown in fig. 6. In all cases, the plots were linear, within the experimental error of the measurements. From the slope of the $\log(j_{\theta=0})$ vs. 1/T, the apparent activation energy was determined for all the solutions. These values are plotted vs. the electrode potential for the different solutions in fig. 7. For the effect of the anions present in solution, two different behaviors can be observed. In the solutions containing perchloric acid, the apparent activation energy is almost independent of the anion present in solution. For these curves, there is a small region between 0.3 and 0.4 V where the activation energy diminishes from values around 55-60 to 45 kJ mol^{-1}. From that potential, the activation energy slowly increases up to 0.7 V. At this point, there is an sharp diminution of the activation energy. On the other hand, for the sulfuric acid solution, there is a continuous diminution of the activation energy from values of ca. 70 kJ mol^{-1} at 0.3 V to 35 kJ mol^{-1} at 0.6 V. From this potential, values increase and reach a stable value of ca. 60 kJ mol^{-1} at 0.8 V. These results clearly indicate that the adsorption of the anions have a strong influence in the kinetics of the reaction. Although the details of this dependence will be discussed in the following section, a preliminary explanation can be given here. The initial diminution in the activation energy can be related to the initial stages of the adsorption of formate or any other anion present in solution. In the absence of strong adsorption, as in the case of 0.1 M $HClO_4$ solutions, after the initial triggering event of the reaction, the activation energy remains nearly constant until OH adsorption occurs on the electrode. For the perchloric acid solutions with acetic acid or sulfuric acid, it is probable that OH replaces the adsorbed anion at the more positive potentials in a process without a significant charge transfer [34]. The adsorption of OH leads to the deactivation of the surface for the direct oxidation and to a significant diminution of the activation energy. For the sulfuric acid solution, there is a clear minimum in the activation energy curve. The region where the minimum activation energy is obtained coincides with the presence of

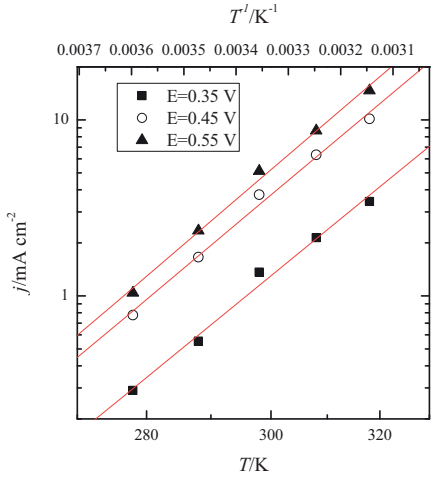

Fig. 6. Arrhenius plots for $j_{\theta=0}$.

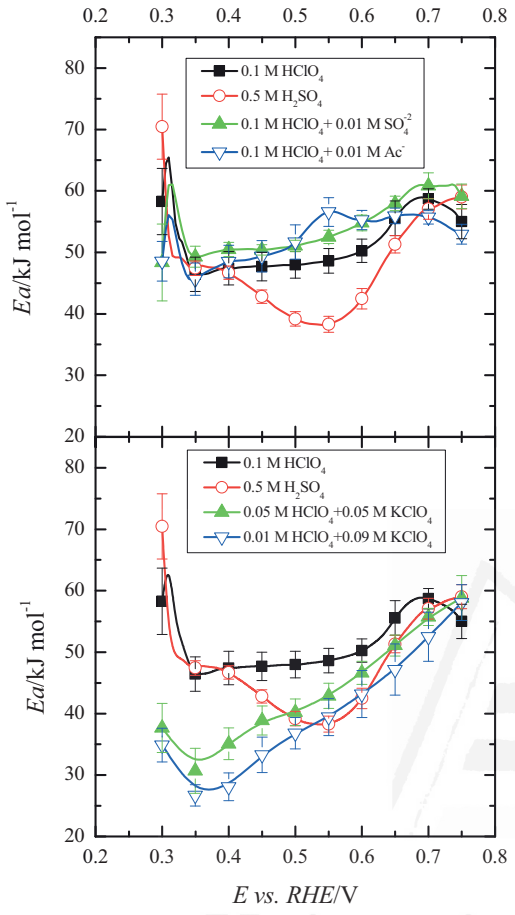

Fig. 7. Apparent activation energy vs. electrode potential determined for the oxidation of 0.1 M HCOOH in different solutions on the Pt(111) electrode.

the small bump that can be observed in the voltammetric profile in the supporting electrolyte (fig. 3). This bump has been associated to an order transition in the sulfate adlayer that leads to the formation of large ordered domains [35–37].

Regarding the pH effect, a clear diminution in the activation energy is observed as the pH increases, which corroborates the results observed by voltammetry (fig. 7, lower panel). The lower apparent activation energy implies that the formation of the reaction intermediate is facilitated at higher pHs. Activation energies as low as 25 kJ/mol are obtained at pH = 1.94. It should be stressed that the measured value is the apparent activation energy with contains not only information on the true activation energy of the rate determining step, but also on the activation energy for all the previous steps [38]. If solution formate is involved in the rate determining step, this species should be produced from the acid/base equilibrium of formic acid/formate at very low pHs. The free energy of this equilibrium reaction contributes in these cases to the apparent activation energy. Thus, the apparent activation energy diminution as the pH increases can be related to the increase in the concentration of solution formate that diminishes the requirements to produce it from formic acid. It should also be highlighted that for the sulfuric acid solution activation energy values are also close to those obtained at higher pH in perchloric acid solutions, which also suggests that adsorbed sulfate facilitates the oxidation of formic acid.

4. Discussion

The results presented here clearly points out the role of several species in the whole mechanism through the direct route. From the dependence of the current densities and activation energy with the pH it is seems clear that formate anion is playing a significant role in the mechanism, as has been already suggested [14]. As the pH increases, the effective concentration of formate for a given initial concentration of formic acid increases and thus current increase. On the other hand, pre-adsorbed anions, as sulfate, have a beneficial effect in the oxidation currents. A clear example of that is the fig. 3, in which a lower onset for the formic acid oxidation reaction is observed in the presence of sulfuric acid. Thus, it can be proposed that adsorbed anions and formate are involved in the oxidation mechanism through the following scheme:

$$Pt + HCOO^- \rightarrow Pt\text{-}HCOO^- \quad (2)$$

$$Pt\text{-}A + Pt\text{-}HCOO^- \rightarrow Pt\text{-}A + Pt + CO_2 + H^+ + 2e \quad (3)$$

where A is an adsorbed anion present on the surface (either sulfate, or acetate or bidentate formate). In the rds, the adsorbed anion and the formate coming from solution interacts with the surface through the C-H bond, according to the equation:

$$Pt - A + Pt - HCOO^-{}_{C-H\ \ down} \rightarrow Pt - A + CO_2 + Pt - H + e^- \quad (4)$$

The C-H down configuration is that in which the H is close to the surface, but it does not imply necessarily that the C-H bond is perpendicular to the surface. Several configurations can be proposed here, such as monodentate adsorbed formate or that proposed in reference [39]. This type of step, in which the oxidation of formate is requires an additional adsorbed anion in the vicinity, has been already proposed by DFT calculations using a continuous solvation model and discrete water molecules [39]. It has been shown that the adsorbed formate molecule in a bridge-bonded bidentate configuration (with the two oxygen atoms in the carboxylic group pointing towards the surface) is a key element in the process. The presence of bridge-bonded bidentate adsorbed formate facilitates the adsorption of an additional formic acid molecule with C-H down configuration. In this position, the cleavage of the H-C has a low activation energy, yielding CO_2 [39].On the other hand, the calculated activation energy for the cleavage of the H-C bond from the bridge bonded bidentate formate is very high and, thus, this event is not likely [39]. With respect to the DFT model, the only significant difference is that formate, not formic acid, is the species that adsorbs with the CH down configuration, in order to justify the dependence of the currents with the pH. Additionally, it will be considered that not only adsorbed formate facilitates the CH down adsorption of the formic acid molecule, but also other adsorbed anions such as sulfate or acetate can play similar roles.

Before formulating a rate equation, it should be also take into account that OH adsorption do not have an active role in the oxidation of formic acid. As can be seen in fig. 2, the presence of adsorbed OH causes the opposite effect. At potentials above 0.6 V in perchloric acid solutions, where OH adsorption occurs, currents diminish and reach negligible values at 0.8 V. Thus, the oxidation of formic acid requires a preadsorbed anion and a free site where formate can adsorb the current for the oxidation of formic acid. The corresponding kinetic equation is then:

$$j = Fk^o \exp\left(\frac{F(E - E^o)}{\alpha RT}\right)\theta_A\left(1 - \theta_A - \theta_{OH}\right)\left[HCOO^-\right] \quad (5)$$

where k^o is the standard rate constant, E^o the standard potential for the oxidation of formic acid, α is the symmetry factor of the reaction, θ_A and θ_{OH} are the specific anion and OH coverages and the rest of symbols have the usual meaning. This equation is the direct consequence of reaction (4), which is the rds. Since the rds is the first

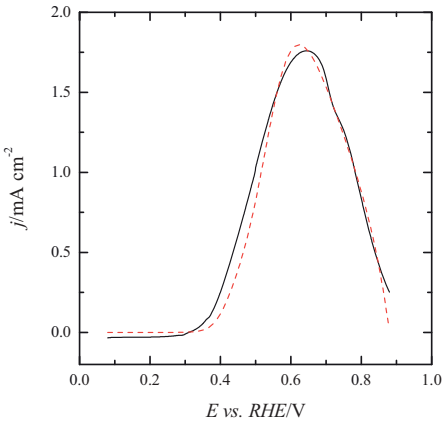

Fig. 8. Comparison of the negative scan direction of the voltammogram recoded in 0.1 M $HClO_4$ +0.05 M HCOOH for the Pt(111) electrode (full line,) and the calculated current using equation (5). θ_A values for this equation are taken from reference [40].

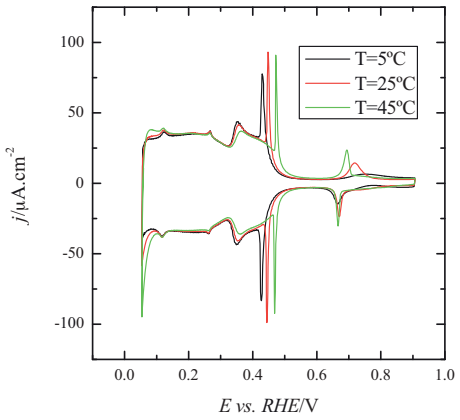

Fig. 9. Voltammetric profile of the Pt(111) electrode in 0.5 M H_2SO_4 at different temperatures.

electron transfer, it should include the potential dependent term $\exp\left(\frac{F(E-E^o)}{\alpha RT}\right)$, with an α value close to 0.5. Also, the step requires the presence of an adsorbed anion (sulfate or bridge-bonded bidentate formate) with represented by its coverage value, θ_A and an adsorbed formate ion in a C-H down configuration. This is an intermediate species, which has been formed through reaction (2) and requires the presence of a free Pt site and a formate ion from solution. Thus, the terms referring to the Pt free sites $\left(1-\theta_A-\theta_{OH}\right)$ and formate solution concentration $\left[HCOO^-\right]$ should appear also in the equation.

This rate equation is different from that proposed in reference [14] to explain the pH behavior of the oxidation current. In this new equation, an additional term, the anion coverage, has been included to explain the lower onset for formic acid oxidation in the presence of sulfate. In phosphate buffer solutions, it was found that the current increases with pH up to values close to 4 and then diminishes from that point [14]. The equation proposed here is also able to reproduce the behavior, since the increase in the with the pH is linked to the formate concentration and the diminution above pH = 4 is associated to the $\left(1-\theta_A-\theta_{OH}\right)$ term, as has been demonstrated in [14]. The addition of θ_A to the rate equation does not alter the behavior proposed in the previous reference, since it is only playing an important role in defining the currents for low coverages, that is, at the onset of formic acid oxidation.

This equation will be tested for the oxidation of formic acid in perchloric acid solutions. For that, the value of the bridge-bonded formate coverage (θ_A) as a function of the electrode potential has to be known from independent measurements. In a previous paper [40], the value of θ_A during formic acid oxidation in perchloric acid solutions was determined by using fast scan voltammetry. Since formic acid oxidation currents are not dependent on the scan rate [41], it is possible to determine adsorption currents for formate at scan rates around 50 V s^{-1}. At 50 mV s^{-1}, the current due to the adsorption of formic acid is negligible in comparison to those obtained for formic acid oxidation. At 50 V s^{-1}, the current for the adsorption process has increases 1000 times, and is much bigger than the oxidation currents and therefore, the curve for formate coverage vs. potential can be estimated from the integration of the voltammetric profile in the region where formate adsorption takes place after subtraction of the typical double layer. From the curve θ_A vs. E from [40], the current density for formic acid oxidation can be calculated according to equation (5) and compared to the experimental current. Fig. 8 shows the comparison between the measured voltammetric profile in the negative scan direction for formic acid oxidation in the solution used to measure θ_A and the calculated current using equation (5). The negative scan direction is used because the surface is free from adsorbed CO. For the calculation, α was equal to 0.45, E^o was 0 V and $Fk^o[HCOO^-]$ was 9.6×10^{-4} mA cm^{-2}. As can be seen, the model is able to reproduce the shape, maximum position and the decay after the maximum for formic acid oxidation. However, the fitting is not perfect probably due to the way the formate coverage was estimated, especially at low potential values. Between 0.3 and 0.45 V, formate adsorption competes with hydrogen adsorption. For the estimation of the coverage, it has been assumed that hydrogen adsorption coverage was equal to that obtained in absence of formic acid in solution and this fact may have led to an underestimated value of the formate coverage. A more accurate method to obtain θ_A would have required the used of the thermodynamic treatment of reference [42]. However, under the present conditions, it is not possible to use such treatment, because the the voltammetric profile at 50 V s^{-1} is not perfectly symmetrical.

The model presented in equation 4 also explains the activation energies measured in fig. 7. The apparent activation energy, which is the measured value, is then defined as:

$$Ea_{app}^{\neq} = -R\frac{d\ln(j)}{d\frac{1}{T}} = -R\left(\frac{d\ln(k^o)}{d\frac{1}{T}}+\frac{d\ln\left(\theta_A\right)}{d\frac{1}{T}}+\frac{d\ln\left(1-\theta_A-\theta_{OH}\right)}{d\frac{1}{T}}\right) \quad (6)$$

In this equation, the real activation energy, which can be related to the value determined by DFT, is:

$$Ea^{\neq} = -R\frac{d\ln(k^o)}{d\frac{1}{T}} \quad (7)$$

It is expected that this value is independent of the electrode potential. The terms related to the anion and OH coverage are clearly dependent on the electrode potential, which causes the different values obtained at different electrode potentials. At low potentials, the dominant term in this potential dependence is $\frac{d\ln(\theta_A)}{d\frac{1}{T}}$. The evolution of the anion coverage with the temperature can be estimated using the voltammetric profile measured at different temperatures. As can be seen in fig. 9 for 0.5 M sulfuric acid solution, the onset of sulfate adsorption is displaced towards more positive values. In the case of acetate, a similar behavior is observed

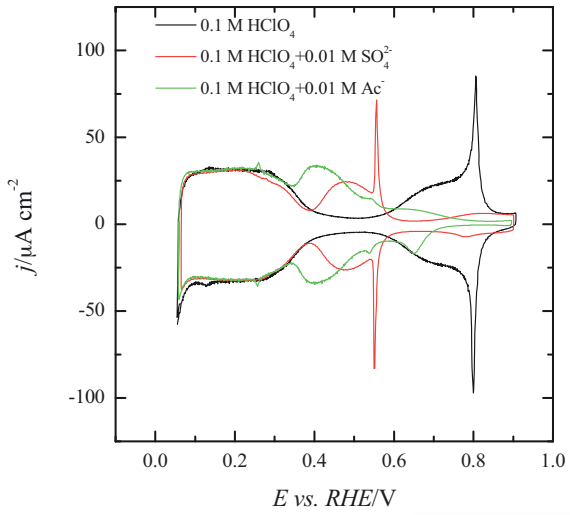

Fig. 10. Voltammetric profile of the Pt(111) electrode in different solutions.

and a similar behavior is also expected for formate adsorption. This implies that at constant electrode potential, the anion coverage diminishes with the temperature, which should lead to a diminution of the activation energy in this potential region, as observed in all solutions. At high potential values, the term that dominates the change with the electrode potential is $\frac{d\ln(1-\theta_A-\theta_{OH})}{d\frac{1}{T}}$. Thus, the way the anion or OH coverage reaches the maximum value and how it evolves with the temperature should determine the changes of the apparent activation energy in this region.

In the case of formate, which will be the adsorbed anion in 0.1 M $HClO_4$, and acetate (in 0.1 M $HClO_4$ + 10 mM HAc), the adsorption strength is similar, as shown in reference [40], and therefore, they have similar values. For the solution containing 0.1 M $HClO_4$ + 10 mM H_2SO_4, the adsorption of sulfate is weaker than that of acetate, as fig. 10 demonstrate. In this case, formate adsorption is probably stronger than sulfate adsorption at this concentration. Therefore, the anion adsorbed on the electrode surface in this supporting electrolyte is formate, which gives apparent activation energies equal to those obtained in pure perchloric acid solution.

The only apparent discrepancy of the proposed model and the obtained results is the order with respect to the formate concentration. According to equation (5), the order should be 1, but the measured order is around 0.4. The real order can only be obtained if the rest of the parameters (coverages and electrode potential) are constant. In fig. 2, the electrode potential is maintained constant. However, the anion coverage is clearly dependent on the pH and for that reason, the measured value deviates from the real value to lower values. This implies that a given electrode potential in the SHE scale, the measured coverage of formate diminishes with the pH.

5. Conclusions

The results presented demonstrate the complexity of the formic acid oxidation reaction, since it involves the presence of at least two adsorbed species: an anion (which could be sulfate, acetate or bridge-bonded bidentate formate) and solution formate. This latter species should interact with the surface with the C-H bond close to the surface, so that the cleavage of the C-H bond could occur. Also, it explains the controversy regarding the role of adsorbed bridge-bonded bidentate formate in the mechanism. It takes part in the mechanism, as ATR-SEIRAS results indicates [9], although it is not the molecule that decomposes to give CO_2. CO_2 is generated from a solution formate which interacts with the surface through the C-H bond.

Acknowledgements

This work has been financially supported by the MICINN (Spain) (project CTQ2010-16271) and Generalitat Valenciana (project PROMETEO/2009/045, FEDER).

References

[1] A. Capon, R. Parsons, J. Electroanal. Chem. 45 (1973) 205.
[2] A. Capon, R. Parsons, J. Electroanal. Chem. 44 (1973) 239.
[3] A. Capon, R. Parsons, J. Electroanal. Chem. 44 (1973) 1.
[4] J. Willsau, J. Heitbaum, Electrochim. Acta 31 (1986) 943.
[5] G. Samjeske, A. Miki, S. Ye, M. Osawa, J. Phys. Chem. B 110 (2006) 16559.
[6] A. Cuesta, G. Cabello, C. Gutierrez, M. Osawa, Phys. Chem. Chem. Phys. 13 (2011) 20091.
[7] Y.X. Chen, M. Heinen, Z. Jusys, R.B. Behm, Angew. Chem. Int. Edit. 45 (2006) 981.
[8] M. Osawa, A. Miki, S. Ye, Abstr. Pap. Am. Chem. Soc. 224 (2002) U445.
[9] Y.X. Chen, S. Ye, M. Heinen, Z. Jusys, M. Osawa, R.J. Behm, J. Phys. Chem. B 110 (2006) 9534.
[10] A. Cuesta, G. Cabello, M. Osawa, C. Gutiérrez, ACS Catal. 2 (2012) 728.
[11] M. Osawa, K. Komatsu, G. Samjeske, T. Uchida, T. Ikeshoji, A. Cuesta, C. Gutierrez, Angew. Chem. Int. Edit. 50 (2011) 1159.
[12] Y.X. Chen, M. Heinen, Z. Jusys, R.J. Behm, Langmuir 22 (2006) 10399.
[13] Y.X. Chen, M. Heinen, Z. Jusys, R.J. Behm, ChemPhysChem 8 (2007) 380.
[14] J. Joo, T. Uchida, A. Cuesta, M.T.M. Koper, M. Osawa, J. Am. Chem. Soc. 135 (2013) 9991.
[15] J. Clavilier, R. Parsons, R. Durand, C. Lamy, J.M. Leger, J. Electroanal. Chem. 124 (1981) 321.
[16] K. Itaya, S. Sugawara, K. Sashikata, N. Furuya, Journal of Vacuum Science & Technology a-Vacuum Surfaces and Films 8 (1990) 515.
[17] J. Solla-Gullón, P. Rodríguez, E. Herrero, A. Aldaz, J.M. Feliu, Phys. Chem. Chem. Phys. 10 (2008) 1359.
[18] J. Clavilier, J. Electroanal. Chem. 236 (1987) 87.
[19] V. Grozovski, V. Climent, E. Herrero, J.M. Feliu, ChemPhysChem 10 (2009) 1922.
[20] V. Grozovski, V. Climent, E. Herrero, J.M. Feliu, Phys. Chem. Chem. Phys. 12 (2010) 8822.
[21] J. Clavilier, D. Armand, S.G. Sun, M. Petit, J. Electroanal. Chem. 205 (1986) 267.
[22] C. Korzeniewski, V. Climent, J.M. Feliu, in: A.J. Bard, C. Zoski (Eds.) Electroanalytical Chemistry: A Series of Advances, Vol 24, vol. 24, 2012, pp. 75.
[23] A. Rodes, K. Elachi, M.A. Zamakhchari, J. Clavilier, J. Electroanal. Chem. 284 (1990) 245.
[24] A.M. Gomez-Marin, J.M. Feliu, Electrochim. Acta 82 (2012) 558.
[25] N. Garcia-Araez, V. Climent, J. Feliu, in: C.G. Vayenas (Ed.) Interfacial Phenomena in Electrocatalysis, vol. 51, Springer New York, 2011, Ch. 1, pp. 1.
[26] J. Mostany, P. Martinez, V. Climent, E. Herrero, J.M. Feliu, Electrochim. Acta 54 (2009) 5836.
[27] M.A. Climent, M.J. Valls, J.M. Feliu, A. Aldaz, J. Clavilier, J. Electroanal. Chem. 326 (1992) 113.
[28] M.D. Maciá, E. Herrero, J.M. Feliu, A. Aldaz, Electrochem. Commun. 1 (1999) 87.
[29] M.D. Maciá, E. Herrero, J.M. Feliu, A. Aldaz, J. Electroanal. Chem. 500 (2001) 498.
[30] E. Herrero, A. Fernández-Vega, J.M. Feliu, A. Aldaz, J. Electroanal. Chem. 350 (1993) 73.
[31] E. Herrero, K. Franaszczuk, A. Wieckowski, J. Phys. Chem. 98 (1994) 5074.
[32] J. Mostany, E. Herrero, J.M. Feliu, J. Lipkowski, J. Phys. Chem. B 106 (2002) 12787.
[33] V. Grozovski, J. Solla-Gullon, V. Climent, E. Herrero, J.M. Feliu, J. Phys. Chem. C 114 (2010) 13802.
[34] A. Rodes, E. Pastor, T. Iwasita, J. Electroanal. Chem. 376 (1994) 109.
[35] N. Garcia-Araez, V. Climent, J.M. Feliu, Electrochim. Acta 54 (2009) 966.
[36] N. Garcia-Araez, V. Climent, P. Rodriguez, J.M. Feliu, Phys. Chem. Chem. Phys. 12 (2010) 12146.
[37] N. Garcia-Araez, V. Climent, P. Rodriguez, J.M. Feliu, Langmuir 26 (2010) 12408.
[38] E. Herrero, J.M. Feliu, S. Blais, Z. Radovic-Hrapovic, G. Jerkiewicz, Langmuir 16 (2000) 4779.
[39] H.-F. Wang, Z.-P. Liu, J. Phys. Chem. C 113 (2009) 17502.
[40] V. Grozovski, F.J. Vidal-Iglesias, E. Herrero, J.M. Feliu, ChemPhysChem 12 (2011) 1641.
[41] M.D. Maciá, E. Herrero, J.M. Feliu, J. Electroanal. Chem. 554 (2003) 25.
[42] E. Herrero, J. Mostany, J.M. Feliu, J. Lipkowski, J. Electroanal. Chem. 534 (2002) 79.

Chapter IV

On the activation energy of the formic acid oxidation reaction on platinum electrodes

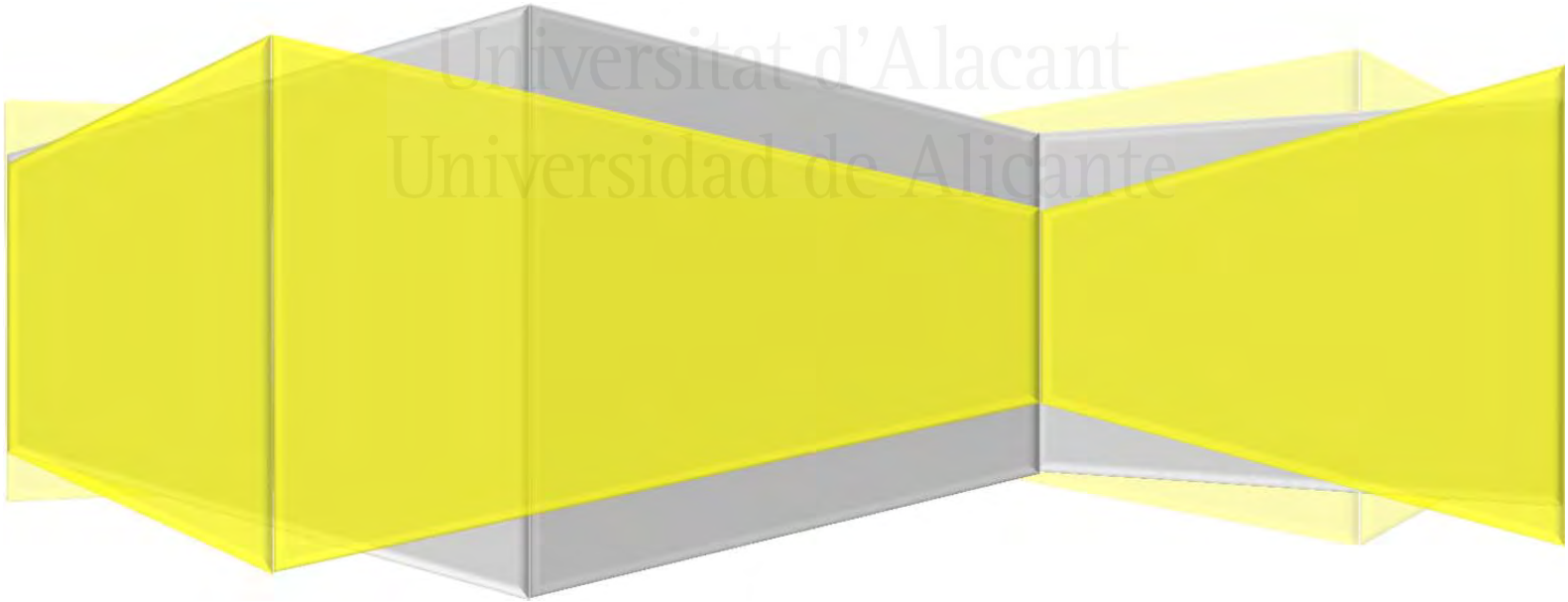

II

Publication II

J. V. Perales-Rondón, E. Herrero and J. M. Feliu, **"On the activation energy of the formic acid oxidation reaction on platinum electrodes"** *Journal of Electroanalytical Chemistry* **2015**, 742, 90-96. **doi:**10.1016/j.electacta.2014.06.057.

Journal of Electroanalytical Chemistry 742 (2015) 90–96

Contents lists available at ScienceDirect

Journal of Electroanalytical Chemistry

journal homepage: www.elsevier.com/locate/jelechem

On the activation energy of the formic acid oxidation reaction on platinum electrodes

Juan V. Perales-Rondón, Enrique Herrero *, Juan M. Feliu

Instituto de Electroquímica, Universidad de Alicante, Apartado 99, E-03080 Alicante, Spain

ARTICLE INFO

Article history:
Received 3 December 2014
Received in revised form 2 February 2015
Accepted 3 February 2015
Available online 11 February 2015

Keywords:
Platinum
Formic acid oxidation
Single crystal electrodes
Fuel cell

ABSTRACT

A temperature dependent study on the formic acid oxidation reaction has been carried out in order to determine the activation energy of this reaction on different platinum single crystal electrodes, namely Pt(100), Pt(111), Pt(554) and Pt(544) surfaces. The chronoamperometric transients obtained with pulsed voltammetry have been analyzed to determine the current densities through the active intermediate and the CO formation rate. From the temperature dependency of those parameters, the activation energy for the direct reaction and the CO formation step have been calculated. For the active intermediate path, the activation energy are in the range of 50–60 kJ/mol. On the other hand, a large dependence on the electrode potential is found for the activation energy of the CO formation reaction on the Pt(100) electrode, and the activation energy values for this process range between 20 and 100 kJ/mol. These results have been explained using a reaction mechanism in which the oxidation of formic acid requires the presence of a pre-adsorbed anion on the electrode surface.

1. Introduction

The formic oxidation reaction has been extensively studied because its potential use as anode reaction in the fuel cell technology. Additionally, from all the possible carbon containing species studied as tentative fuels, it has the simplest oxidation mechanism [1–3]. In fact, its oxidation to CO_2 only requires the cleavage of two bonds: O–H and C–H. The break of the O–H bond is relatively simple, since the OH group is involved in the acid/base equilibria of the molecule. For the second one, a surface with affinity for hydrogen and dehydration reactions is required. For that reason, the platinum and palladium electrodes show the highest activity.

In spite of the apparent simplicity of the reaction, additional complications in the oxidation mechanism appear on platinum surfaces. On these electrodes, CO formation at low potentials is observed [1]. To produce adsorbed CO, the cleavage of two different bonds should take place: the C–H and the C–OH bonds. The formation of CO creates additional problems in the oxidation of the formic acid molecule. CO is strongly adsorbed on the Pt surface and its final oxidation to CO_2 requires the transfer of an OH group. This latter step has a large overpotential. For this reason, CO is also called the poisoning intermediate, since it blocks the surface for the reaction to continue. On the other hand, the reaction route which gives directly CO_2 is called the direct oxidation route. For this route, the nature of the intermediate is still subject of discussion [4–11].

In order to get insight into the oxidation mechanism, extensive DFT calculations have been carried out using well defined surfaces [12–15]. In these studies, different intermediates and reaction schemes have been proposed. However, in order to validate those reaction mechanism, the theoretical data for the calculated activation energies should be compared with those obtained experimentally. In this manuscript the activation energies for the formic acid oxidation reaction are measured on single crystal electrodes using different electrolytes. The activation energies will be analyzed in view of the proposed mechanism, and compared with previous results, in order to obtain additional details on the oxidation mechanism. In this way, the measured values will be compared with those obtained from DFT calculations to validate the proposed mechanism.

2. Experimental procedure and numerical treatment of data

2.1. Experimental procedure

Platinum single crystal electrodes were oriented, cut and polished from small single crystal beads (ca. 2.5 mm diameter) following the procedure described by Clavilier [16,17]. The electrodes used in this study were the Pt(111) and Pt(100) low index planes

* Corresponding author.
E-mail address: herrero@ua.es (E. Herrero).

http://dx.doi.org/10.1016/j.jelechem.2015.02.003
1572-6657/

and two stepped surfaces: Pt(544) and Pt(554). These surfaces have 9 atom-wide (111) terraces separated by monoatomic (100) and (110) steps, respectively. Before every use, the electrodes were cleaned by flame annealing, cooled down in H_2/Ar and protected with water in equilibrium with this atmosphere. It is known that this procedure gives rise to surfaces whose atomic arrangement corresponds to the nominal one [18]. The voltammetric profile of the electrode in 0.5 M H_2SO_4 is always recorded to assure that the surface is well prepared and clean. The upper potential limit is always chosen so that oxide formation is avoided, to prevent surface disordering [19,20].

Experiments were carried out in a classical two-compartment electrochemical cell deaerated by using Ar (N50, Air Liquide in all gases used), including a large platinum counter electrode and a reversible hydrogen (N50) electrode (RHE) as reference. For the temperature controlled experiments, the electrochemical cell was immersed in a water bath to control the temperature. Temperature dependent measurements were conducted in a range between 278 and 333 K, using 5 K intervals. For the different experiments, the reference electrode was kept at room temperature (298 K). To transform the direct potential reading to the RHE scale at 298 K values, the direct potential reading should be corrected for the thermodiffusion potential using the procedure explained in reference [21]. Solutions were prepared from sulfuric acid, perchloric acid, formic acid (Merck suprapur in all cases) and ultrapure water from Elga.

The potential program for the pulse voltammetry, which allowed obtaining the current transients, was generated with an arbitrary function generator (Rigol, DG3061A) together with a potentiostat (eDAQ, EA161) and a digital recorder (eDAQ, ED401). To avoid any interference of the diffusion of formic acid in the reaction rate, stationary conditions were attained by using a hanging meniscus rotating disk configuration at 1600 rpm (controlled by a Radiometer CTV 101). Full experimental details on the pulsed voltammetry can be found in reference [22]. In summary, the potential program consists in a series of steps between an upper potential (0.9 V for $T < 298$ K and 0.85 V for $T \geqslant 298$ K) to oxidized the accumulated CO on the surface and the sampling potential. The duration of the steps was always 1 s.

2.2. Numerical treatment of the transients

In a previous work, transients obtained in the pulsed voltammetry as those shown in Fig. 1 were simulated with a model which took into account direct formic acid oxidation and CO formation through the dehydration reaction [22]. For the oxidation through the active intermediate, it was supposed that the current density depended on the fraction of the surface not covered by CO, $(1-\theta_{CO})$, and the current that would have been obtained in absence of CO, $j_{\theta=0}$.

$$j = j_{\theta=0}(1-\theta_{CO}) \tag{1}$$

In turn, the CO coverage will depend on the on the dehydration step, for which the reaction rate was written as:

$$\frac{d\theta_{CO}}{dt} = k_{ads}(1-\theta_{CO})^p \tag{2}$$

where k_{ads} is the poison formation reaction rate and p is the number of Pt sites required for the dehydration step to occur. The integration of Eq. (2), and substitution in Eq. (1) yielded:

$$j = j_{\theta=0}\left(\frac{1}{1+k_{ads}t(p-1)}\right)^{\frac{1}{p-1}} \tag{3}$$

This model was used to obtain the values of $j_{\theta=0}$, k_{ads} and p from the fits of this equation to the experimental transients. The fits were very

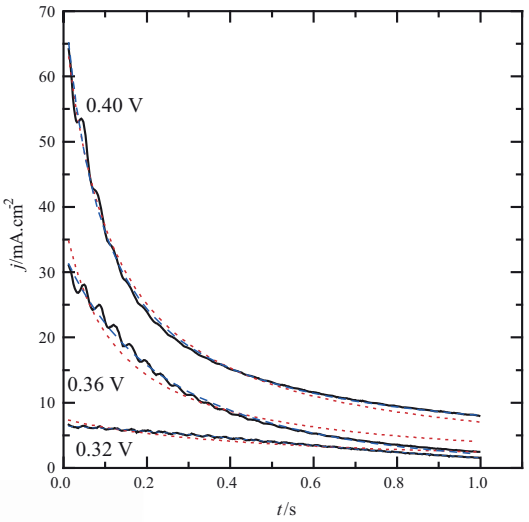

Fig. 1. Transient currents measured during the pulsed voltammetry at different potentials on the Pt(100) electrode at 40 °C in 0.5 H_2SO_4 + 0.1 M HCOOH and fittings according to Eq. (3) (dotted line) and Eq. (8) (dashed line).

good at room temperature, which supported the validity of the model [22,23]. In all cases, p was close to two, which implies that the dehydrogenation reaction requires two contiguous free platinum sites to proceed. However, when this equation is used for $T > 298$ K for the transients obtained in this work, the model deviates from experimental transients (Fig. 1, dotted line). In the model represented by Eq. (3), possible contributions to the total current from the adsorbed CO oxidation process according to the reaction

$$CO + H_2O \rightarrow CO_2 + 2H^+ + 2e \tag{4}$$

were not taken into account, because it was experimentally verified that, the CO oxidation rate was negligible at the potentials where CO was formed [22,23]. In the worst case scenario, the Pt(100) electrode, CO formation takes place at $E < 0.50$ V and for those potentials CO oxidation is negligible at room temperature. However, the temperature increase has two major effects: to accelerate CO oxidation process and also to increase the potential window where CO formation occurs. For this reason, the deviations from previous model are due to the contribution of the CO oxidation process to the measured current and, thus, such contribution should be taken into account for the transients at $T > 298$ K. Eq. (2) should be then modified incorporating the possibility of change of CO coverage due to its oxidation according to the proposed mean field Langmuir-Hinselwood mechanism [3,24,25] as:

$$\frac{d\theta_{CO}}{dt} = k_{ads}(1-\theta_{CO})^p - k_{ox}\theta_{CO}(1-\theta_{CO}) \tag{5}$$

where k_{ox} is the rate constant for the CO oxidation process. In the same way, the equation for the current density should incorporate the contributions to the measured current of the CO oxidation reaction as:

$$j = j_{\theta=0}(1-\theta_{co}) + qk_{ox}\theta_{co}(1-\theta_{co}) \tag{6}$$

where q is the charge involved to the oxidation of a monolayer of CO (320 μC cm^{-2} for the Pt(100) electrode). In order to solve Eq. (5) for θ_{CO}, p was fixed to 2, because this was the value obtained experimentally [22]. Assuming that $k_{ads} \gg k_{ox}$, θ_{CO} is then:

$$\theta_{CO} = k_{ads}\frac{\exp(k_{ox}t)-1}{k_{ox}\exp(k_{ox}t)+k_{ads}\exp(k_{ox}t)-k_{ads}} \tag{7}$$

Substituting into Eq. (6) gives:

$$j = \frac{k_{ox}[(1-\exp(-k_{ox}t))(j_{\theta=0}k_{ads} + qk_{ads}k_{ox}) + j_{\theta=0}k_{ox}]}{[k_{ox} + k_{ads}(1-\exp(-k_{ox}t))]^2} \quad (8)$$

Of course, when k_{ox} tends to 0, Eq. (8) transforms into Eq. (3) with $p = 2$. As can be seen, the model, which also contains 3 adjustable parameters, as the previous one, is able to perfectly fit the experimental transients (Fig. 1, dashed line).

3. Results and discussion

3.1. Temperature effects on the behavior of the electrodes in the pure supporting electrolyte

It has been shown that the formic acid oxidation reaction is affected by the anion adsorption process. In fact, it has been proposed that anion adsorption is required for the oxidation to proceed [26]. For the Pt(111) electrode, the proposed model suggests that the formic acid oxidation reaction requires the presence of an anion adsorbed on the surface and a contiguous free site. On this free site, formate, the proposed reactive species [8], can interact with the surface in a configuration which favors the C–H bond cleavage [27]. DFT calculations indicate that the activation energy for the cleavage of the C–H bond is low when this bond is directed to the surface [14], and thus it can be proposed that the formate species should have the C–H bond directed to the surface. The adsorbed anion that facilitates the adsorption of formate in the C–H down configuration can be either a formate species bonded to the surface through one or two oxygen atoms or any other anion such as acetate or sulfate [26]. Thus, the adsorption of the anion and how this process is influenced by the temperature is an important parameter that can affect the measured activation energy.

Fig. 2 shows the voltammetric profiles of the electrodes used in this work at different temperatures. For the Pt(111) electrode, as the temperature increases, sulfate adsorption shifts slightly toward more positive potentials [28,29]. All the signals related to sulfate adsorption move slightly to more positive potentials, but the effect is clearer when the position of the spike at ca. 0.45 V is compared for the different temperatures. This spike marks the position of the disorder–order transition of the sulfate layer [30], and this transition, which takes place at a constant coverage [31], moves toward positive potentials. This fact clearly indicates that the adsorption of anions is disfavored as the temperature increases. The second feature, the small bump at 0.6–0.7 is related to the completion of the sulfate layer [32]. In this case, this process is more reversible with the temperature, as the peak separation between positive and negative scan direction diminishes, but there is no significant peak shift.

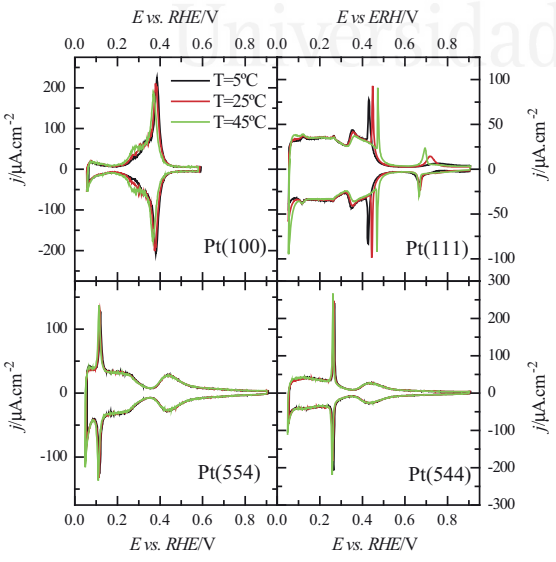

Fig. 2. Effect of the temperature in the voltammetric profiles of the electrodes in 0.5 M H_2SO_4. Scan rate: 50 mV s^{-1}.

The situation for the Pt(100) electrode is different. For this electrode, there is no clear separation between hydrogen and anion adsorption processes. The peak at ca. 0.37 V marks the point where hydrogen adsorbed atoms are being replaced by adsorbed sulfate [33]. As can be seen, this peak shifts toward negative potential values, but is less sharp [29]. This fact indicates that the onset for the adsorption process takes place at lower potentials. However, the sharpness of the peak indicates how narrow the window is for the replacement of the adsorbed hydrogen atoms by sulfate. This would suggest that the adsorption of the sulfate anion starts at lower potentials but the completion of the full adlayer shifts toward higher potential values as the temperature increases. For the other two surfaces, there is no noticeable change of the voltammetric profile as the temperature increases, which indicates no major changes in anion adsorption with temperature.

The differences in the anion adsorption between the low index and stepped surfaces stress the significant effects of the long range order in the adsorption of anion for large planar surfaces. For the Pt(100) and Pt(111) electrodes, achieving a long range order in the sulfate adlayer is the key factor for the completion of the anion layer [32]. As aforementioned, the small bump between 0.6 and 0.7 V for the Pt(111) electrode is related to the completion of the adlayer. This process becomes more reversible as the temperature increases, revealing a strong effect of the temperature on this process. On the other hand, when the terrace size diminishes, the long range order effects are less important in the adsorption processes, because it is interrupted by the presence of steps, and thus, the adlayer formation is depends only on the individual adsorption energies of the different sites, which are less affected by the temperature.

3.2. Effects of the temperature and anion adsorption on the formic acid oxidation reaction

The voltammetric profiles for the formic acid oxidation reaction at 298 K in perchloric and sulfuric acid solutions are shown in Fig. 3. In all cases, there is an hysteresis between positive and negative scan directions, due to the formation of CO through the dehydration reaction at low potentials [22,23]. Thus, currents in the positive scan direction are affected by the presence of adsorbed CO, which blocks the surface for the direct oxidation reaction. At high potentials ($E > 0.75$ V), CO is readily oxidized and the surface recovers its activity. In the negative scan direction, the surface is not blocked by CO for $E > 0.5$ V and for that reason, currents are much higher. The relative difference between the currents in positive and negative san directions is related to the kinetics of CO formation at low potentials. For the Pt(100), since the CO formation rate is the highest of all basal planes, currents are almost zero in the positive scan direction. A similar situation is observed for the Pt(554), because the CO formation rate on the (110) monoatomic step is also high [23]. On the other hand, for the Pt(111), the hysteresis is very small, since CO formation is related to defects. An intermediate situation is observed for the Pt(544) electrode, where the activity of the (100) steps for the CO formation step is not very high [23].

As expected, maximum currents for formic acid oxidation in perchloric acid are higher than those measured in sulfuric acid.

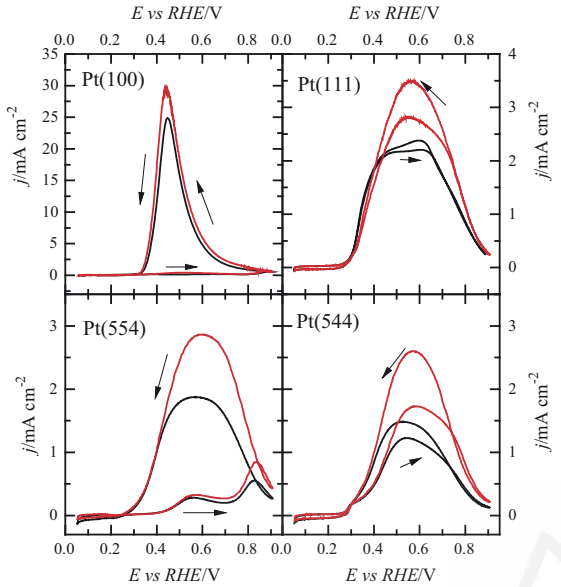

Fig. 3. Voltammetric profiles of the electrodes in 0.5 M H_2SO_4 + 0.1 M HCOOH (black line) and 0.1 M $HClO_4$ + 0.1 M HCOOH (red line). Scan rate: 50 mV s^{-1}. (For interpretation of the references to color in this figure legend, the reader is referred to the web version of this article.)

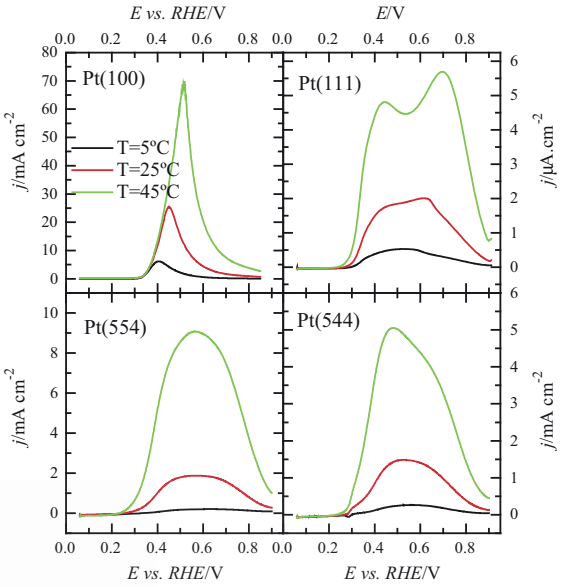

Fig. 4. Effect of the temperature in the voltammetric profiles of the electrodes in 0.5 M H_2SO_4 + 0.1 M HCOOH. Only the negative scan direction is shown, for simplicity. Scan rate: 50 mV s^{-1}.

However, the difference for the Pt(100) and Pt(111) are very small. Moreover, for the Pt(111) electrode, currents at $E < 0.4$ V are larger in sulfuric acid. These facts reveal that adsorbed sulfate is not inhibiting formic acid oxidation on these two surfaces. On the other hand, for the stepped surfaces, the differences are somehow larger. Since the behavior of the (111) plane for the oxidation is the same in perchloric and sulfuric acid solutions, as Fig. 3 demonstrates, the larger differences should be then associated to the different activity of the steps. For these surfaces, adsorbed sulfate on the steps should have an inhibiting behavior, whereas the adsorption on the (100) or (111) planes is neutral or even facilitates the formic acid oxidation reaction [27].

The effect of the temperature on the formic acid oxidation reaction is shown in Fig. 4. For simplicity, only negative scan directions are shown. The activity is mainly related to the direct oxidation of formic acid for this scan direction, since the surface is free from CO at the beginning of the scan ($E = 0.90$ V). For the Pt(100) electrode, currents at $E < 0.4$ V are almost independent of the temperature and above 0.4 V, a clear increase is observed. A priori, this constant value would suggest that the activation energy is zero for $E < 0.4$ V, since the dependence of the current with temperature is negligible. However, the decay in the current in the negative scan direction after the peak is mainly related to the formation of CO which blocks the surface [22], and thus, the activation energy for the direct path should be higher. As will be shown later, the rate for CO formation in this region also increases with the temperature, and the observed behavior is just a consequence of two opposing factors: the increasing rate of the direct reaction and of the dehydration step to yield CO, which results in currents that are almost independent of the temperature. For the other surfaces, a clear increase in current with the temperature is observed in all cases.

3.3. Activation energy for the reaction through the active intermediate

The different transients measured with the pulsed voltammetry were analyzed using Eq. (8) and the values of $j_{\theta=0}$ and k_{ads} from the different electrodes at different potentials and temperatures were calculated. Fig. 5 shows the values of $j_{\theta=0}$ for the different electrodes used in this study. The voltammetric profile in the negative scan direction at 45 °C is also shown for comparison. For the Pt(111), Pt(544) and Pt(554) electrodes, values of $j_{\theta=0}$ and measured current densities in negative scan direction of the voltammogram are almost identical for $E < 0.3$ V, which indicates that poison is not formed in this potential region, as was observed previously

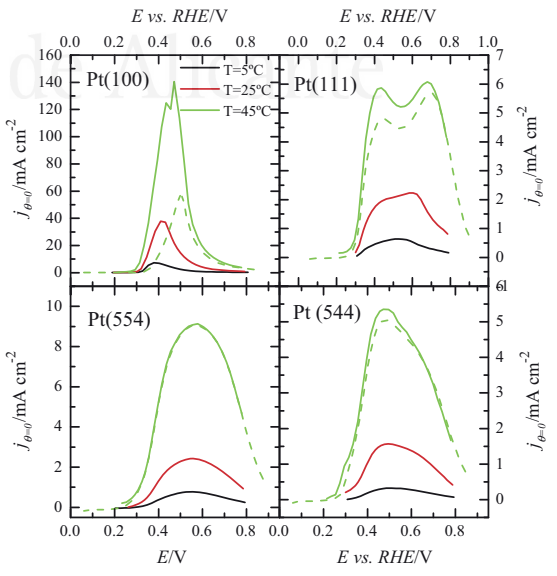

Fig. 5. Measured values of $j_{\theta=0}$ at three different temperatures in 0.5 M H_2SO_4 + 0.1 M HCOOH for the different electrodes. The negative scan direction at 45 °C of the voltammetric profile is also shown for comparison (dashed line).

for room temperature [23]. Also, oxidation transients are almost horizontal and the k_{ads} values obtained from the fittings are negligible. In fact, for the Pt(544) and Pt(554), CO is formed in the around the peaks associated to the adsorption of hydrogen on the steps in the potential region around 0.26 and 0.13 V, respectively (see Fig. 1) [23]. For the Pt(100) electrode, there is a significant difference between $j_{\theta=0}$ and the measured current for $E < 0.5$ V. The lower currents in the voltammetry are clearly related to the blocking of the surface by CO through the dehydration reaction, which is formed at $E < 0.5$ V (see Fig. 8).

Activation energies for the direct oxidation were obtained from Arrhenius plots ($\log(j_{\theta=0})$ vs. $1/T$). In all cases, these plots are linear. It should be stressed that the measured activation energy is an apparent activation energy ($Ea^{\neq}_{app}$) and contains terms that are not directly related to the activation energy of the different steps. It has been proposed that the oxidation through the active intermediate follows the rate equation [27]:

$$j_{\theta=0} = Fk^o \exp\left(\frac{\alpha F(E-E^o)}{RT}\right)\theta_A(1-\theta_A-\theta_{OH})[HCOO^-] \quad (9)$$

where k^o is the standard rate constant, E^o the standard potential for the oxidation of formic acid, α is the symmetry factor of the reaction, θ_A and θ_{OH} are the specific anion and OH coverages and the rest of symbols have the usual meaning. This rate equation corresponds to a mechanism whose rds is a step in which a formate anion interacts with the surface (in a free site) in the C–H down configuration

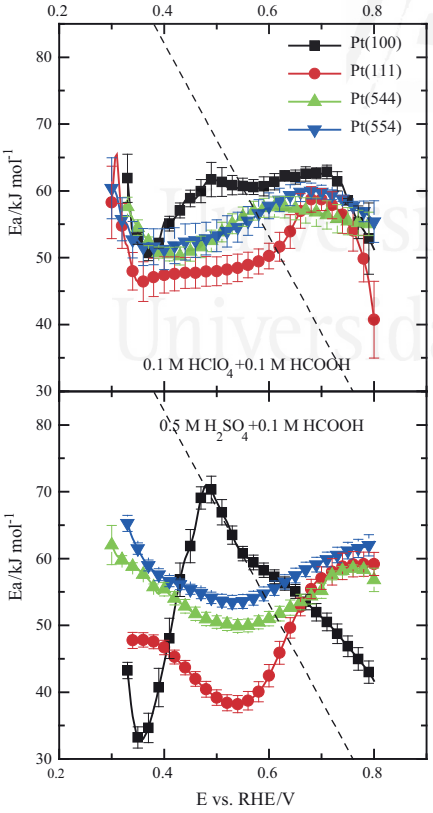

Fig. 6. Calculated apparent activation energy for the direct oxidation of formic acid for the different electrodes in 0.5 M H_2SO_4 + 0.1 M HCOOH and 0.1 M $HClO_4$ + 0.1 M HCOOH. The dashed line shows the expected behavior from Eq. (13), for $\alpha = 1.5$ and an arbitrary value of $Ea^{\neq}$.

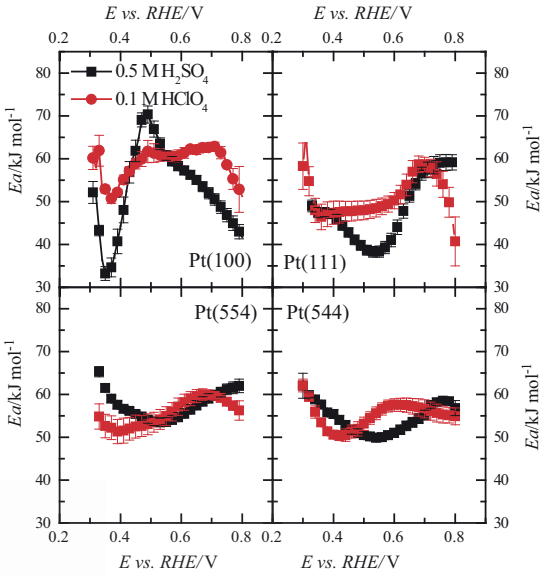

Fig. 7. Effect of the electrolyte composition in the apparent activation energy for the direct oxidation of formic acid of the electrodes 0.5 M H_2SO_4 + 0.1 M HCOOH (black curves) and 0.1 M $HClO_4$ + 0.1 M HCOOH (red curves). (For interpretation of the references to color in this figure legend, the reader is referred to the web version of this article.)

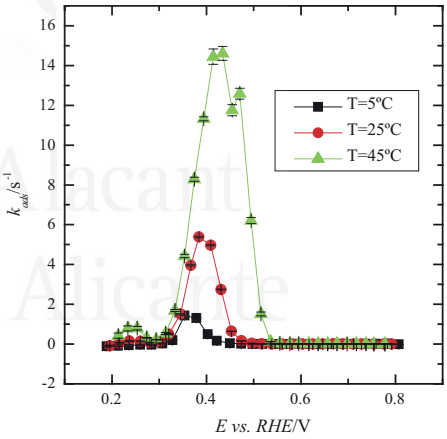

Fig. 8. Measured values of k_{ads} at three different temperatures in 0.5 M H_2SO_4 + 0.1 M HCOOH for the Pt(100) electrode.

close to an adsorbed anion (formate or sulfate), as has been proposed by the pH dependence of the oxidation rate of formic acid [8]. This rds, in which the C–H bond is cleaved and an electron is transferred, corresponds to the second electron transfer.

$$Pt-A+Pt-HCOO^-_{C-H\ down} \rightarrow Pt-A+CO_2+Pt-H+e^- \quad (10)$$

The activation energy of the reaction is defined as:

$$Ea^{\neq} = -R\left(\frac{d\ln(k^o)}{d\frac{1}{T}}\right)_{E,\theta,[HCOO]} \quad (11)$$

whereas the actually measured activation energy corresponds to the derivative $\ln(j_{\theta=0})$ vs. $1/T$, according to:

$$Ea^{\neq}_{app} = -R\left(\frac{d\ln(j_{\theta=0})}{d\frac{1}{T}}\right)_E = Ea^{\neq} - R\left(\frac{d\ln(\theta_A)}{d\frac{1}{T}} + \frac{d\ln(1-\theta_A-\theta_{OH})}{d\frac{1}{T}}\right)_E - \alpha F\left(E-E^0\right) \quad (12)$$

Thus, it contains terms that are related to the effect of the temperature on the anion and OH coverage and the electrode potential, which can affect the measured activation energy and modify its value. If the terms related to the coverages were negligible (that is, they were independent of the temperature), the apparent activation energy for the oxidation reaction should diminish with the electrode potential according to:

$$Ea^{\neq}_{app} = -R\left(\frac{d\ln(j_{\theta=0})}{d\frac{1}{T}}\right)_E = Ea^{\neq} - \alpha F\left(E-E^0\right) \quad (13)$$

If this is not true, that is, if the terms related to the coverages are temperature dependent, deviations from this slope must be observed. The potential regions where those terms can have a larger impact in the measured values are at the initial and final stages of the adsorption of the anions and OH. In the initial stages, the term $\frac{d\ln(\theta_A)}{d\frac{1}{T}}$ should have the larger effect, since, at these potentials, temperature changes can have a relative large effect on the anion coverage. On the other hand, the $\frac{d\ln(1-\theta_A-\theta_{OH})}{d\frac{1}{T}}$ term should have large values at the final stages of the adsorption process.

Figs. 6 and 7 show the apparent activation energies obtained in perchloric and sulfuric acid solutions for the different electrodes. The dashed line shows the expected behavior for the apparent activation energy from Eq. (13) with $\alpha = 1.5$ (the typical value for a mechanism in which the second electron transfer is the rds) and an arbitrary value of $Ea^{\neq}$. As can be seen, experimental values deviates clearly from the expected slope, which can be a consequence of the impact of the terms related to the anion and OH coverages in the formic acid oxidation process. The behavior of the Pt(111) electrode and the two vicinal surfaces Pt(554) and Pt(544) will be discussed first. In perchloric acid solutions, values are almost constant for these electrodes between 0.35 and 0.65 V. Apparent activation energies are ca. 47, 50 and 52 kJ mol^{-1} for the Pt(111), Pt(544) and Pt(554) in this region. First of all, the difference between these surfaces should be related to the activation energy on the (100) and (110) step sites. These values suggests that the activation energy on those sites is higher than in the (111) plane. Second, the almost constant value suggests that the terms related to the anion coverage either are very important, that is, significant changes in the anion coverages are observed with the temperature, or that additional factors, which have not been taken into account, play a role in the mechanism. From $E > 0.65$ V, the activation energy diminishes, with a behavior similar to that of Eq. (13). In this region, the formate coverage has reached to a maximum value, and probably, no change in the coverage is observed with the temperature.

In sulfuric acid solution, values for the Pt(554) and Pt(544) are very similar to those obtained in perchloric acid solution (Fig. 7). This fact indicates that adsorbed sulfate or formate, species that are required for the oxidation of formic acid, have very similar behavior, and supports the proposed mechanism [27]. There are only small changes at the onset potential, probably due to small difference on how temperature affects the initial stages of this process. Larger differences are observed on the Pt(111) electrode, for which, a diminution of the activation energy is observed around 0.6 V in sulfuric acid solutions. The diminution should be then related to the changes in the sulfate coverage, since, in this region the sulfate layer rearranges to reach the maximum coverage [21].

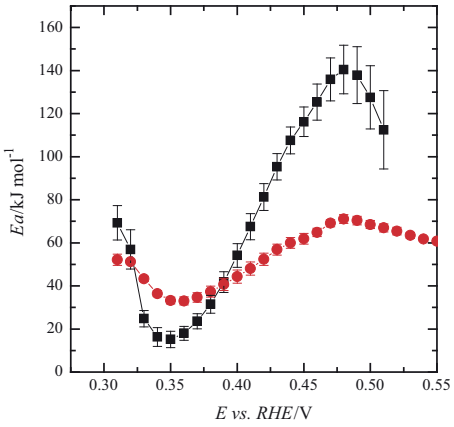

Fig. 9. Calculated apparent activation energy for the formation of CO from formic acid (black points) and the direct oxidation of formic acid (red points) in 0.5 M H_2SO_4 + 0.1 M HCOOH on the Pt(100) electrode. (For interpretation of the references to color in this figure legend, the reader is referred to the web version of this article.)

For the Pt(100) electrode in perchloric acid solution, there is an initial diminution, as predicted by Eq. (13), followed by a fast increase with the potential, reaching an almost constant value of 60 kJ mol^{-1} for $E > 0.5$ V. The increase is related to the adsorption of anions, and it is more evident in sulfuric acid solutions. As temperature effects in the blank voltammetric profiles demonstrate, the anion coverages diminishes for $E > 0.36$ V, which leads to an increase of the apparent activation energy due to the contribution of the $\frac{d\ln(1-\theta_A-\theta_{OH})}{d\frac{1}{T}}$ term. In sulfuric acid solutions, the shape of the apparent activation energy curve in sulfuric acid solutions is similar to that measured in perchloric acid, but the local maxima and minima are more pronounced, related to a large effect of the temperature on the adsorption of sulfate over formate. As before, for this medium and $E > 0.5$ V, the observed behavior follows Eq. (13), because sulfate coverage has reached to a maximum value, and the terms related to the coverage are temperature independent in this region.

In summary, the apparent activation energies for the different surfaces are in the range of ca. 50–60 kJ mol^{-1}, once the effects of the anion adsorption in the measured activation energies are subtracted. This results contrasts with the significant larger currents measured for the Pt(100) electrode. Thus, the larger currents and, therefore, the larger kinetic constant for this latter electrode should be then linked to a higher pre-exponential factor in kinetic constant. Since the pre-exponential factor is related to the probability of reaching the configuration of the activated complex, this could imply that the initial configuration giving rise to the activated complex is more probable on the Pt(100) surface. This would suggests that, from the different adsorption modes of formate, the one having the configuration required for the reaction to proceed is more likely on the Pt(100) surface than in the rest.

3.4. Activation energy of the dehydrogenation process of formic acid to yield adsorbed CO

As aforementioned, for the Pt(111), Pt(554) and Pt(544), k_{ads} values were negligible for the region where non-zero oxidation transients for the formic acid oxidation reaction are obtained ($E > 0.3$ V). However, for the Pt(100), it was possible to determine the values of k_{ads} from the transients in this region. Fig. 8 shows the

measured values for k_{ads} on this electrode at three representative temperatures. As can be seen, CO formation takes place in a potential region between 0.3 and 0.5 V with a maximum rate located close to the potential of zero total charge of the electrode [22]. This narrow regions expands as the temperature increase. The onset potential for the reaction shifts slightly toward lower potential values, whereas the upper limit for the reaction shifts markedly to higher values as the temperature increases.

Apparent activation energies for this reaction were calculated as before and the results are plotted in Fig. 9. In this figure, the apparent activation energy for the direct oxidation measured in the same experiment is also shown for comparison. As can be seen, the curve for the dehydration reaction presents the same features, with local minima and maxima located in the same potential, at 0.35 and 0.48 V. The only differences are the values and the intensities of the maxima and minima. If we accept that the deviations from the expected value are related to the anion coverage terms in the kinetic equation, the kinetic equation should be similar but with a higher order for the terms related to the anions in the kinetic equation. In fact, in the fittings of the transients, it was assumed that the reaction requires two free sites to proceed [22], and thus, it can be written that the rate for the reaction is:

$$k_{ads} = k^{o}_{ads}\theta_{A}(1-\theta_{A}-\theta_{OH})^{2}[HCOO^{-}] \quad (14)$$

where k^{o}_{ads} is the standard rate constant for the process. This equation qualitatively justifies the larger change in the activation energy due to the changes in the anion coverage due to the exponential factor of the $(1-\theta_{A}-\theta_{OH})$ term and also the observed shape of the curves of k_{ads} vs. potential, which should have a maximum located at $\theta_{A}=1/3$ and an onset potential which coincides with the onset potential of the anion and a final potential in the region where the anion adlayer is completed (or the anion has been replaced by adsorbed OH). It is not possible to predict the exact shape of the curves, since isotherms for the anion adsorption on the Pt(100) are not currently available, but the general shape agrees with the model. Incidentally, the changes with the temperature are also in agreement with the observed behavior of the anion adsorption on the Pt(100) electrode as the temperature increases. As aforementioned, the onset for anion adsorption is displaced to lower values as the temperature increases, and the same behavior is observed for k_{ads}. Also, the completion of the anion adlayer requires higher applied potentials, and thus, the window where CO formation takes place expands toward positive values.

4. Conclusions

In this manuscript, the apparent activation energies for the formic acid oxidation reaction on different platinum single crystal electrodes have been calculated, both for the direct and poisoning routes. It has been shown that the potential dependent behavior of the activation energies for the direct route is in agreement with a mechanism in which the adsorbed anions present on the surface play an active role in the oxidation mechanism. It has been proposed that these anions (sulfate or formate itself) facilitates the adsorption of the formic acid molecule in a configuration in which the C–H bond is directed toward the surface. Thus, the kinetic equation for the oxidation currents through the active intermediate contains the potential dependence, a term related to the pre-adsorbed anion coverage and another corresponding to a free site, where the incoming formate species should adsorb in the C–H down configuration. In this configuration, results from the literature show that the activation energy is low. For the poisoning route, the adsorbed anions are also important. However, two free sites are required for the anion to adsorb. It is important to stress that the complete understanding of an oxidation mechanism can only be achieved if experimental results using different techniques are combined with theoretical calculations.

Conflict of interest

Authors declare no conflict of interest.

Acknowledgments

This work has been financially supported by the MICINN (Spain) (project 2013-44083-P) and Generalitat Valenciana (Spain) (project PROMETEOII/2014/013, -FEDER).

References

[1] R. Parsons, T. Vandernoot, J. Electroanal. Chem. 257 (1988) 9.
[2] J.M. Feliu, E. Herrero, in: W. Vielstich, H. Gasteiger, A. Lamm (Eds.), Handbook of Fuel Cells – Fundamentals, Technology and Applications, vol. 2, John Wiley & Sons Ltd, Chichester, 2003.
[3] M.T.M. Koper, S.C.S. Lai, E. Herrero, in: M.T.M. Koper (Ed.), Fuel Cell Catalysis, A Surface Science Approach, John Wiley & Sons Inc, Hoboken, NJ, 2009, p. 159.
[4] Y.X. Chen, M. Heinen, Z. Jusys, R.J. Behm, Langmuir 22 (2006) 10399.
[5] G. Samjeske, M. Osawa, Angew. Chem. Int. Ed. 44 (2005) 5694.
[6] G. Samjeske, A. Miki, S. Ye, M. Osawa, J. Phys. Chem. B 110 (2006) 16559.
[7] M. Osawa, K. Komatsu, G. Samjeske, T. Uchida, T. Ikeshoji, A. Cuesta, C. Gutierrez, Angew. Chem. Int. Ed. 50 (2011) 1159.
[8] J. Joo, T. Uchida, A. Cuesta, M.T.M. Koper, M. Osawa, J. Am. Chem. Soc. 135 (2013) 9991.
[9] Y.X. Chen, M. Heinen, Z. Jusys, R.B. Behm, Angew. Chem. Int. Ed. 45 (2006) 981.
[10] Y.X. Chen, M. Heinen, Z. Jusys, R.J. Behm, Chem. Phys. Chem. 8 (2007) 380.
[11] S. Brimaud, J. Solla-Gullon, I. Weber, J.M. Feliu, R.J. Behm, Chem. Electron. Chem. 1 (2014) 1075.
[12] M. Neurock, M. Janik, A. Wieckowski, Faraday Discuss. 140 (2009) 363.
[13] W. Gao, J.A. Keith, J. Anton, T. Jacob, J. Am. Chem. Soc. 132 (2010) 18377.
[14] H.-F. Wang, Z.-P. Liu, J. Phys. Chem. C 113 (2009) 17502.
[15] J.V. Perales-Rondon, A. Ferre-Vilaplana, J.M. Feliu, E. Herrero, J. Am. Chem. Soc. 136 (2014) 13110.
[16] J. Clavilier, D. Armand, S.G. Sun, M. Petit, J. Electroanal. Chem. 205 (1986) 267.
[17] C. Korzeniewski, V. Climent, J.M. Feliu, in: A.J. Bard, C. Zoski (Eds.), Electroanalytical Chemistry: A Series of Advances, vol. 24, CRC Press, Boca Raton, 2012, p. 75.
[18] E. Herrero, J.M. Orts, A. Aldaz, J.M. Feliu, Surf. Sci. 440 (1999) 259.
[19] K. Itaya, S. Sugawara, K. Sashikata, N. Furuya, J. Vac. Sci. Technol., A 8 (1990) 515.
[20] A.M. Gomez-Marin, J.M. Feliu, Electrochim. Acta 82 (2012) 558.
[21] N. Garcia-Araez, V. Climent, J. Feliu, in: C.G. Vayenas (Ed.), Mod Asp Electrochem, vol. 51, Springer, New York, 2011, p. 1 (Chapter 1).
[22] V. Grozovski, V. Climent, E. Herrero, J.M. Feliu, Chem. Phys. Chem. 10 (2009) 1922.
[23] V. Grozovski, V. Climent, E. Herrero, J.M. Feliu, Phys. Chem. Chem. Phys. 12 (2010) 8822.
[24] M. Bergelin, E. Herrero, J.M. Feliu, M. Wasberg, J. Electroanal. Chem. 467 (1999) 74.
[25] N.P. Lebedeva, M.T.M. Koper, E. Herrero, J.M. Feliu, R.A. van Santen, J. Electroanal. Chem. 487 (2000) 37.
[26] V. Grozovski, F.J. Vidal-Iglesias, E. Herrero, J.M. Feliu, Chem. Phys. Chem. 12 (2011) 1641.
[27] J.V. Perales-Rondon, E. Herrero, J.M. Feliu, Electrochim. Acta 140 (2014) 511.
[28] S. Blais, G. Jerkiewicz, E. Herrero, J.M. Feliu, Langmuir 17 (2001) 3030.
[29] E. Herrero, B. Alvarez, J.M. Feliu, S. Blais, Z. Radovic-Hrapovic, G. Jerkiewicz, J. Electroanal. Chem. 567 (2004) 139.
[30] A.M. Funtikov, U. Linke, U. Stimming, R. Vogel, Surf. Sci. 324 (1995) L343.
[31] E. Herrero, J. Mostany, J.M. Feliu, J. Lipkowski, J. Electroanal. Chem. 534 (2002) 79.
[32] N. Garcia-Araez, V. Climent, P. Rodríguez, J.M. Feliu, Electrochim. Acta 53 (2008) 6793.
[33] J. Clavilier, J.M. Orts, R. Gómez, J.M. Feliu, A. Aldaz, in: B.E. Conway, G. Jerkiewicz (Eds.), The Electrochemical Society, vols. 94–21, INC., Pennington, NJ, 1994, p. 167.

Chapter V

Further Insights into the Formic Acid Oxidation Mechanism on Platinum: pH and Anion Adsorption Effects

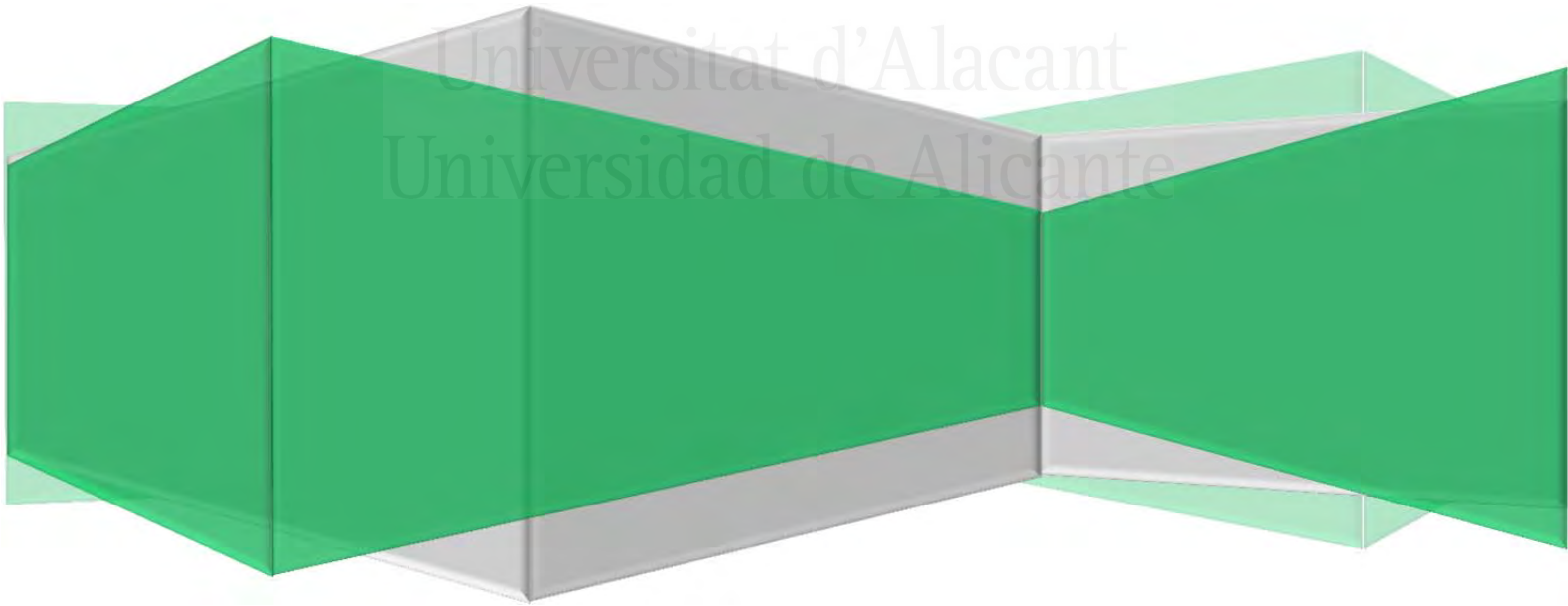

III

Publication III

J. V. Perales-Rondón, S. Brimaud, J. Solla-Gullón, E. Herrero, R. Jürgen Behm and J. M. Feliu, **"Further Insights into the Formic Acid Oxidation Mechanism on Platinum: pH and Anion Adsorption Effects"** *Electrochimica Acta* **2015**, 180, 479-485. **doi:**10.1016/j.electacta.2015.08.155.

Electrochimica Acta 180 (2015) 479–485

Contents lists available at ScienceDirect

Electrochimica Acta

journal homepage: www.elsevier.com/locate/electacta

Further Insights into the Formic Acid Oxidation Mechanism on Platinum: pH and Anion Adsorption Effects

Juan V. Perales-Rondón[a], Sylvain Brimaud[b,1], Jose Solla-Gullón[a,1,*], Enrique Herrero[a,c,1], R. Jürgen Behm[b,1], Juan M. Feliu[a,c,1]

[a] Instituto de Electroquímica, Universidad de Alicante Apartado 99, E-03080 Alicante, Spain
[b] Institut für Oberflächenchemie und Katalyse, Universität Ulm, Albert-Einstein-Alle 47, D-89069 Ulm, Germany
[c] Departamento de Química-Física, Universidad de Alicante Apartado 99, E-03080 Alicante, Spain

ARTICLE INFO

Article history:
Received 27 May 2015
Received in revised form 10 July 2015
Accepted 30 August 2015
Available online 1 September 2015

Keywords:
Formic acid oxidation
Pt electrode
Specific anion adsorption
pH effects
formic acid oxidation mechanism

ABSTRACT

The influence of the electrolyte pH in the formic acid oxidation reaction on a polyoriented Pt electrode in the presence of different anions, including sulfate, perchlorate, phosphate and chloride, in different concentrations has been investigated, using cyclic voltammetric measurements. The curves of the peak currents in the negative scan direction vs. the pH in pure sulfate and perchlorate solutions are very similar. For these solutions, the maximum oxidation currents increase steadily with increasing pH up to pH ≈ 5, followed by a plateau until pH 10. This suggests that the reaction proceeds via a similar reaction mechanism, in which the concentration of $HCOO^-$ anions in solution plays a key role. For phosphate or chloride containing solutions, in contrast, the maximum oxidation currents show a bell-shaped pH-oxidation current correlation, whose exact shape depends on the anion concentration. We suggest that in these cases the pH-current relation is modified by competing specific adsorption of anions which act as site blocking spectator species. These results will be discussed in relation with compatible mechanistic proposals.

1. Introduction

Formic acid electrooxidation is one of the most relevant electrocatalytic reactions, not only because it is a model reaction for a two-electron-transfer reaction, but also for its potential use as fuel in direct formic acid fuel cells, in particular for portable applications and small power generation devices [1]. It is widely accepted that the oxidation of formic acid takes place through a dual path mechanism [2–4] a direct pathway via an adsorbed reactive intermediate and a pathway involving the formation of adsorbed CO that acts as a poison for the reaction, being further oxidized to CO_2 at higher overpotentials ('indirect pathway'). This second route has been well established and the presence of adsorbed CO was clearly identified by in situ infrared spectroscopy [5,6]. Nevertheless, the nature and role of the reactive intermediate in the direct pathway is still matter of strong discussion in the literature. Osawa et al. early proposed adsorbed bidentate formate species as the reactive intermediate after their detection by *in situ* surface-enhanced infrared absorption spectroscopy in an attenuated total reflection configuration (ATR-SEIRAS) [7] and they also found a qualitative correlation between the observed reactivity and the amount of adsorbed formate [8]. In this way, this adsorbed bidentate formate has been considered to be the reactive intermediate species in subsequent contributions [9–13]. However, in other reports, this adsorbed bidentate formate has been considered, conversely, as a site-blocking spectator species, and the oxidation has been proposed to proceed via a weakly adsorbed HCOOH [14–17]. Currently, the nature and role of the reactive intermediate are still under debate [17,18] and more insights are still required to clarify these mechanistic considerations.

Interestingly, after some previous approaches [19–21], the effect of the solution pH on the reaction kinetics has been very recently reincorporated in the discussion about the reaction mechanism. Osawa and co-workers performed HCOOH oxidation experiments on a rotating Pt disc electrode over a wide range of pH (0–12) in phosphate buffer solutions [22,23]. They found a bell-shaped pH-current activity, showing a maximum activity at a pH equal to the pK_a of the formic acid in solution ($pK_a = 3.7$). From this experimental evidence, these authors concluded that the increase of the activity with increasing pH, in the range of low pH values (pH < pK_a of formic acid), was due to the increasing concentration

* Corresponding author.
E-mail address: jose.solla@ua.es (J. Solla-Gullón).
[1] ISE member.

http://dx.doi.org/10.1016/j.electacta.2015.08.155
0013-4686/

of $HCOO^-$ in the electrolyte, thus suggesting that this species, rather than HCOOH, was the reactive species. The decay in activity at higher pH values ($pH > pK_a$) was attributed to a competitive adsorption of OH^-, whose concentration increases with increasing pH, thus leading to a decreasing reactivity as a consequence of an increasing site blocking at higher pH values.

Almost in parallel, Behm and co-workers also carried out pH experiments using both Au and Pt electrodes [24]. For Au electrodes, they observed an analogous bell-shaped pH-current correlation, with also a maximum current obtained for solution pH at the pK_a of HCOOH. However, for Pt electrodes, and in contrast with Osawa's observation, they found that the catalytic activity increases steadily with increasing pH up to pH ≈ 5, followed by a plateau until pH 10, in agreement with early observations [20,21]. Based on these observations, they suggested that different reaction mechanisms operate for HCOOH oxidation on Pt and Au electrodes, as a consequence of the different adsorption strengths of the adsorbed species involved in the reaction. Focusing our attention to the case of Pt electrodes, it is of fundamental importance to understand the reasons for the observation of the distinctly different pH-current dependencies in these two research groups. At this point, it is worth noting the different nature of the electrolyte employed (phosphate in [22,23] and sulfate/perchlorate in [24]). The specific adsorption of the anion present in the solution could play, together with the particular pH, a critical role on the reaction kinetics and/or modify the reaction mechanism (i.e., the most favorable reaction pathway).

To complete this overview, in a more recent contribution, Herrero and co-workers performed formic acid oxidation experiments on a Pt(111) electrode in solutions containing perchloric, sulfuric and acetic acids in the pH range between 0 and 2 [25]. They concluded that the reaction requires the presence of at least two species, an adsorbed anion (sulfate, acetate or bridge-bonded bidentate formate) and solution formate. Interestingly, these authors proposed that the solution formate would react with the C-H bond close to the surface to produce its cleavage and thus forming CO_2, being this step facilitated by the adsorbed anion. Furthermore, this reaction scheme was in good agreement with findings in previous DFT calculations [26]. In this sense, it is also worth noting the contributions reported by Jacob et al. [27,28]. Using DFT calculations, they studied the electrooxidation mechanism of the formic acid in a Pt(111) electrode with a particular solvation model and under the influence of an electrode potential to mimic electrochemical conditions. They interestingly observed that the *preferred* HCOOH oxidation reaction pathway was potential-dependent, and consequently, the overall rate constant also depended on the electrode potential.

In order to improve our understanding of the combined effects of solution pH and anion specific adsorption on the HCOOH oxidation current, we conducted a systematic study of formic acid oxidation on polycrystalline platinum electrodes in a wide range of pH values (0–12), employing different and combined supporting electrolytes. We will confirm that the active species for formic acid oxidation is most likely the formate ion in solution and will show that the relationship between the Pt electrode activity and the solution pH depends on the electrolyte counter-ion, i.e., it is mainly controlled by the specific adsorption of anions like phosphates. Finally, our results will be discussed regarding to previous mechanistic proposals.

2. Experimental

The experiments were performed in a classical three-electrode cell, using a Pt wire as counter electrode. The potentials were measured against a reversible hydrogen electrode (RHE) connected to the cell via a Luggin capillary or a palladium-hydrogen electrode. All potentials were referred to the RHE. Appropriate amounts of H_2SO_4 (suprapure, Merck) or $HClO_4$ (suprapure, Merck) and Na_2SO_4 (99.99%, Aldrich) or $NaClO_4$ (99.99%, Sigma–Aldrich) and NaOH (99.99%, Sigma–Aldrich) were added to MilliQ® water (Millipore, 18 MΩ cm) in order to prepare electrolytes at various pH values, maintaining a constant (bi) sulfate or perchlorate concentration (0.5 M). Phosphate solutions (0.2 M) with different pHs were prepared from appropriate amounts of H_3PO_4 (98%, Merck), NaH_2PO_4 (99.99%, Merck), Na_2HPO_4 (99.999%, Fluka) and Na_3PO_4 (Puriss., Sigma). NaCl (suprapure, Merck) was used for the preparation of chloride containing solutions. For all experiments, the initial concentration of HCOOH was fixed at 0.1 M. Thus, depending on the electrolyte pH, formic acid will be more or less dissociated, but the overall concentration of formic acid + formate ions was constant and equivalent to 0.1 M for all experiments. The solutions were purged by Ar bubbling (Alpha Gaz™ 99.999%). Particular attention was paid to the cleanness of the experimental set-up.

An EDI-101 rotating disk electrode (2 mm Pt tip, Radiometer) was used. The rotation rate was controlled by a Radiometer CTV 101 apparatus. Prior to the use of the Pt RDE, the electrode was electrochemically cleaned (cycles between surface oxidation and hydrogen adsorption-desorption regions, i.e., 0.05 V and 1.50 V) in 0.5 M H_2SO_4 until a stable voltammetric response was obtained. All experiments were conducted at room temperature, using a potentiostat-galvanostat AUTOLAB PGSTAT302N (Metrohm Autolab).

3. Results

3.1. Formic acid oxidation in phosphate solutions at different pH's

Fig. 1 shows representative cyclic voltammograms of 0.1 M formic acid oxidation recorded at a rotating Pt disk electrode in 0.2 M phosphate solutions at various pH values. For the sake of simplicity, only three voltammograms are shown, which correspond to the three main pH regions of interest, that is, below, at, and above the pK_a (3.7) of formic acid. The results are in good agreement with those reported by Osawa and co-workers [22,23], who employed a similar electrolyte, both in terms of the voltammetric profiles as well as by the observation of a maximum oxidation peak current which takes place at a pH close to the pK_a. This is illustrated by plotting the maximum oxidation current in

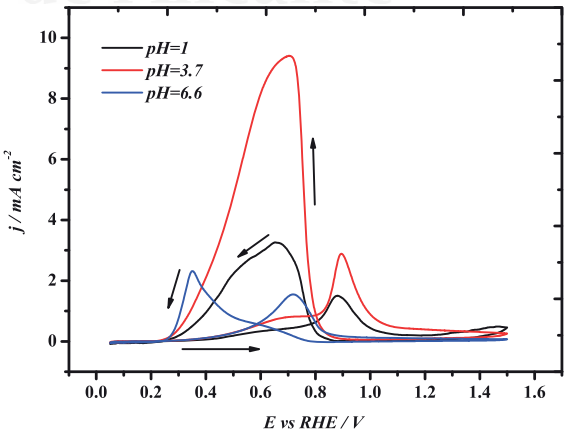

Fig. 1. Cyclic voltammograms of a rotating Pt disk electrode in 0.1 M HCOOH + 0.2 M phosphate solutions. Scan rate 50 mV s^{-1}. Black line (pH 1); red line (pH 3.7); blue line (pH 6.6). Rotation rate: 1000 rpm. (For interpretation of the references to color in this figure legend, the reader is referred to the web version of this article.)

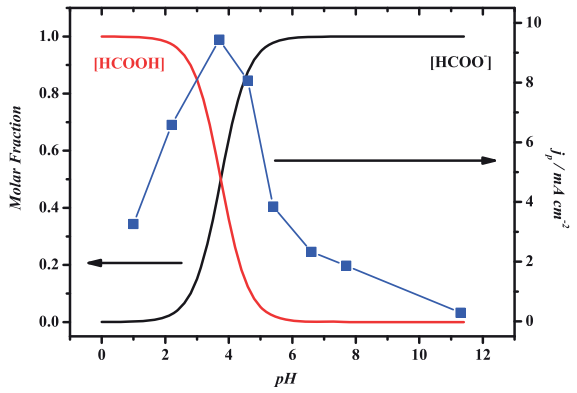

Fig. 2. The pH dependence of the peak current density (j_p) on the negative-going scan (blue line) in 0.1 M HCOOH + 0.2 M phosphate solutions obtained with a Pt rotating disk electrode with a rotation rate of 1000 rpm at a scan rate of 50 mV s^{-1}. The black and red line represent the molar fractions of HCOOH and HCOO$^-$, respectively, in the solution. (For interpretation of the references to color in this figure legend, the reader is referred to the web version of this article.)

the negative-going scan after the reduction of the Pt surface oxide versus the pH of the solution (Fig. 2). This maximum current provides a good measure of the behavior of the electrode although, in a more rigorous point of view, a pulsed voltammetry analysis with its corresponding fitting would be required to evaluate the intrinsic activity of the electrode, that is, the activity at t = 0 [29–31]. The plot results in a bell shaped activity curve, with a maximum at the pK_a of formic acid, similar to that previously reported (the current is about twice because the concentration is two times that used in the previous work) [22].

3.2. Formic acid oxidation in perchlorate and sulfate solutions at different pH's

As it has been previously underlined that for solutions having low buffering capability [24,32] and for large HCOOH oxidation currents obtained with a Pt electrode (2–15 mA cm^{-2}) it is important to ensure that the electrochemical release of protons during the oxidation reaction does not significantly alter the local pH in the vicinity of the electrode and consequently the relationship between the electrode activity and the pH of the bulk solution. Local changes of the interfacial pH can significantly

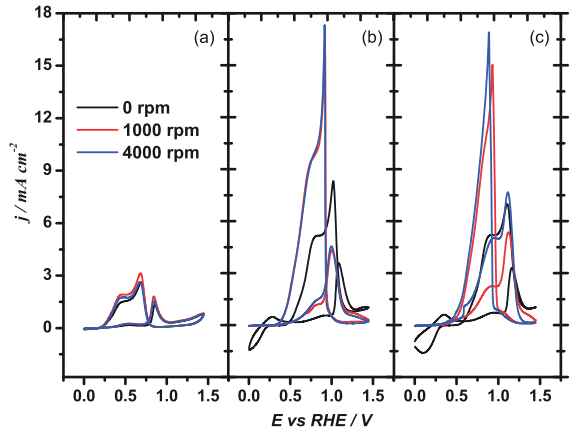

Fig. 3. Cyclic voltammograms of a rotating Pt disk electrode in 0.1 M HCOOH + 0.5 M perchlorate solutions. Scan rate 50 mV s^{-1}. (a) pH 0.9; (b) pH 6.5; (c) pH 9.1.

affect the rate and mechanism during the course of an electrodic reaction as recently shown for ethanol oxidation at Pt electrodes in alkaline media [33]. Fig. 3 shows voltammograms obtained with a Pt electrode in 0.1 M HCOOH containing perchlorate solutions, at different pHs and for different rotation rates of the Pt working electrode, including quiescent conditions. As expected, in strongly acidic solutions (Fig. 3a) a lowering of the diffusion layer thickness by a stepwise increase of Pt electrode rotation rate barely affects the current values as compared to measurements performed in quiescent conditions. However, for higher pH values (Fig. 3b and c), the main voltammetric features in the oxidation process in quiescent conditions are significantly shifted to higher potentials compared to measurements performed at 1000 rpm and 4000 rpm (between these two rotation rates, the changes are minimal). In addition, in quiescent conditions, a contribution related to the reduction of protons, formed and accumulated in the diffusion layer during the oxidation reaction, is clearly observed. Subsequently, in the positive-going sweep, an oxidative process, associated with oxidation of the electrochemically formed hydrogen, is also observed. One should also note that the oxidation current densities are much higher (ca. doubled) when the diffusion away from the Pt electrode of the protons released upon the oxidation reaction is enhanced by rotating the electrode. Nevertheless, only minor changes in the shape of the current traces are observed with the rotation rates employed, confirming that in the whole potential range the HCOOH oxidation reaction is not controlled by mass transport limitations. Therefore, under present experimental conditions local modification of the pH in the vicinity of the Pt electrode, coming from proton released after HCOOH oxidation, can be neglected at electrode rotation rates equal to or higher than 1000 rpm, in agreement with earlier findings [34]. In addition, it should be noted that relatively high rotation rates such as 4000 rpm cause only a minor increase in the current density (recorded from the current of the oxidation peak, in the negative-going scan, after the reduction of the Pt surface oxide) for pH values higher than 7. Therefore, and in order to minimize possible surface contaminations taking place at very high rotation rates, we decided to use a rotation rate of 1000 rpm as standard value to compare results on different solution. In this regard, it is worth reporting that this conclusion is also valid for experiments conducted in phosphate solutions (see section above), in particular for those pH values with low buffering properties.

The voltammetric profiles and maximum oxidation currents of the current traces obtained in perchlorate solutions are essentially identical to those previously reported in sulfate containing solutions, employing similar experimental conditions [24]. In fact, as illustrated in Fig. 4, the changes in the maximum oxidation current density as function of the electrolyte pH, both in sulfate and perchlorate solutions, are very similar; that is, the oxidation current increases steadily with increasing pH up to a pH value of approximately 5, from which the current density remains practically stable until a pH close to 9–10. Above this pH, the oxidation current decreases dramatically, which is considered to be a consequence of OH adsorption (or oxide formation) on the electrode surface, as suggested in refs [35,36].

These experimental findings strongly suggest that the oxidation reaction seems to proceed via a similar reaction mechanism in both electrolytes. This fact also implies that the specific adsorption of sulfate anions on the Pt surface does not significantly alter the reaction kinetics compared to that obtained in the absence of specific anion adsorption (ClO_4^- solutions). In addition, taking into account that this pH-oxidation current relationship follows remarkably well the HCOOH dissociation proportion to HCOO$^-$ anions in the bulk of the electrolyte, these results suggest that formate anions are the precursors for the oxidation reaction, as was concluded in the recent paper by Joo et al. [22,23]. From the

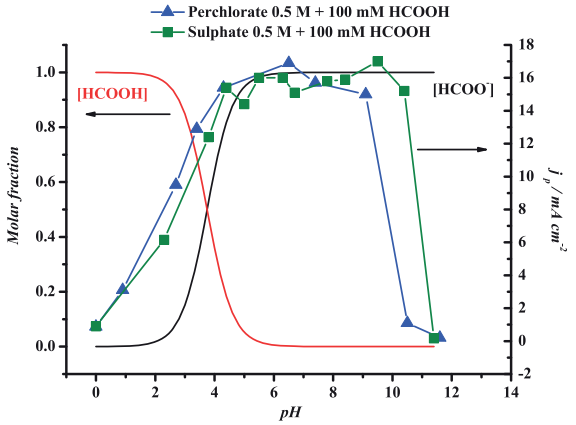

Fig. 4. The pH dependence of the peak current density (j_p) in the negative-going scan in 0.5 M perchlorate (blue line) and 0.5 M sulfate (green line) electrolyte. Electrode: Pt rotating disk electrode with a rotation rate of 1000 rpm. The black and red line represent the molar fractions of HCOOH and $HCOO^-$, respectively, in the solution. (For interpretation of the references to color in this figure legend, the reader is referred to the web version of this article.)

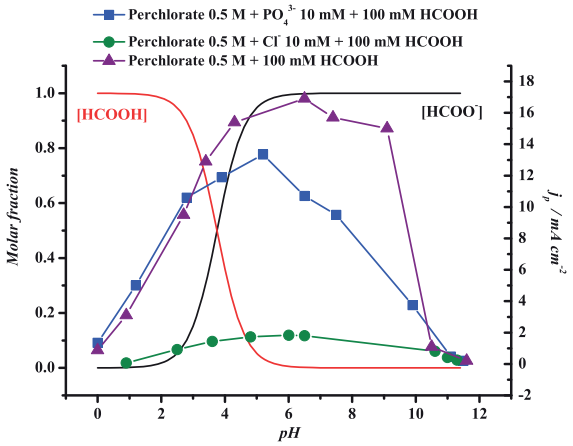

Fig. 5. The pH dependence of the peak current density (j_p) in the negative-going scan in 0.5 M perchlorate + 10 mM PO_4^{3-} (blue line), 0.5 M perchlorate + 10 mM Cl^- (green line) and 0.5 M perchlorate (purple line) solution. Electrode: Pt rotating disk electrode with a rotation rate of 1000 rpm. Both, black and red line represents the molar fractions of HCOOH and $HCOO^-$ respectively in the solution. (For interpretation of the references to color in this figure legend, the reader is referred to the web version of this article.)

absence of a measurable competition resulting from specifically adsorbed anions in the presence of strongly adsorbing anions (SO_4^{2-}), we might conclude that (1) either the turnover frequency of the reaction is very high and thus a partial site blocking by adsorbed anions is not detected, or (2) the adsorption strength of the activated complex is higher than that of those species present in solution, or (3) both (1) and (2) operate. As will be discussed later, none of those possible explanations can justify the whole set of experiments, and other justifications will be proposed for the observed behavior. Finally, it is important to highlight that not only the pH-oxidation current relationship obtained in sulfate and perchlorate solutions is different to that obtained in phosphate solutions (see Fig. 2), but also the maximum current densities which are ca. 50% lower in the latter solutions. This seems to indicate that in phosphate solutions the HCOOH oxidation reaction is slowed down by an adsorbed species.

3.3. Formic acid oxidation in deliberately modified perchlorate solutions. Effect of the specific anion adsorption

The specific adsorption of anions on a Pt surface is well-known to play a critical role in Electrocatalysis and, for many reactions of interest, determine the resulting electrocatalytic activity [37–41]. Consequently, the understanding of the different adsorption strengths of the species present in solution is a question of outstanding importance. This fact implies that, if a particular anion adsorbs stronger than the reactive molecule, the reaction mechanism of the process could be modified with respect to that taking place in the absence of this particular anion. In order to reveal whether specific adsorption of anions is responsible for the differences in the oxidation current-solution pH relationship between sulfate/perchlorate and phosphate solutions, we have carried out additional experiments in perchlorate solutions in which a low amount (10 mM) of Cl^- and phosphate was deliberately added. The results are displayed in Fig. 5.

The addition of these anions produces a remarkable lowering in the maximum current density compared to pure perchlorate solutions. Interestingly, in both cases the current-pH relationship exhibits a broad, bell-shape form, with the maximum oxidation currents at different pH values. In the presence of Cl^-, the decrease of the activity is particularly dramatic, with the electrocatalytic activity of the Pt surface being almost suppressed as a consequence of the strongly adsorbed Cl^- anions. Obviously, these act as site-blocking species. For the perchlorate solution containing 10 mM phosphate anions, at solution pH lower than 3, the reactivity remains essentially similar to that observed in the absence of phosphate anions. However, at higher pH values, a clear diminution of the oxidation current is observed. One should also note that the relationship oxidation current-solution pH exhibits a bell-shape with a maximum at a solution pH close to 5–6. Comparing the results for 10 mM phosphate containing 0.5 M perchlorate solution to those in 0.2 M phosphate solution (see Fig. 6), we emphasize that (i) the oxidation currents in 0.2 M phosphate solutions are systematically lower in the whole pH range and that (ii) the maximum of the bell-shaped oxidation current-solution pH is also shifted to lower pH values in these latter solutions.

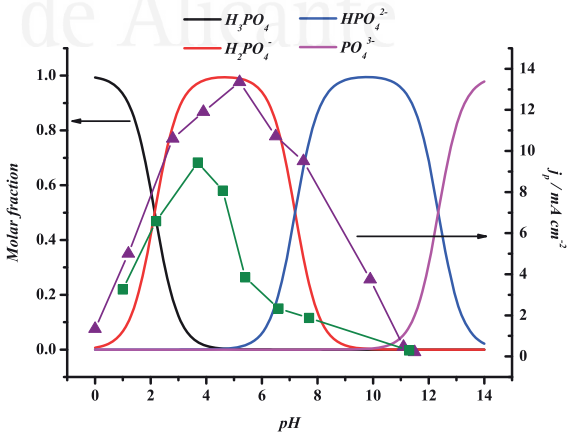

Fig. 6. The pH dependence of the peak current density (j_p) in the negative-going scan in perchlorate 0.5 M + 10 mM PO_4^{3-} (purple line) and 0.2 M phosphate (green line). Electrode: Pt rotating disk electrode with a rotation rate of 1000 rpm. Black, red, blue and magenta lines represent the molar fractions of H_3PO_4, $H_2PO_4^-$, HPO_4^{2-} and PO_4^{3-}, respectively, in the solution. (For interpretation of the references to color in this figure legend, the reader is referred to the web version of this article.)

These results strongly suggest that the origin of the decay of the oxidation current density for solution pH values higher than the pK_a of formic acid is related to the specific adsorption of phosphate species rather than to Pt surface oxidation or OH adsorption, as was previously suggested by Joo et al. [22,23]. Also, by simply plotting the anion phosphate species distribution as a function of the pH (see Fig. 6), we can intuit that the presence of $H_2PO_4^-$ and/or HPO_4^{2-} may be responsible of the evident decrease of the oxidation activity. In this sense, it is worth noting that previous FTIR studies on electrodes showed changes in the nature or configuration of the adsorbed phosphate species with the solution pH and potential [42–45].

3.4. Discussion of the mechanism of the formic acid oxidation

The results presented and discussed above provide new and relevant insights into the mechanism of the formic acid oxidation reaction on Pt electrode surfaces. In particular, the reaction mechanism seems to be controlled by two different aspects, (1) the pH of the solution, which determines the concentration of formate anion in solution, and (2) the specific adsorption of other species present in the solution. This latter step is essentially determined by the different adsorption strengths of such species and their nature. First of all, the almost identical peak currents measured in perchloric and sulfuric acid solutions will be discussed. As aforementioned, this behavior could be interpreted in two different ways. In the first hypothesis, the turnover frequency is so high than the diminution in turnover frequency due to the presence of a relatively strong adsorbing anion, such as sulfate, is not translated into a diminution in the measured current. This situation is achieved when the reaction is purely controlled by the diffusion of the reactant species to the electrode surface, so that this is the slowest step in the reaction. Any rate diminution in the other steps is not translated into a change in the current, provided that the diffusion step is still the rate determining step. However, as shown in Fig. 3, this is not the case. At low pH values, the oxidation currents are independent of the rotation rate, which clearly indicates that these currents are totally controlled by the kinetic of the oxidation process. At higher pH values, an increase in the currents is observed below 1000 rpm, but above this value, the measured currents are constant. Therefore, also in this case the currents measured at 1000 rpm are controlled by the reaction kinetics as well, and not by the transport of species between the bulk solution and the interphase.

The second possible explanation is that the adsorption strength of the reactive intermediate is higher than that of the anions present in solution. It should be taken into account that in the case of perchloric acid solution at low pH values, bridge-bonded bidentate formate species are the species specifically adsorbed on the surface, as shown by FTIR and electrochemical experiments [8,12]. Although it has been evidenced that perchlorate anions can adsorb on the surface [46], the adsorption strength of these formate species is much higher than that of perchlorate anions. Therefore, the former one represents the adsorbed species in formic acid containing solutions. Thus, the adsorption strength of formate and sulfate anions should then be compared. For Pt(111) electrodes, the adsorption of sulfate in 0.5 M sulfuric acid solutions would seem stronger than that of formate [12,47] and thus a diminution in the oxidation currents should have been expected. However, using vibrational broadband sum-frequency generation (SFG) measurements, Braunschweig and Wieckowski reported that, in presence of HCOOH, the contributions related to (bi) sulfate anions were absent and the spectra were dominated by the contribution associated with the symmetric carboxylate stretching vibration of adsorbed formate [48]. This finding would suggest that the formate is adsorbing more strongly than (bi) sulfate anions. In any case, it has been proposed that both adsorbed formate and sulfate have a beneficial effect in the oxidation currents [25]. Thus, it was reported that for a Pt(111) electrodes and in the pH range between 0 and 2, adsorbed formate or sulfate would facilitate the adsorption of a second formate ion in a C–H down configuration [25,47]. In fact, in this latter configuration, the cleavage of the C–H bond has been reported to have a low activation energy [26]. This formate with the C–H down configuration would be the reactive intermediate, whose interaction with the surface is stabilized by the presence of an additional adsorbed species (e.g., the adsorbed bidentate formate, or an adsorbed sulfate anion). Therefore, the active intermediate can, in fact, also be considered as a dimer. It should be mentioned that formic acid dimers are present in aqueous solutions, as have been postulated on the basis of thermodynamic measurements [49,50], and that the presence of a bisulfate-formic acid dimer is also possible, due to the possible formation of hydrogen bonds. At this point, it is important to note that this mechanistic proposal has been exclusively postulated for Pt(111) surfaces, although recent results seems to indicate that a similar scenario takes place for Pt(100) electrodes [51]. However, due to the fact that the Pt electrode was electrochemically cleaned (cycles between surface oxidation and hydrogen adsorption-desorption regions, i.e., 0.05 V and 1.50 V) in 0.5 M H_2SO_4 prior to the formic acid experiments, the presence of (111) and (100) facets can be discarded [25] in the present contribution. This fact, however, does not necessarily imply a modification of the oxidation mechanism because both species, bridge-bonded formate and sulfate, can be absorbed on polyoriented/polycrystalline Pt surfaces.

On the other hand, it should be mentioned that at pH > 5–6 sulfate is probably not adsorbed on the platinum surface. For Pt(111) electrodes, the onset of adsorption is shifted in the RHE scale to higher potential values as the pH increases to about 4, so that it almost coincides with the onset of OH adsorption on this electrode [52]. Thus, at higher pH values, sulfate anions cannot compete with the adsorption of OH, and this species is the one controlling the reactivity. A similar situation is expected for the formate adsorption in the bidentate configuration, whose coverage decreases to zero at pH > 6 [22]. However, despite the absence of any specific anion adsorption, the oxidation currents remain not only constant in the pH range between 5 and 9–10, but also at their maximum current value. This observation may suggest that the presence of an adsorbed anion is not required to facilitate the interaction with a formate ion in a C–H down configuration and that the reaction depends exclusively on the concentration of formate ions in solution, which is determined by its pH. However, it should be borne in mind that as the pH increases, the potential window in the SHE scale is displaced to negative values. Thus, the surface would have an increasing negative net charge [53], which could favor the interaction with the formate anion in the C–H down configuration. Finally, at pH values > 9–10, the oxidation current decreases dramatically as a consequence of an increasing OH_{ad} coverage or oxide formation, which in turn results from the increasing OH^- concentration.

Different from this behavior, the presence of chloride anions in solution essentially diminish the reactivity of the electrode. Chloride anions are known to adsorb stronger than sulfate, and there is no possibility of an interaction through hydrogen bonds between the formic acid molecule and the adsorbed chloride species. Thus the observed behavior in the reaction is that of a purely site blocking species.

In the presence of phosphate anions, whose adsorption strength can be considered to be in between those of sulfate and chloride, the behavior is a mixture of both limiting cases: perchloric acid solution and chloride solution. At pH < 3 and for low phosphate concentrations (10 mM), the measured peak currents are similar to

those in perchlorate or sulfate solutions, whereas above this pH value the currents decrease (Fig. 5). The exact pH for the onset of the decrease depends on the concentration of the phosphate species. Thus, some change in the interphase of the electrode should occur around a pH of 3. Examining the voltammograms of the polycrystalline platinum and Pt(111) electrodes between pH 0 and 12, however, no significant change can be detected [54]. These voltammograms have the typical characteristics observed for Pt electrodes in the presence of strongly adsorbing anions, implying that these anions are always present in the interphase in the potential range where formic acid oxidation takes place. Therefore, there must be an additional factor which is responsible for the change in the reaction behavior. Indeed, FTIR studies of the adsorption of phosphate revealed an important difference in the adsorption behavior compared to that of sulfate. For sulfate, no change in the bands is observed with pH or potential, indicating that the adsorbed species is always the same [55]. On the other hand, for adsorbed phosphate species there are clear changes in the related bands with potential and pH [43,45]. Although it is difficult to establish the exact nature of the adsorbed species on the interphase, due to the changes in the configuration upon adsorption [56], the data indicate clear changes in the configuration/nature of the adsorbed species. At low pH values, $H_3PO_{4,ad}$ has been postulated as the adsorbed species, which transforms into $H_2PO_{4,ad}$ at high potentials [43,45]. At a pH value around 3, the adsorbed species is $H_2PO_{4,ad}$ at lower potentials, while at higher potentials this is replaced by $HPO_{4,ad}$. Probably, at higher pH values, the main species adsorbed on the electrode surface is $H_2PO_{4,ad}$. Thus, the change in the behavior of the formic acid oxidation current curves versus pH, can be related to changes in the dominant adsorbed species on the surface. The species identified as adsorbed H_3PO_4 or as $H_2PO_{4,ad}$ do not markedly affect the adsorption of the formate species in the C-H down configuration (they may even support this process, as in the case of sulfate), whereas $HPO_{4,ad}$ will act as site blocking species for the reaction, strongly lowering its rate.

Taking into account this complex scenario, a plausible reaction mechanism would involve the following scheme, in which the concentration of $HCOO^-$ anions in the electrolyte is controlled by the pH of the solution:

$$HCOO^-_{sol} \rightarrow [intermediate]_{ads} \rightarrow CO_2 + H^+ + 2e^- \quad (1)$$

The active intermediate could be a formate species in a C-H down configuration. For pH values between 0 and 5, the adsorption of this formate species may be facilitated by the presence of an adsorbed species, Pt-A (adsorbed sulfate or adsorbed bidentate formate) and thus:

$$Pt-A + Pt-HCOO^-_{C-Hdown} \rightarrow Pt-A + CO_2 + Pt + H^+ + 2e^- \quad 0 < pH < 5 \quad (2)$$

In contrast, for pH values between 5 and 10, where the adsorbed anions are absent, the adsorption of the formate species in a C–H down configuration would be promoted by the negative net charge of the surface. This negative charge is a consequence of the pH shift that displaces, in the SHE scale, the potential window to negative values. In this case the reaction is expected to proceed via:

$$Pt-HCOO^-_{C-Hdown} \rightarrow CO_2 + Pt + H^+ + 2e^- \quad 5 < pH < 10 \quad (3)$$

In the presence of strongly adsorbed anions as present in chloride or phosphate solutions, the reaction is clearly perturbed or even inhibited, and the resulting activity is dominated by site blocking spectator species.

Finally, it is important to recall that, as previously suggested by Jacob et al., the *dominant* or *preferred* reaction pathway may change with the electrode potential [27,28]. To properly evaluate this effect, new pH-dependent experiments using pulse voltammetry are in progress to evaluate both paths (direct and indirect) independently, and to determine the reaction kinetics parameters as previously shown [29–31]. In addition, these experiments will be also carried with Pt single crystals (Pt(100) and Pt(111) electrodes) to re-evaluate the well-established surface structure sensitivity of this reaction but at different pHs [25,51]. All this information will help us to achieve a better understanding of the formic acid oxidation reaction.

4. Conclusions

The effect of the electrolyte pH in the formic acid oxidation reaction on a polyoriented Pt electrode in the presence of different anions has been investigated, focusing on anion effects. The results obtained show that in the case of sulfate and perchlorate solutions, the evolution of the electrocatalytic activity with increasing pH is very similar, with the maximum oxidation current steadily increasing up to pH ≈ 5, followed by a plateau up to a pH value of ~10. In contrast, for phosphate or chloride containing solutions, the evolution of the maximum oxidation current is completely different and shows a bell-shaped pH-oxidation current correlation. This pH-current correlation suggests that the specific adsorption of anions is a critical parameter, which strongly determines the resulting pH-current dependency. Based on these findings, a mechanism is proposed, in which a formate anion interacting with the surface in a C–H down configuration could be the active intermediate.

For pH values between 0 and 5, the interaction with this formate species in a C–H down configuration may be supported and even facilitated by the presence of an adsorbed anion like sulfate and or formate (bidentate adsorbed formate); while for pH values between 5 and 10, the adsorption of the suggested active intermediate would be facilitated by the negative net charge of the surface. The presence of strongly adsorbing anions such as chloride or phosphate anions, leads to a bell-shaped pH-oxidation current correlation, where the decay of the maximum current at higher pH values results from the specific adsorption of these anions, which act as site blocking spectator species.

Acknowledgments

This work has been financially supported by the MICINN (Spain) (projects CTQ2013-44083-P and CTQ2013-48280-C3-3-R) and Generalitat Valenciana (project PROMETEOII/2014/013, FEDER), as well as by the Deutsche Forschungsgemeinschaft via the project BE 1201 / 17-1.

References

[1] S. Uhm, H.J. Lee, J. Lee, Understanding underlying processes in formic acid fuel cells, Phys. Chem. Chem. Phys. 11 (2009) 9326–9336.
[2] A. Capon, R. Parsons, The oxidation of formic acid at noble metal electrodes: I. Review of previous work, J. Electroanal. Chem. 44 (1973) 1–7.
[3] A. Capon, R. Parsons, The oxidation of formic acid on noble metal electrodes: II. A comparison of the behaviour of pure electrodes, J. Electroanal. Chem. 44 (1973) 239–254.
[4] A. Capon, R. Parsons, The oxidation of formic acid at noble metal electrodes Part III. Intermediates and mechanism on platinum electrodes, J. Electroanal. Chem. 45 (1973) 205–231.
[5] B. Beden, A. Bewick, C. Lamy, A study by electrochemically modulated infrared reflectance spectroscopy of the electrosorption of formic-acid at a platinum-electrode, J. Electroanal. Chem. 148 (1983) 147–160.
[6] K. Kunimatsu, H. Kita, Infrared spectroscopic study of methanol and formic acid adsorbates on a platinum electrode. Part II. Role of linear COads derived from methanol and formic acid in the electrocatalytic oxidation of CH_3OH and HCOOH, J. Electroanal. Chem. 218 (1987) 153.
[7] A. Miki, S. Ye, M. Osawa, Surface-enhanced IR absorption on platinum nanoparticles: an application to real-time monitoring of electrocatalytic reactions, Chem. Commun. (2002) 1500–1501.

[8] G. Samjeske, M. Osawa, Current oscillations during formic acid oxidation on a Pt electrode: Insight into the mechanism by time-resolved IR spectroscopy, Angew. Chem. Int. Ed. 44 (2005) 5694–5698.
[9] G. Samjeske, A. Miki, S. Ye, M. Osawa, Mechanistic study of electrocatalytic oxidation of formic acid at platinum in acidic solution by time-resolved surface-enhanced infrared absorption spectroscopy, J. Phys. Chem. B 110 (2006) 16559–16566.
[10] A. Cuesta, G. Cabello, C. Gutierrez, M. Osawa, Adsorbed formate: the key intermediate in the oxidation of formic acid on platinum electrodes, Phys. Chem. Chem. Phys. 13 (2011) 20091–20095.
[11] M. Osawa, K. Komatsu, G. Samjeske, T. Uchida, T. Ikeshoji, A. Cuesta, C. Gutierrez, The Role of Bridge-Bonded Adsorbed Formate in the Electrocatalytic Oxidation of Formic Acid on Platinum, Angew. Chem. Int. Ed. 50 (2011) 1159–1163.
[12] V. Grozovski, F.J. Vidal-Iglesias, E. Herrero, J.M. Feliu, Adsorption of Formate and Its Role as Intermediate in Formic Acid Oxidation on Platinum Electrodes, ChemPhysChem 12 (2011) 1641–1644.
[13] A. Cuesta, G. Cabello, M. Osawa, C. Gutiérrez, Mechanism of the Electrocatalytic Oxidation of Formic Acid on Metals, ACS Catal. 2 (2012) 728–738.
[14] Y.X. Chen, M. Heinen, Z. Jusys, R.B. Behm, Kinetics and mechanism of the electrooxidation of formic acid—Spectroelectrochemical studies in a flow cell, Angew. Chem. Int. Ed. 45 (2006) 981–985.
[15] Y.X. Chen, M. Heinen, Z. Jusys, R.J. Behm, Bridge-bonded formate: Active intermediate or spectator species in formic acid oxidation on a Pt film electrode? Langmuir 22 (2006) 10399–10408.
[16] Y.X. Chen, M. Heinen, Z. Jusys, R.J. Behm, Kinetic isotope effects in complex reaction networks: Formic acid electro-oxidation, ChemPhysChem 8 (2007) 380–385.
[17] J. Xu, D.F. Yuan, F. Yang, D. Mei, Z.B. Zhang, Y.X. Chen, On the mechanism of the direct pathway for formic acid oxidation at a Pt(111) electrode, Phys. Chem. Chem. Phys. 15 (2013) 4367–4376.
[18] H. Okamoto, Y. Numata, T. Gojuki, Y. Mukouyama, Different behavior of adsorbed bridge-bonded formate from that of current in the oxidation of formic acid on platinum, Electrochim. Acta 116 (2014) 263–270.
[19] G. Crépy, C. Lamy, S. Maximovitch, Oxidation de l'acide formique sur électrode d'or, J. Electroanal. Chem. 54 (1974) 161–179.
[20] H. Kita, T. Katagiri, K. Kunimatsu, Electrochemical oxidation of HCOONa on Pt in acidic solutions, J. Electroanal. Chem. 220 (1987) 125–138.
[21] J.L. Haan, R.I. Masel, The influence of solution pH on rates of an electrocatalytic reaction: Formic acid electrooxidation on platinum and palladium, Electrochim. Acta 54 (2009) 4073–4078.
[22] J. Joo, T. Uchida, A. Cuesta, M.T.M. Koper, M. Osawa, Importance of Acid-Base Equilibrium in Electrocatalytic Oxidation of Formic Acid on Platinum, J. Am. Chem. Soc. 135 (2013) 9991–9994.
[23] J. Joo, T. Uchida, A. Cuesta, M.T.M. Koper, M. Osawa, The effect of pH on the electrocatalytic oxidation of formic acid/formate on platinum: A mechanistic study by surface-enhanced infrared spectroscopy coupled with cyclic voltammetry, Electrochim. Acta 129 (2014) 127–136.
[24] S. Brimaud, J. Solla-Gullon, I. Weber, J.M. Feliu, R.J. Behm, Formic Acid Electrooxidation on Noble-Metal Electrodes: Role and Mechanistic Implications of pH, Surface Structure, and Anion Adsorption, ChemElectroChem 1 (2014) 1075–1083.
[25] J.V. Perales-Rondon, E. Herrero, J.M. Feliu, Effects of the anion adsorption and pH on the formic acid oxidation reaction on Pt(111) electrodes, Electrochim. Acta 140 (2014) 511–517.
[26] H.-F. Wang, Z.-P. Liu, Formic Acid Oxidation at Pt/H_2O Interface from Periodic DFT Calculations Integrated with a Continuum Solvation Model, J. Phys. Chem. C 113 (2009) 17502–17508.
[27] W. Gao, J.A. Keith, J. Anton, T. Jacob, Theoretical Elucidation of the Competitive Electro-oxidation Mechanisms of Formic Acid on Pt(111), J. Am. Chem. Soc. 132 (2010) 18377–18385.
[28] W. Gao, J.E. Mueller, Q. Jiang, T. Jacob, The Role of Co-Adsorbed CO and OH in the Electrooxidation of Formic Acid on Pt(111), Angew. Chem. Int. Ed. 51 (2012) 9448–9452.
[29] V. Grozovski, V. Climent, E. Herrero, J.M. Feliu, Intrinsic Activity and Poisoning Rate for HCOOH Oxidation at Pt(100) and Vicinal Surfaces Containing Monoatomic (111) Steps, ChemPhysChem 10 (2009) 1922–1926.
[30] V. Grozovski, V. Climent, E. Herrero, J.M. Feliu, Intrinsic activity and poisoning rate for HCOOH oxidation on platinum stepped surfaces, Phys. Chem. Chem. Phys. 12 (2010) 8822–8831.
[31] J. Clavilier, Pulsed linear sweep voltammetry with pulses of constant level in a potential scale, a polarization demanding condition in the study of platinum single-crystal electrodes, J. Electroanal. Chem. 236 (1987) 87–94.
[32] M.D. Maciá, E. Herrero, J.M. Feliu, Formic acid oxidation on Bi-Pt(111) electrode in perchloric acid media. A kinetic study, J. Electroanal. Chem. 554 (2003) 25–34.
[33] M.C. Figueiredo, R.M. Arán-Ais, V. Climent, T. Kallio, J.M. Feliu, Evidence of Local pH Changes during Ethanol Oxidation at Pt Electrodes in Alkaline Media, ChemElectroChem (2015) , doi:http://dx.doi.org/10.1002/celc.201500151.
[34] M. Auinger, I. Katsounaros, J.C. Meier, S.O. Klemm, P.U. Biedermann, A.A. Topalov, M. Rohwerder, K.J.J. Mayrhofer, Near-surface ion distribution and buffer effects during electrochemical reactions, Phys. Chem. Chem. Phys. 13 (2011) 16384–16394.
[35] P.A. Christensen, A. Hamnett, D. Linares-Moya, The electro-oxidation of formate ions at a polycrystalline Pt electrode in alkaline solution: an in situ FTIR study, Phys. Chem. Chem. Phys. 13 (2011) 11739–11747.
[36] J. John, H. Wang, E.D. Rus, H.D. Abruña, Mechanistic Studies of Formate Oxidation on Platinum in Alkaline Medium, J. Phys. Chem. C 116 (2012) 5810–5820.
[37] J.M. Orts, J.M. Gómez, A. Feliu, J. Clavilier, Potentiostatic charge displacement by exchanging adsorbed species on Pt(111) electrodesóacidic electrolytes with specific anion adsorption, Electrochim. Acta 39 (1994) 1519–1524.
[38] M.C. Santos, D.W. Miwa, S.A.S. Machado, Study of anion adsorption on polycrystalline Pt by electrochemical quartz crystal microbalance, Electrochem. Commun. 2 (2000) 692–696.
[39] E. Herrero, K. Franaszczuk, A. Wieckowski, Electrochemistry of Methanol at Low Index Crystal Planes of Platinum: An Integrated Voltammetric and Chronoamperometric Study, J. Phys. Chem. 98 (1994) 5074–5083.
[40] F. Colmati, G. Tremiliosi-Filho, E.R. Gonzalez, A. Berna, E. Herrero, J.M. Feliu, Surface structure effects on the electrochemical oxidation of ethanol on platinum single crystal electrodes, Faraday Discuss. 140 (2008) 379–397.
[41] M.J. Prieto, G. Tremiliosi-Filho, The influence of acetic acid on the ethanol electrooxidation on a platinum electrode, Electrochem. Commun. 13 (2011) 527–529.
[42] T. Iwasita, F.C. Nart, H. Polligkeit, An in-situ FTIR study of the behaviour of phosphate species at platinum. Bulk effects and their influence on the spectra for adsorbed ions, Ber. Bunsen-Ges. Phys. Chem. 95 (1991) 638.
[43] F.C. Nart, T. Iwasita, On the adsorption of H_2PO_4- and H_3PO_4 on Pt: an in-situ FTIR study, Electrochim. Acta 37 (1992) 385.
[44] F.C. Nart, T. Iwasita, M. Weber, In-situ FTIR study on the adsorption of phosphate species on well-ordered Pt(111) single crystal surfaces, Ber. Bunsen-Ges. Phys. Chem. 97 (1993) 737.
[45] M. Weber, F.C. Nart, I.R. deMoraes, T. Iwasita, Adsorption of phosphate species on Pt(111) and Pt(100) as studied by in situ FTIR spectroscopy, J. Phys. Chem. 100 (1996) 19933–19938.
[46] G.A. Attard, A. Brew, K. Hunter, J. Sharman, E. Wright, Specific adsorption of perchlorate anions on Pt{hkl} single crystal electrodes, Phys. Chem. Chem. Phys. 16 (2014) 13689–13698.
[47] J.V. Perales-Rondon, A. Ferre-Vilaplana, J.M. Feliu, E. Herrero, Oxidation Mechanism of Formic Acid on the Bismuth Adatom-Modified Pt(111) Surface, J. Am. Chem. Soc. 136 (2014) 13110–13113.
[48] B. Braunschweig, A. Wieckowski, Surface spectroscopy of Pt(111) single-crystal electrolyte interfaces with broadband sum-frequency generation, J. Electroanal. Chem. 716 (2014) 136–144.
[49] A. Katchalsky, H. Eisenberg, S. Lifson, Hydrogen Bonding and Ionization of Carboxylic Acids in Aqueous Solutions, J. Am. Chem. Soc. 73 (1951) 5889–5890.
[50] E.E. Schrier, M. Pottle, H.A. Scheraga, The Influence of Hydrogen and Hydrophobic Bonds on the Stability of the Carboxylic Acid Dimers in Aqueous Solution, J. Am. Chem. Soc. 86 (1964) 3444–3449.
[51] J.V. Perales-Rondón, E. Herrero, J.M. Feliu, On the activation energy of the formic acid oxidation reaction on platinum electrodes, J. Electroanal. Chem. 742 (2015) 90–96.
[52] N. Garcia-Araez, V. Climent, P. Rodríguez, J.M. Feliu, Thermodynamic analysis of (bi) sulphate adsorption on a Pt(111) electrode as a function of pH, Electrochim. Acta 53 (2008) 6793–6806.
[53] R. Rizo, E. Sitta, E. Herrero, V. Climent, J.M. Feliu, Towards the understanding of the interfacial pH scale at Pt(111) electrodes, Electrochim. Acta 162 (2015) 138–145.
[54] R. Gisbert, G. García, M.T.M. Koper, Adsorption of phosphate species on poly-oriented Pt and Pt(111) electrodes over a wide range of pH, Electrochim. Acta 55 (2010) 7961–7968.
[55] Z.F. Su, V. Climent, J. Leitch, V. Zamlynny, J.M. Feliu, J. Lipkowski, Quantitative SNIFTIRS studies of (bi) sulfate adsorption at the Pt(111) electrode surface, Phys. Chem. Chem. Phys. 12 (2010) 15231–15239.
[56] A. Berna, A. Rodes, J.M. Feliu, F. Illas, A. Gil, A. Clotet, J.M. Ricart, Structural and spectroelectrochemical study of carbonate and bicarbonate adsorbed on Pt (111) and Pd/Pt(111) electrodes, J. Phys. Chem. B 108 (2004) 17928–17939.

Chapter VI

Oxidation Mechanism of Formic Acid on the Bismuth Adatom-Modified Pt(111) Surface

IV

Publication IV

J. V. Perales-Rondon, A. Ferre-Vilaplana, J. M. Feliu and E. Herrero, **"Oxidation Mechanism of Formic Acid on the Bismuth Adatom-Modified Pt(111) Surface"** *Journal of the American Chemical Society* **2014**, 136, 13110-13113. **doi:** 10.1021/ja505943h.

JACS
JOURNAL OF THE AMERICAN CHEMICAL SOCIETY

Communication

pubs.acs.org/JACS

Oxidation Mechanism of Formic Acid on the Bismuth Adatom-Modified Pt(111) Surface

Juan Victor Perales-Rondón,[†] Adolfo Ferre-Vilaplana,[‡,§] Juan M. Feliu,[†] and Enrique Herrero*[,†]

[†]Instituto de Electroquímica, Universidad de Alicante, Apdo. 99, E-03080 Alicante, Spain

[‡]Instituto Tecnológico de Informática, Ciudad Politécnica de la Innovación, Camino de Vera s/n, E-46022 Valencia, Spain

[§]Departamento de Sistemas Informáticos y Computación, Escuela Politécnica Superior de Alcoy, Universidad Politécnica de Valencia, Plaza Ferrándiz y Carbonell s/n, E-03801 Alcoy, Spain

Supporting Information

ABSTRACT: In order to improve catalytic processes, elucidation of reaction mechanisms is essential. Here, supported by a combination of experimental and computational results, the oxidation mechanism of formic acid on Pt(111) electrodes modified by the incorporation of bismuth adatoms is revealed. In the proposed model, formic acid is first physisorbed on bismuth and then deprotonated and chemisorbed in formate form, also on bismuth, from which configuration the C−H bond is cleaved, on a neighbor Pt site, yielding CO_2. It was found computationally that the activation energy for the C−H bond cleavage step is negligible, which was also verified experimentally.

Cleaner energy based on the oxidation of small organic molecules (i.e., formic acid, methanol, ethanol, etc.) in fuel cells requires efficient electrocatalysts capable of operating at low overpotentials and high current densities. To guide the development of optimal catalysts, the oxidation mechanisms of the fuels have to be fully understood. The oxidation of formic acid to CO_2, involving the exchange of only two electrons and the cleavage of a single C−H bond, is probably the simplest among the processes considered.[1,2] In order to activate the aforementioned C−H bond cleavage, platinum surfaces are particularly effective, giving rise to overpotentials lower than those observed in the oxidation of small organic molecules on others metals. However, even on pure platinum, the measured oxidation currents, at low overpotentials, are still low. To increase the activity of the catalyst, modifications of platinum with other elements have been proposed. Intermetallic PtBi nanoparticles have shown an excellent performance, where high currents at very low overpotentials have been recorded.[3−6] Nevertheless, the role played by Bi, or any other modifier, in the considered oxidation process is still unknown. In this work, using a combination of DFT calculations and experimental results on single-crystal electrodes, the electro-oxidation mechanism of formic acid on the bismuth adatom-modified Pt(111) surface is completely elucidated. Note that single-crystal electrodes allow direct comparison between computational and experimental results.

The electrooxidation of formic acid on pure platinum electrodes can evolve following two main routes: through CO, which remains strongly adsorbed on the electrode, and thus is difficult to oxidize, and through an active intermediate, which is the desired route.[2,7] For this route, the nature of the intermediate is still under discussion.[8−13] Electrocatalytic reaction rates depend on the surface structure of the electrodes. So, Pt(111) electrodes exhibit low activity through the active intermediate and negligible CO formation, whereas Pt(100) surfaces show the highest activity for both routes.[14,15] Moreover, to increase the reaction rate through the direct route, pure platinum electrodes have been modified incorporating other species. Bismuth has given rise to very promising results.[16−18] The addition of Bi adatoms to pristine Pt(111) single-crystal electrodes diminishes the overpotentials and increases the current density up to 30−40 times that measured for the unmodified surface.[15] Such improvement is clearly related to the deposition of Bi on the terraces, since it reaches the maximum for coverages close to the saturation value. For low and moderate Bi coverages, only isolated or <1 nm islands have been seen by scanning tunneling microscopy, which supports the random distribution model of adatoms on the surface.[19] Also, statistical models suggest that a Bi−Pt ensemble would be the reactive site, although the role played by each atom in the considered oxidation process has not yet been described.[20]

It has been pointed out that adsorbed formate plays an important role in the process of oxidation of formic acid on pure platinum electrodes. This species has been detected by FTIR[9−13] and voltammetry,[21] showing that the onset for the oxidation process coincides with that for the adsorption of formate.[21] Also, density functional theory calculations indicate that adsorbed formate is a key part of the considered oxidation process.[22,23] More specifically, it has been suggested that adsorbed formate facilitates the adsorption of a new formic acid (or formate) molecule with the C−H bond directed toward the surface.[24] From such a configuration, the activation energy for the cleavage of the C−H bond would be low (ca. 0.5 eV), yielding CO_2 as the final product. To adsorb the formate−formic dimer, a Pt ensemble with several Pt atoms is required. Thus, the initial hypothesis could be that bismuth facilitates the adsorption of formate on Pt sites.

To detect adsorption of formate on single-crystal electrodes, fast-scan voltammetry can be used.[21] During formic acid

Received: June 13, 2014
Published: September 4, 2014

dx.doi.org/10.1021/ja505943h | J. Am. Chem. Soc. 2014, 136, 13110−13113

oxidation, voltammetric currents come from two different processes: the oxidation process itself and adsorption processes (mainly hydrogen and anions) on the electrode surface. At low scan rates, oxidation currents are much higher than adsorption currents. However, adsorption currents are proportional to the scan rate, whereas oxidation currents are much less affected by the scan rate.[18] By using high scan rates, adsorption currents can dominate the voltammetric profile.[21] For a Bi adatom-modified Pt(111) electrode with a coverage of 0.25, which is very close to the maximum activity, both types of experiments (low and high scan rate voltammetry) are shown in Figure 1.

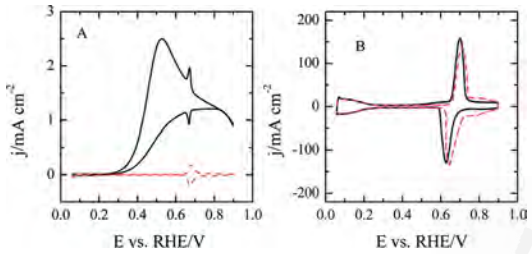

Figure 1. Voltammetric profiles of Bi−Pt(111) electrode with θ_{Bi} = 0.25 in 0.5 M $HClO_4$ + 0.05 M HCOOH (full line) and 0.5 M $HClO_4$ (dashed lines) at (A) 0.05 and (B) 50 V/s.

The same kinds of experimental results are shown in the Supporting Information, Figures S1−S3, for the bare electrode and two additional coverages. As can be seen by comparison of the voltammetries in presence and absence of formic acid, at 50 mV/s (Figures 1A and S1A−S3A), adsorption currents are much smaller than those corresponding to formic acid oxidation, the shape of the voltammogram indicating an irreversible oxidation process that is inhibited at high potentials. At high bismuth coverages and above 0.5 V, the incoming molecules are immediately oxidized on the electrode.

However, at 50 V/s (Figures 1B and S1B−S3B), adsorption currents have increased 3 orders of magnitude, making adsorption the dominant process recorded in the voltammetry. In presence of formic acid, the voltammograms are practically symmetrical through the potential axis, which indicates that currents are mainly due to adsorption processes, and thus, the contribution from oxidation processes can be discarded. Comparison with the voltammograms measured in the absence of formic acid enables us to establish the formate adsorption range on platinum. In perchloric acid solutions, a hydrogen adsorption region appears at potentials below 0.3 V, whereas bismuth redox give rise to a pair of peaks between 0.6 and 0.7 V, in a similar way to what is found at 50 mV/s (Figures 1B and S4). Above 0.7 V, the signals corresponding to OH adsorption on Pt sites can be detected. In presence of formic acid at 50 V/s, some changes can be observed in the voltammograms. First, depending on the coverage, a signal corresponding to formate adsorption can be seen between 0.4 and 0.6 V in the positive scan direction (Figure S5). In Figure 1B, since bismuth coverage is high, the amount of free Pt sites is small, and therefore, the total amount of adsorbed formate on platinum is also small. However, in Figure S5, the signal corresponding to formate adsorption diminishes as the coverage increases. For bismuth-modified surfaces, the voltammograms in the presence of formic acid at 50 V/s are almost identical to those measured in sulfuric acid solutions in the absence of formic acid, which corroborates that these processes are due to the adsorption of the formate anion.[25] As the amount of bismuth coverage increases, the onset for the formate anion adsorption is displaced toward higher potential values (see Figure S5).[26] In parallel to the appearance of the new signal between 0.4 and 0.6 V, those signals corresponding to the adsorption of OH above 0.7 V disappear, and a small shift in the bismuth redox peaks is observed. All these results indicate that, for θ_{Bi} = 0.25, formate is present on platinum sites only above 0.5 V, whereas on the unmodified Pt(111) electrode it can be detected at 0.35 V.[21] On the other hand, the onset potential for formic acid oxidation diminishes as the bismuth coverage increases. Thus, it is clear that the catalytic effect of bismuth is not linked to the adsorption of formate on Pt sites.

In order to gain insight into the mechanisms explaining the higher performance of bismuth modified electrodes, DFT calculations, modeling different aspects of the investigated process, were carried out. Adsorption of bismuth on fcc and hcp sites of the Pt(111) surface was found to be favorable by 3.20 and 3.17 eV, respectively. The adsorption of bismuth causes a redistribution of electron density on the bare surface. The results corresponding to fcc sites are displayed in Figure 2;

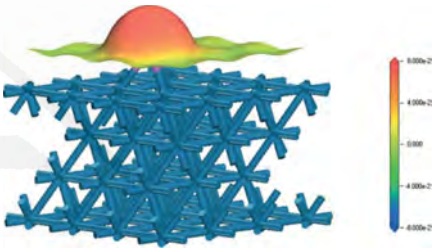

Figure 2. Electrostatic potential [Ha/e] mapped on electron isodensity surface for a density value ρ = 0.01 e/Å^3 for a Bi adatom adsorbed on the Pt(111) surface.

the ones corresponding to hcp sites are virtually identical. From Figure 2, it can be inferred that an excess of positive charge would be concentrated on the adatom, while the compensating negative charge would be distributed among the platinum atoms close to the adatom. Thus, bismuth has cationic character when adsorbed on Pt(111). Here we propose that the formation of the identified cationic site determines the oxidation process of formic acid on the Bi−Pt(111) surface, driving its mechanism.

It was found that physisorption of hydrated formic acid near the adatom is favorable by ca. 0.26 eV. In its lower energy configuration, the carbonyl group is directed toward the adatom (Figure S6), with changes in the bonds geometry being observed. In such a configuration, the O−H distance of the carboxylic group increases, whereas the distance to the corresponding hydrogen bond diminishes as compared to the distances calculated in absence of surface. Adatoms favoring physisorption of formic acid in the C−H down configuration have been previously found,[27] though the evolution of formic acid on the adatom site was not studied, and only the generic argument that the configuration facilitates the cleavage of the C−H bond is provided. Here, the relevance of the role played by the adatom during the oxidation process is established, and the complete oxidation mechanism is revealed.

From the described physisorbed configuration, the deprotonation of the formic acid molecule would be assisted by the fact that, from this location, formate was found to be favorably chemisorbed by 0.39 eV on the bismuth adatom without barrier. Therefore, the two processes of formic acid deprotonation and formate chemisorption on bismuth would take place simultaneously. The above-described physisorption- and formate chemisorption-related observations suggest that the pK_a of formic acid near the surface would be lower than that in the bulk. Physisorption, deprotonation, and formate chemisorption would all be driven by the positive charge located on the adatom.

Once formate chemisorption on the adatom has taken place, it was assumed that the electron in excess exits toward the circuit. So, the evolution of the HCOO fragment bonded to the bismuth modified platinum surface was analyzed. Running quantum mechanical molecular dynamics simulations, it was found that, transiting among different configurations whose energies fluctuate within the error of the calculations, the chemisorbed HCOO fragment evolves in a rotating process for which the Bi−O and O−C bonds play the role of rotation axis, until a sufficiently favorable C−H down configuration is reached. From this configuration the C−H bond is cleaved to yield CO_2 and an adsorbed H atom (Figure 3). The activation

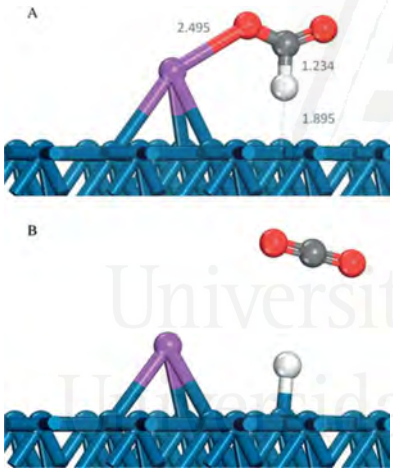

Figure 3. (A) HCOO fragment adsorbed on the Bi−Pt(111) surface and (B) final products in the oxidation of formic acid.

energy estimated from the calculations for the C−H bond cleavage step was negligible, presenting a favorable energy of 1.21 eV. Comparison with previous results on unmodified Pt(111) electrodes[24] shows a significant diminution in activation energy for the C−H bond cleavage step, from 0.5 to 0 eV.

In summary, the oxidation reaction model proposed here draws a bifunctional catalyst in which the bismuth adatom plays a determinant role in the formic acid adsorption and evolution to chemisorbed formate, whereas an adjacent Pt site is responsible for the cleavage of the C−H bond, which is in agreement with previous analysis suggesting that the catalytic site is a Bi−Pt ensemble.[20]

To corroborate the proposed reaction mechanism, activation energies for different bismuth coverages on Pt(111) electrodes were experimentally estimated. To do so, voltammetric profiles for the oxidation process were recorded at different temperatures (Figure 4A). Since CO formation on these electrodes is

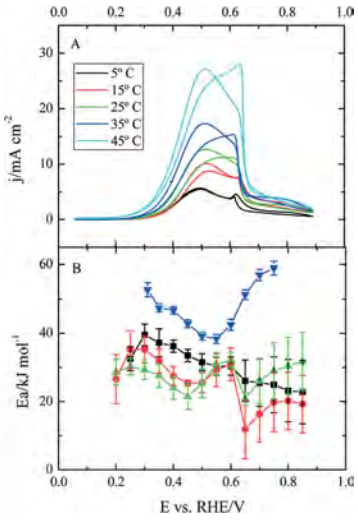

Figure 4. (A) Voltammetric profile of a Bi−Pt(111) electrode with θ_{Bi} = 0.25 in 0.5 M H_2SO_4 + 0.1 M HCOOH at 0.05 V/s at different temperatures. (B) Measured activation energy for different Bi coverages θ_{Bi}: (▼) 0.00, (■) 0.10, (●) 0.22, and (▲) 0.28.

negligible,[15,17] the measured currents correspond to the direct route. So, the logarithm of the current density at constant potential can be charted vs T^{-1} in an Arrhenius plot to determine the apparent activation energy (Figure S7). Activation energies vs electrode potentials for different bismuth coverages are displayed in Figure 4B. For comparison, the activation energy for the unmodified Pt(111) electrode is also included. For the bare electrode, the activation energy was determined from the intrinsic activity of the electrode through the active intermediate reaction measured at different temperatures.[14,15]

In Figure 4B, as bismuth coverage increases, a significant diminution in the activation energy of the process can be observed. For the electrode with the highest activity, the diminution is around 20 kJ/mol with respect to that corresponding to the unmodified Pt(111) electrode. It should be borne in mind that experimentally estimated activation energies are apparent activation energies, which are a combination of the activation energies of all the different steps involved in a mechanism, whereas computationally estimated activation energies correspond to a single step in a process. Additionally, in the case of the bismuth-modified Pt(111) electrodes, the measured activation energy is an average of the activation energies for all the different kinds of reactive sites on the surface. For the investigated surfaces, two different kinds of active sites are considered: the Pt−Bi ensemble of Figure 3, and the Pt ensemble on which the reaction occurs through the formate−formic dimer. If the activation energy for the Pt−Bi ensemble is much lower than that for the Pt sites, it is clear that the measured activation energy should diminish when increasing bismuth coverage, as found experimentally. For the bismuth coverage with the

highest catalytic activity (θ_{Bi} = 0.28), the measured activation energy is not zero because of the contribution of other previous steps and also from some Pt ensembles still accessible on the surface. At 0.45 V, the measured activation energy for θ_{Bi} = 0.28 is 21 kJ/mol, whereas on the unmodified surface it is 42 kJ/mol. From these data, the contribution of the different steps/processes to the apparent activation energy at this bismuth coverage can be estimated. Since each bismuth adatom blocks three platinum sites, at the considered coverage, the number of free Pt sites is 0.16. This implies that the contribution of these sites to the total energy would be 0.16 × 42 = 6.7 kJ/mol. The remaining 14.3 kJ/mol (or 0.15 eV) should arise, then, from the previous steps for the reaction on the Bi−Pt ensemble, probably from the deprotonation of the formic acid close to the Bi adatom to give rise to formate, which will adsorb immediately on the Bi adatom.

Finally, it should be stressed that the reaction mechanism suggested by our DFT calculations is in very good agreement with a broad set of experimental data. First, unlike the Pt(111) electrodes, for which currents increase with the pH,[12] the currents measured on the bismuth-modified Pt(111) electrodes do not depend on the pH for values between 0 and 2,[18] which implies that the formic acid molecule is the reactant species at these pH values. As has been shown, a formic acid molecule close to the Bi adatom would have a lower pK_a, which would facilitate its adsorption as formate on the bismuth adatom; therefore, the presence of a formate molecule close to the adatom is not required. Second, the activation energy diminishes with the bismuth coverage. Third, the proposed reaction mechanism helps to explain why the onset of the reaction is between 0.2 and 0.3 V for the different bismuth coverages. In the final step, adsorbed hydrogen is formed, "poisoning" the active site. In order to reactivate the active site, hydrogen should be desorbed. Thus, a steady current for formic acid oxidation is possible only at potentials at which hydrogen is easily desorbed from the Pt sites, that is, where hydrogen equilibrium coverage on the surface is low. On the unmodified Pt(111) surface, hydrogen coverage is low above 0.30 V, and this potential value diminishes as the bismuth coverage increases (see Figure S4). Thus, the onset potential for the reaction shifts accordingly. And, fourth, the proposed mechanism also explain why the activation energy diminishes from 0.2 to 0.5 V. Hydrogen desorption also contributes to the measured activation energy, since it can be considered also the first step in the reaction at potentials where hydrogen is adsorbed. As the potential is made more positive, this step is faster (i.e., with a lower activation energy), which results in a diminution of the overall activation energy. As a conclusion, it can be verified that the computational results presented here are in very good agreement with a broad set of experimental data, thus explaining them, which rigorously supports the proposed reaction model.

■ ASSOCIATED CONTENT

Supporting Information

Experimental details, computational methods, and additional figures. This material is available free of charge via the Internet at http://pubs.acs.org.

■ AUTHOR INFORMATION

Corresponding Author

herrero@ua.es

Notes

The authors declare no competing financial interest.

■ ACKNOWLEDGMENTS

This work has been financially supported by the MINECO (Spain) (project CTQ2013-44083-P) and Generalitat Valenciana (project PROMETEOII/2014/013).

■ REFERENCES

(1) Parsons, R.; Vandernoot, T. *J. Electroanal. Chem.* **1988**, *257*, 9.
(2) Koper, M. T. M.; Lai, S. C. S.; Herrero, E. In *Fuel cell catalysis, a surface science approach*; Koper, M. T. M., Ed.; John Wiley & Sons, Inc.: Hoboken, NJ, 2009; p 159.
(3) Roychowdhury, C.; Matsumoto, F.; Zeldovich, V. B.; Warren, S. C.; Mutolo, P. F.; Ballesteros, M.; Wiesner, U.; Abruña, H. D.; Disalvo, F. J. *Chem. Mater.* **2006**, *18*, 3365.
(4) Roychowdhury, C.; Matsumoto, F.; Mutolo, P. F.; Abruna, H. D.; DiSalvo, F. J. *Chem. Mater.* **2005**, *17*, 5871.
(5) Casado-Rivera, E.; Gal, Z.; Angelo, A. C. D.; Lind, C.; DiSalvo, F. J.; Abruna, H. D. *ChemPhysChem* **2003**, *4*, 193.
(6) Blasini, D. R.; Rochefort, D.; Fachini, E.; Alden, L. R.; DiSalvo, F. J.; Cabrera, C. R.; Abruna, H. D. *Surf. Sci.* **2006**, *600*, 2670.
(7) Feliu, J. M.; Herrero, E. In *Handbook of fuel cells—fundamentals, technology and applications*; Vielstich, W., Gasteiger, H., Lamm, A., Eds.; John Wiley & Sons, Ltd.: Chichester, 2003; Vol. 2.
(8) Samjeske, G.; Miki, A.; Ye, S.; Osawa, M. *J. Phys. Chem. B* **2006**, *110*, 16559.
(9) Chen, Y. X.; Ye, S.; Heinen, M.; Jusys, Z.; Osawa, M.; Behm, R. J. *J. Phys. Chem. B* **2006**, *110*, 9534.
(10) Cuesta, A.; Cabello, G.; Gutierrez, C.; Osawa, M. *Phys. Chem. Chem. Phys.* **2011**, *13*, 20091.
(11) Osawa, M.; Komatsu, K.; Samjeske, G.; Uchida, T.; Ikeshoji, T.; Cuesta, A.; Gutierrez, C. *Angew. Chem., Int. Ed.* **2011**, *50*, 1159.
(12) Joo, J.; Uchida, T.; Cuesta, A.; Koper, M. T. M.; Osawa, M. *J. Am. Chem. Soc.* **2013**, *135*, 9991.
(13) Chen, Y. X.; Heinen, M.; Jusys, Z.; Behm, R. J. *Langmuir* **2006**, *22*, 10399.
(14) Grozovski, V.; Climent, V.; Herrero, E.; Feliu, J. M. *ChemPhysChem* **2009**, *10*, 1922.
(15) Grozovski, V.; Climent, V.; Herrero, E.; Feliu, J. M. *Phys. Chem. Chem. Phys.* **2010**, *12*, 8822.
(16) Clavilier, J.; Fernández-Vega, A.; Feliu, J. M.; Aldaz, A. *J. Electroanal. Chem.* **1989**, *258*, 89.
(17) Herrero, E.; Fernández-Vega, A.; Feliu, J. M.; Aldaz, A. *J. Electroanal. Chem.* **1993**, *350*, 73.
(18) Maciá, M. D.; Herrero, E.; Feliu, J. M. *J. Electroanal. Chem.* **2003**, *554*, 25.
(19) Kim, J.; Rhee, C. K. *Electrochem. Commun.* **2010**, *12*, 1731.
(20) Leiva, E.; Iwasita, T.; Herrero, E.; Feliu, J. M. *Langmuir* **1997**, *13*, 6287.
(21) Grozovski, V.; Vidal-Iglesias, F. J.; Herrero, E.; Feliu, J. M. *ChemPhysChem* **2011**, *12*, 1641.
(22) Neurock, M.; Janik, M.; Wieckowski, A. *Faraday Discuss.* **2009**, *140*, 363.
(23) Gao, W.; Keith, J. A.; Anton, J.; Jacob, T. *J. Am. Chem. Soc.* **2010**, *132*, 18377.
(24) Wang, H.-F.; Liu, Z.-P. *J. Phys. Chem. C* **2009**, *113*, 17502.
(25) Clavilier, J.; Feliu, J. M.; Aldaz, A. *J. Electroanal. Chem.* **1988**, *243*, 419.
(26) Climent, V.; Herrero, E.; Feliu, J. M. *Electrochem. Commun.* **2001**, *3*, 590.
(27) Peng, B.; Wang, H.-F.; Liu, Z.-P.; Cai, W.-B. *J. Phys. Chem. C* **2010**, *114*, 3102.

Supporting information

Oxidation Mechanism of Formic Acid on the Bismuth Adatom-Modified Pt(111) Surface.

Juan Victor Perales-Rondón[†], Adolfo Ferre-Vilaplana[‡,§], Juan M. Feliu[†] and Enrique Herrero[†]*.

[†]Instituto de Electroquímica, Universidad de Alicante, Apdo. 99, E-03080 Alicante, Spain

[‡]Instituto Tecnológico de Informática, Ciudad Politécnica de la Innovación, Camino de Vera s/n, E-46022 Valencia, Spain,

[§]Departamento de Sistemas Informáticos y Computación, Escuela Politécnica Superior de Alcoy, Universidad Politécnica de Valencia, Plaza Ferrándiz y Carbonell s/n, E-03801 Alcoy, Spain

Experimental and computational methods.

Experimental methods.

Platinum single crystal electrodes were oriented, cut and polished from small single crystal beads (2.5 mm diameter) following the procedure described by Clavilier and co-workers.[1,2] The electrodes were cleaned by flame annealing, cooled down in H_2/Ar and protected with water in equilibrium with this gas mixture to prevent contamination before immersion in the electrochemical cell, as described in detail elsewhere.[2,3] The voltammetric profiles, and therefore the surface structure of the electrodes, are stable upon cycling provided that oxide formation is avoided. It is known that oxidation/reduction cycles create defects on the electrode surface.[4,5]

Bismuth adlayer were prepared by the irreversible adsorption technique. The prepared electrode surface is put in contact in a separate vessel with a solution of Bi_2O_3 (10^{-5}–10^{-4} M) in 0.1 M perchloric acid for a short period of time (5–60 s).[6] The modified electrode was then rinsed with water and immersed again in the electrochemical cell. The presence of irreversibly adsorbed bismuth was estimated voltammetrically by the inspection of the new peak that appeared in the voltammogram centered at 0.67 V. Bismuth coverage is given as the number of Bi atoms per Pt surface atoms and has been calculated according to the procedure described in reference.[7] Experiments were carried out in a classical two-compartment electrochemical cell deaerated by using Ar (N50, Air Liquide in all gases used), including a large platinum counter electrode and a reversible hydrogen (N50) electrode (RHE) as reference. For the determination of the activation energy, the electrochemical cell was immersed in a water bath to control the temperature in a range between 278 and 333 K. The reference electrode was kept at room temperature (298 K) and all the measured potentials are referred to a RHE electrode at 298 K. For that reason, the measured potentials were corrected with the thermodiffusion potential using the procedure explained in reference [8]. All the potentials are quoted vs. the RHE at 298 K unless otherwise stated. Solutions were prepared from sulfuric acid, perchloric acid, sodium perchlorate, acetic acid, formic acid (Merck suprapur in all cases) and ultrapure water from Elga. The cleanliness of the solutions was tested by the stability of the characteristic voltammetric features of well-defined single crystal electrodes.

The potential program for the transients was generated with an arbitrary function generator (Rigol, DG3061A) together with a potentiostat (eDAQ EA161) and a digital recorder (eDAQ, ED401). To avoid any interference of the diffusion of formic acid in the reaction rate, stationary conditions were attained by using a hanging meniscus rotating disk configuration at 900 rpm (controlled by a Radiometer CTV 101).

Computational methods.

All DFT calculations were carried out using numerical basis sets,[9] semicore pseudopotentials[10] (which include scalar relativistic effects) and the RPBE functional[11] as implemented in the Dmol^3 code.[12] With the exception of the bismuth adatom binding energy estimation, which was performed under high vacuum conditions, implicit solvation effects were taken into account by the COSMO model.[13] The effects of non-zero dipole moments, in the supercells, were cancelled by means of external fields.[14]

The Pt(1 1 1) surface was modeled by means of a periodic supercell comprising 36 Pt atoms (four layers of metal atoms) and a vacuum slab of 20 Å. The bottom 18 Pt atoms were frozen

in their bulk crystal locations. The remaining 18 Pt atoms were completely relaxed joint to the adsorbates. The shortest distance between periodic images was 8.51 Å.

Optimal configurations (adsorbent/adsorbate, reactants, products and transition states) were searched for using numerical basis sets of double-numerical quality. During this phase of the calculations, Brillouin zones were sampled, under the Monkhorst-Pack method,[15] using grids corresponding to distances in the reciprocal space of the order of 0.05 1/Å, and convergence was facilitated introducing 0.005 Ha of thermal smearing.

Assuming the previously optimized configurations, binding energies, reaction energies and barriers were estimated using numerical basis sets of double-numerical quality plus polarization. In this case, Brillouin zones were sampled, also under the Monkhorst-Pack method, but using grids corresponding to distances in the order of 0.04 1/Å, and convergence was facilitated introducing only 0.005 Ha of thermal smearing. Moreover, energies were extrapolated to 0°K.

Finally, molecular dynamic simulations were run, under the NVE thermodynamic ensemble, using the same numerical setup used for optimization calculations and 1 femtosecond of time step.

Additional Figures

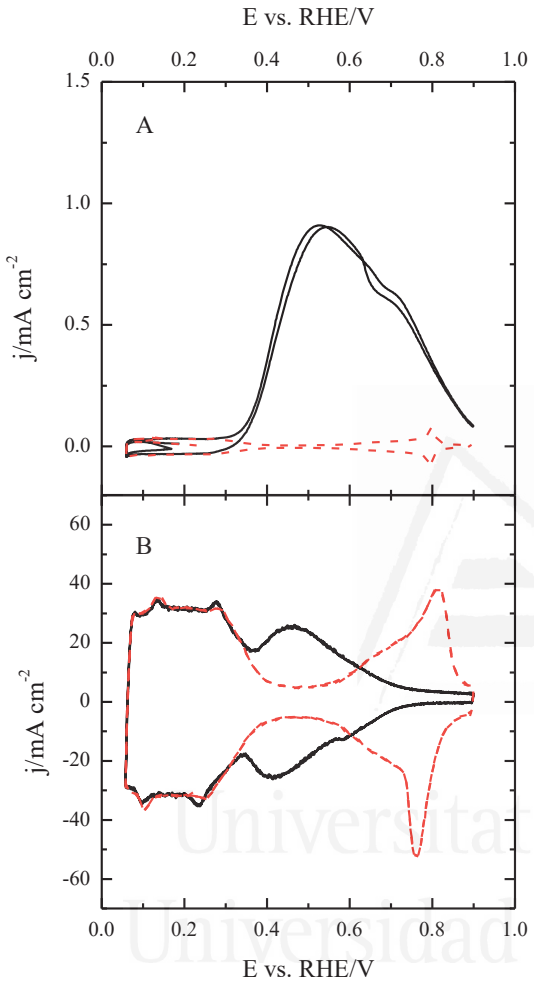

Figure S1. Voltammetric profiles of the unmodified Pt(111) electrode in 0.5 M $HClO_4$ + 0.05 M HCOOH (full line) and 0.5 M $HClO_4$ (dashed lines) at (A) 0.05 V s^{-1} and (B) 50 V s^{-1}.

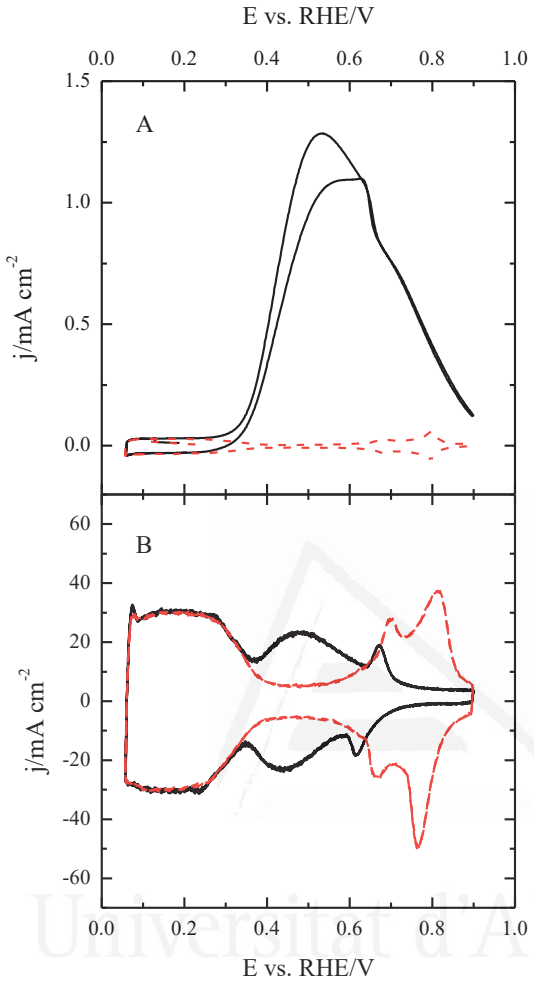

Figure S2. Voltammetric profiles of the Bi-Pt(111) electrode with θ_{Bi}=0.04 in 0.5 M $HClO_4$ + 0.05 M HCOOH (full line) and 0.5 M $HClO_4$ (dashed lines) at (A) 0.05 V s^{-1} and (B) 50 V s^{-1}.

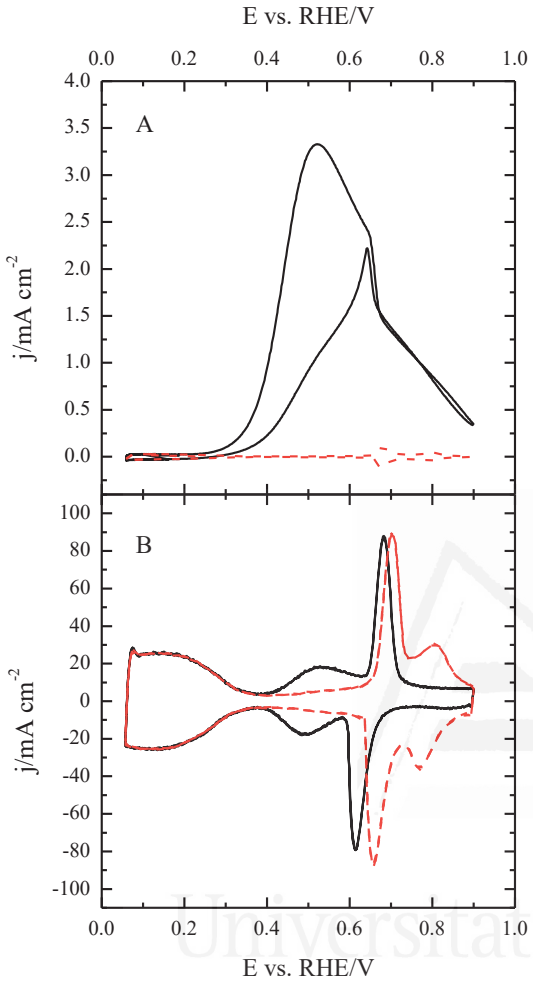

Figure S3. Voltammetric profiles of the Bi-Pt(111) electrode with θ_{Bi}=0.12 in 0.5 M $HClO_4$ + 0.05 M HCOOH (full line) and 0.5 M $HClO_4$ (dashed lines) at (A) 0.05 V s^{-1} and (B) 50 V s^{-1}.

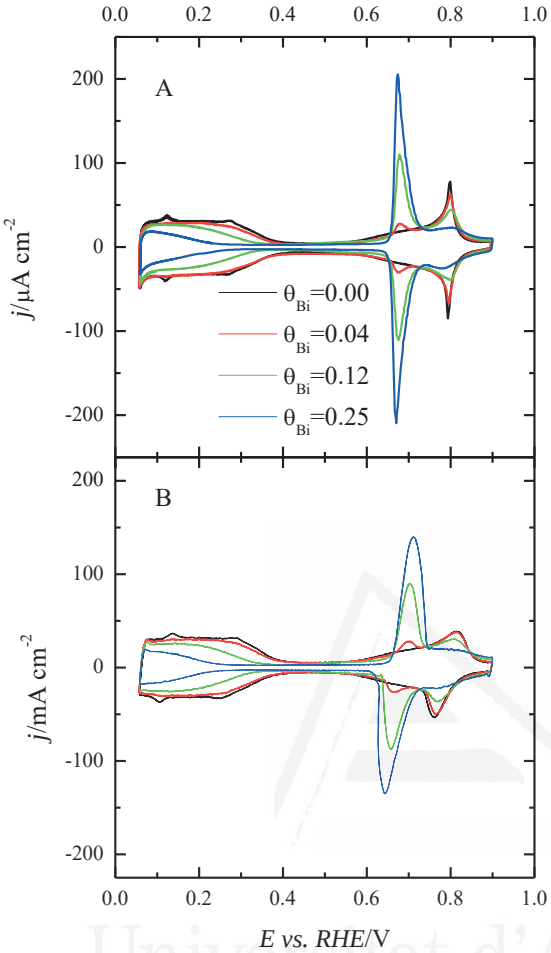

Figure S4. Voltammetric profile of the Bi-Pt(111) electrode with different bismuth coverages in 0.5 M $HClO_4$ at (A) 50 mV s^{-1} and (B) 50 V s^{-1}.

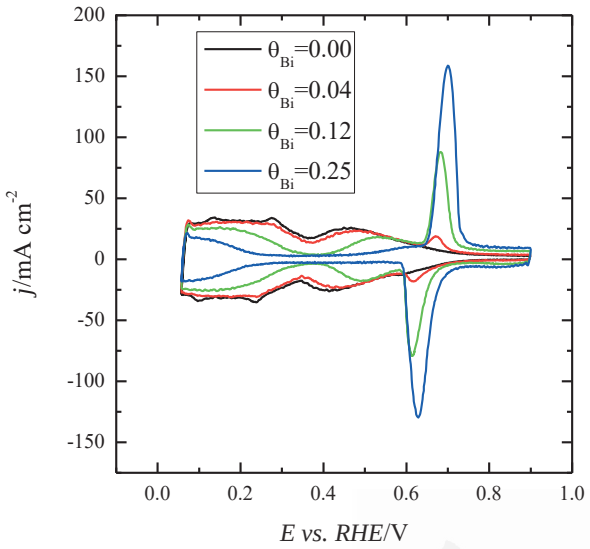

Figure S5. Voltammetric profile of the Bi-Pt(111) electrode with different bismuth coverages in 0.5 M $HClO_4$ + 0.01 M HCOOH at 50 V s^{-1}.

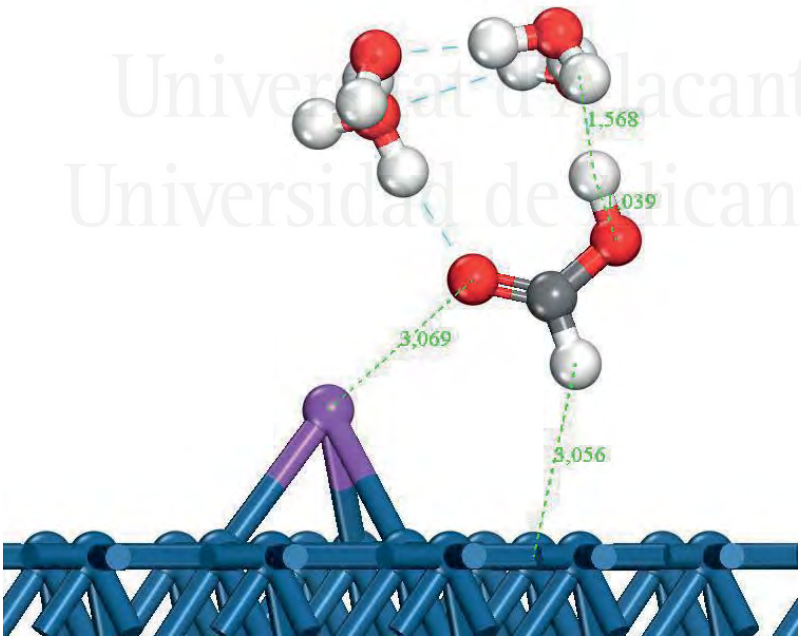

Figure S6. Hydrated formic acid physisorbed on the Bi-Pt(111) surface.

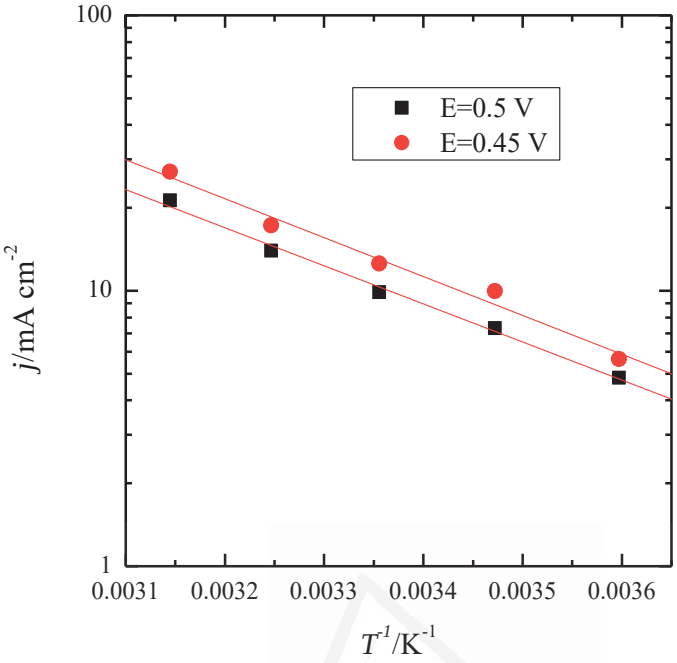

Figure S7. Arrhenius plot for currents at two different potentials measured for a Bi-Pt(111) electrode with θ_{Bi}=0.22 in 0.5 M H_2SO_4 + 0.1 M HCOOH

References

(1) Clavilier, J.; Armand, D.; Sun, S. G.; Petit, M. *J. Electroanal. Chem.* **1986**, *205*, 267.
(2) Korzeniewski, C.; Climent, V.; Feliu, J. M. In *Electroanalytical chemistry: A series of advances, vol 24*; Bard, A. J., Zoski, C., Eds. 2012; Vol. 24, p 75.
(3) Rodes, A.; Elachi, K.; Zamakhchari, M. A.; Clavilier, J. *J. Electroanal. Chem.* **1990**, *284*, 245.
(4) Itaya, K.; Sugawara, S.; Sashikata, K.; Furuya, N. *Journal of Vacuum Science & Technology a-Vacuum Surfaces and Films* **1990**, *8*, 515.
(5) Gomez-Marin, A. M.; Feliu, J. M. *Electrochim. Acta* **2012**, *82*, 558.
(6) Clavilier, J.; Feliu, J. M.; Aldaz, A. *J. Electroanal. Chem.* **1988**, *243*, 419.
(7) Maciá, M. D.; Herrero, E.; Feliu, J. M. *J. Electroanal. Chem.* **2003**, *554*, 25.
(8) Garcia-Araez, N.; Climent, V.; Feliu, J. In *Interfacial phenomena in electrocatalysis*; Vayenas, C. G., Ed.; Springer New York: 2011; Vol. 51, p 1.
(9) Delley, B. *J. Chem. Phys.* **1990**, *92*, 508.
(10) Delley, B. *Phys. Rev. B* **2002**, *66*, 155125.
(11) Hammer, B.; Hansen, L. B.; Nørskov, J. K. *Phys. Rev. B* **1999**, *59*, 7413.
(12) Delley, B. *J. Chem. Phys.* **2000**, *113*, 7756.
(13) Delley, B. *Mol. Simul.* **2006**, *32*, 117.
(14) Neugebauer, J.; Scheffler, M. *Phys. Rev. B* **1992**, *46*, 16067.
(15) Monkhorst, H. J.; Pack, J. D. *Phys. Rev. B* **1976**, *13*, 5188.

Unpublished Articles

Chapter VII

Formic acid electrooxidation on thallium modified platinum single crystal electrodes

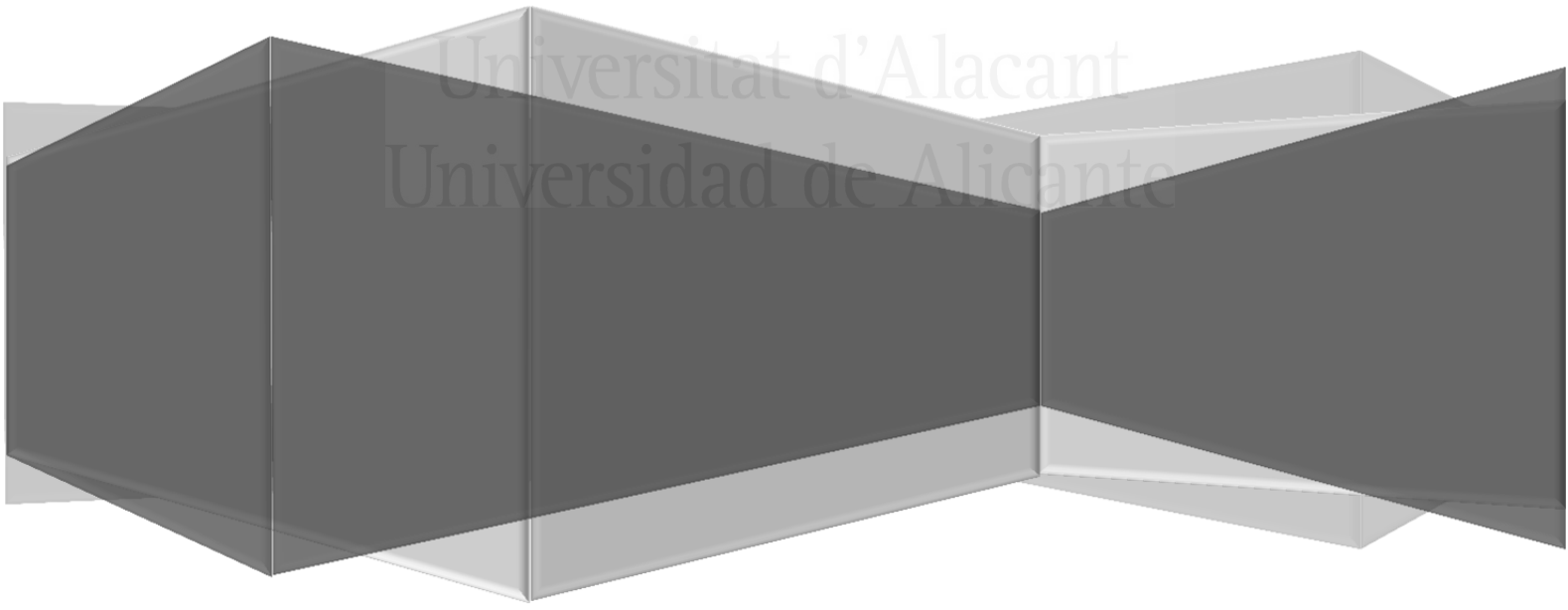

V

Publication V

J. V. Perales-Rondón, C. Busó-Rogero, J. Solla-Gullón, E. Herrero and J. M. Feliu, **"Formic acid electrooxidation on thallium modified platinum single crystal electrodes"**. **In preparation**.

Formic acid electrooxidation on thallium modified platinum single crystal electrodes.

J. V. Perales-Rondón[b], C. Busó-Rogero[b], J. Solla-Gullón[b], E. Herrero,[a, b] and J. M. Feliu[a, b].

[a]Departamento de Química-Física, Universidad de Alicante Apartado 99, E-03080, Alicante, Spain.

[b]Instituto de Electroquímica, Universidad de Alicante Apartado 99, E–03080, Alicante, Spain.

Abstract

Formic acid electrooxidation on Tl modified Pt single crystal electrodes has been carried out in sulfuric acid media. Voltammetric experiments demonstrated that Pt(100) modified by Tl displays a significant enhancement towards formic acid oxidation both lowering the oxidation onset potential and increasing the maximum current density in the positive going-sweep. A similar behavior has been observed in *Pt(s)[(100)x(111)]* stepped surfaces. On the other hand, for Pt(111) surfaces, the incorporation of Tl also induced a shift of the oxidation onset to lower potential values, a diminution of the hysteresis between the positive and negative going-sweep and also an increase of the oxidation currents. These results have been corroborated using *in situ* FTIR experiments, where the CO adsorption band disappears completely when Pt(100) and its vicinal surfaces are modified by Tl adatom, leading to the formation of CO_2 at lower overvoltages.

7.1. Introduction

Formic acid oxidation is known to be a very important reaction in electrocatalysis [1, 2]. It can be used as a model reaction for more complex organic molecules, given that i) its oxidation process only involves two electrons, ii) an additional oxygen atom is not required to produce CO_2, and finally, iii) it is a clear example of a reaction sensitive to the surface structure of the electrocatalyst. In addition, formic acid has been proposed as a possible fuel for fuel cells with portables and small power applications [1, 3, 4]. Although this species emerges as a possible fuel in direct formic acid fuel cells (DFAFC), its application is limited by a low power density and the poisoning of the catalyst. Therefore, high active catalysts towards formic acid oxidation are required.

It is well accepted that formic acid oxidation reaction (FAOR) proceeds via two different routes in Pt electrodes: the so-called indirect pathway, where CO (poisoning intermediate) is formed on the electrode surface, being then oxidized to CO_2 at high potentials; and the second route (direct pathway), which involves the formation of an active intermediate, presumably a formate weakly adsorbed species [5, 6], and its subsequent oxidation into CO_2 at low potentials. This dual pathway mechanism sets one of the main problems to be solved in order to catalyze this reaction in Pt electrodes, which is suppressing the poison formation route and enhancing the oxidation through the direct pathway.

There are two classical approaches to enhance the activity of the electrocatalyst, namely, modifying the surface structure, or changing the composition of the electrode. The first one consists in preparing electrodes with different atomic arrangement, providing specific surface symmetry that favors the formic acid oxidation by the direct pathway [7, 8]. The second one implies the modification of the platinum surfaces with the adsorption of

foreign atoms. This second approach has been widely studied over the past years. Adatoms such as bismuth (Bi) [9], antimony (Sb) [10, 11], arsenic (As) [11] or palladium (Pd) [12] provide an important improvement in the catalytic activity, not only in terms of maximum current density, but also shifting the oxidation onset potential to lower values. One reason for this enhancement is the so-called, third body effect [13], in which one of the metals acts with a steric influence to suppress the poison formation, enhancing the activity through the other pathway. However, some of the adatoms promote also an important bifunctional effect [13-15], where the adatom act as a promotor of the active intermediate in a specific configuration, decreasing the activation energy of the process through the direct pathway. The case of Bi modification is a clear example of this bifunctional effect [16].

In recent years, an increasing interest has been set on those metals that have been less studied, among this, thallium adatom. In earlier studies, Clavilier *et al.* [17] perfomed the underpotential deposition (UPD) of Tl^+ on Pt(111) electrode, arguing that there is an equilibrium in the adsorption-desorption process. More recently, Rodriguez *et al.* [18] has studied extensively either the UPD and irreversible adsorption of Tl on Pt(111) and vicinal surfaces. They were able to ascribe the processes Tl/Tl^+ oxidation and anion adsorption on the Tl-modified surface. Additionally, the results obtained with stepped surfaces indicated that some of the features are clearly associated to the presence of (111) surface domains (terraces).

On the other hand, some few works has studied the FAOR on Tl modified Pt electrodes. For instance, Hartung *et al.*[19] reported the effect of Tl deposition on Pt electrodes towards formic acid oxidation, concluding that Tl catalyse the direct oxidation of bulk HCOOH. More recently, Tl modified shape-controlled Pt nanoparticles showed an important enhancement of the FAOR [20], concluding that preferentially (100) Pt

nanoparticles (cubic shape) modified by Tl were more active than the (111) Pt nanoparticles (octahedral shape) in the entire range of Tl coverages. However, despite these previous contributions, a fundamental study dealing with the activity of Tl modified Pt single crystal electrodes have not been conducted yet. For that reason, in this contribution, an electrochemical and spectroscopic study of formic acid oxidation on Tl modified Pt single crystal electrodes, both using basal planes and stepped surfaces are presented.

7.2. Experimental

Platinum single crystal electrodes were oriented, cut and polished from small single crystal Pt beads (2.5 mm diameter) following the method developed by Clavilier *et al.*[21]. Before all the experiments, working electrodes were flame annealed during 15 s, cooled down in a H_2/Ar atmosphere and quenched in ultrapure water in equilibrium with this atmosphere before immersion in the electrochemical cell [22]. Tl deposition on Pt was performed by cycling between 0.06 V and 0.65 V for Pt(100) and *Pt(s)[(100x111)]* stepped surfaces, and between 0.06 V and 0.50 V for Pt(111) electrodes. The upper potential was chosen in order to preserve the surface order and also to avoid problems of Tl desorption at higher potentials. Diluted solutions of Tl^+ (Tl_2SO_4, Aldrich® 99.995%) with concentrations between 10^{-5} ~ 10^{-6} M in 0.5 M H_2SO_4 were used.

Experiments were carried out at room temperature (25ºC), in a classical electrochemical cell, including a large platinum counter electrode and a reversible hydrogen (N50) electrode (*RHE*) as reference. All potentials used in this work are referred to *RHE*. The solutions were prepared by using H_2SO_4 (Merck KGaA Suprapur® 96%),

formic acid (Merck KGaG 98 %) and ultrapure water (Elga PureLab Ultra 18.2 MΩ cm), preparing 0.1 M HCOOH + 0.5 M H_2SO_4 solution. Ar (N50, Air Liquide) was used for deoxygenating the solutions. All the electrochemical measurements (cyclic voltammetry) were performed using a waveform generator (EG&G PARC 175) coupled to a potentiostat (eDAQ EA161) and a digital recorder (eDAQ ED401).

In situ FTIR measurements were performed in a Nicolet 8700 spectrometer equipped with a mercury cadmium telluride (MCT) detector, according with the external reflection configuration for a transparent prism of CaF_2 beveled at 60º [23] and coupled with the spectroelectrochemical cell. For each spectrum, 100 interferograms were averaged to increase the signal-to-noise ratio, using a resolution of 8 cm^{-1}. For all the experiments, *p*-polarized light was used, allowing the detection of species adsorbed on the electrode surface and other species in the electrolyte solution. Spectra were presented in absorbance units, $A = -log\,(R_1 - R_2)/R_1$, in which R_1 and R_2 are the reflectance values for the single-beam spectra recorded at the sample and the reference potential respectively. Positive bands in spectra are related to species formed at the sampling potential with respect to the reference potential, whereas negative bands correspond to species consumed. IR spectra were collected at intervals of 50 mV between 0.05 V and 0.5 V, and 100 mV between 0.5 V and 0.9 V *vs. RHE*. Spectrum taken at 0.05 V was used as a reference in all spectra presented.

7.3. Results and discussion

7.3.1. FAOR on Tl modified Pt(100) and Pt(111) electrodes

Figure 7.1 shows the voltammetric profiles corresponding to a) Pt(100) and b) Pt(111) modified with Tl at different coverages in 0.5 M H_2SO_4. In the case of Pt(100), two

different regions can be distinguished. The first one, located between 0.06 V and 0.20 V, where a new peak centered at 0.17 V appears for increasing thallium coverages and a second one involving the decrease of the contributions from 0.2 V to 0.5 V, related to the competitive adsorption between hydrogen and sulfate anions on the Pt surface.

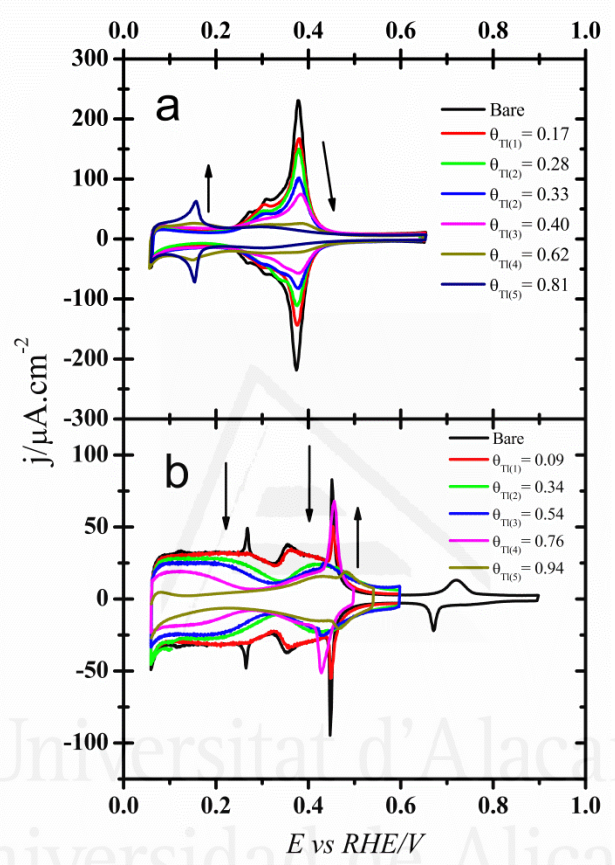

Figure 7.1. Cyclic voltammetry of Tl modified Pt single crystal electrodes taken in H_2SO_4 0.5 M at different Tl coverages. (a) Tl modified Pt(100) electrode; (b) Tl modified Pt(111) electrode. Scan rate 50 $mV.s^{-1}$.

In order to find out the nature of the peak at 0.17 V, the peak potential position (in the hydrogen electrode scale (SHE)) was plotted against solution pH (figure 7.2). A slope value of 52 mV was obtained, very near to 59 mV, which implies that one proton is exchanged per electron in the surface redox reaction. Since the charge of this process is small and the peak is only well defined at high coverages, it can be proposed that the

reaction is associated to the hydrogen adsorption process on a Pt site surrounded by Tl adatoms. Thus, considering Tl as an electropositive adatom, this finding suggests that its presence modifies the adsorption of hydrogen profile, lowering the potential where the adsorption starts to occur.

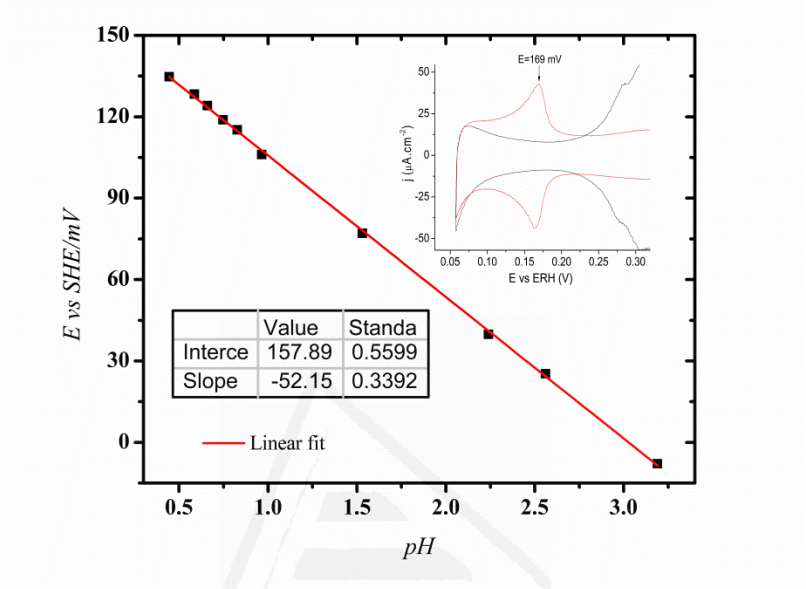

Figure 7.2. Linear relationship between the peak potential of the reversible feature in Tl modified Pt(100) electrode (inset) and the solution pH.

On the other hand, for Pt(111), there is a clear decrease of the voltammetric profile comparing to the blank, both the hydrogen adsorption/desorption region and the anion adsorption/desorption regions [17]. However, a new peak around 0.48 V appears very close to the spike in the unmodified surfaces. This sharp spike is related to the order disorder transition in the sulfate layer [17, 18, 24]. Thus, it can be proposed that Tl is modifying the energetics of this order-disorder transition. Moreover, an additional proves for that can be obtained when the voltammetric profiles in the absence and presence of sulfate. Figure 7.3 displays the appearance of a new small peak around 0.48-0.50 V for a Tl modified Pt(111) after adding small amounts of sulfate into a perchloric acid solution. This result suggests that the peak at 0.48 V is related to the rearrangement of the sulfate layer

adsorbed on the Tl modified Pt surface. The latter result was demonstrated by Rodriguez *et al.* by the observation of the displacement of this peak when changing the sulfate concentration in the solution at a constant pH [18].

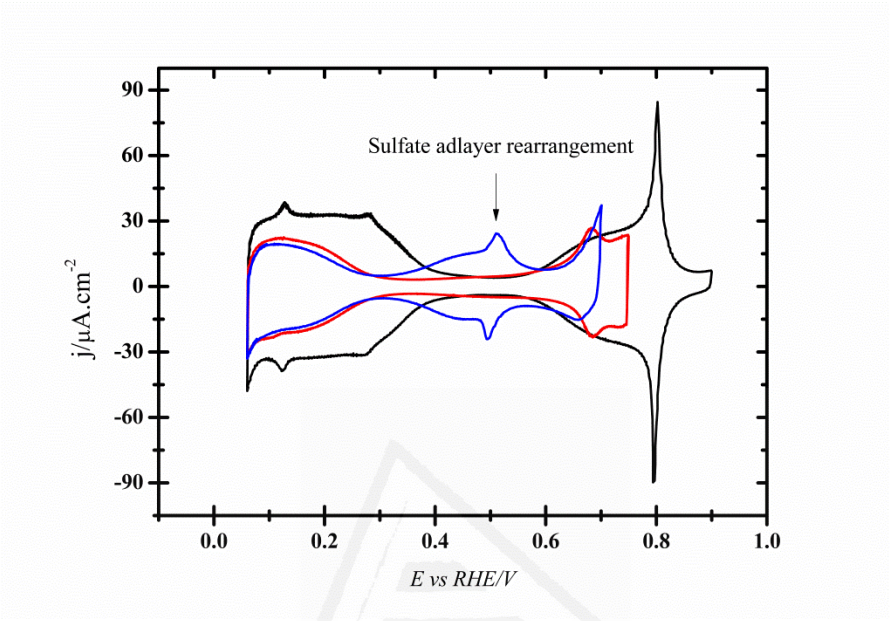

Figure 7.3. Comparison between voltammetric profile of the Pt(111) modified by Tl adatom in: perchloric acid (red line) and perchloric acid with sulfate anions (blue line). The black line represents the voltammetric profile for the blank in perchloric acid. Scan rate: 0.05 V s^{-1}

The results shown in figure 7.1 can be also use to monitor the deposition of Tl adatom, by the decreasing of the currents in the main region related to hydrogen and anion adsorption desorption, as previously done in a former work [20]. Thus, since Tl coverage could be followed through the decreasing of the hydrogen adsorption/desorption region at each Pt electrode profile, the Tl coverage could be calculated by using the equation 7.1:

$$\theta_{Tl} = 1 - \theta_{H} = \frac{q_H^0 - q_H^{Tl}}{q_H^0} \qquad \textit{Eq. 7.1}$$

where q_H^0 and q_H^{Tl} are the hydrogen adsorption charges of the clean and thallium modified electrodes respectively, calculated after the subtraction of the double layer charging

contribution. This equation have been extensively used in the calculation of coverage of a large number of adatoms [2], considering that an adatom can blocked a specific number of Pt sites where hydrogen adsorption takes place. For Pt(100) the coverage was calculated between 0.22 and 0.50 V, whereas for Pt(111) the potential limits were set between 0.06 and 0.325 V in order to avoid some contribution coming from signals belonging to Tl redox surface processes.

Both Tl modified electrodes were used to study FAOR. Figure 7.4 a and b show the formic acid oxidation activity as a function of the Tl coverage (only positive going sweeps are shown). For the Pt(100) electrode, the activity in the positive sweep is almost zero (black line), due to the important poisoning of the electrode by CO that takes place between 0.25 and 0.4 V, widely documented in previous works [1, 25-27]. The first effect of the Tl modification is the evident diminution of the onset potential of the oxidation, which starts at about 0.15 V for intermediate coverages. In addition, a clear increase of the current density for the FAOR is observed showing a peak at about 0.5 V. Interestingly, the current density grows as the Tl coverage increase, reaching a maximum value at $\theta_{Tl} \cong 0.33$ (small coverage values). From this coverage, the current density decreases, although the onset potential remains similar to that obtained for $\theta_{Tl} \cong 0.33$. Finally, at the maximum coverage studied ($\theta_{Tl} \cong 0.78$), a significant decrease of the current and a shift of the onset potential to more positive values are observed.

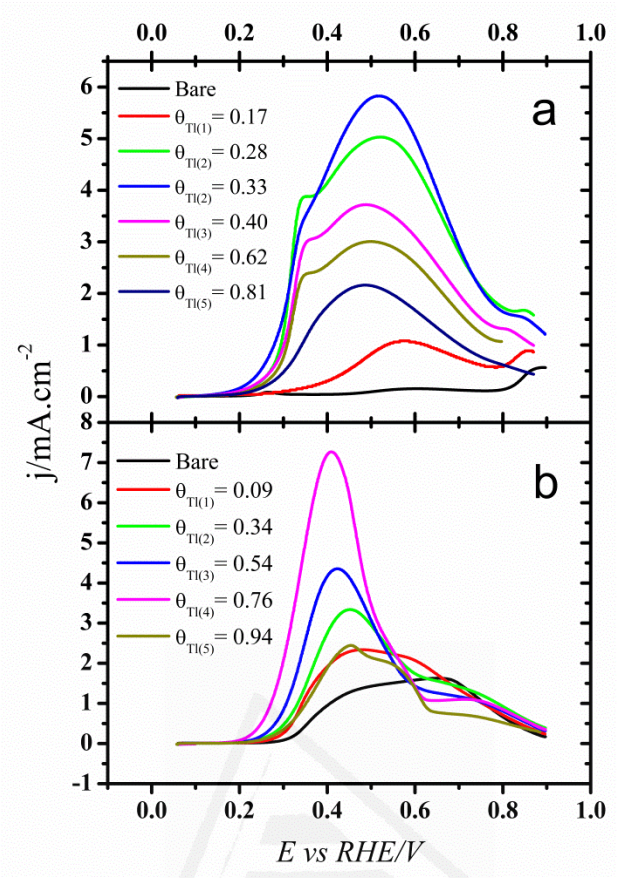

Figure 7.4. Positive sweep voltammetry for 0.1 M HCOOH oxidation in H_2SO_4 0.5 M for: (a) Tl modified Pt(100) and (b) Tl modified Pt(111) single crystal electrodes. Scan rate 0.02 V s^{-1}.

This fact indicates that the presence of Tl at high coverages has a negative effect, presumably due to the blockage of a large number of Pt sites to achieve the oxidation of formic acid. The last observation is in agreement with the actuation mechnanisms of the adatomos proposed in [13]. Thus, with increasing amounts of Tl until a maximum value ca. $\theta_{Tl} \cong 0.30$, the indirect pathway (through CO poisoning) is hindered, promoting formic acid oxidation through the direct pathway.

Figure 7.4b shows the results obtained with a Pt(111) surface. The results also suggest that the incorporation of Tl have a positive effect in the activity of the electrode, specially, increasing the current density of the oxidation in the low potential region. Also a shift in the onset potential of the oxidation can be achieved. For low coverages ($\theta_{Tl} \approx 0.10$), the

improvement in the activity is less significant, being similar at high coverages ($\theta_{Tl} \approx 0.82$). Nevertheless, the main effect is achieved at medium-high coverages, i.e. $\theta_{Tl} \approx 0.70$. In fact, at $\theta_{Tl} \approx 0.76$, the current density reach maximum values (7 mA.cm^{-2}). In the voltammetric profile can be seem that the current starts to increases at potential as low as 0.15 V, reaching the highest activity at 0.4 V. In this case, it is clear that Tl has a positive effect for the FAOR. For adatoms, such as Tl, which are electropositive with respect to Pt, the catalytic effect has been explained using a bifunctional mechanism, in which the adatom facilitate the adsorption of formate in the right position, so that the C-H bond cleavage is facilitated [16, 28] . This mechanism is in agreement with the maximum catalytic activity found for $\theta_{Tl} \approx 0.76$, since for this coverage the number of Pt-Tl ensembles, which are the catalytic active site, are maximized [13].

It is important to highlight that these results are different from those reported previously [20] by our research group. Such a difference is attributed to the stability of the Tl adlayer on the electrode surface. In the previous experiments, after modifying the electrode, and before being immersed into the cell containing formic acid, the electrode was rinsed with ultrapure water. We have recently observed that this rinsing step gives rise to an important removal of the Tl adsorbed on the surface of the electrode. This fact is the reason for which, in the previous contribution [20], the enhanced activity displayed by the Tl modified surfaces is much lower than that reported in the present contribution. In this work, a special care has been taken in order to keep as stable as possible the coverage of Tl on the electrode. Thus, after modifying the electrode with Tl and testing it in the electrolytic solution, this was taken directly into the cell containing formic acid 0.1M, avoiding the loss of Tl because of the rinsing step.

Figure 7.5 shows a normalization of the current density ($j_{\theta_{Tl}}/j_{Bare}$) at the coverage where the maximum current is reached for each of the electrodes (black and red curves).

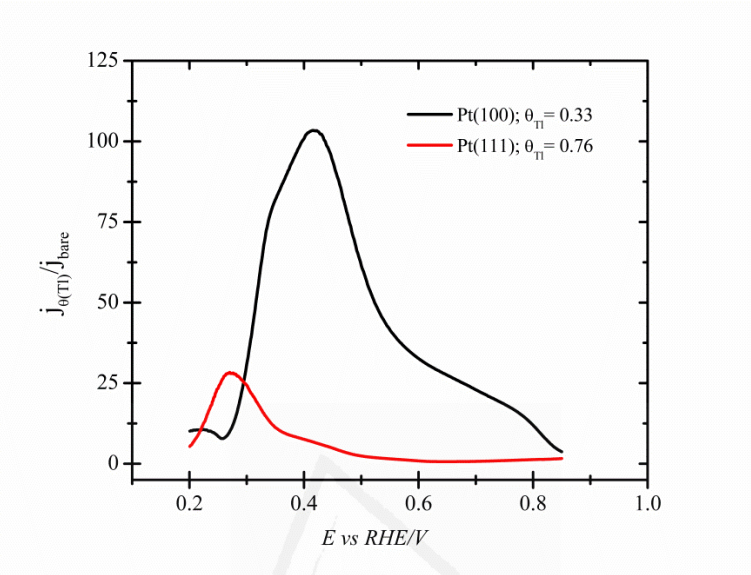

Figure 7.5. FAOR current densities normalized using the bare and Tl-modified Pt(100) (black line) and Pt(111) (red line). Data taken from Figure 7.4.

It is clear from the figure that the "improvement factor" for the case of Pt(100) modified by Tl is bigger than that shown for Tl-Pt(111), except for potentials below 0.3 V, where Tl-Pt(111) has a better improvement than Tl-Pt(100). It is important to notice that the potential where Tl-Pt(111) reach the maximum improvement factor is lower (0.25 V) compared with 0.35 V which is the potential at the maximum improvement in the case of Tl-Pt(100).

As a conclusion, since CO adsorption from formic acid has specific Pt free sites requirements [29, 30], Tl adsorbed on Pt(100) has a positive effect because it enables preventing the CO formation (third body effect), whereas in the case of Pt(111) (which is an ideally poisoning resistant surface[15]), the main effect involves lowering the activation energy possibly by promoting the adsorption of the active intermediate in a configuration

which facilitate the oxidation into CO_2, similar with those effect described for Bi adatom previously [16, 28].

7.3.2. FAOR on Tl modified Pt(s)[n(100)x(111)]

Figures 7.6A, C and E show the voltammetric profile for some electrodes belonging to the series *Pt(s)[n(100)x(111)]*, that is, surfaces with (100) terraces and (111) steps, for increasing Tl coverages. In all the cases, as is observed for the Pt(100) electrode, the hydrogen adsorption/desorption region decreases as the Tl coverage increases. Additionally, a small peak around 0.17 V can be again observed in the voltammetric profile for the Pt(23 1 1) and Pt(15 1 1) at high Tl coverages, feature that disappears for Pt(711) electrode. This fact suggests that long-range (100) domains are required to form those structures leading to the appearance of this particular feature. Another interesting point is that associated with the selective adsorption of the Tl adatom. For Pt(711), it is observed that Tl is adsorbed in the steps prior to the terraces, according to the Smoluchowski for electropositive adatoms [31]. This effect is not observed for the surfaces with longer terraces, similarly to what has been observed for this series of surfaces with bismuth [32]. It is important to highlight that the later behavior could be interesting to be applied in futures works to combine two types of adatoms in a stepped modified surface. For instance, modifying the steps with Tl adatom to suppress the poison formation combined with the modification with another adatom to promote the formic acid oxidation by the direct pathway.

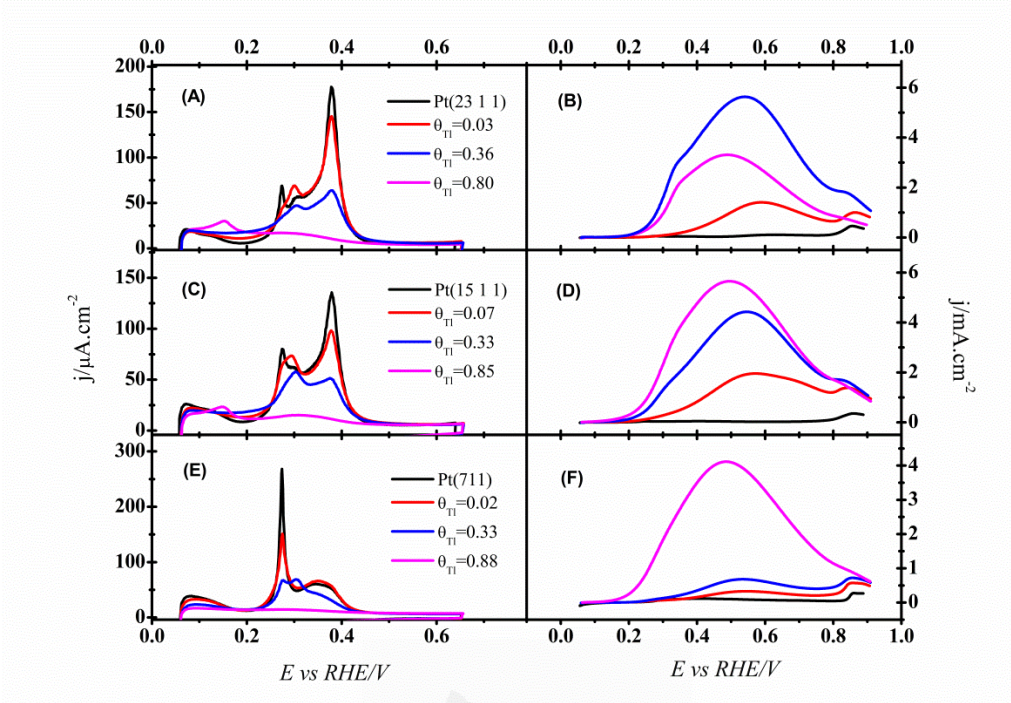

Figure 7.6. Positive sweep voltammetry for 0.1 M HCOOH oxidation in H_2SO_4 0.5 M for: (A) Tl modified Pt(23 1 1); (C) Tl modified Pt(15 1 1) and (E) Tl modified Pt(711) single crystal electrodes. Scan rate 0.02 V s^{-1}. Positive sweep voltammetry in H_2SO_4 0.5 M for: (B) Tl modified Pt(23 1 1); (D) Tl modified Pt(15 1 1) and (F) Tl modified Pt(711) single crystal electrodes. Scan rate 0.05 V s^{-1}.

Figures 7.6B, D and F show the activity for those Tl modified Pt electrodes towards formic acid oxidation. For Pt(23 1 1), that is, a surface still having wide (100) terraces, the maximum activity is achieved at coverage values about $\theta_{Tl} \approx 0.30 - 0.40$, in good agreement with the case of Pt(100). Again, when the coverage becomes maximum, the activity decreases and the reaction is less favored, shifting the onset potential of the oxidation to more positive values. For the case of Pt(15 1 1) and Pt(711) the response is clearly different to that previously shown and the activity systematically improves as the Tl coverage increases, being maximum at higher values. This behavior is quite similar to that observed previously for (100)-Pt NPs modified by Tl, in which at maximum coverage was found the higher activity towards formic acid oxidation [20]. This fact points out the similitude between a shaped controlled nanoparticles and a stepped electrode in terms of

surface structure and would suggest that the Tl has a positive effect in the electrocatalysis of formic acid through the direct pathway, as happens for the Pt(111)electrode.

Comparing the activities at $\theta_{Tl} = 0.33{\sim}0.36$ (figure 7.7), it can be seen that the current density decreases when the step density increases. This suggests that the surface arrangement reached in long-ranges (100) terraces is more effective to catalyze the reaction by the direct pathway. It is also important to point out that CO forms easily in step sites, independently of its crystallographic orientation [33, 34], which explains the lower activity when the terraces become shorter. Although the presence of steps in (100) terraces has minor effects on the modification of electrochemical properties than that one found for stepped Pt(111) surfaces [35], however, these changes are magnified with the modification by an adatom.

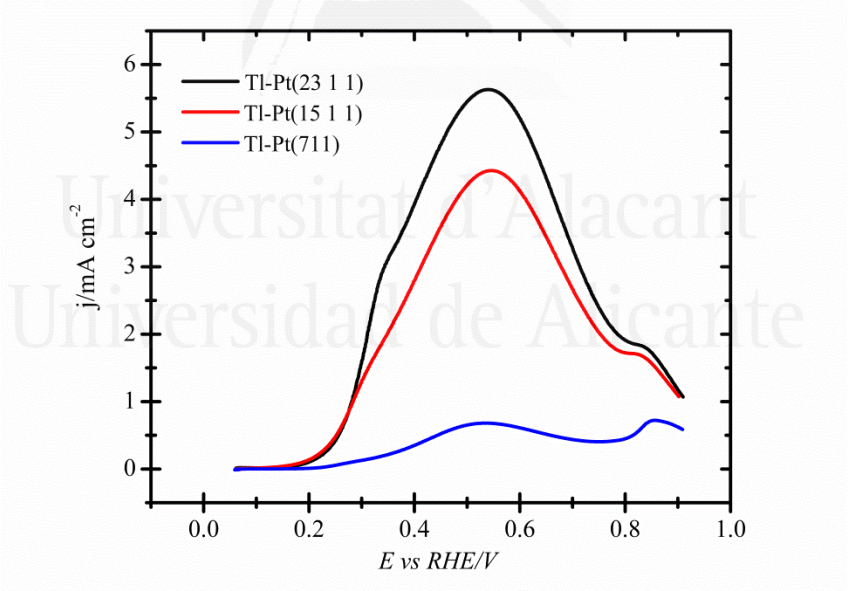

Figure 7.7. Comparison of the positive sweep for formic acid oxidation on Tl modified Pt single crystal belonging to the series *Pt(s)[n(100)x(111)]* at a coverage $\theta_{Tl} = 0.33{\sim}0.36$. Values taken form the activities in figure 7.6.

7.3.3. FAOR on Tl modified Pt(s)[n(111)x(100)]

Figure 7.8 reports the evolution of electrodes belonging to the series *Pt(s)[n(111)x(100)]*, namely, Pt(11 10 10) and Pt(544), after being modified with Tl. The results obtained again show a decrease in all signals corresponding to the hydrogen and anion adsorption/desorption process, as the Tl coverage increases. The small peak centered around 0.45 V (associated to sulfate/bisulfate order transition) is presented in long (111) terraces stepped surfaces, being lost in Pt(544) electrode (see Figure 7.8 A and C).

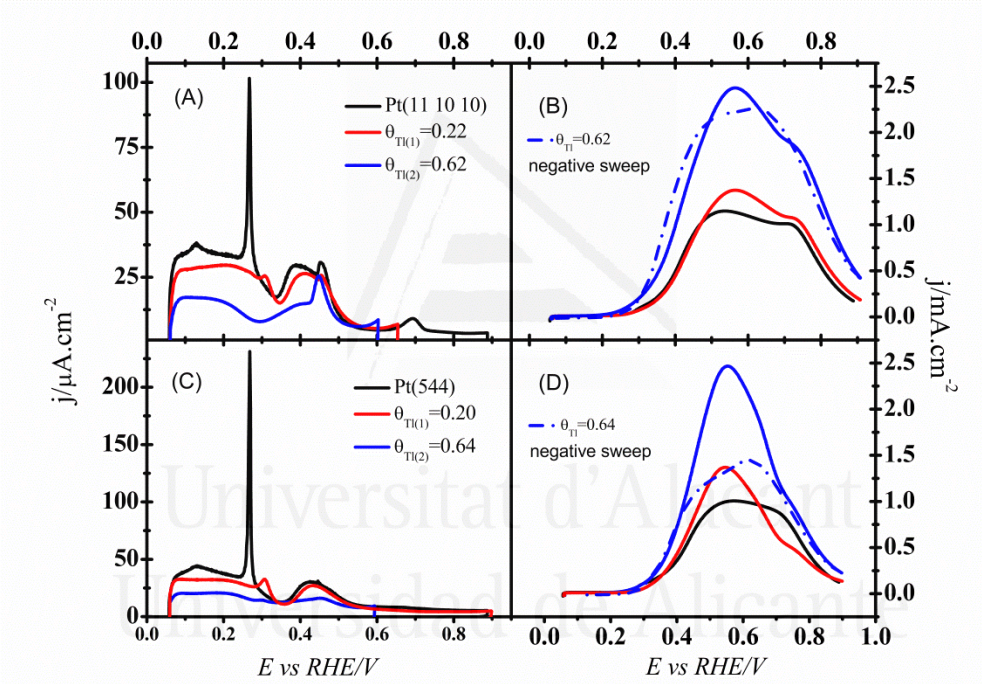

Figure 7.8. Positive sweep voltammetry for 0.1 M HCOOH oxidation in H_2SO_4 0.5 M for: (A) Tl modified Pt(11 10 10) and (C) Tl modified Pt(544) single crystal electrodes. Scan rate 0.02 V s^{-1}. Positive sweep voltammetry in H_2SO_4 0.5 M for: (B) Tl modified Pt(11 10 10) and (D) Tl modified Pt(544) single crystal electrodes. Scan rate 0.05 V s^{-1}.

Figures 7.8B and D display the corresponding formic acid electrooxidation activity. The results show that, for increasing Tl coverages, the oxidation current increases and the oxidation onset potential shifts the lower potential values, although these effects are less significant than that obtained with Pt(100) and its vicinal surfaces. Interestingly, the

voltammetry for each Pt bare electrode shows that the CO formation is hindering the FAOR by the direct pathway, because of the smaller current density in the positive sweep compared with the negative one, being responsible for the hysteresis observed. When modifying the electrode with Tl, the enhancement is quite similar for both electrodes. The only notorious difference is evidenced in the hysteresis between the positive and negative voltammetric cycles. For Pt(11 10 10) the hysteresis is lost almost completely at $\theta_{Tl} \cong 0.60$ (which could be considered as a high coverage). On the other hand, for Pt(544), even the positive sweep is higher than the negative one, suggesting that the insertion of a bigger step density, i.e. make it the (111) terraces shorter, favors those adsorbed structures that prevent the CO formation, leading such an unusual "inverse" hysteresis effect at Pt(544) electrode.

7.3.4. In situ FTIR experiments on Pt(100) and Pt(111)

From the previous voltammetric experiments, it is evident that the incorporation of Tl is directly related to the suppression of the CO formation. However, to deepen on this aspect, some spectroscopic evidences (*in situ* FTIR experiments) will strongly contribute to elucidate the role played by the Tl adatom during FAOR [23]. In this regard, it is worth noting that during the *in situ* FTIR experiments, the formic acid concentration was diminished with the aim of decreasing the huge amount of CO_2 formed during the experiment, which importantly destabilizes the thin-layer configuration. In addition, sulfuric acid concentration was reduced in order to avoid possible damage in the CaF_2 prism due to the higher acid concentrations.

Figure 7.9 shows some selected spectra obtained with Tl modified and unmodified Pt(100) and Pt(111) surfaces. For bare Pt(100) and Pt(111), it is clear the presence of CO adsorbed on the electrode surface in both linear and bridge configuration (for Pt(111) electrode only linear CO is present) at 2030-2070 cm^{-1} and 1840-1870 cm^{-1} , respectively [36-38]. It is worthy to clarify that the presence of CO adsorbed on Pt(111) is due to the presence of some defects on the electrode used to carry out these experiments. These bands are clearly present even at 0.5 V where the incipient CO oxidation takes place. Consequently, at 0.4 V, the formation of CO_2 starts for both electrodes, as deduced from the band at 2340 cm^{-1}.

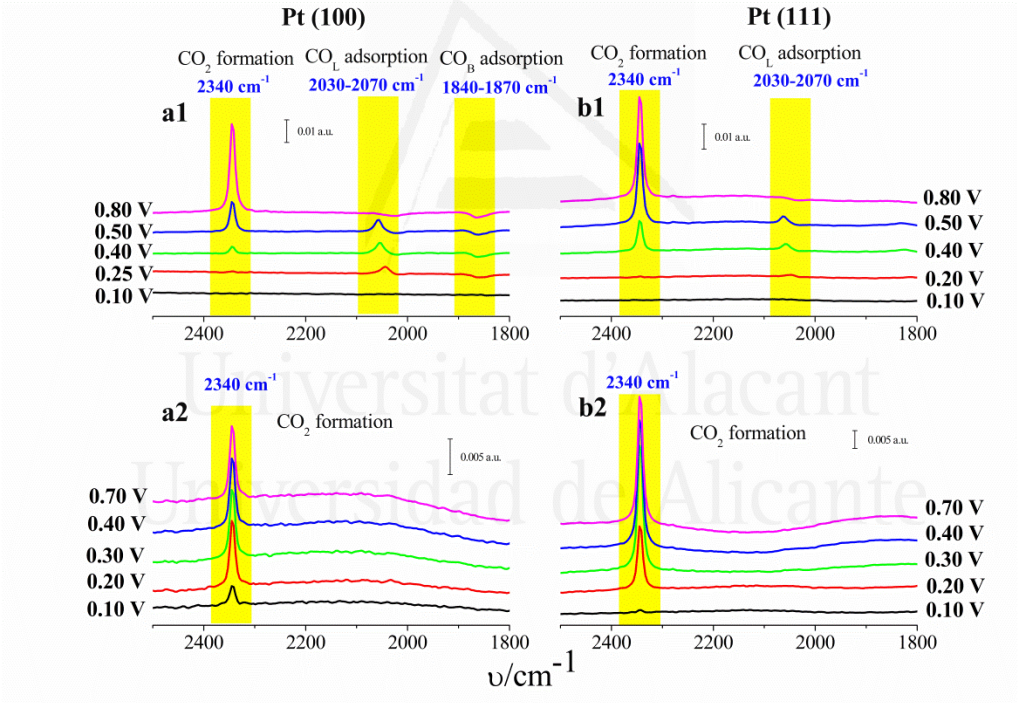

Figure 7.9. *In* situ FTIR experiments in 0.05 M HCOOH + 0.1 M H_2SO_4 for: (a) Pt (100) and (b) Pt (111) electrode. Spectra denoted as '1' correspond to the bare Pt electrode whereas '2' indicates spectra collected in Pt electrodes modified with Tl at the maximum coverage.

When the electrodes are modified by Tl (at maximum coverage), the CO band is absent and the CO_2 band is observed at very low potentials (even before 0.1 V).

Similar *in situ* FTIR experiments were also performed with the *Pt(s)[n(111)x(100)]* electrodes. For the sake of comparison, figure 7.10 shows the integration of the CO_2 band normalized to the same integrated CO_2 band at 0.8 V for each experiment. At 0.1 V, it is observed that the Pt(711) displays the highest ratio, thus indicating the positive contribution of the (111) steps for this reaction. In fact, in figure 7.7, can be seen that the onset of the oxidation is the lowest compared with the other stepped surfaces. Interestingly, for the three electrodes studied, an almost complete CO_2 formation/production (90%) is reached at a potential about 0.2 V regardless the electrode employed. These results confirm the third body effect played by the Tl in the modified electrode [13].

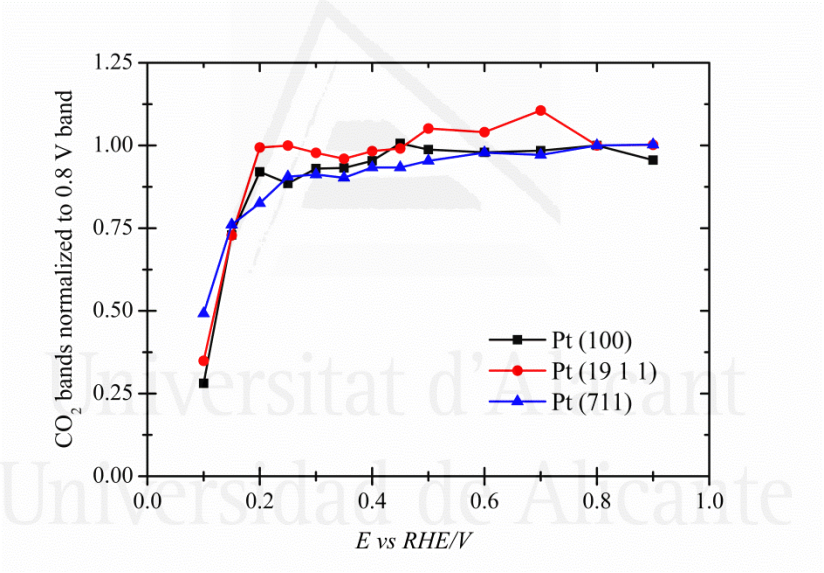

Figure 7.10. Ratio between integrated intensities of the CO_2 bands and the integral of the same CO_2 band at 0.8 V for the Tl-modified Pt electrodes at the maximum coverage at different potentials.

7.4. Conclusions

A systematic FAOR study on Pt single crystal electrodes modified by Tl has been done. Voltammetric experiments in Pt(100) and vicinal surfaces, *Pt(s)[(100)x(111)]*, modified by Tl present an important enhancement towards formic acid oxidation, lowering

the onset potential of oxidation and increasing the current density in the positive sweep voltammetry. For Pt(111), the main effect of Tl is notorious in the diminution of the onset potential of the oxidation, as well as the lowering in the potential where the current density reach maximum values, suggesting a bifunctional effect of the Tl adatom. On the other hand, for *Pt(s)[(111)x(100)]* stepped surfaces, was found that Tl modification reduce the hysteresis between positive and negative cycle, whereas the activity in the whole potential range is also improved. Although there is an important improvement in both, Pt(111) and Pt(100) electrodes modified by Tl, the enhancement is more significant in the case of Pt(100)

In situ FTIR experiments show that CO band disappear completely when Pt(100) and Pt(111) have been modified by Tl adatom, leading CO_2 production at lower potentials (even at 0.1 V). By combining voltammetric and spectroscopic data it can be concluded that Tl presents a third body effect for the formation of CO. Its role can be summarized as follow: when modifying Pt(100) and its vicinal surfaces with Tl, the indirect pathway (CO adsorption) is hindered by the arrangement of Tl on the electrode surface. The diminution of the onset potential for the oxidation also indicates that Tl is promoting formic acid oxidation through the direct pathway through bifunctional effect, leading a similar behavior to that found for Bi-Pt previously.

Acknowledgments

This work has been financially supported by the MICINN (Spain) (projects CTQ2013-44083-P and CTQ2013-48280-C3-3-R) and Generalitat Valenciana (project PROMETEOII/2014/013, FEDER).

7.5. References

[1] J. M. Feliu and E. Herrero, "Formic acid oxidation", in *Handbook of Fuel Cells - Fundamentals, Technology and Applications, vol. 2*, W. Vielstich, H. Gasteiger and A. Lamm (Eds.) John Wiley & Sons, Ltd., Chichester, **2003**, pp. 625-634.

[2] M. T. M. Koper, "Fuel Cell Catalysis: A Surface Science Approach", *Electrocatalysis and Electrochemistry* A. Wieckowski (Ed.), John Wiley & Sons, Hoboken, New Jersey, **2009**.

[3] C. Rice, R. I. Ha, R. I. Masel, P. Waszczuk, A. Wieckowski and T. Barnard, "Direct formic acid fuel cells" *Journal of Power Sources* **2002**, 111, 83-89.

[4] C. Rice, S. Ha, R. I. Masel and A. Wieckowski, "Catalysts for direct formic acid fuel cells" *Journal of Power Sources* **2003**, 115, 229-235.

[5] J. V. Perales-Rondon, E. Herrero and J. M. Feliu, "Effects of the anion adsorption and pH on the formic acid oxidation reaction on Pt(111) electrodes" *Electrochimica Acta* **2014**, 140, 511-517.

[6] H.-F. Wang and Z.-P. Liu, "Formic Acid Oxidation at Pt/H2O Interface from Periodic DFT Calculations Integrated with a Continuum Solvation Model" *Journal of Physical Chemistry C* **2009**, 113, 17502-17508.

[7] V. Grozovski, V. Climent, E. Herrero and J. M. Feliu, "Intrinsic Activity and Poisoning Rate for HCOOH Oxidation at Pt(100) and Vicinal Surfaces Containing Monoatomic (111) Steps" *ChemPhysChem* **2009**, 10, 1922-1926.

[8] V. Grozovski, V. Climent, E. Herrero and J. M. Feliu, "Intrinsic activity and poisoning rate for HCOOH oxidation on platinum stepped surfaces" *Physical Chemistry Chemical Physics* **2010**, 12, 8822-8831.

[9] S. P. E. Smith, K. F. Ben-Dor and H. D. Abruna, "Structural effects on the oxidation of HCOOH by bismuth-modified Pt(111) electrodes with (100) monatomic steps" *Langmuir* **1999**, 15, 7325-7332.

[10] Y.-Y. Yang, S.-G. Sun, Y.-J. Gu, Z.-Y. Zhou and C.-H. Zhen, "Surface modification and electrocatalytic properties of Pt(100), Pt(110), Pt(320) and Pt(331) electrodes with Sb towards HCOOH oxidation" *Electrochimica Acta* **2001**, 46, 4339-4348.

[11] A. Boronat-Gonzalez, E. Herrero and J. M. Feliu, "Fundamental aspects of HCOOH oxidation at platinum single crystal surfaces with basal orientations and modified by irreversibly adsorbed adatoms" *Journal of Solid State Electrochemistry* **2014**, 18, 1181-1193.

[12] F. J. Vidal-Iglesias, J. Solla-Gullón, E. Herrero, A. Aldaz and J. M. Feliu, "Formic acid oxidation on Pd-modified Pt(100) and Pt(111) electrodes: A DEMS study" *Journal of Applied Electrochemistry* **2006**, 36, 1207-1214.

[13] E. Leiva, T. Iwasita, E. Herrero and J. M. Feliu, "Effect of adatoms in the electrocatalysis of HCOOH oxidation. A theoretical model" *Langmuir* **1997**, 13, 6287-6293.

[14] M. Shibata, N. Furuya, M. Watanabe and S. Motoo, "Electrocatalysis by ad-atoms. Part XXIV. Effect of arrangement of Bi ad-atoms on formic acid oxidation" *Journal of Electroanalytical Chemistry* **1989**, 263, 97-108.

[15] E. Herrero, A. Fernández-Vega, J. M. Feliu and A. Aldaz, "Poison formation reaction from formic acid and methanol on Pt(111) electrodes modified by irreversibly adsorbed Bi and As " *Journal of Electroanalytical Chemistry* **1993**, 350, 73-88.

[16] J. V. Perales-Rondon, A. Ferre-Vilaplana, J. M. Feliu and E. Herrero, "Oxidation Mechanism of Formic Acid on the Bismuth Adatom-Modified Pt(111) Surface" *Journal of the American Chemical Society* **2014**, 136, 13110-13113.

[17] J. Clavilier, J. P. Ganon and M. Petit, "A comparative study of the underpotential deposition of two monovalent cations, Tl^+ and H^+, on Pt (111) as a way to the interpretation of the unusual adsorption states" *Journal of Electroanalytical Chemistry* **1989**, 265, 231-245.

[18] P. Rodriguez, N. García-Aráez, E. Herrero and J. M. Feliu, "New insight on the behavior of the irreversible adsorption and underpotential deposition of thallium on platinum (111) and vicinal surfaces in acid electrolytes" *Electrochimica Acta* **2015**, 151, 319-325.

[19] T. Hartung, J. Willsau and J. Heitbaum, "Catalytic effects of Hg and Tl submonolayers on the electrooxidation of formic acid on Pt" *Journal of Electroanalytical Chemistry and Interfacial Electrochemistry* **1986**, 205, 135-149.

[20] C. Buso-Rogero, J. V. Perales-Rondon, M. J. S. Farias, F. J. Vidal-Iglesias, J. Solla-Gullon, E. Herrero and J. M. Feliu, "Formic acid electrooxidation on thallium-decorated shape-controlled platinum nanoparticles: an improvement in electrocatalytic activity" *Physical Chemistry Chemical Physics* **2014**, 16, 13616-13624.

[21] J. Clavilier, D. Armand, S. G. Sun and M. Petit, "Electrochemical adsorption behaviour of platinum stepped surfaces in sulphuric acid solutions " *Journal of Electroanalytical Chemistry* **1986**, 205, 267-277.

[22] J. Clavilier, K. El Achi, M. Petit, A. Rodes and M. A. Zamakhchari, "Electrochemical monitoring of the thermal reordering of platinum single crystal surfaces after metallographic polishing from the early stage to the equilibrium surfaces" *Journal of Electroanalytical Chemistry* **1990**, 295, 333.

[23] T. Iwasita and F. C. Nart, "In situ infrared spectroscopy at electrochemical interfaces" *Progress in Surface Science* **1997**, 55, 271-340.

[24] R. R. Adzic, J. X. Wang, O. M. Magnussen and B. M. Ocko, "Structure of Tl adlayers on the Pt(111) electrode surface: Effects of solution pH and bisulfate coadsorption" *Journal of Physical Chemistry* **1996**, 100, 14721-14725.

[25] S. Gilman, "The Mechanism of Electrochemical Oxidation of Carbon Monoxide and Methanol on Platinum. II. The "Reactant-Pair" Mechanism for Electrochemical Oxidation of Carbon Monoxide and Methanol" *Journal of Physical Chemistry B* **1964**, 68, 70.

[26] J. Clavilier and S. G. Sun, "Electrochemical Study of the Chemisorbed Species Formed from Formic-Acid Dissociation at Platinum Single-Crystal Electrodes" *Journal of Electroanalytical Chemistry* **1986**, 199, 471-480.

[27] J. Willsau and J. Heitbaum, "Analysis of adsorbed intermediates and determination of surface potential shifts by DEMS" *Electrochimica Acta* **1986**, 31, 943-948.

[28] A. Ferre-Vilaplana, J. V. Perales-Rondon, J. M. Feliu and E. Herrero, "Understanding the Effect of the Adatoms in the Formic Acid Oxidation Mechanism on Pt(111) Electrodes" *ACS Catalysis* **2015**, 5, 645-654.

[29] M. J. Llorca, E. Herrero, J. M. Feliu and A. Aldaz, "Formic acid oxidation on Pt(111) electrodes modified by irreversibly adsorbed selenium" *Journal of Electroanalytical Chemistry* **1994**, 373, 217-225.

[30] S. C. Chang, Y. Ho and M. J. Weaver, "Applications of real-time infrared spectroscopy to electrocatalysis at bimetallic surfaces. I. Electrooxidation of formic acid and methanol on bismuth-modified Pt(111) and Pt(100)" *Surface Science* **1992**, 265, 81-94.

[31] E. Herrero, V. Climent and J. M. Feliu, "On the different adsorption behavior of bismuth, sulfur, selenium and tellurium on a Pt(775) stepped surface" *Electrochemistry Communications* **2000**, 2, 636-640.

[32] R. Gisbert, V. Climent, E. Herrero and J. M. Feliu, "Underpotential Deposition of Copper on Pt(S)[n(100)x(110)] Stepped Surfaces" *Journal of Electrochemistry* **2012**, 18, 410-426.

[33] M. D. Maciá, E. Herrero, J. M. Feliu and A. Aldaz, "Formic acid self-poisoning on bismuth-modified stepped electrodes" *Journal of Electroanalytical Chemistry* **2001**, 500, 498-509.

[34] M. D. Maciá, E. Herrero, J. M. Feliu and A. Aldaz, "Formic acid self-poisoning on bismuth-modified Pt(755) and Pt(775) electrodes" *Electrochemistry Communications* **1999**, 1, 87-89.

[35] A. Ferre-Vilaplana, R. Gisbert and E. Herrero, "On the electrochemical properties of platinum stepped surfaces vicinal to the (100) pole. A computational study" *Electrochimica Acta* **2014**, 125, 666-673.

[36] K. Kunimatsu, "Infrared spectroscopic study of methanol and formic acid adsorbates on a platinum electrode: Part I. Comparison of the infrared absorption intensities of linear CO(a) derived from CO, CH_3OH and HCOOH " *Journal of Electroanalytical Chemistry* **1986**, 213, 149-157.

[37] K. Kunimatsu, H. Seki, W. G. Golden, J. G. Gordon and M. R. Philpott, "Carbon monoxide adsorption on a platinum electrode studied by polarization modulated FTIR reflection-absorption spectroscopy. 2.CO adsorbed at a potential in the hydrogen region and its oxidation in acids" *Langmuir* **1986**, 2, 464.

[38] S. G. Sun, J. Clavilier and A. Bewick, "The mechanism of electrocatalytic oxidation of formic acid on Pt (100) and Pt (111) in sulphuric acid solution: an emirs study" *Journal of Electroanalytical Chemistry* **1988**, 240, 147-159.

Chapter VIII

Enhanced catalytic activity and stability for the electrooxidation of formic acid on lead modified shape controlled platinum nanoparticles

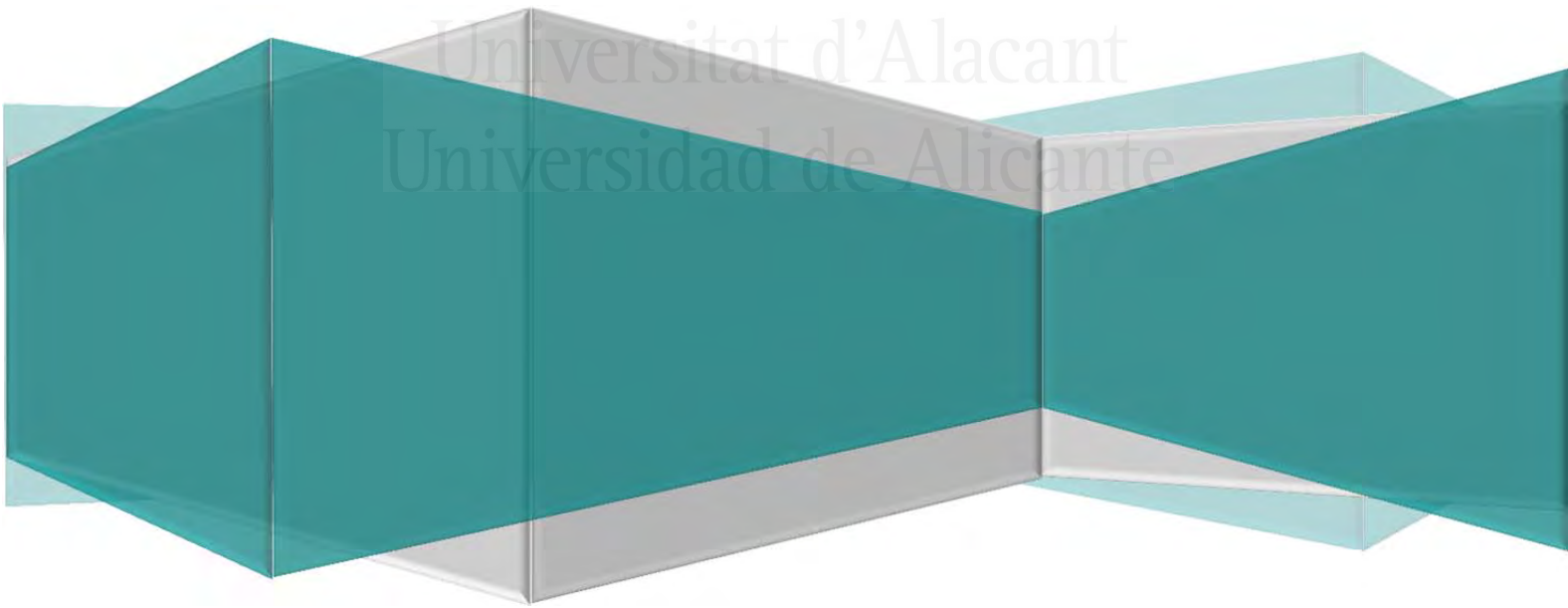

VI

Publication VI

J.V. Perales-Rondón, J. Solla-Gullón, E. Herrero and C.M. Sánchez-Sánchez, **"Enhanced catalytic activity and stability for the electrooxidation of formic acid on lead modified shape controlled platinum nanoparticles"**. **Under revision**. Article submitted to the Journal *Applied Catalysis B.*

Enhanced catalytic activity and stability for the electrooxidation of formic acid on lead modified shape controlled platinum nanoparticles

Juan Víctor Perales-Rondón[*,a,b], Jose Solla-Gullón[b], Enrique Herrero[a,b] and Carlos Manuel Sánchez-Sánchez[c]*

[a]*Departamento de Química-Física, Instituto Universitario de Electroquímica, Universidad de Alicante Ap. 99, E–03080, Alicante, Spain.*

[b]*Instituto de Electroquímica, Universidad de Alicante Apartado 99, E–03080, Alicante, Spain.*

[c]*Sorbonne Universités, UPMC Univ Paris 06, CNRS, Laboratoire Interfaces et Systèmes Electrochimiques, 4 place Jussieu, F-75005 Paris, France*

**e-mail adress: juanvictor.perales@ua.es (Juan Víctor Perales-Rondón).*

Abstract

High catalytic activity for formic acid oxidation reaction (FAOR) is demonstrated in Pb modified shape controlled platinum (Pt) nanoparticles (NPs). Cyclic voltammetry is used to follow the effective modification of Pt NPs by Pb. Octahedral shaped Pt NPs modified by Pb have proved to be the most active electrocatalyst studied towards FAOR and display a catalytic activity of c.a. 7 mA cm^{-2} at 0.5 V in 0.1 M formic acid solution. This current density represents an enhancement factor 29.5 with respect to the bare shaped Pt NPs and

this is 2.7 and 2.3 times higher than that found for Tl_{θ} /100-Pt NPs and Sb_{θ} /111-Pt NPs, respectively, some of the most active electrocatalysts based on adatoms modified Pt NPs reported so far. This outstanding activity is displayed at maximum Pb coverage and also confers a wide electrocatalyst stability over the entire potential range studied. FAOR is also studied using scanning electrochemical microscopy (SECM) by the MD/SC working mode as a preliminary rapid test to identify active electrocatalysts. The activity of a Pt ultramicroelectrode (100 μm diameter) modified by Pb exhibits a remarkable improvement in SECM (13 times the current density of pristine Pt electrode at 0.3 V). Thus, this technique emerges as a suitable and fast method to test, and in some cases quantify, catalyst activity for reactions of interest in fuel cell applications.

8.1. Introduction

Formic acid oxidation reaction (FAOR) represents a very important reaction in electrocatalysis, since it can be used as a model in fundamental studies for other small organic molecules (SOMs) such as methanol or ethanol [1]. Moreover, formic acid has been proposed as a fuel for direct liquid fuel cells (DLFCs), which can be used as small power supply [2, 3] in electronic devices, since FAOR presents fast oxidation kinetics, safety in the manipulation and less fuel crossover through the ion exchange membrane than other fuels such as methanol [4]. In a direct formic acid fuel cell (DFAFC) [5], the thermodynamic cell potential is 1.428 V, which makes it more interesting than hydrogen fuel cells from an available energy point of view. Nevertheless, the overpotential for the FAOR at present needs to be improved in order to reach commercial applications.

Platinum (Pt) is one of the most studied metals in electrocatalysis [1]. In particular, FAOR on Pt electrodes has been widely studied over the last decades due to the high activity of this metal for the oxidation of different SOMs. Since FAOR has probably the simplest oxidation mechanism among all different SOMs, a deep understanding of the FAOR mechanism on Pt should be very useful for other important electrocatalytic oxidation reactions. It is well accepted that FAOR on Pt electrodes follows two different reaction pathways [6-8]. One of then, the so-called indirect via, involves the formation of CO on the electrode surface, which acts as a poison intermediate. The other pathway is known as the direct via, and implies the formation of an active intermediate, which is immediately oxidized into CO_2. On the other hand, it is also well-known that FAOR is a surface sensitive reaction [9, 10]. Studies on Pt single crystal electrodes (Pt(*hkl*)) have allowed a better comprehension

of some of the elementary steps in FAOR, proving that Pt(100) is the most active electrode for both paths, while Pt(111) is the less active one, in spite of the fact that the formation of CO is almost negligible on this electrode [11].

The modification of the surface chemical composition on the Pt(*hkl*) electrodes is one of the most widely employed methods to increase the catalytic activity for the FAOR. This strategy is mainly based on the incorporation of different adatoms, which can be either metals or semi-metals, on the surface of the Pt(*hkl*) electrodes. This epitaxial adsorption and deposition of a sub-monolayer of adatoms on a foreign metal substrate is usually performed either by irreversible adsorption at open circuit potential or by underpotential depostion (UPD). These two interesting methods to modify noble metals may generate surface alloys in some cases [12]. In the case of modified Pt electrodes, the UPD method [13] is based on the electrodeposition of an adatom monolayer from a solution containing the adatom dissolved as a cation at potentials significantly less negative than that for the bulk electrodepositon of the adatom. The main difference between UPD and irreversible adsorption methods is the fact that irreversible adsorbed adatoms remain stable on the Pt surface in the absence of the adatom cation in solution, but on the contrary, UPD adatoms are not stable on the Pt surface. Moreover, irreversible adsorption allows achieving adatom coverages independently of the applied potential, as far as it remains within the adatom electrochemical stability limits. In addition, this approach also avoids the problem of accuracy in the coverage quantification that appears when the UPD method is used, due to its dependency with the applied potential and solution composition. The well accepted positive effect of the presence of some adatoms on the electrocatalytic activity of Pt electrodes towards FAOR is visualized by an

evident shift to lower potential values on the onset oxidation potential and/or by increasing current densities of the oxidation reaction. In this sense, it is proposed that adatoms may act following three main different mechanisms; *i*) the *third body* effect in which the foreign adatom modifies the reaction mechanism by steric interference, since it blocks specific adsorption sites on the Pt surface preventing CO formation [14], *ii*) the *electronic* effect [15, 16], where the modification of the Pt electronic structure due to the presence of foreign adatoms enhances the activity of the surface and *iii*) the *bifunctional* effect [17], in which the adatom and the Pt surface sites have distinct roles in the oxidation mechanism [18].

Over the last decades, adatoms such as bismuth (Bi) [19, 20], arsenic (As) [21], antimony (Sb) [22], palladium (Pd) [23] and lead (Pb) [24-26] adsorbed on Pt(*hkl*) electrodes has been studied, showing an important improvement in the FAOR activity, by following at least one of the proposed mechanisms mentioned above. Nowadays, the next challenge is to transfer all that knowledge from single crystal electrodes to nanoparticles (NPs) with a preferential surface structure. In this sense, the role of some adatoms such as Bi [27], Sb [28] and Tl [29] modifying shape controlled Pt NPs have been already reported. Particularly, Bi adatom has shown a significant enhancement in the activity of the (111) preferential Pt NPs towards FAOR [30], which agrees with previous studies using Bi modified Pt single crystal electrodes [31]. Despite the number of adatoms already studied modifying Pt NPs, there are still some of them untested. This is the case of Pb adatom on shape controlled Pt NPs for FAOR, which is studied herein. However, Pb has been already used in Pt-Pb bimetallic alloys [32-34] to improve conventional spherical Pt NPs activity towards FAOR. The main goal of this contribution is to address that

question in order to explore the feasibility of using Pb modified shape controlled Pt NPs as catalyst for fuel cell applications. The use of conventional Pb or PtPb NPs in real electrochemical filter press reactors either for electroorganic synthesis [35] or DFAFCs [36] have been already demonstrated in the literature.

Finally, the use of novel electroanalytical techniques for studying the reaction mechanism in electrocatalytic reactions provides new tools for electrocatalyst interrogation [37-41]. Among them, the scanning electrochemical microscopy (SECM) [42], which is based on the steady-state diffusion controlled regime provided by either an ultramicroelectrode (UME) or a micropipette, has already demonstrated its utility for studying FAOR [43-45]. However, no SECM imaging studies have been devoted to prove the activity improvement of adatomos modifying Pt electrodes in FAOR. So far, only a voltammetric study of FAOR on Bi modified Pt UME has been reported [46]. In the present work, we provide for the first time SECM images comparing the activity for FAOR on pristine Pt and Pb modified Pt (Pb-Pt) electrodes in order to increase the scope of SECM in studying electrocatalytic reactions.

8.2. Experimental section

8.2.1. Chemicals

1,2-dichloroethane (CH_2Cl-CH_2Cl, DCE) anhydrous 99.8%, octyltriethoxysilane 97.5%, lead (II) perchlorate hydrate $Pb(ClO_4)_2 \cdot H_2O$ (Aldrich® 99.995%), H_2SO_4 (Merck KGaA Suprapur® 96%), HCOOH (Merck KGaG 98 %), polyethylene glycol dodecyl ether (Brij® 30), n-heptane (ACROS Organics,

Analysis), sodium borohydride (Aldrich® 99.99%), sodium polyacrylate (Aldrich®), K_2PtCl_4 (Aldrich® 99.99%), $H_2PtCl_6 \cdot 6H_2O$ (Aldrich® 37.50%), HCl (Aldrich® 37%), NaOH (Merck, Pellets for analysis). All solutions were prepared with ultrapure water (18.2 MΩ cm, Purelab Ultra system, Elga-Vivendi).

8.2.2. Pb modified shape controlled Pt NPs (Pb_θ/Pt NPs)

Three types of shape controlled Pt NPs dispersed in water with surface area to volume ratios of 0.03 cm^2 μL^{-1} for Cubic 100-Pt NPs and 0.017 cm^2 μL^{-1} for octahedral 111-Pt NPs and for quasi-spherical poly-Pt NPs were used. The chemical synthesis of those NPs was carried out as previously described in detail [47]. The Pt NPs morphology/shape was confirmed by transmission electron microscopy (TEM). The average particle size of the cubic and octahedral NPs was around 9-10 nm, whereas the size of the quasi-spherical NPs was around 4-5 nm. Before being modified with Pb, the Pt NPs were electrochemically characterized and a CO adsorption-stripping experiment was performed in order to clean the Pt NPs surface, as has been reported previously [47, 48]. In brief, this procedure consists in blocking the Pt NPs electrode surface by bubbling CO in solution for about 30 s. After this time the electrode is kept at potential 0.1 V for about 15 min, while the solution is bubbled with Ar(g) in order to remove any CO traces in solution. Finally, the CO adsorbed on the Pt NPs electrode surface is stripped and converted into CO_2 by running a CV at slow scan rate (20 mV s^{-1}), which reaches a high enough positive potential (0.8 V vs RHE). Then, each type of Pt NPs was electrochemically characterized in 0.5 M H_2SO_4 solution before and after the irreversible adsorption of

Pb adatoms on its surface. The Pt NPs active surface area was determined by the charge involved in the hydrogen UPD region (between 0.05 V and 0.50 V for 100-Pt NPs; 0.05 V and 0.45 V for poly-Pt NPs, and 0.05 V and 0.65 V for 111-Pt NPs) after the subtraction of the double layer [48]. Then, Pb adatoms were irreversibly adsorbed on each type of Pt NPs outside the electrochemical cell by simple immersion of Pt NPs at open circuit potential within dilute solutions of $10^{-3} \sim 10^{-5}$ M $Pb(ClO_4)_2$ in 0.5 M $HClO_4$ and following a common procedure for the irreversible adsorption of different adatoms on Pt [49]. After this, the electrode was rinsed with ultrapure water (except for the maximum coverage case, where the electrodes were not rinsed before being immersed into the solution) and transferred to an electrochemical cell (different to the one used for Pt NPs electrochemical characterization) to perform the electrocatalytic test for FAOR in deaerated 0.1 M HCOOH and 0.5 M H_2SO_4 solution. By varying the adatom concentration in solution as well as the electrode immersion time, different Pb adatom coverages can be reached on the Pt NPs surface. Finally, the Pb coverage (θ_{Pb}) on the Pt NPs surface was quantified by following the decrease of the charge involved in the hydrogen adsorption or desorption peaks present in the hydrogen UPD region of the corresponding cyclic voltammetry, according to the equation 8.1:

$$\theta_{Pb} = 1 - \theta_{H} = \frac{q_H^0 - q_H^{Pb}}{q_H^0} \qquad Eq.\ 8.1$$

where q_H^0 and q_H^{Pb} are the hydrogen desorption charges for the pristine and Pb modified Pt electrodes respectively, calculated after the subtraction of the double layer contribution [29, 30]. However, as it was already described for Sb [28] and Tl [29] modified Pt NPs, the characterization of θ_{Pb} is not possible at high Pb coverage,

since the decrease in the hydrogen adsorption/desorption peaks shown in the hydrogen UPD region is compensated by the appearance of a new peak associated with a surface Pb oxidation/reduction signal from the Pb adsorbed on the gold substrate electrode, discarding the quantification of high Pb coverages by this procedure. Thus, the maximum Pb coverage obtained on each type of Pt NPs studied here is not quantified and it is identified as θ_{max}. Then, the three types of Pb modified Pt NPs are named: *i*) Pb_{θ} /100-Pt NPs, *ii*) Pb_{θ} /111-Pt NPs and *iii*) Pb_{θ} /poly-Pt NPs.

8.2.3. Electrochemical experiments

8.2.3.1. Voltammetric and chronoamperometric studies

Cyclic voltammetry (CV) and chronoamperometry (CA) were performed using a conventional electrochemical glass cell of 3 electrodes at room temperature and a potentiostat-galvanostat AUTOLAB PGSTAT302N (Metrohm Autolab B. V.) or a potentiostat CHI 760E. The working electrode was prepared by adding 4 μL of each type of Pt NPs (2 μL for 100-Pt NPs) coating a 3 mm diameter gold (Au) disc electrode, which is used as a NPs support and current collector, and allowing the water solvent to be evaporated before entering the electrode in the cell. The sample volume of 4 μL was selected after performing a calibration curve that proved no diffusion limitations for FAOR due to the thickness of that layer of NPs deposited on the gold disc electrode. Each Pt NPs suspension was sonicated for 2 min before being used. A gold wire was used as a counter electrode, and a reversible hydrogen electrode (*RHE*) within a Luggin capillary was employed as a reference electrode.

All potentials used in this paper are referred to *RHE*. CVs for Pt surface area quantification were carried out in a deaerated 0.5 M H_2SO_4 solution. CVs and CAs for studying the electrocatalytic activity for FAOR were carried out in deaerated 0.1 M HCOOH and 0.5 M H_2SO_4 solution. An electrochemical pre-treatment for removing the CO_{ads} accumulated at the electrode surface from previous FAOR experiments was performed before starting each CA. This consists in holding the electrode potential at 0.8 V for 5 s. The potential window where it is possible to work avoiding structure modifications on the shape controlled Pt NPs surface is between 0.05 V and 0.8 V.

8.2.3.2. Scanning Electrochemical Microscopy (SECM)

The working electrode for SECM experiments was a 100 μm diameter pristine Pt UME and the same electrode after in-situ surface modification by irreversible adsorption of Pb (3 min immersed in a diluted $Pb(ClO_4)_2$ solution) (Pb-Pt). SECM images were carried out using the micropipette delivery/substrate collection (MD/SC) mode [44] of SECM using a CHI 910B microscope (CH Instruments) and a three-electrodes configuration cell at room temperature. The micropipettes used to deliver the HCOOH in the vicinity of the studied electrodes presented an opened diameter of ca. 15-20 μm and were loaded with a mixture 50:50 (v/v) DCE:HCOOH. They were fabricated by pulling borosilicate capillaries with O.D.: 1.5 mm, I.D.: 1.0 mm and length 90 mm using a laser-based puller P-2000 from Sutter Instrument Co. The inner walls of the micropipettes were made hydrophobic following a well-established silanization protocol [50, 51] by filling them with octyltriethoxylsilane overnight and finally, drying them exhaustively. For MD/SC

SECM imaging [44, 52], a gold wire, 0.5 mm diameter, was used as counter electrode and a commercial Hg/Hg_2SO_4 (K_2SO_4 sat.) electrode within a Luggin capillary as reference, although all potential values have been referred in the article to *RHE* ($E_{(Hg/Hg2SO4)}$ = +0.64 V vs *RHE*). The electrochemical cell employed was built in Teflon with a 2 mm diameter aperture, where the Pt UME perfectly fitted facing up and was held at a potential value positive enough to produce the electrochemical oxidation of HCOOH at the electrode surface. An electrochemical pre-treatment for removing the CO_{ads} accumulated at the electrode surface was performed before each SECM image. This consists in holding the electrode potential constant at 0.8 V for 5 s. The micropipette was located at a constant tip-substrate distance in Z (d = 50 μm) facing the Pt UME and the MD/SC SECM images were obtained recording the substrate current while the micropipette was scanned on the X-Y plane in an argon saturated 0.5 M H_2SO_4 solution. The tip scan rate was 75 μm s^{-1}, using increments of 15 μm each 0.2 s.

8.3. Results and discussion

8.3.1. FAOR activity enhancement on modified Pb-Pt electrodes by SECM imaging

Figure 8.1 displays several SECM images for FAOR on pristine and Pb-modified with the highest coverage (θ_{max}) Pt electrodes, using the MD/SC mode of the SECM for imaging. In this mode, the species of interest (HCOOH) is delivered within the solution through a micropipette by crossing the liquid-liquid interface between two immiscible phases, DCE and H_2O, within and without the

micropipette, respectively. Moreover, HCOOH delivery rate is controlled by its partition coefficient in both immiscible phases [44]. These SECM images were taken at two different potentials, namely, 0.3 V and 0.5 V. Brown color in the figure corresponds to the background current, and green color means an increase in the oxidation current because of the oxidation of HCOOH on the electrode.

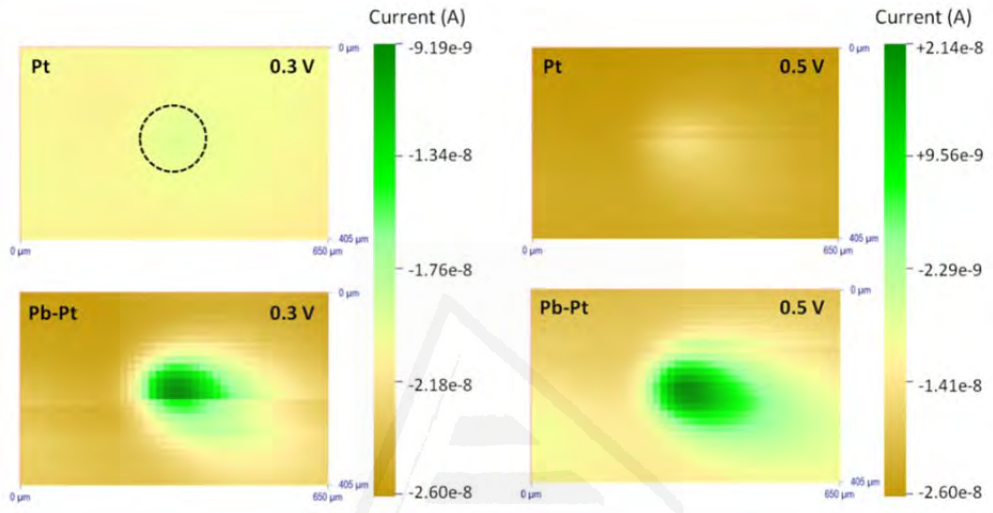

Figure 8.1. SECM MD/SC images displaying the substrate current collected for HCOOH oxidation at different potentials in a 0.5 M H_2SO_4 solution at pristine and Pb-modified (θ_{max}) Pt UME (diameter = 100 µm). The micropipette tip scan rate was 75 µm.s^{-1} and the micropipette-substrate electrode distance was 50 µm. Micropipette filled with 50:50 (v/v) DCE:HCOOH.

Figure 8.1 shows a much higher net oxidation current appearing when the micropipette scans above Pb-Pt than on Pt electrode at both studied potentials. In fact, the current collected at 0.3 V on Pt is so low that a dashed circle has been added into the image to mark the exact Pt electrode location. Thus, these facts clearly point out that the current collection for FAOR (difference between the maximum current at the electrode location and the background current in the SECM image at a given tip-substrate distance [53]) is significantly higher in the case of Pb modified Pt electrode. Table 8.1 summarizes the collected current for Pt and Pb-Pt

electrodes at both potentials exhibiting values from 1.1 to 34.8 nA. Moreover, the catalytic enhancement factor, which in this case is defined as the ratio between the collected current on Pb-Pt electrode versus that collected on Pt electrode at the same potential and tip-substrate distance, is calculated and included in Table 8.1.

Table 8.1. Current collected on the SECM images and catalytic enhancement factor comparing those currents for Pt and Pb-Pt electrodes at 0.3 and 0.5 V.

Applied potential (V)	$I_{collected}$ (nA) Pt	$I_{collected}$ (nA) Pb-Pt	Catalytic enhancement factor
0.3	1.1	14.31	13
0.5	8.7	34.8	4

8.3.2. Characterization and stability of Pb modified shape controlled Pt NPs.

Once the FAOR activity enhancement on modified Pb-Pt electrodes has been demonstrated by preliminary rapid SECM imaging, it is necessary to transfer those results into Pt NPs in order to gain insight into the catalytic mechanism and to envisage the potential feasibility of using Pb modified Pt NPs as electrocatalysts for real DFAFCs. Before preparing the Pb modified Pt NPs, a careful verification of the current contribution provided by the substrate electrode used as a support and current collector should be conducted. In order to carry out such verification, the Pb surface modification (maximum coverage) of an Au disk electrode was performed. The voltammetric profiles of Pb modified Au disk (black plot) and Pb modified 111-Pt NPs supported on Au disk electrode (red plot) are displayed in figure 8.2. The main feature observed in both curves corresponds to a sharp anodic peak around

0.22 V, which is associated with Pb UPD/dissolution at different crystal faces of the Au substrate [54]. This is evident in figure 8.2a when comparing the response of 111-Pt NPs on Au substrate (red plot) and on glassy carbon (GC) substrate (blue plot), where the main difference corresponds to the sharp peak displayed at 0.22 V only present in the Au substrate case. A broad redox signal extended from 0.3 V to 0.8 V only appears when the electrode contains 111-Pt NPs, suggesting Pb redox processes on the Pt surface taking place at more positive potentials than on Au.

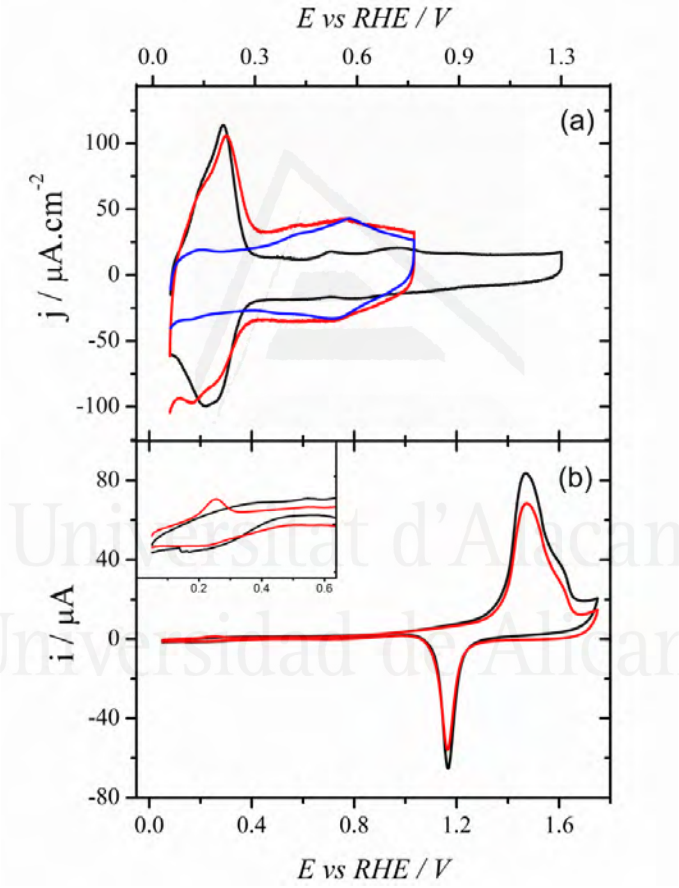

Figure 8.2. (a) Voltammetric profiles in argon saturated 0.5 M H_2SO_4 solution for Pb modified Au substrate electrode (black plot); Pb_θ /111-Pt NPs on Au substrate (red plot) and Pb_θ /111-Pt NPs on GC substrate (blue plot) at maximum coverage (θ_{Pb}) in all three cases. (b) Voltammetric profile in argon saturated 0.1 M HCOOH and 0.5 M H_2SO_4 solution on gold pristine disk electrode (black plot) and on Pb modified gold disk electrode (red plot). Scan rate: 0.05 $V.s^{-1}$.

Furthermore, the presence of 111-Pt NPs in the electrode causes an important increase in the apparent double layer capacitance current, probably associated to the Pb redox process. Finally, figure 8.2b exhibits the response of Pb modified Au and bare Au electrodes for the FAOR, showing no activity increase when the Au electrode is modified by Pb. This fact rules out any relevant contribution in the electrocatalytic behavior displayed by the Pt NPs studied here coming from the Au substrate electrode.

Figure 8.3 shows the electrochemical characterization of all three types of shape controlled Pt NPs modified with different coverage of Pb in sulfuric acid solution. The voltammetric profiles without Pb modification ($\theta_{Pb} = 0$) agree with those reported already in the literature for shaped controlled Pt NPs [55]. Then, for the three types of shape controlled Pt NPs modified with different amount of Pb, the charge associated within the hydrogen adsorption and desorption region on Pt clearly decreases when the amount of Pb is increased. The Pb coverage is estimated using equation 8.1. Nevertheless, the peak appeared around 0.22 V when the amount of Pb is significantly increased (θ_{Pb} = max), which is due to a redox process associated to Pb adsorbed on the Au polycrystalline surface [54, 56] prevent a proper Pb coverage quantification. For this reason, the maximum Pb coverage is not quantified (θ_{max}).

The stability of the Pb adlayer on Pt NPs is shown in Figure 8.4 at both, high (θ_{max}) and low coverage (θ_{Pb}/100-Pt = 0.27 and θ_{Pb}/111-Pt = 0.31). At low Pb coverage (black plots), the Pb deposition is more unstable and the characteristic hydrogen features are clearly identified after FAOR experiment (dash dotted black plot), due to the partial dissolution of Pb [57]. A similar behavior is found when

increasing the number of electrochemical cycles that reach 0.8 V as a positive cycle limit (not shown). On the contrary, at maximum Pb coverage (red plots), the modified electrode profile before and after FAOR remains stable, which may suggest the formation of a chemically stable Pb surface alloy on Pt when high coverages are reached, which avoids its rapid dissolution and confers more durability to the catalyst.

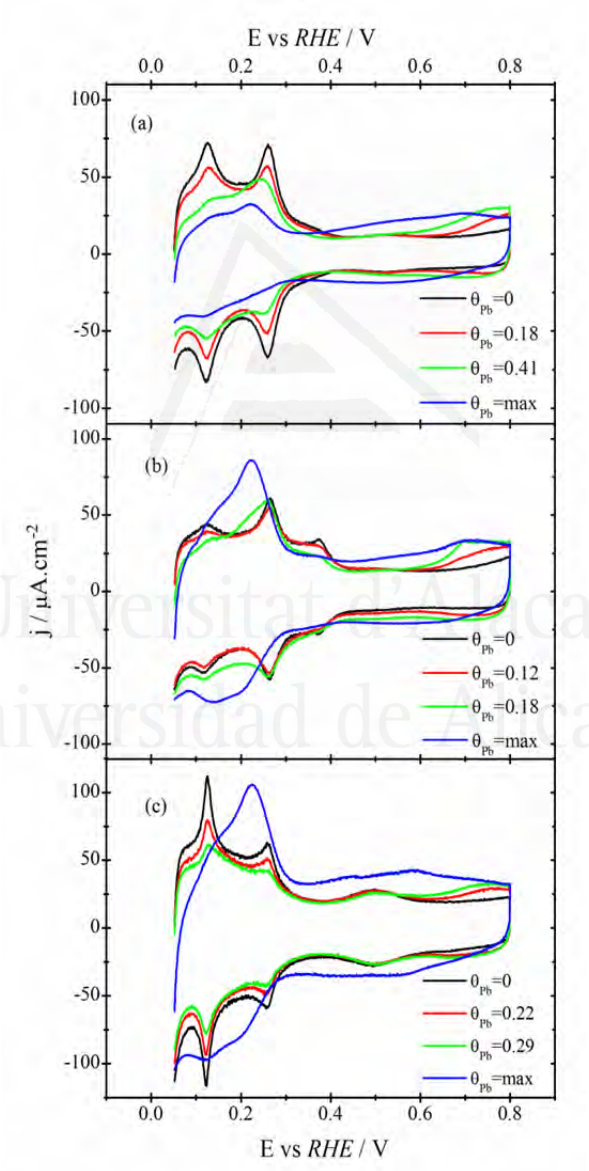

Figure 8.3. Voltammetric profiles: (a) Pb_{θ} /poly-Pt NPs, b) Pb_{θ} /100-Pt NPs and c) Pb_{θ} /111-Pt NPs with different Pb coverage (θ_{Pb}). Scan rate: 0.05 $V.s^{-1}$. Test solution: argon saturated 0.5 M H_2SO_4.

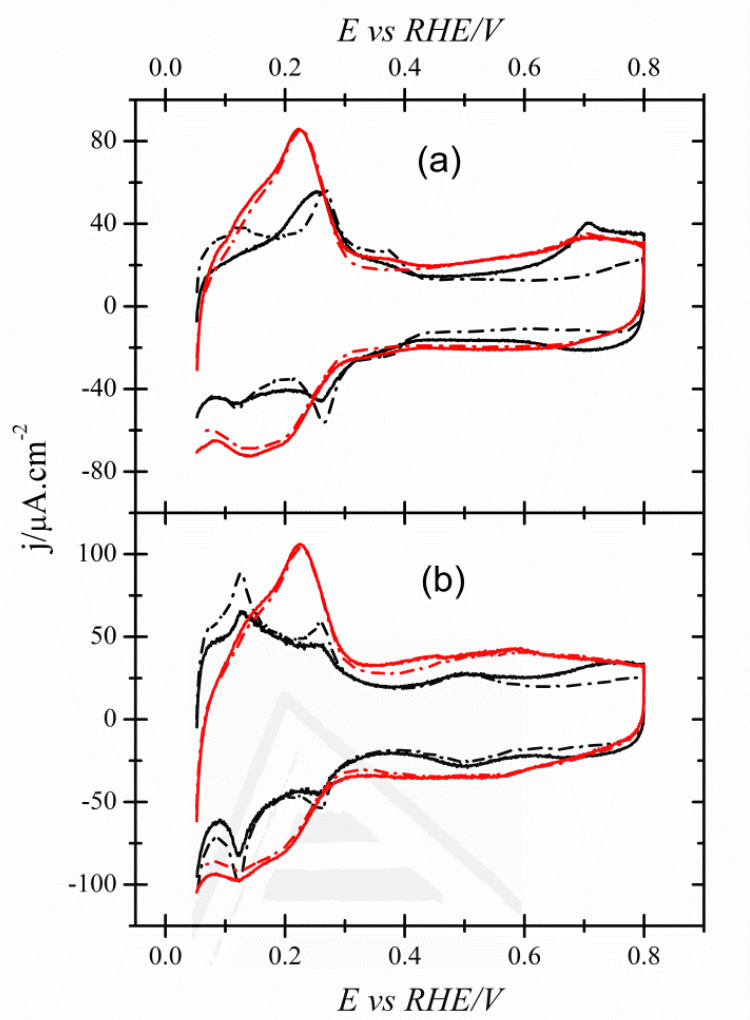

Figure 8.4. Voltammetric profiles: (a) Pb_{θ}/100-Pt NPs and b) Pb_{θ}/111-Pt NPs at low (θ_{Pb}/100-Pt = 0.27 and θ_{Pb}/111-Pt = 0.31) (black plots) and at maximun Pb coverage (θ_{max}) (red plots). Solid plots represent CVs before FAOR experiments, whereas dash dotted plots represent CVs after FAOR experiments. Scan rate: 0.05 $V.s^{-1}$. Test solution: argon saturated 0.5 M H_2SO_4.

8.3.3. FAOR on Pb modified shape controlled Pt NPs.

Figure 8.5 presents the positive scan direction of CVs for all three different type of shape controlled Pt NPs at different Pb coverage, and the negative scan direction only for θ_{Pb} = 0 and θ_{Pb} = max. In particular, Figure 8.5a exhibits pristine and Pb modified poly-Pt NPs. This type of Pt NPs represents the most comparable

case to the bulk Pt electrode used for SECM imaging (Figure 8.1). Moreover, the current density at potentials below 0.30 V is almost negligible in the positive potential scan in all three types of pristine Pt NPs shown in Figure 8.5 (see Table 8.2), which is due to CO_{ads} poisoning effects. However, this behavior is particularly important in the pristine 100-Pt NPs (figure 8.5b, solid black plot), which perfectly agrees with previous Pt(*hkl*) studies, which demonstrated that (100) domains are the most active for the CO formation during FAOR [16]. Above 0.3 V, the current density on pristine Pt NPs increases slowly until ~0.80 V. In contrast, the negative potential scans (dashed black plots in Figure 8.5) show significantly higher current densities producing an important hysteresis in all three cases because the CO is removed from the electrode surface at 0.8 V. Figure 8.5 also shows a significant increase in the oxidation current densities when Pb is present on the surface of all three types of Pt NPs, even at low Pb coverages ($\theta_{Pb} < 0.2$), reaching a maximum at ~0.50 V. Moreover, this activity enhancement is displayed in both positive and negative scan directions, exhibiting a very small hysteresis when Pb is present on the Pt NPs surface. In fact, for Pb_{θ}/poly-Pt NPs there is not hysteresis between both scans, whereas in the cases of Pb_{θ}/100-Pt NPs and Pb_{θ}/111-Pt NPs, this effect is somehow more visible, being always the current in the positive scan larger than in the negative one. This behavior is completely different from that observed in unmodified Pt NPs and indicates suppression of CO formation when Pb is present on the Pt NPs surface. Furthermore, there is a shift of the onset potential for the FAOR with respect to the unmodified Pt NPs towards less positive potentials (~0.15 V) in all three cases. More importantly, a significant current increase is observed for Pb_{θ}/111-Pt NPs and particularly at maximum Pb coverage (6718 μA cm^{-2} at 0.5 V).

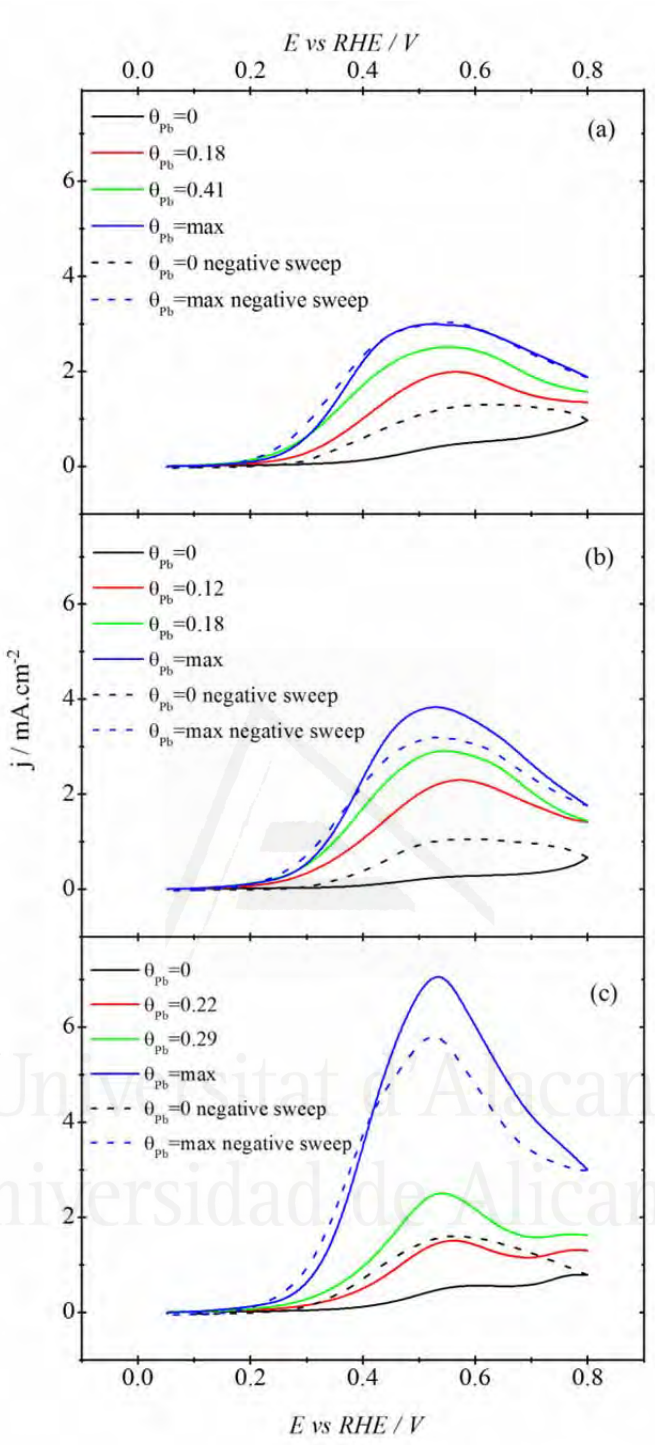

Figure 8.5. Voltammetric profiles for FAOR. Solid line, positive scan direction and dashed line, negative scan direction. (a) Pb_{θ} /poly-Pt NPs, b) Pb_{θ} /100-Pt NPs and c) Pb_{θ} /111-Pt NPs with different Pb coverages (θ_{Pb}). Scan rate: 0.02 $V.s^{-1}$. Test solution: argon saturated 0.1 M HCOOH in 0.5 M H_2SO_4.

Table 8.2 summarizes the density current values reached at 0.3 V and 0.5 V in the positive scan direction for each type of shape controlled Pt NPs at θ_{Pb} maximum. Additionally, in order to achieve a proper comparison with other adatoms already studied in the literature, comparable results for FAOR using Sb [28] modified Pt NPs and Tl [29] modified Pt NPs are also included in Table 8.2.

Table 8.2. Density current at 0.3 and 0.5 V from the positive-sweep voltammetric profile performed at 0.02 V s^{-1} in 0.1 M HCOOH and 0.5 M H_2SO_4 solution for each type of shape controlled Pt NPs modified at maximum coverage by Pb and Tl and at optimum coverage by Sb. Their corresponding catalytic enhancement factors are also included. They are all calculated in comparison with the current densities on pristine Pt NPs reported here.

	j at (0.3 V) / µA cm^{-2}	**Catalytic enhancement factor at 0.3 V**	**j at (0.5 V) / µA cm^{-2}**	**Catalytic enhancement factor at 0.5 V**
poly-Pt NPs	46.6		341	
100-Pt NPs	32.7		210	
111-Pt NPs	41.7		372	
Pb_θ/poly-Pt NPs	628	13.5	2975	8.7
Pb_θ/100-Pt NPs	553	16.9	3770	18
Pb_θ/111-Pt NPs	642	15.4	6718	18
[a]Sb_θ/poly-Pt NPs	520	9	2150	6.3
[a]Sb_θ/100-Pt NPs	260	8	1070	5.1
[a]Sb_θ/111-Pt NPs	820	19.7	2880	7.7
[b]Tl_θ/100-Pt NPs	712	21.8	2447	11.7
[b]Tl_θ/111-Pt NPs	425	10.2	1670	4.5

[a] From reference [28]

[b] From reference [29]

That comparison points out that Sb_θ/111-Pt NPs and Tl_θ/100-Pt NPs exhibit a little bit larger current densities than any of the Pb modified Pt NPs at 0.3 V (1.2 and

1.1 times higher than Pb_{θ} /111-Pt NPs, respectively). Nevertheless, the maximum current reported for FAOR on Pt NPs modified by adatoms at higher potentials (at 0.5 V) is the one exhibited by Pb_{θ} /111-Pt NPs (2.7 times higher than on Tl_{θ} /100-Pt NPs and 2.3 higher than on Sb_{θ} /111-Pt NPs). In addition to this, all three types of Pb modified Pt NPs exhibit higher current densities than Sb or Tl modified Pt NPs at 0.5 V, independently of the preferential Pt surface structure. Furthermore, the modification by Pb provides the highest average current comparing all 3 adatoms and considering the average of all three types of NPs for each case, both at 0.3 and 0.5 V, since the reaction is less sensitive to the surface structure of the NPs, which also supports the possible formation of a chemically stable Pb-Pt surface alloy [58].

Figure 8.6 shows the catalytic enhancement factor for FAOR as a function of applied potential calculated from the corresponding positive-sweep voltammetric profiles displayed in Figure 8.5. This factor of normalization is defined as the ratio between the current densities of Pb modified Pt NPs at maximum Pb coverage and that obtained in the corresponding pristine Pt NPs. It can be seen that, despite Pb_{θ} /111-Pt NPs is the most active electrode comparing absolute values of current density, the normalized activity is very similar with that of Pb_{θ} /100-Pt NPs. However, Pb_{θ} /poly-Pt NPs show a lower increase in the activity. In fact, the maximum normalized activity is reached around 0.37 - 0.40 V, and the catalytic enhancement factor is 29.5 and 28.5 for Pb_{θ} /111-Pt NPs and Pb_{θ} /100-Pt NPs, respectively, and 18 for Pb_{θ} /poly-Pt NPs. This fact could be related with a NPs size effect. Since poly-Pt NPs are significantly smaller than the others, they have a larger fraction of edge atoms on their surface, which affords a smaller catalytic enhancement factor. Thus, a Pb adatom deposited neighboring to an edge will have

a lower amount of neighboring Pt surface atoms and the increase in activity is proportional to the number of Pt-Pb ensembles created by the adatom deposition, that is, to the number of Pt neighboring the Pb adatom [14]. It is clear that the deposition of Pb close to an edge will result in an increase of activity lower than that measured when the adatom is deposited in the middle of a large domain.

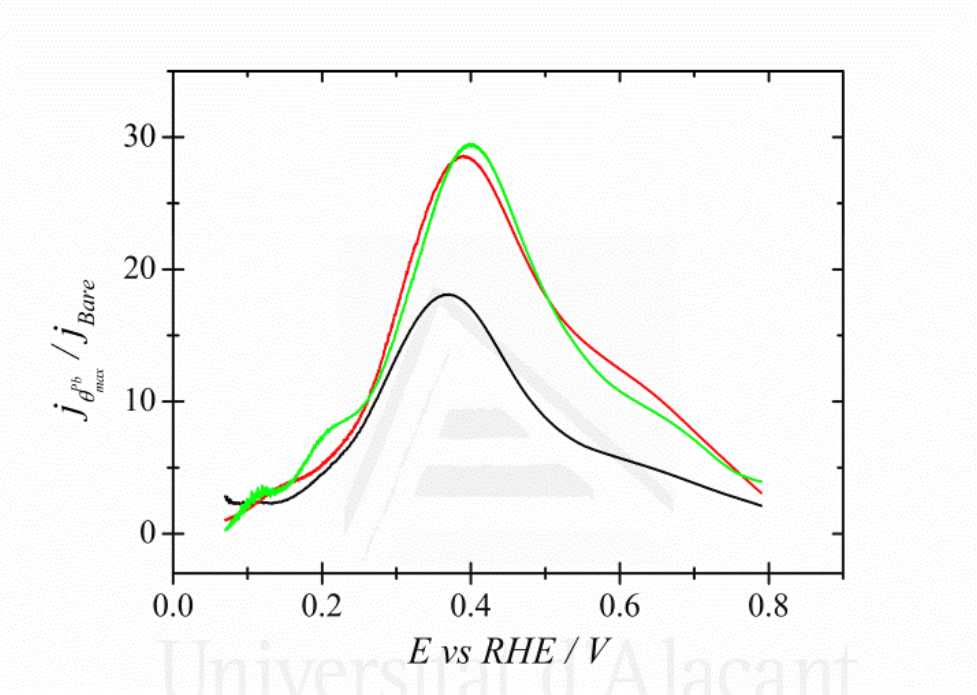

Figure 8.6. Catalytic activity comparison between the three types of pristine and Pb-modified (θ_{max}) shape-controlled Pt NPs by calculating the catalytic enhancement ratio from the corresponding current densities displayed in Figure 8.5. Pb_θ /poly-Pt NPs, black solid plot; Pb_θ /100-Pt NPs, red solid plot and Pb_θ /111-Pt NPs, green solid plot.

However, despite a lower increase, the shape of the curve in figure 8.5 is the same in all three cases, which indicates that the actuation mechanism is similar in all Pb modified Pt NPs. Furthermore, no difference is observed when comparing the catalytic enhancement factor at 0.3 V calculated from the current collected within the SECM images (13, see Table 8.1) and the one calculated from the positive-sweep voltammetric profiles in Figure 8.5a for Pb modified poly-Pt NPs (13.5, see

Table 8.2), since that potential fits into the charge transfer control regime. In contrast, the same comparison at 0.5 V, a potential at which diffusion may play a role in the kinetics, denotes a clear underestimation of the catalytic enhancement factor when it is calculated from SECM images, mainly due to the tip-substrate distance used in figure 8.1, which does not allow a 100% collection efficiency.

Figures 8.7 and 8.8 show the chronoamperometric experiments for 600 s at 0.3 and 0.5 V, respectively, obtained with all three types of Pb modified Pt NPs. Chronoamperometric experiments not only provide information about the catalytic enhancement at any specific potential, but also it can give some light about the stability of the catalytic activity vs. time. For this reason, they may be used to calculate the deactivation rate, which is defined as $(j_{60s} - j_{600s}) / j_{60s}$ and it is reported in Table 8.3. In particular, Figure 8.7 shows that all three types of Pb modified Pt NPs provide similar current density values (aprox. 400 μA cm^{-2}, see Table 8.3) at maximum Pb coverage after 600 s, which implies that there is not a specific surface structure effect in the activity when modifying by Pb at this potential, as was also suggested by the voltammetric behavior. However, when the cronoamperometric experiment is performed at 0.5 V (figure 8.8), the Pb_θ /111-Pt NPs at maximum Pb coverage clearly exhibits the highest current density value after 600 s (4190 μAcm^{-2}, see Table 8.3), showing also a moderate deactivation rate (15%, see Table 8.3) similar to the one already reported for Sb_θ /111-Pt NPs at optimum Sb coverage [28].

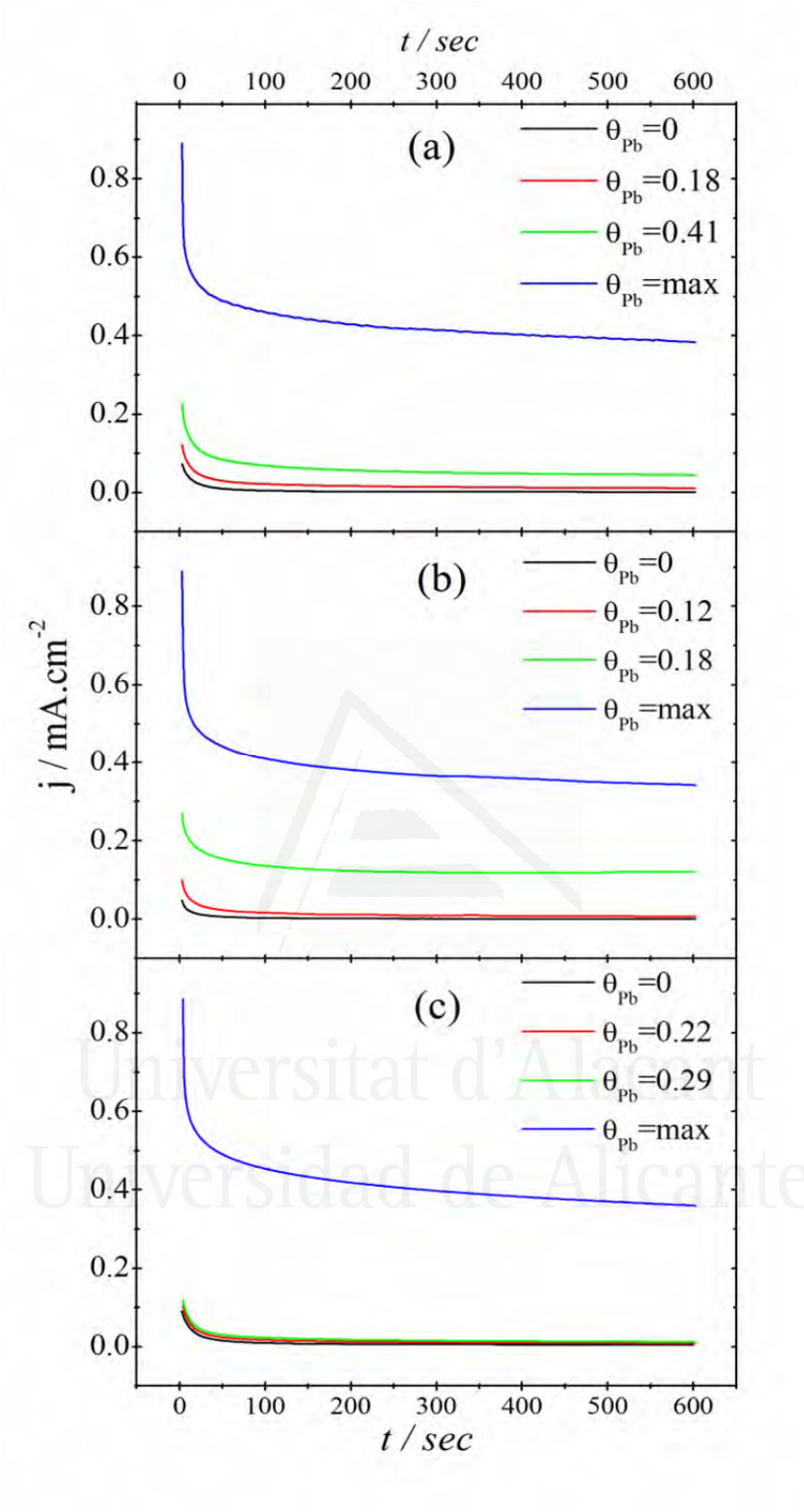

Figure 8.7. Chronoamperometric curves recorded at 0.3 V vs *RHE* for catalytic evaluation of FAOR. (a) Pb_{θ} /poly-Pt NPs, b) Pb_{θ} /100-Pt NPs and c) Pb_{θ} /111-Pt NPs with different Pb coverages (θ_{Pb}). Test solution: argon saturated 0.1 M HCOOH in 0.5 M H_2SO_4.

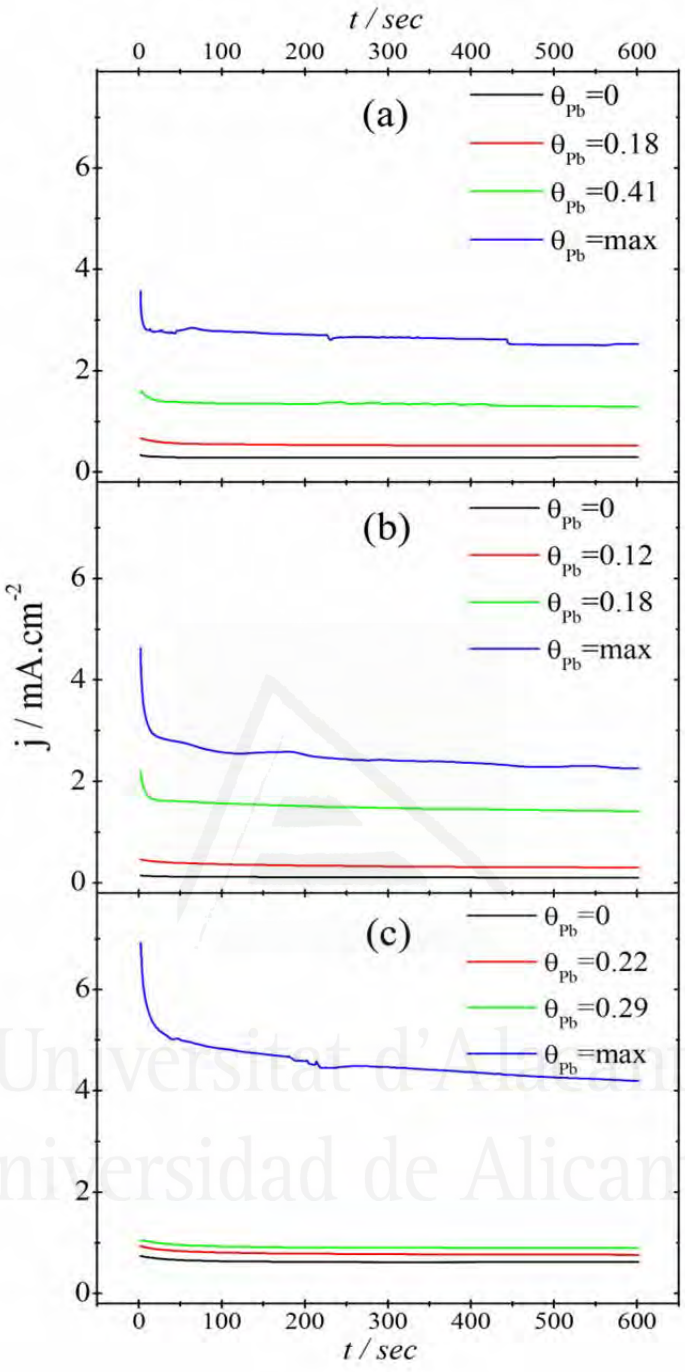

Figure 8.8. Chronoamperometric curves recorded at 0.5 V vs *RHE* for catalytic evaluation of FAOR. (a) Pb_{θ} /poly-Pt NPs, b) Pb_{θ} /100-Pt NPs and c) Pb_{θ} /111-Pt NPs with different Pb coverages (θ_{Pb}). Test solution: argon saturated 0.1 M HCOOH in 0.5 M H_2SO_4.

Table 8.3. Chronoamperometric activities at 600 s and deactivation percentage at 0.3 and 0.5 V for each shape controlled Pt NPs modified by Pb calculated by comparing the current density in the corresponding chronoamperometry at 60 s and 600s.

	j a 600 s (0.3 V) / μA cm^{-2}	j a 600 s (0.5 V) / μA cm^{-2}	Deactivation at 0.3 V (%)	Deactivation at 0.5 V (%)
Pb_θ/poly-Pt NPs	380	2530	20	10
Pb_θ/100-Pt NPs	340	2250	20	17
Pb_θ/111-Pt NPs	350	4190	27	15

8.3.4. FAOR mechanism discussion for Pb modified shaped controlled Pt NPs

As it is well known, HCOOH can yield adsorbed CO by a dehydration reaction [59]. This process has specific surface site requirements [14, 60], which makes the reaction susceptible of control by adding adatoms, which can act as an "impurity", blocking some surface Pt ensemble sites and hindering in this way the CO formation. From the voltammetric profiles shown in Figure 8.5 it is clear that the CO adsorption is hindered by the presence of Pb on the Pt NPs surface, at low and high coverage, because of a third body effect [20, 61]. This is more evident by the loss of the hysteresis between the positive and negative potential sweep at each case compared with the unmodified Pt NPs.

As in the case of other electropositive adatoms such as Bi, Sb or Te, their presence on Pt promotes the adsorption of the formate on the adatom in a configuration which facilitates the cleavage of the C-H bond with almost no activation energy on a neighboring Pt site, justifying the bifunctional mechanims. This is well documented and demonstrated in recent contributions [20, 61]. This

behavior is certain assuming only the formation of a submonolayer of adatom on the electrode surface. In parallel, the presence of Pb hinders the dehydration reaction of HCOOH [62]. Thus, the net result of both processes is that the formation of CO is completely inhibited and much higher currents are reached.

8.4. Conclusions

Pb modified shape controlled Pt NPs represents a highly efficient method for improving the catalytic activity for FAOR of Pt NPs by reaching catalytic enhancement factors as high as 29.5. In particular, Pb_{θ} /111-Pt NPs at θ_{max} reaches 2.7 times higher current density than Tl_{θ} /100-Pt NPs [29] and 2.3 higher than Sb_{θ} /111-Pt NPs [28] at 0.5 V in 0.1 M HCOOH and 0.5 M H_2SO_4 solution, so far, two of the most active catalysts reported for FAOR under low reactant concentration conditions (0.1 M). It should be also highlighted that all three types of Pb modified Pt NPs studied at maximum Pb coverage exhibit higher current density at 0.5 V than Tl_{θ} /100-Pt NPs and Sb_{θ} /111-Pt NPs, which could suggest the formation of a Pb surface alloy on the Pt surface at high Pb coverage and an important bifunctional effect leading the FAOR mechanism towards the direct reaction pathway and suppressing the CO formation by a third body effect. Moreover, at maximum Pb coverage, the modified electrode voltammetric profile remains stable after FAOR in a wide potential range, which confers a remarkable durability to the Pb modified Pt electrodes and opens up its application in diffusion gas electrodes for fuel cells. Finally, it should be pointed out that the SECM imaging by the MD/SC mode emerges as a suitable and fast method to perform preliminary catalytic tests, and in

some cases quantify, the catalyst activity for reactions of interest in fuel cell applications, such as FAOR, providing a fast method to test in advance the effect of a specific adatom adsorbed on metallic electrodes.

Acknowledgements

This work has been financially supported by the MICINN (Spain) (projects CTQ2013-44083-P and CTQ2013-48280-C3-3-R), Generalitat Valenciana (project PROMETEOII/2014/013, FEDER) and CNRS (project Défi Instrumentation aux limites 2015).

8.5. References

[1] M. T. M. Koper, "Fuel Cell Catalysis: A Surface Science Approach", *Electrocatalysis and Electrochemistry* A. Wieckowski (Ed.), John Wiley & Sons, Hoboken, New Jersey, **2009**.

[2] C. Rice, R. I. Ha, R. I. Masel, P. Waszczuk, A. Wieckowski and T. Barnard, "Direct formic acid fuel cells" *Journal of Power Sources* **2002**, 111, 83-89.

[3] N. V. Rees and R. G. Compton, "Sustainable energy: A review of formic acid electrochemical fuel cells" *Journal of Solid State Electrochemistry* **2011**, 15, 2095-2100.

[4] S. Uhm, H. J. Lee and J. Lee, "Understanding underlying processes in formic acid fuel cells" *Physical Chemistry Chemical Physics* **2009**, 11, 9326-9336.

[5] X. Yu and P. G. Pickup, "Recent advances in direct formic acid fuel cells (DFAFC)" *Journal of Power Sources* **2008**, 182, 124-132.

[6] A. Capon and R. Parsons, "The oxidation of formic acid at noble metal electrodes: I. Review of previous work " *Journal of Electroanalytical Chemistry* **1973**, 44, 1-7.

[7] A. Capon and R. Parsons, "The oxidation of formic acid on noble metal electrodes: II. A comparison of the behaviour of pure electrodes " *Journal of Electroanalytical Chemistry* **1973**, 44, 239-254.

[8] A. Capon and R. Parsons, "The oxidation of formic acid at noble metal electrodes Part III. Intermediates and mechanism on platinum electrodes " *Journal of Electroanalytical Chemistry* **1973**, 45, 205-231.

[9] V. Grozovski, V. Climent, E. Herrero and J. M. Feliu, "Intrinsic Activity and Poisoning Rate for HCOOH Oxidation on Platinum Stepped Surfaces" *Physical Chemistry Chemical Physics* **2010**, 12, 8822-8831.

[10] S. G. Sun and Y. Y. Yang, "Studies of kinetics of HCOOH oxidation on Pt(100), Pt(110), Pt(111), Pt(510) and Pt(911) single crystal electrodes" *Journal of Electroanalytical Chemistry* **1999**, 467, 121-131.

[11] V. Climent and J. M. Feliu, "Thirty years of platinum single crystal electrochemistry" *Journal of Solid State Electrochemistry* **2011**, 15, 1297-1315.

[12] F. J. Vidal-Iglesias, A. Al-Akl, D. Watson and G. A. Attard, "Electrochemical characterization of PtPd alloy single crystal surfaces prepared using Pt basal planes as templates" *Journal of Electroanalytical Chemistry* **2007**, 611, 117-125.

[13] E. Herrero, L. J. Buller and H. D. Abruna, "Underpotential deposition at single crystal surfaces of Au, Pt, Ag and other materials" *Chemical Reviews (Washington, DC, United States)* **2001**, 101, 1897-1930.

[14] E. Leiva, T. Iwasita, E. Herrero and J. M. Feliu, "Effect of adatoms in the electrocatalysis of HCOOH oxidation. A theoretical model" *Langmuir* **1997**, 13, 6287-6293.

[15] M. Shibata, N. Furuya, M. Watanabe and S. Motoo, "Electrocatalysis by ad-atoms. Part XXIV. Effect of arrangement of Bi ad-atoms on formic acid oxidation" *Journal of Electroanalytical Chemistry* **1989**, 263, 97-108.

[16] E. Herrero, A. Fernández-Vega, J. M. Feliu and A. Aldaz, "Poison formation reaction from formic acid and methanol on Pt(111) electrodes modified by irreversibly adsorbed Bi and As " *Journal of Electroanalytical Chemistry* **1993**, 350, 73-88.

[17] M. Watanabe and S. Motoo, "Electrocatalysis by ad-atoms: Part III. Enhancement of the oxidation of carbon monoxide on platinum by ruthenium ad-atoms" *Journal of Electroanalytical Chemistry* **1975**, 60, 275-283.

[18] N. M. Markovic, H. A. Gasteiger, P. N. Ross, X. D. Jiang, I. Villegas and M. J. Weaver, "Electrooxidation Mechanisms of Methanol and Formic-Acid on Pt-Ru Alloy Surfaces" *Electrochimica Acta* **1995**, 40, 91-98.

[19] S. P. E. Smith, K. F. Ben-Dor and H. D. Abruna, "Structural effects on the oxidation of HCOOH by bismuth-modified Pt(111) electrodes with (100) monatomic steps" *Langmuir* **1999**, 15, 7325-7332.

[20] J. V. Perales-Rondon, A. Ferre-Vilaplana, J. M. Feliu and E. Herrero, "Oxidation Mechanism of Formic Acid on the Bismuth Adatom-Modified Pt(111) Surface" *Journal of the American Chemical Society* **2014**, 136, 13110-13113.

[21] A. Boronat-Gonzalez, E. Herrero and J. M. Feliu, "Fundamental aspects of HCOOH oxidation at platinum single crystal surfaces with basal orientations and modified by irreversibly adsorbed adatoms" *Journal of Solid State Electrochemistry* **2014**, 18, 1181-1193.

[22] Y.-Y. Yang, S.-G. Sun, Y.-J. Gu, Z.-Y. Zhou and C.-H. Zhen, "Surface modification and electrocatalytic properties of Pt(100), Pt(110), Pt(320) and Pt(331) electrodes with Sb towards HCOOH oxidation" *Electrochimica Acta* **2001**, 46, 4339-4348.

[23] F. J. Vidal-Iglesias, J. Solla-Gullón, E. Herrero, A. Aldaz and J. M. Feliu, "Formic acid oxidation on Pd-modified Pt(100) and Pt(111) electrodes: A DEMS study" *Journal of Applied Electrochemistry* **2006**, 36, 1207-1214.

[24] J. M. Feliu, A. Fernández-Vega, J. M. Orts and A. Aldaz, "The behavior of lead and bismuth adatoms on well-defined platinum surfaces" *Journal de Chimie Physique et de Physico-Chimie Biologique* **1991**, 88, 1493-1518.

[25] X. H. Xia and T. Iwasita, "Influence of underpotential deposited lead upon the oxidation of HCOOH in HClO4 at platinum electrodes" *Journal of the Electrochemical Society* **1993**, 140, 2559-2565.

[26] H. W. Lei, H. Hattori and H. Kita, "Electrocatalysis by Pb adatoms of HCOOH oxidation at Pt(111) in acidic solution" *Electrochimica Acta* **1996**, 41, 1619-1628.

[27] A. López-Cudero, F. J. Vidal-Iglesias, J. Solla-Gullón, E. Herrero, A. Aldaz and J. M. Feliu, "Formic acid electrooxidation on Bi-modified polyoriented and preferential (111) Pt nanoparticles" *Physical Chemistry Chemical Physics* **2009**, 11, 416-424.

[28] F. J. Vidal-Iglesias, A. Lopez-Cudero, J. Solla-Gullon and J. M. Feliu, "Towards More Active and Stable Electrocatalysts for Formic Acid Electrooxidation: Antimony-Decorated Octahedral Platinum Nanoparticles" *Angewandte Chemie-International Edition* **2013**, 52, 964-967.

[29] C. Buso-Rogero, J. V. Perales-Rondon, M. J. S. Farias, F. J. Vidal-Iglesias, J. Solla-Gullon, E. Herrero and J. M. Feliu, "Formic acid electrooxidation on thallium-decorated shape-controlled platinum nanoparticles: an improvement in electrocatalytic activity" *Physical Chemistry Chemical Physics* **2014**, 16, 13616-13624.

[30] Q. S. Chen, Z. Y. Zhou, F. J. Vidal-Iglesias, J. Solla-Gullon, J. M. Feliu and S. G. Sun, "Significantly Enhancing Catalytic Activity of Tetrahexahedral Pt Nanocrystals by Bi Adatom Decoration" *Journal of the American Chemical Society* **2011**, 133, 12930-12933.

[31] M. D. Maciá, E. Herrero and J. M. Feliu, "Formic acid oxidation on Bi-Pt(111) electrode in perchloric acid media. A kinetic study" *Journal of Electroanalytical Chemistry* **2003**, 554, 25-34.

[32] M. Gong, F. Li, Z. Yao, S. Zhang, J. Dong, Y. Chen and Y. Tang, "Highly active and durable platinum-lead bimetallic alloy nanoflowers for formic acid electrooxidation" *Nanoscale* **2015**, 7, 4894-4899.

[33] E. Casado-Rivera, D. J. Volpe, L. Alden, C. Lind, C. Downie, T. Vázquez-Alvarez, A. C. D. Angelo, F. J. DiSalvo and H. D. Abruña, "Electrocatalytic Activity of Ordered Intermetallic Phases for Fuel Cell Applications" *Journal of the American Chemical Society* **2004**, 126, 4043-4049.

[34] F. Matsumoto, C. Roychowdhury, F. J. DiSalvo and H. D. Abruna, "Electrocatalytic activity of ordered intermetallic PtPb nanoparticles prepared by borohydride reduction toward formic acid oxidation" *Journal of the Electrochemical Society* **2008**, 155, B148-B154.

[35] A. Saéz, C. M. Sánchez-Sánchez, J. Solla-Gullón, E. Expósito and V. Montiel, "Electrosynthesis of L-cysteine on a dispersed Pb/carbon black electrode" *Journal of the Electrochemical Society* **2009**, 156, E154-E160.

[36] S. Uhm, S. T. Chung and J. Lee, "Activity of Pt anode catalyst modified by underpotential deposited Pb in a direct formic acid fuel cell" *Electrochemistry Communications* **2007**, 9, 2027-2031.

[37] C. M. Sánchez-Sánchez and A. J. Bard, "Hydrogen Peroxide Production in the Oxygen Reduction Reaction at Different Electrocatalysts as Quantified by Scanning Electrochemical Microscopy" *Analytical Chemistry* **2009**, 81, 8094-8100.

[38] M. Villanueva-Rodríguez, C. M. Sánchez-Sánchez, V. Montiel, E. Brillas, J. M. Peralta-Hernández and A. Hernández-Ramírez, "Characterization of ferrate ion electrogeneration in acidic media by voltammetry and scanning electrochemical microscopy. Assessment of its reactivity on 2,4-dichlorophenoxyacetic acid degradation" *Electrochimica Acta* **2012**, 64, 196-204.

[39] C. M. Sanchez-Sanchez, J. Souza-Garcia, A. Saez, V. Montiel, E. Herrero, A. Aldaz and J. M. Feliu, "Imaging decorated platinum single crystal electrodes by scanning electrochemical microscopy" *Electrochimica Acta* **2011**, 56, 10708-10712.

[40] C. M. Sanchez-Sanchez, J. Solla-Gullon, F. J. Vidal-Iglesias, A. Aldaz, V. Montiel and E. Herrero, "Imaging Structure Sensitive Catalysis on Different Shape-

Controlled Platinum Nanoparticles" *Journal of the American Chemical Society* **2010**, 132, 5622-5624.

[41] C. M. Sanchez-Sanchez, "Studying Electrocatalytic Activity Using Scanning Electrochemical Microscopy" *The Electrochemical Society Interface* **2014**, 23, 43-45.

[42] A. J. Bard and M. V. Mirkin, "Scanning Electrochemical Microscopy", in, N. Y. CRC Press, US (Ed.), **2012**.

[43] C. Jung, C. M. Sánchez-Sánchez, C.-L. Lin, J. Rodríguez-López and A. J. Bard, "Electrocatalytic Activity of Pd−Co Bimetallic Mixtures for Formic Acid Oxidation Studied by Scanning Electrochemical Microscopy" *Analytical Chemistry* **2009**, 81, 7003-7008.

[44] C.-L. Lin, J. Rodríguez-López and A. J. Bard, "Micropipet Delivery−Substrate Collection Mode of Scanning Electrochemical Microscopy for the Imaging of Electrochemical Reactions and the Screening of Methanol Oxidation Electrocatalysts" *Analytical Chemistry* **2009**, 81, 8868-8877.

[45] J. Rodríguez-López and A. J. Bard, "Scanning Electrochemical Microscopy: Surface Interrogation of Adsorbed Hydrogen and the Open Circuit Catalytic Decomposition of Formic Acid at Platinum" *Journal of the American Chemical Society* **2010**, 132, 5121-5129.

[46] S. Daniele and S. Bergamin, "Preparation and voltammetric characterisation of bismuth-modified mesoporous platinum microelectrodes. Application to the electrooxidation of formic acid" *Electrochemistry Communications* **2007**, 9, 1388-1393.

[47] J. Solla-Gullón, F. J. Vidal-Iglesias, A. López-Cudero, E. Garnier, J. M. Feliu and A. Aldaz, "Shape-dependent electrocatalysis: methanol and formic acid electrooxidation on preferentially oriented Pt nanoparticles" *Physical Chemistry Chemical Physics* **2008**, 10, 3689-3698.

[48] J. Solla-Gullón, P. Rodríguez, E. Herrero, A. Aldaz and J. M. Feliu, "Surface characterization of platinum electrodes" *Physical Chemistry Chemical Physics* **2008**, 10, 1359-1373.

[49] C. M. Sánchez-Sánchez, J. Souza-Garcia, E. Herrero and A. Aldaz, "Electrocatalytic reduction of carbon dioxide on platinum single crystal electrodes modified with adsorbed adatoms" *Journal of Electroanalytical Chemistry* **2012**, 668, 51-59.

[50] Y. Shao and M. V. Mirkin, "Probing Ion Transfer at the Liquid/Liquid Interface by Scanning Electrochemical Microscopy (SECM)" *The Journal of Physical Chemistry B* **1998**, 102, 9915-9921.

[51] D. A. Walsh, J. L. Fernández, J. Mauzeroll and A. J. Bard, "Scanning Electrochemical Microscopy. 55. Fabrication and Characterization of Micropipet Probes" *Analytical Chemistry* **2005**, 77, 5182-5188.

[52] O. Lugaresi, J. V. Perales-Rondon, A. Minguzzi, J. Solla-Gullon, S. Rondinini, J. M. Feliu and C. M. Sanchez-Sanchez, "Rapid screening of silver nanoparticles for the catalytic degradation of chlorinated pollutants in water" *Applied Catalysis B* **2015**, 163, 554-563.

[53] F. Zhou, P. R. Unwin and A. J. Bard, "Scanning electrochemical microscopy. 16. Study of second-order homogeneous chemical reactions via the feedback and generation/collection modes" *The Journal of Physical Chemistry* **1992**, 96, 4917-4924.

[54] R. Adzic, E. Yeager and B. D. Cahan, "Optical and Electrochemical Studies of Underpotential Deposition of Lead on Gold Evaporated and Single-Crystal Electrodes" *Journal of the Electrochemical Society* **1974**, 121, 474-484.

[55] Z. Y. Zhou, N. Tian, Z. Z. Huang, D. J. Chen and S. G. Sun, "Nanoparticle catalysts with high energy surfaces and enhanced activity synthesized by electrochemical method" *Faraday Discussions* **2008**, 140, 81-92.

[56] M. J. Henderson, E. Bitziou, A. R. Hillman and E. Vieil, "Lead Underpotential Deposition on Polycrystalline Gold Electrode in Perchloric Acid Solution: A Combined Electrochemical Quartz Crystal Microbalance and Probe Beam Deflection Study" *Journal of the Electrochemical Society* **2001**, 148, E105-E111.

[57] J. Clavilier, J. M. Orts, J. M. Feliu and A. Aldaz, "Study of the conditions for irreversible adsorption of lead at Pt(h,k,l) electrodes " *Journal of Electroanalytical Chemistry* **1990**, 293, 197-208.

[58] M. P. Mercer, D. Plana, D. J. Fermín, D. Morgan and N. Vasiljevic, "Growth of Epitaxial Pt1–xPbx Alloys by Surface Limited Redox Replacement and Study of Their Adsorption Properties" *Langmuir* **2015**, 31, 10904-10912.

[59] M. J. Llorca, E. Herrero, J. M. Feliu and A. Aldaz, "Formic acid oxidation on Pt(111) electrodes modified by irreversibly adsorbed selenium" *Journal of Electroanalytical Chemistry* **1994**, 373, 217-225.

[60] E. Herrero, J. M. Feliu and A. Aldaz, "Poison formation reaction from formic acid on Pt(100) electrodes modified by irreversibly adsorbed bismuth and antimony " *Journal of Electroanalytical Chemistry* **1994**, 368, 101-108.

[61] A. Ferre-Vilaplana, J. V. Perales-Rondon, J. M. Feliu and E. Herrero, "Understanding the Effect of the Adatoms in the Formic Acid Oxidation Mechanism on Pt(111) Electrodes" *ACS Catalysis* **2015**, 5, 645-654.

[62] H. Wang, L. Alden, F. J. DiSalvo and H. D. Abruna, "Electrocatalytic mechanism and kinetics of SOMs oxidation on ordered PtPb and PtBi intermetallic compounds: DEMS and FTIRS study" *Physical Chemistry Chemical Physics* **2008**, 10, 3739-3751.

Chapter IX

Conclusions

Conclusiones

El objetivo general de la tesis estuvo centrado en estudiar la oxidación de ácido fórmico en electrodos de Pt y Pt modificado con un adátomo (M-Pt), tanto desde un punto de vista fundamental, usando electrodos poliorientados y monocristalinos, como a un nivel más aplicado, sintetizando y usando nanopartículas con forma controlada. A continuación se enumeran los hallazgos principales de esta tesis doctoral:

De los capítulos 3 y 4 se desprende que la E_a^{app} de la oxidación de ácido fórmico es sensible a la estructura superficial del electrodo y depende de otros parámetros como la presencia de aniones adsorbidos o el pH de la disolución. Esto plantea una mayor complejidad de la reacción dado que en su mecanismo está implicada la participación del anión, así como la del formiato en disolución, lo que lleva la inclusión del término θ_A (recubrimiento del anión) en la ecuación cinética de la reacción, que queda expresada de la siguiente manera:

$$j = Fk^o \exp\left(\frac{\alpha F\left(E - E^o\right)}{RT}\right)\theta_{\mathrm{A}}\left(1-\theta_{\mathrm{A}}-\theta_{\mathrm{OH}}\right)\left[\mathrm{HCOO^-}\right] \qquad \textit{Eq. 9.1}$$

Según los resultados obtenidos en esta tesis, esta última especie (formiato en disolución) debe ser precursora del intermediario activo, que se propone como el formiato adsorbido con el enlace C-H orientado en dirección hacia la superficie electródica (*w*-$HCOO_{C\text{-}H\ down}$). Se demuestra además el papel del formiato adsorbido en configuración puente (*b*-$HCOO_{ads}$), el cual actúa como promotor de la adsorción de *w*-$HCOO_{C\text{-}H\ down}$.

Finalmente, en estos 2 capítulos se pone de manifiesto que a pesar de la diferencia de reactividad de las superficies Pt(111) y Pt(100), el mecanismo parece ser el mismo en ambos casos.

En el capítulo 5 se demuestra la dependencia de la corriente de oxidación de ácido fórmico en Pt poliorientado en función del pH de la disolución. A medida que se aumenta el pH, la corriente máxima de oxidación va aumentando hasta llegar a un plató, donde alcanza un valor constante de densidad de corriente. Este comportamiento es altamente dependiente de la presencia de aniones que puedan presentar adsorción específica en la disolución. En esta tesis se ha logrado establecer un mecanismo que da explicación al comportamiento de la densidad corriente en todo el rango de pHs. El mecanismo se describe como sigue:

$$Pt\text{-}A + Pt\text{-}HCOO^-_{C\text{-}H\ down} \rightarrow Pt\text{-}A + CO_2 + Pt + H^+ + 2e^- \quad 0 < pH < 5 \qquad \textit{Eq. 9.2}$$

$$Pt\text{-}HCOO^-_{C\text{-}H\ down} \rightarrow CO_2 + Pt + H^+ + 2\,e^- \quad 5 < pH < 10 \qquad \textit{Eq. 9.3}$$

donde A corresponde al anión del electrolito.

El mecanismo anterior establece que por debajo de pH 5, el *w*-$HCOO_{C\text{-}H\ down}$ se adsorberá en la superficie electródica favorecido por la presencia de un anión adsorbido (A = sulfato, formiato en configuración puente, etc). Por otro lado, entre pH 5 y 10, donde la adsorción de aniones no está favorecida, la adsorción de *w*-$HCOO_{C\text{-}H\ down}$ está promovida por la carga negativa neta de la superficie en estas condiciones.

La segunda parte de esta tesis estuvo dedicada a la modificación superficial de electrodos de Pt con adátomos para mejorar su actividad catalítica para la reacción de oxidación de ácido fórmico. Aunque también hay una parte dedicada al estudio mecanístico de la reacción sobre este tipo de electrodos. Concretamente, y gracias a la

corroboración de los datos experimentales por medio de simulaciones DFT, fue posible proponer un mecanismo de reacción para un electrodo de Pt(111) modificado con Bi, el cual propone que el formiato (o ácido fórmico) es adsorbido sobre un átomo de Bi, quedando en una configuración *w*-$HCOO_{C\text{-}H\ down}$. En estas condiciones la ruptura del enlace C-H sobre Pt esta favorecida, con una energía de activación muy baja, lo que conlleva la formación espontánea de CO_2.

Por otro lado, y desde el punto de vista de mejora de la actividad catalítica, se estudiaron los electrodos Pt(100) y Pt(111) modificados con Tl y 3 tipos de nanopartículas de Pt modificadas con Pb. Al modificar un electrodo de Pt(100) con Tl , la mejora en actividad es evidente, especialmente por la disminución del potencial de inicio de la oxidación, así como de la densidad de corriente máxima. Comparado con el Tl-Pt(111), el Tl-Pt(100) presenta el mayor factor de mejora de actividad. Esto se debe principalmente a la acción de dos efectos por parte del adátomo: El de tercer cuerpo, y un efecto bifuncional. Asimismo, se demostró como la presencia de Pb adsorbido en nanopartículas de Pt con forma, provoca un importante aumento de la actividad en la oxidación de ácido fórmico. La utilización del SECM combinado con las cronoamperometrías permitió hacer una comparación detallada de la actividad y la estabilidad de las diferentes nanopartículas de Pt modificadas con Pb. Las nanopartículas Pb_θ /111-Pt resultaron ser las más activas para la oxidación de ácido fórmico, alcanzando actividades máximas de 7 $mA.cm^{-2}$ a 0.5 V vs RHE en una disolución de ácido fórmico 0.1 M. En estas mismas condiciones experimentales, las Pb_θ /111-Pt NPs resultaron ser 2.7 y 2.3 veces más activas que las Tl_θ /100-Pt NPs y Sb_θ /111-Pt NPs, respectivamente, lo que las posiciona como uno de los sistemas basado en nanomateriales más activos para la oxidación de ácido fórmico descrito

hasta la fecha. Además, los recubrimientos de Pb máximos en estas nanopartículas presentan una alta estabilidad frente al tiempo de uso del catalizador.

Finalmente, es importante señalar que, los hallazgos descritos en esta tesis doctoral arrojan luz para una mejor comprensión del mecanismo de oxidación del ácido fórmico y, por ende, para el diseño de electrocatalizadores más activos y duraderos.

Conclusions

The main goal of this thesis was focused on study the formic acid oxidation reaction at Pt and Pt modified (M-Pt) electrodes, both at a fundamental level (using Pt polycrystalline and single crystals) and at an applied level, using shape controlled Pt nanoparticles. Thus, the final remarks found in the doctoral thesis may be summarized as follows:

Chapters 3 and 4 showed that the E_a^{app} of formic acid oxidation is sensitive to the surface structure of the electrode. It also depends on the anion adsorption and the solution pH. These facts points out a more complex scene due to the incorporation of the electrolyte anion and/or the formate in solution into the kinetic model. The new kinetic expression includes the term θ_A (electrolyte anion coverage) and is written as follows:

$$j = Fk^o \exp\left(\frac{\alpha F\left(E - E^o\right)}{RT}\right)\theta_{\mathrm{A}}\left(1-\theta_{\mathrm{A}}-\theta_{\mathrm{OH}}\right)\left[\mathrm{HCOO^-}\right] \qquad \textit{Eq. 9.1}$$

From the results obtained in this thesis, the formate in solution may be appointed as the precursor of the active intermediate, which is proposed as formate adsorbed with the C-H bond towards the electrode surface (*w*-$HCOO_{C\text{-}H\ down}$). Furthermore, it is revealed the relevant role of formate under bridge bonded configuration (*b*-$HCOO_{ads}$), which acts as an adsorption promotor of *w*-$HCOO_{C\text{-}H\ down}$. Finally, in these two chapters, the similitude in the oxidation mechanism for Pt(111) and Pt(100) electrodes is stressed out, despite of the difference in reactivity.

In chapter 5 is described the dependency of the formic acid oxidation rate on a polycrystalline Pt electrode as a function of the solution pH. As the pH increases, the oxidation current density increases and finally reaches a plateau, where the maximum value is achieved. This behaviour is highly dependent on the presence of electrolyte anions that present specific adsorption strength. This doctoral thesis provides as an outcome a plausible mechanism, which fits the current density-pH behaviour within the entire pH range studied. The overall mechanism equation is written as follows:

$$Pt\text{-}A + Pt\text{-}HCOO^-_{C\text{-}H\ down} \rightarrow Pt\text{-}A + CO_2 + Pt + H^+ + 2e^- \quad 0 < pH < 5 \qquad \textit{Eq. 9.2}$$

$$Pt\text{-}HCOO^-_{C\text{-}H\ down} \rightarrow CO_2 + Pt + H^+ + 2\,e^- \quad 5 < pH < 10 \qquad \textit{Eq. 9.3}$$

where A stands for the electrolyte anion.

In the previous mechanism, at pH below 5 the *w*-$HCOO_{C\text{-}H\ down}$ is adsorbed on the electrode surface favoured by the presence of an adsorbed anion (A = sulphate, bridge bonded formate, etc). On the other hand, at pH between 5 and 10, where the anion adsorption is not favoured, the *w*-$HCOO_{C\text{-}H\ down}$ adsorption is promoted by the negative net charge on the electrode surface in these conditions.

The second part of this thesis is focused on the surface modification of Pt electrodes, using adatoms, in order to improve its activity towards formic acid oxidation reaction, although some mechanistic studies are also included. In fact, using some DFT calculations for experiments validation was possible to propose a reaction mechanism for the Bi-Pt(111) electrode, which proposes that formate (or formic acid) is adsorbed on a Bi atom, leading towards a *w*-$HCOO_{C\text{-}H\ down}$ configuration. Under those conditions the cleavage of the C-H bond is favoured on Pt, with a negligible activation energy, which leads to the spontaneous formation of CO_2.

From the improvement in the catalytic activity point of view, it was studied Pt(100) and Pt(111) electrodes modified by Tl and three types of shape controlled Pt nanoparticles modified by Pb. Thus, when modifying Pt(100) by Tl, is evident an enhancement in the catalytic activity, especially for the diminution of the onset potential of the oxidation, and an increasing in the maximum current density reached. Comparing both electrodes, the highest improvement factor in catalytic activity is achieved in Tl-Pt(100). This is explained because of the action of two main effects: third body and bifunctional effects. Moreover, it was demonstrated the beneficial effect on their catalytic activity of modifying shape controlled Pt nanoparticles by Pb adatoms. The combined use of several electrochemical techniques such as SECM and cronoamperometry allowed setting a detailed comparison of the activity and stability of the different Pt nanoparticles modified by Pb. Pb_{θ} /111-Pt NPs were the most active nanoparticles to formic acid oxidation, reaching a maximum activity of 7 $mA.cm^{-2}$ at 0.5 V vs RHE in a 0.1 M formic acid solution. Under comparable experimental conditions, Pb_{θ} /111-Pt NPs exhibit 2.7 and 2.3 times more current density than Tl_{θ} /100-Pt NPs and Sb_{θ} /111-Pt NPs, respectively, which places them as one of the most active systems for formic acid oxidation studied so far. Additionally, the maximum Pb coverage reached on Pt nanoparticles presents a very high stability versus reaction time.

Finally, it is important to stress out that the findings described in this doctoral thesis give a deep insight to help in the comprehension of the reaction mechanism of the formic acid oxidation and, thus, for the design of new efficient and stable electrocatalysts.

List of Publications

List of publications in the scope of this Thesis

Published Articles

[1] C. Buso-Rogero, J. V. Perales-Rondon, M. J. S. Farias, F. J. Vidal-Iglesias, J. Solla-Gullon, E. Herrero and J. M. Feliu, "Formic acid electrooxidation on thallium-decorated shape-controlled platinum nanoparticles: an improvement in electrocatalytic activity" *Physical Chemistry Chemical Physics* **2014**, 16, 13616-13624.

[2] J. V. Perales-Rondon, A. Ferre-Vilaplana, J. M. Feliu and E. Herrero, "Oxidation Mechanism of Formic Acid on the Bismuth Adatom-Modified Pt(111) Surface" *Journal of the American Chemical Society* **2014**, 136, 13110-13113.

[3] J. V. Perales-Rondon, E. Herrero and J. M. Feliu, "Effects of the anion adsorption and pH on the formic acid oxidation reaction on Pt(111) electrodes" *Electrochimica Acta* **2014**, 140, 511-517.

[4] A. Ferre-Vilaplana, J. V. Perales-Rondon, J. M. Feliu and E. Herrero, "Understanding the Effect of the Adatoms in the Formic Acid Oxidation Mechanism on Pt(111) Electrodes" *ACS Catalysis* **2015**, 5, 645-654.

[5] O. Lugaresi, J. V. Perales-Rondon, A. Minguzzi, J. Solla-Gullon, S. Rondinini, J. M. Feliu and C. M. Sanchez-Sanchez, "Rapid screening of silver nanoparticles for the catalytic degradation of chlorinated pollutants in water" *Applied Catalysis B* **2015**, 163, 554-563.

[6] J. V. Perales-Rondón, E. Herrero and J. M. Feliu, "On the activation energy of the formic acid oxidation reaction on platinum electrodes" *Journal of Electroanalytical Chemistry* **2015**, 742, 90-96.

[7] J. V. Perales-Rondón, S. Brimaud, J. Solla-Gullón, E. Herrero, R. Jürgen Behm and J. M. Feliu, "Further Insights into the Formic Acid Oxidation Mechanism on Platinum: pH and Anion Adsorption Effects" *Electrochimica Acta* **2015**, 180, 479-485.

Unpublished Articles

[8] J. V. Perales-Rondón, C. Busó-Rogero, J. Solla-Gullón, E. Herrero and J. M. Feliu, "Formic acid electrooxidation on thallium modified platinum single crystal electrodes". **In preparation**.

[9] J.V. Perales-Rondón, J. Solla-Gullón, E. Herrero and C.M. Sánchez-Sánchez, "Enhanced catalytic activity and stability for the electrooxidation of formic acid on lead modified shape controlled platinum nanoparticles". **Under revision**. Article submitted to the Journal *Applied Catalysis B.*